VISIT…

Metallurgy of Steel for Bladesmiths & Others who Heat Treat and Forge Steel

John D. Verhoeven
Emeritus Professor
Iowa State University

March 2005

Preface

For the past 15 years or so I have been working with practicing bladesmiths on problems related to forging and heat treating steel blades. It has become apparent to me in that time that there is a need for a book that explains the metallurgy of steel for people who heat treat and forge steels and have had no formal metallurgical education. This book is an effort to provide such a treatment. I have discovered that bladesmiths are generally very quick to catch on to the ideas of metallurgy and consequently an attempt was made to set the level of detail presented here for the needs of those wanting a fairly complete understanding of the subject.

Most chapters in the book contain a summary at the end. These summaries provide a short review of the contents of each chapter. It may be useful to read these summaries before and perhaps after reading the chapter contents.

The Materials Information Society, ASM International, has published a book that contains a wealth of information on available steels and is extremely useful to those who work and heat treat steel: Heat Treater's Guide, Practices and Procedures for Irons and Stteels, 2nd Edition, (1995), Materials Park, OH 44073. A major goal of this book is to provide the necessary background which will permit a practicing metal worker to understand how to use the information in the ASM book, as well as other handbooks published by ASM International.

I would like to acknowledge the help of two bladesmiths who have contributed to this book in several ways, Alfred Pendray and Howard Clark. Both men have helped me understand the level of work being done by U.S. bladesmiths and they have also contributed to some of the experiments utilized in this book. They are also responsible for the production of this book because of their encouragement to write it. In addition I would like to acknowledge many useful discussions with William Dauksch and my colleague, Prof. Brian Gleeson, who made many useful suggestions on the stainless steel chapter.

I am particularly indebted to Iowa State University and their Materials Science and Engineering Department for providing me with the opportunity to teach metallurgical engineering students about steel for over two decades, as well as to the Ames Laboratory, DOE, that supported most of my research activity. Many of the pictures and methods of presentation in this book result from my experience teaching students and doing research at Iowa State University.

My professional career has been supported by publicly funded institutions. Therefore, I grant any user copyright permission to download and print a copy of this book for personal use or any teacher to do the same for their students. I do not grant rights to the text for commercial uses. The copyrights to all figures with citations belong to the original publishers. Copyright permissions were obtained for inclusion of these figures.

Index Index

Chapter	Title of chapter or subtopic	Page
1	**Pure Iron**	1
	Summary	4
2	**Solutions and Phase Diagrams**	5
	Solutions	5
	Phase Diagrams	6
	Summary	7
3	**Steel and the Fe-C Phase Diagram**	8
	Low Carbon Steels (Hyoeutectoid Steels)	10
	High Carbon Steels (Hypereutectoid Steels)	11
	Eutectoid Steels	13
	The A_1, $A_{e1,}A_{c1}$, A_{r1} Nomenclature	15
	References	16
	Summary	17
4	**The Various Microstructures of Room Temperature Steel**	19
	Optical Microscope Images of Steel Grains	19
	Room Temperature Microstructures of Hypo- and Hypereutectoid Steels	20
	Microstructure of Quenched Steel	23
	Martensite	24
	Two Types of Martensite	25
	The M_s and M_f Temperatures	26
	Martensite and Retained Austenite	27
	Bainite	29
	Spheroidized Microstructures	32
	Summary	34
5	**Mechanical Properties**	36
	The Tensile Test	36
	The Hardness Test	38
	The Notched Impact Test	42
	Fatigue Failure and Residual Stresses	45
	References	47
	Summary	48
6	**The Low Alloy AISI Steels**	50
	Manganese in Steel	52
	Effect of Alloying Elements on Fe-C Phase Diagram	54
	References	56
	Summary	56
7	**Diffusion**	58
	Carburizing and Decarburizing	61
	References	63
	Summary	64
8	**Control of Grain Size by Heat Treatment and Forging**	66
	Grain Size	66
	Grain Growth	67
	New Grains formed by Phase Transformation	69
	New Grains formed by Recrystallization	70
	Effects of Alloying Elements	72
	Particle Drag	73
	Solute Drag	74
	References	76
	Summary	76
8	**Hardenability of Steel**	78
	IT Diagrams	79
	Hardenability Demonstration Experiment	83
	CT Diagrams	85
	The Jominy End Quench	88
	Hardenability Bands	91
	References	91
	Summary	92

10	**Tempering**	95
	Tempered Martensite Embrittlement (TME)	96
	Effect of %C on toughness	97
	Effect of Alloying Elements	98
	References	101
	Summary	101
11	**Austenitization**	103
	Single Phase Austenitization	103
	Homogenization	106
	Austenite Grain Growth	106
	Two-Phase Austenitization	108
	References	110
	Summary	110
12	**Quenching**	113
	Special Quenching techniques	113
	Martempering	114
	Austempering	115
	Variation on Conventional Austempering	117
	Characterization of Quench Bath Cooling Perfomance	120
	Oil Quenchants	122
	Polymer Quenchants	124
	Salt Bath Quenchants	124
	References	125
	Summary	126
13	**Stainless Steels**	128
	Ferritic Stainless Steels	129
	Martensitic Stainless Steels	132
	Optimizing Martensitic Stainless Steels for Cutlery Applications	134
	Example Heat Treatment using AEB-L	139
	Austenitic Stainless Steels	141
	Precipitation Hardening Stainless Steels (PHSS)	145
	References	147
	Summary	147
14	**Tool Steels**	151
	Tool Steel Classification	151
	The Carbides in Tool Steels	153
	Special heat treatment effects with tool steels	155
	References	157
	Summary	158
15	**Solidification**	159
	Factor 1 - Microsegregation	160
	Factor 2 - Grain Size and Shape	165
	Factor 3 - Porosity	166
	References	168
	Summary	168
16	**Cast Irons**	170
	Gray and White Cast Irons	171
	Ductile and Malleable Cast Iron	179
	References	182
	Summary	183
Index		184
Appendix	A - Temperature Measurement	A1
	Thermocouples	A1
	Radiation Pyrometers	A3
	References	A7
	B – Stainless Steels for Knife-makers	B8

1 - Pure Iron

Most steels are over 95% iron, so a good starting point to understanding steel is to study the nature of solid iron. Consider the following experiment. A 1 inch diameter bar of pure iron is sectioned to form a thin disk in the shape of a quarter. A face of the disk is now polished on polishing wheels starting first with a coarse grit polish and proceeding in steps with ever finer grits until one ends up with the face having the appearance of a shinny mirror. The shinny disk is now immersed for around 20-30 seconds in a mixture of 2 to 5 % nitric acid (HNO_3) in methyl alcohol (called nital, nit for the acid and al for the alcohol), a process known as etching. The etch causes the shinny surface to become a dull color. If the sample is now viewed in an optical microscope at a magnification of 100x, it is found to have the appearance shown on the right of Fig. 1. The individual regions such as those numbered 1 to 5 are called iron grains and the boundaries between them, such as that between grains 4 and 5 highlighted with an arrow, are called grain boundaries. The average size of the grains is quite small. At the 100x magnification of this picture a length of 200 microns is shown by the arrow so labeled. The average grain diameter for this sample has been measured to be 125 microns, where 1 micron = 0.001 mm. Although a small number, this grain size is much larger than most commercial irons. (It is common to use the term μm for micron and 25 μm = 0.001 inches = 1 mil. The thickness of aluminum foil and the diameter of a hair both run around 50 μm.)

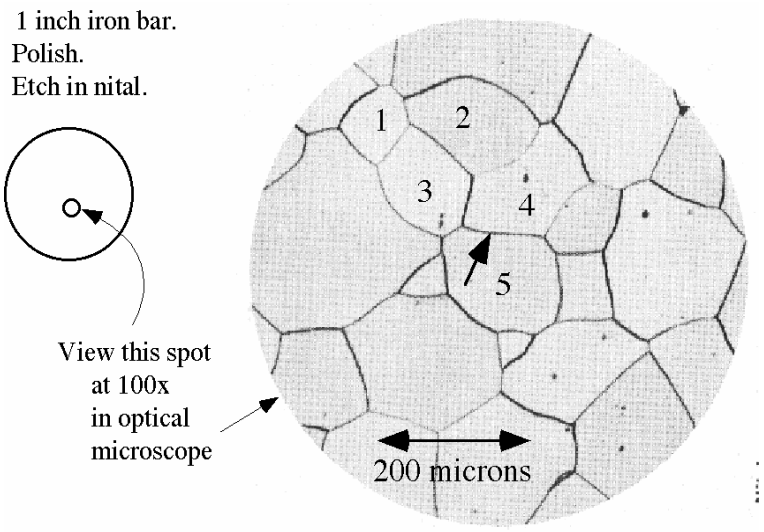

Figure 1.1 Optical microscope image of surface of a polished and etched iron bar viewed at a magnification of 100x. [1.1]

The basic building blocks of solids like salt and ice are molecules, which are units made up of two or more atoms. For example, sodium + chlorine in table salt (NaCl) and hydrogen + oxygen in ice (H_2O). In metals, however, the basic building blocks are the individual atoms of the metal, i.e., iron (Fe) atoms in a bar of iron, or copper (Cu) atoms in copper wire. Each one of the grains in Fig. 1.1 is what we call a crystal. In a crystal made up of atoms, all of the atoms are uniformly arranged on layers. As shown in Fig. 1.2, if you draw lines connecting the centers of the atoms you generate a 3-dimensional array of little cubes stacked together to fill space. In iron at room temperature the cubes have an atom at each of the 8 corners and one atom right in the middle of the cube. This crystal structure is called a BCC (body centered cubic) structure, and the geometric arrangement of atoms is often called a BCC ***lattice***. Notice that the crystal lattice can be envisioned as 3 sets of intersecting planes of atoms with each plane set parallel to one face of the cube. Iron with a BCC structure is called ***ferrite***. Another name for ferrite is alpha iron, or α-iron, where α is the symbol for the Greek letter a.

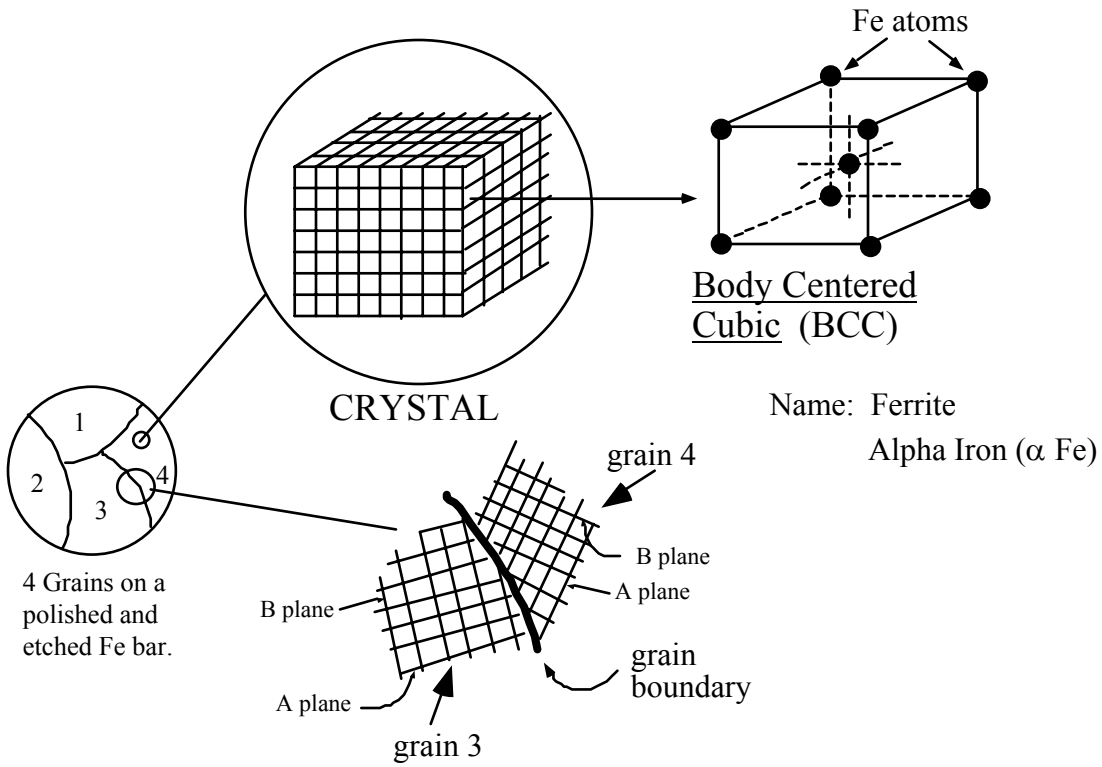

Figure 1.2 The crystal structure of the grains and the nature of the grain boundaries.

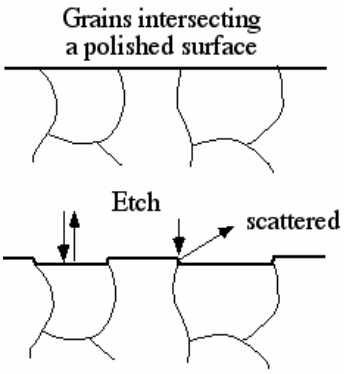

The nature of a grain boundary is illustrated at the bottom center of Fig. 1.2. The boundary is a planar interface, generally curved, along which two grains of different orientation intersect. The A planes in grain 4 make a much steeper angle with the horizontal than do the A planes of grain 3. If grain 4 were rotated clockwise to cause its A planes to line up with the A planes of grain 3, then the grain boundary would go away and the 2 grains would become one larger grain. An interesting question is why do these grain boundaries show up on the etched surface? When a metal is etched in an acid, atoms are chemically removed from the surface. It turns out that the rate of removal of iron atoms by nital depends on the orientation of the crystal that is facing the acid. Because each grain presents a different orientation, each grain etches down at a different rate. For example, the planes that form the faces of the body centered cubes etch far slower than other crystal planes. Hence, after a period of etching small steps develop at the grain boundaries. For example, at the boundary of a fast etching grain, one would see a step -up to the surrounding grains. The step generally causes light to be scattered away from your eye and you see the boundaries as dark lines.

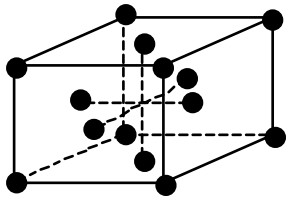

Face Center
Cubic (FCC)

Names: Austenite or Gamma Iron (γ Fe)

If iron is heated to 912 ^{o}C (1674 ^{o}F) a somewhat magical effect occurs, the crystal structure changes spontaneously from body centered cubic to a new structure called face centered cubic (FCC). This structure is shown in Fig. 1.3, where it is seen that, as the name suggests, the atoms lie on the corners of a cube as well as one atom at each of the 6 faces of the cube. Like

Figure 1.3 The crystal structure of iron that forms at high temperatures.

the low temperature BCC structure, this structure has two names, either ***austenite*** or gamma iron (γ iron), where γ is the symbol for the Greek form of the letter c.

Historical Note: The first 3 letters of the Greek alphabet are alpha, beta, gamma (α, β, γ) but there is no structure of iron called beta iron. When the structure of iron was being discovered in the late 19th century, the magnetic transition in iron which occurs at 770 ^{o}C (1418 ^{o}F), caused scientists to theorize a structure of iron they called beta iron, which was later shown not to exist.

When the ferritic iron is heated to 912 ^{o}C (1674 ^{o}F) the old set of ferrite grains changes (transforms) into a new set of austenite grains. Imagine that the ferrite grain structure shown in Fig. 1.2 has just reached the transformation temperature. What one would see is, first, the formation of a new set of very small austenite grains forming on the old ferrite grain boundaries, and second, the growth of these grains until all the old ferrite grains were gone. Two important effects occur when ferrite changes to austenite. (1) Just like it takes heat energy to transform ice to water, it takes heat energy to change the ferrite grains into austenite grains. Therefore, on heating, the iron temperature will remain close to 912 ^{o}C (1674 ^{o}F) until all the ferrite grains are transformed. (2) The ferrite to austenite (α to γ) transformation is accompanied by a volume change. The density of austenite is 2% higher than ferrite, which means that the volume per atom of iron is less in austenite.

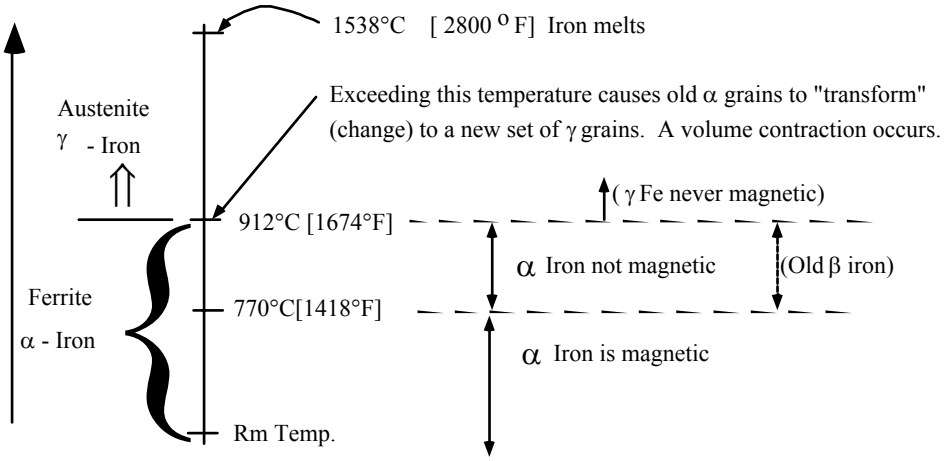
1538°C [2800 O F] Iron melts
Exceeding this temperature causes old α grains to "transform"
(change) to a new set of γ grains. A volume contraction occurs.
Austenite
γ - Iron
(γ Fe never magnetic)
912°C [1674°F]
α Iron not magnetic
(Old β iron)
Ferrite
α - Iron
770°C[1418°F]
α Iron is magnetic
Rm Temp.

Figure 1.4 Changes occurring in iron shown on a plot of increasing temperatre.

It is helpful to represent the ideas discussed above geometrically on a diagram where one plots temperature on a vertical scale and identifies the changes that occur at significant temperatures, as shown in Fig. 1.4. Following are two experiments one can do to illustrate these changes. Exp. 1: Heat a bar of iron up above 1418 ^{o}F (770 ^{o}C) and as it cools place a magnet near it. When the temperature reaches 1418 ^{o}F (770 ^{o}C) the hot sample will begin to become pulled toward the magnet. As the diagram of Fig. 1.4 shows, BCC iron (α iron) is only magnetic below 1418 ^{o}F (770 ^{o}C), and FCC iron (γ iron) is never magnetic. Exp. 2: Obtain a piece of black (non-galvanized) iron picture wire and string it horizontally between 2 electrical posts spaced 3 feet apart. Hang a weight from the center of the wire and pass an electrical current through the wire heating it above 1674 ^{o}F (912 ^{o}C), which will be past a red color to an orange-yellow color. (Note:

You will need to increase the voltage slowly using a high current capacity variable power source, such as a variac.) As you heat the wire it expands and the weight drops. Now turn off the power and watch the wire cool in a darkened room. You will see the above two effects that occur at the 1674 ^{o}F (912 ^{o}C) transformation temperature. 1) As the wire cools the accompanying volume contraction will raise the center weight, but this rising will be temporarily reversed when the wire expands as the less dense ferrite forms. 2) Heat liberated by the transformation will cause a visible pulse of color temperature increase to be seen in a darkened room. Both of these effect can be observed in reverse order on heating, but they are less dramatic due to the difficulty of heating rapidly. You can understand why heat is given off when austenite changes to ferrite on cooling by thinking about the water-ice transformation. It is clear that one needs to cool water to make it transform to ice (freeze). This means heat is removed from the liquid at the freezing temperature. The same effect occurs when metals freeze, heat is removed from the metal. So when a hot metal cools to its freezing point we find that heat is given off from the freezing liquid. The transformation from liquid to solid is a **phase transformation** between the liquid phase and the solid phase. Phase transformations that occur on cooling liberate heat. When austenite transforms to ferrite on cooling we have a solid-solid (rather than a solid-liquid) phase transformation and heat is liberated. On heating the reverse occurs, heat is absorbed when ferrite goes to austenite.

References

1.1 Metals Handbook, Volume 7, 8th Edition, ASM (1972).

Summary of the major ideas of this chapter.

1 A piece of iron consists of millions of small crystals all packed together.

2 Each crystal is called a ***grain***. A typical grain diameter is 30 to 50 microns.
(25 micron = 25 μm = 0.001inch = 1 mil)

3 The boundaries between the crystals are called ***grain boundaries***.

4 Below 1167 ^{o}F (912 ^{o}C) iron is called either ***ferrite*** or ***alpha*** (α) iron. The iron atoms in ferrite are arranged on a body center cubic (BCC) geometry. It is common to call the arrangement of atoms a body centered cubic (BCC) ***lattice***.

5 Above 1167 ^{o}F (912 ^{o}C) iron is called either ***austenite*** or ***gamma*** (γ) iron. The iron atoms in austenite are arranged on a face center cubic (FCC) lattice.

6 Heating ferrite to 1167 ^{o}F (912 ^{o}C) causes tiny grains of austenite to form on the ferrite grain boundaries. Continued heating causes these new γ grains to grow converting all the old α grains into a new set of smaller γ grains. On cooling below 1167 ^{o}F (912 ^{o}C) the same type of change occurs, but in reverse order, where α grains replace γ grains.

2 - Solutions and Phase Diagrams

In order to understand how the strength of steels is controlled it is extremely useful to have an elementary understanding of two topics: Solutions and Phase Diagrams.

Solutions The idea of a solution can be explained by the following simple example. Take a glass of water and put a tea spoon full of either sugar or salt into it. Initially you will be able to see most of the solid white sugar or salt floating on the water or sinking to the bottom of the glass. However, after stirring with the spoon adequately you will see that all of the sugar or salt disappears and you only see the clear water that you started with. We say that the sugar or salt has ***dissolved*** into the water and the final liquid is said to be a ***solution*** of sugar or salt in water.

What has happened to the sugar or salt? Consider the salt because its molecule (sodium chloride [NaCl] for table salt or calcium chloride [$CaCl_2$] for the salt used on icy roads) is more simple than sugar. When the salt goes "into solution" the individual molecules break apart into their component atoms and these atoms in-turn are pulled into the liquid water and are trapped in the water as charged atoms (called ions) between the water molecules [H_2O] that make up the liquid we call water. For table salt the NaCl molecules decompose following the reaction: $NaCl \Rightarrow Na^+ + Cl^-$, where the symbol Na^+ refers to a positively charged sodium atom, called an ion, and the symbol Cl^- refers to a negatively charged chorine atom. You no longer see the solid salt because the chemical bonds that held the atoms together in the solid have been relaxed causing the former solid structure to disappear as its component atoms became incorporated into the liquid water between the water molecules.

In general, when a solution is formed by dissolving something into a liquid the freezing temperature of the liquid will decrease. This, of course, is why we add calcium chloride ($CaCl_2$) salt to our streets and sidewalks during the winter months. The salt dissolves into the rain water and drops its freezing temperature so that ice will not form until the temperature has been lowered below the pure water freezing temperature of 32 ^oF (0 ^oC). This effect can be represented graphically as shown in Fig. 2.1. Here, temperature is plotted on the vertical axis and the amount of salt dissolved into the water on the horizontal axis. The amount of salt dissolved in the water is given here as a weight percent of the total liquid solution. Two terms are often used to

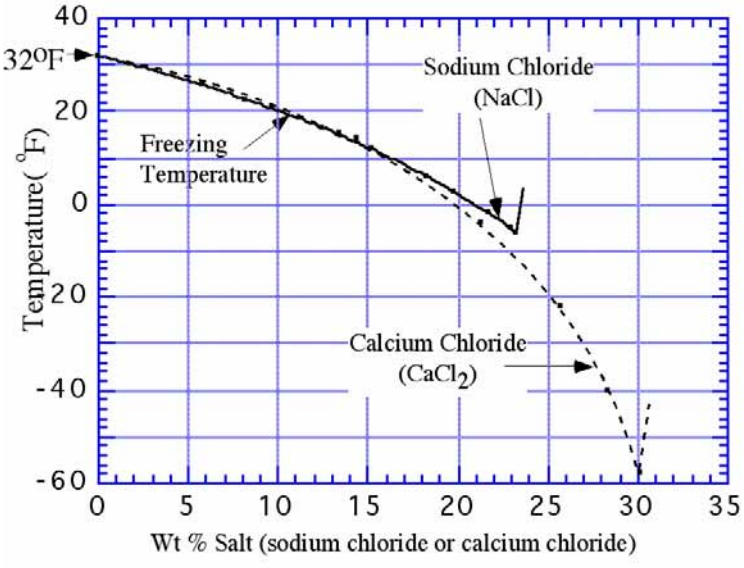

Figure 2.1 The lowering of the freezing temperature of water versus the weight % of two different salts dissolved in the water.

describe the amount of stuff that has been dissolved, A 10 wt. % sodium chloride value can be called the ***concentration*** of salt in the solution, or the ***composition*** of the solution. Notice on Fig. 2.1 that after a certain maximum amount of the salt has dissolved in the solution the freezing temperature suddenly begins to rise quite rapidly. This maximum composition is called the ***eutectic*** composition and it will be discussed more later. The curves show why it is preferable to use calcium chloride over sodium chloride to prevent ice formation on your sidewalks.

Phase Diagrams The geometric arrangement of the molecules in water (called the molecular structure) is the same, on average, from point to point in the water. The water is called a liquid ***phase***. Similarly, the molecular structure in ice is the same from point to point in the ice, and the ice is called a solid phase. However, the molecular structures of ice and water are very different from each other, one being a liquid and the other a solid. Therefore, liquid water and ice are 2 different phases.

As shown in Fig. 2.1, the freezing point of water is suppressed as salt is dissolved into the water forming a solution. The molecular structure of the salt solution is essentially the same as that of pure water since the salt ions fit in-between the H_2O molecules without disturbing their geometric arrangement relative to each other. So pure water and the salt solution generated by dissolving salt in the water are the same phase.

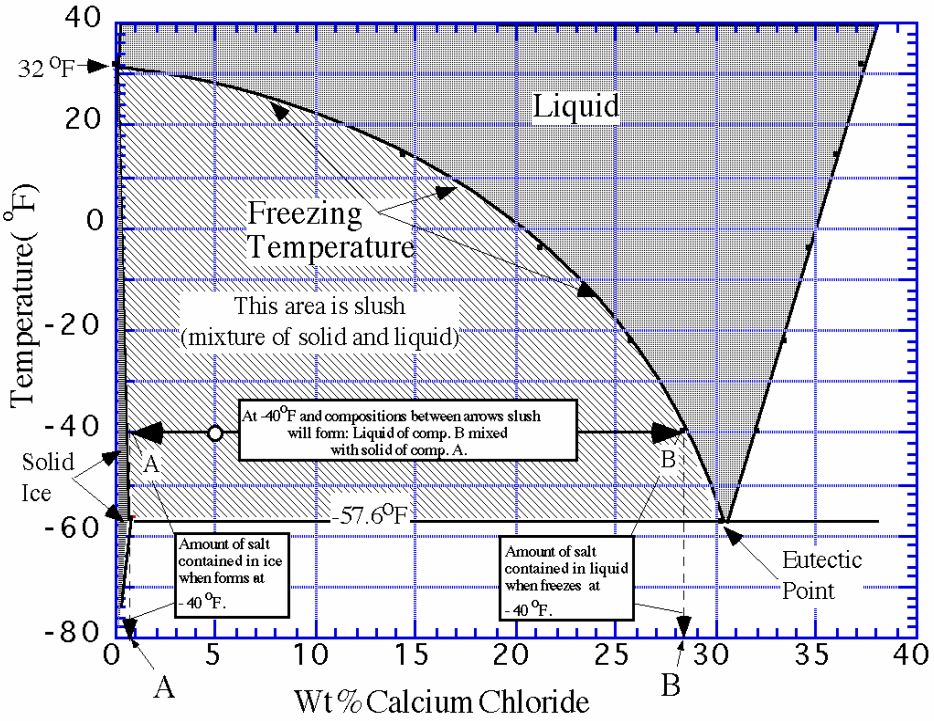

Figure 2.2 A portion of the water-clacium chloride phase diagram.

A phase diagram is a temperature versus composition map that locates on the map the temperature-composition coordinates where the various phases can exist. Fig. 2.2 presents part of the water-calcium chloride phase diagram. Just as in Fig. 2.1 the diagram has temperature plotted vertically and composition (in wt. % salt) plotted horizontally. The

freezing temperature line for the liquid salt solution is the same as on Fig. 2.1, only now the sharp rise in freezing temperature beyond the eutectic point is extended to the maximum temperature of the diagram. The shaded region labeled "Liquid" above the freezing temperature line maps out all possible temperature-compositions that are found to be liquid. Notice that at the extreme left of the diagram there is a thin shaded region labeled "Solid Ice". This solid ice has the same molecular structure as pure water ice, but now it contains a very small amount of salt dissolved in it. It is the same phase as the pure water ice. Hence this thin region is a map of where solid ice occurs on the diagram.

Now consider a salt solution containing 5 wt. % calcium chloride that is cooled to -40 ^{o}F (small circle on Fig. 2.2). This point on the phase diagram map does not lie in either the liquid or the solid (ice) regions. Hence, this solution at - 40 ^{o}F cannot be all solid or all liquid. Figure 2.2 shows a horizontal line at -40 ^{o}F that terminates with arrow heads labeled A and B. What the diagram tells us is that this 5 % solution at -40 ^{o}F is a mixture of solid ice having composition A (about 0.7 % salt[*]) and liquid water having composition B (about 28.3 % salt). Hence, it tells us we have a slush (a water-ice mixture) and it tells us the compositions of the ice and water in the slush. A solution corresponding to any point in the shaded slush region of the phase diagram is going to be a slush, consisting of a mixture of water with ice. Hence, each region on the phase diagram tells us what phases, in this case solid or liquid, are present. If we are in the 2-phase region (the shaded slush region) it also tells us the composition of each of the 2 phases once we pick a temperature. However, if we are in the 1-phase solid or 1-phase liquid region it does not tell us the composition of the phase once we pick the temperature. It only tells us that we must have all solid or all liquid. In these cases the compositions are the overall average composition that you started with, a number not predicted by the phase diagram.

Summary of major ideas of chapter 2.

1 A liquid ***solution*** occurs when a substance dissolves in a liquid, such as salt into water. A solid solution is similar, like when salt dissolves in ice.

2 The stuff that dissolves into solution (salt in salt solutions, carbon in steel) loses its identity and is hidden from view as its atoms become incorporated into the solution.

3 Solutions have the same molecular structure or atomic structure from point to point within themselves. Each solution is called a ***phase***.

4 A phase diagram is a map having coordinates of temperature on the vertical axis and composition or concentration on the horizontal axis. The phase diagram map identifies those temperature-composition coordinates where a certain phase will exist.

5 A phase diagram also maps out temperature-composition coordinates where only phase mixtures can exist. For example on the Fig. 2.2 phase diagram the shaded slush region locates where slush mixtures of solid ice and liquid water exist.

[*] The real value is much less than 0.7%. The value was increased so it would be clear on the diagram.

3 - Steel and the Fe-C Phase Diagram

Steel is made by dissolving carbon into iron. Pure iron melts at an extremely high temperature, 2800 ^{o}F (1538 ^{o}C), and at such temperatures carbon readily dissolves into the molten iron generating a liquid solution. When the liquid solution solidifies it generates a "solid solution", in which the C atoms are dissolved into the solid iron. The individual C atoms lie in the holes between the iron atoms of the crystalline grains of austenite (high temperatures) or ferrite (low temperatures). If the amount of C dissolved in the molten iron is kept below 2.1 weight percent we have steel, but if it is above this value we have cast iron. Although liquid iron can dissolve C at levels well above 2.1%, solid iron cannot. This leads to a different solid structure for cast irons (iron with total %C greater 2.1%) which is discussed in more detail in Chapter 16.

In addition to C all modern steels contain the element manganese, Mn, and low levels of the impurity atoms sulfur, S, and phosphorous, P. Hence we can think of steels as an alloy of 3 or more elements given as Fe + C + X, where Fe and C are the chemical element symbol for iron and carbon, and X can be thought of as 3rd element additions and impurities. In the United States most steels are classified by a code developed by the American Iron and Steel Institute (AISI). It is customary to partition steel compositions into 2 categories, plain carbon steels and alloy steels. In plain carbon steels, X consists only of Mn, S and P, whereas in alloy steels one or more additional alloying elements are

Table 3.1 Composition (weight %) of some steels

Steel Type	American Iron&Steel Institute code (AISI number)	%C	%Mn	% Other	%S	%P
Plain carbon	1018	0.18	0.75	-	0.05 (max)	0.04 (max)
	1095	0.95	0.40	-	"	"
Alloy	5160	0.60	0.82	0.8 Cr	"	"

added. Table 3.1 lists the composition of 2 common plain carbon steels and one sees that the amount of C (in weight %) is related to the last 2 numbers of the code. The Mn level is not related to the code and must be looked up in a table. The first 2 numbers of the code, 10, identify the steel as a plain carbon steel. These 2 numbers are changed for alloy steels, and the table lists one example for a chromium (Cr) alloy steel. The alloy steels will be discussed in more detail later.

Solid solutions are similar to the liquid salt solution discussed in the last chapter, in that, after the substance has become dissolved its presence is no longer evident to an observer as it had been previous to the dissolving. This may be illustrated for steel as shown in Fig. 3.1. On the left one has a starting condition of a round iron containing only 3 grains. The iron is surrounded by a thin layer of graphite and heated to 1832 ^{o}F (1000 ^{o}C). After a period of several hours the graphite layer disappears. The C atoms of the graphite have migrated into the solid iron by a

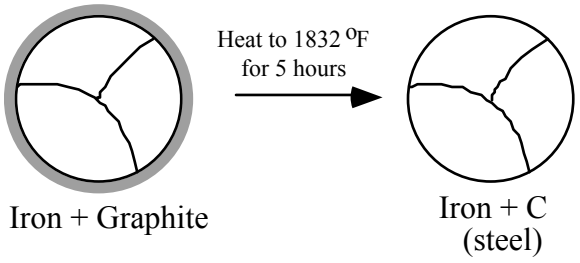

Figure 3.1 Converting a rod of iron containing only 3 grains to steel by dissolving carbon in it.

process called diffusion which is discussed in Chapter 7. All of the C atoms have fit themselves into the holes that exist between the iron atoms of the FCC austenite present at this temperature. This solid solution of C in Fe is steel.

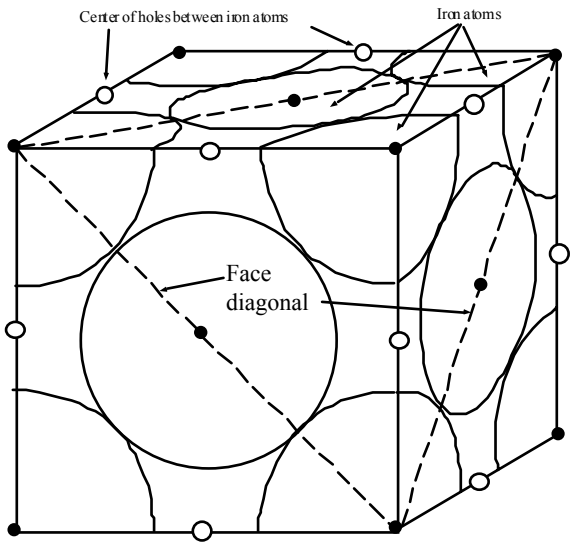

Figure 3.2 Location of iron atoms in FCC austenite. Small circles locate centers of holes between the iron atoms.

Figure 1.3 locates the center of the iron atoms in the FCC lattice. Allow each of the little dots of Fig. 1.3 to expand until they touch each other and you end up with the model of FCC iron shown in Fig. 3.2. The expanded iron atoms touch each other along the face diagonals of the cube. The small open circles locate the center of the void spaces between the iron atoms. If you expand these small circles until they touch the iron atoms you find that their maximum diameter equals 41.4 % of the iron atom diameter. This means that X atoms smaller than around 42% of the iron atom diameter should fit into the holes between the iron atoms. Carbon atoms are small, but the diameter of carbon atoms is estimated to be 56 % of the diameter of iron atoms in austenite. Hence, when C dissolves in iron it pushes the iron atoms apart a small amount. The more carbon dissolved the further the iron atoms are pushed apart. Hence there is a limit to how much C can dissolve in iron.

Historical Note: The iron age dates to around 1000 BC, when our ancestors first learned to reduce the plentiful iron oxide ores found on earth into elemental iron. The iron was made in furnaces that were heated by charcoal fires that were not able to get hot enough to melt the iron. They produced an iron called bloomery iron which is similar to modern wrought iron. Even though charcoal was used in these furnaces, very little carbon became dissolved in the iron. So, to make steel, carbon had to be added to the bloomery iron. (Even to this day steel cannot be economically made directly from the iron ore. The modern 2 step process first makes high carbon pig iron and the second step reduces the carbon composition to the steel range.) Our ancestors did not know the nature of the element C until around 1780-90AD, and steel and cast iron played a key role in its discovery. Until shortly before that time, the production of steel was primarily the result of blacksmiths heating bloomery iron in charcoal fires. This process is tricky as a charcoal fire can just as easily remove C as add it (see p. 63). Therefore, steel was made on a hit and miss basis from the start of the iron age, and the quality of such steel varied widely. The successful blacksmiths guarded their methods carefully.

In pure iron the difference in ferrite and austenite is a difference in their atomic structure. As illustrated in Figs. 1.2 and 1.3, the iron atoms are arranged with a BCC crystal structure in ferrite and a FCC crystal structure in austenite. In both ferrite grains and austenite grains this atomic structure does not change as one moves around in the grain. Hence, similar to ice and water of the last chapter, both ferrite and austenite are individual ***phases***.

When C is added to austenite to form a solid solution, as illustrated above in Fig. 3.1, the solid solution has the same FCC crystal structure as in pure iron. As discussed with reference to Fig. 3.2, the C from the graphite just fits in-between the iron atoms. The crystal structure remains FCC, the only change being that the iron atoms are pushed

very slightly farther apart. Pure austenite and austenite with C dissolved in it are both the same phase. Hence, austenite with C dissolved in it, and ferrite with C dissolved in it are two different phases, both of which are steel.

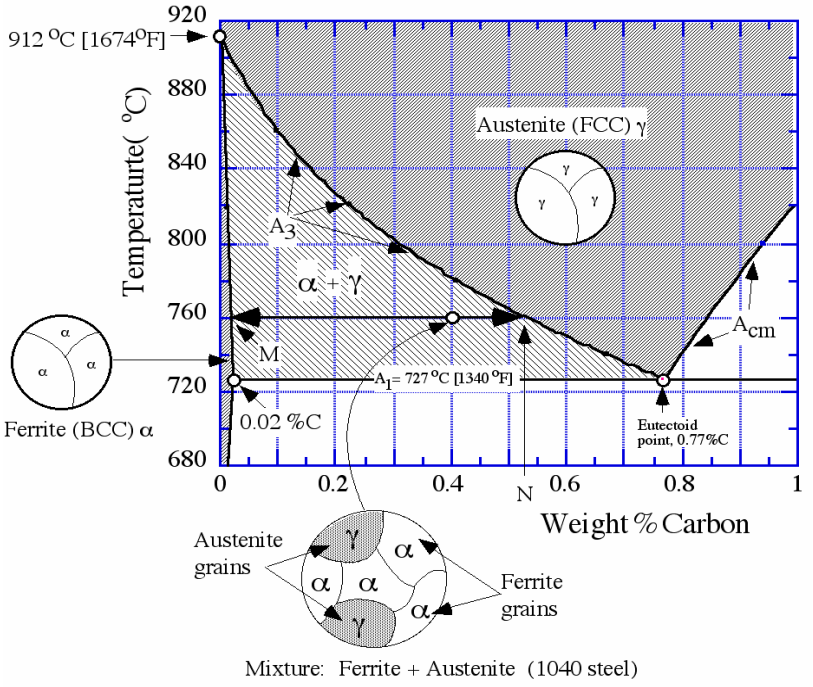

Figure 3.3 Portion of Fe-C phase diagram for hypoeutectoid alloys. (%C less than 0.77%)

Low Carbon Steels (Hypoeutectoid Steels)

The Fe-C phase diagram provides us with a temperature-composition map that tells us where on this map the two phases, austenite and ferrite, will occur. It also shows us where on the map we can expect to get mixtures of these 2 phases, just like the slush region on the ice-salt phase diagram. A portion of the Fe-C phase diagram is shown on Fig. 3.3 and it seen that there is a strong similarity to the salt diagram of Fig. 2.2. In pure iron, austenite transforms to ferrite on cooling to 912 °C (1674 °F). This transition temperature is traditionally called the A_3 temperature and the diagram shows that, just as adding salt to water lowers the freezing point of water, adding C to iron lowers the A_3 temperature. Whereas, the maximum lowering occurs at what is called the eutectic point in water-salt, a similar maximum lowering occurs in Fe-C, but here it is called the ***eutectoid*** point, and also, the ***pearlite*** point. The eutectoid point has a composition of 0.77 % C and steels with compositions less than this value are called ***hypoeutectoid*** steels, as illustrated in the title of Fig. 3.3. The eutectoid temperature is traditionally called the A_1 temperature.

Steels that are 100 % austenite must have temperature-composition coordinates within the central upper dark area of Fig. 3.3. Steels that are ferrite must have temperature composition coordinates in the skinny dark region at the left side of Fig. 3.3. The maximum amount of C that will dissolve into ferritic iron is only 0.02 %, which occurs at the eutectoid temperature of 727 °C (1340 °F). This means that ferrite is essentially pure iron because it is always 99.98% or purer with respect to C. Notice however, that austenite may dissolve much more carbon than ferrite. At the eutectoid temperature austenite dissolves 0.77 % C, which is roughly 38 times more C than ferrite will hold at this temperature. Austenite holds more C than ferrite because the holes between iron atoms are larger in the FCC structure than the BCC structure.

Remember that in the salt-water phase diagram the shaded slush region mapped the temperature composition points where one obtains slush: a mixture of the water and ice. Similarly, the central shaded region labeled $\alpha+\gamma$ of Fig. 3.3 maps temperature-composition points where steel consists of a mixture of ferrite and austenite. Suppose your were able to utilize a hot stage microscope to look at a polished steel having a

composition of 0.4 % C after it was heated to 760 °C (1400 °F). Since this temperature-composition point lies in the central shaded region labeled α+γ, the steel must be a mixture of ferrite and austenite. What you would observe would be a mixture of ferrite grains and austenite grains, as shown at the bottom of Fig. 3.3. The phase diagram also tells you information about the composition of the two phases. The austenite grains must have the composition given as N, and the ferrite the composition given as M on Fig. 3.3.

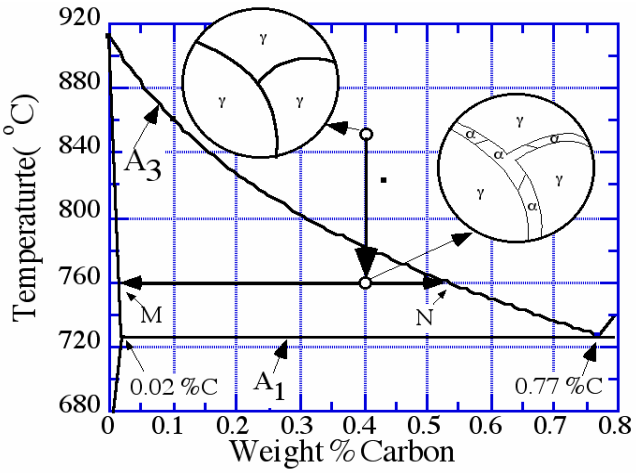

Figure 3.4 Change in microstructure on cooling a 1040 steel from 850 °C to 760 °C.

As a further illustration of the usefulness of the phase diagram consider the following simple experiment. A steel of composition 0.4 %C is first heated to 850 °C (1562 °F) and held for around 10 minutes. After this short hold all the grains in this steel would consist of pure FCC austenite grains with a composition of 0.4 % C. To make the illustration simple image that we are looking at the steel in a hot stage microscope and we see a region of only 3 grains as shown on Fig. 3.4. Now the hot stage temperature is reduced to 760 °C (1400 °F) and the sample slowly cools to this temperature. What happens to the microstructure? The phase diagram tells us that after cooling the steel must become 2-phase, a mixture of austenite and ferrite. Experiments show that the ferrite that forms in the pure austenite as it cools virtually always forms on the austenite grain boundaries. This is illustrated in the lower microstructure of Fig. 3.4, where the ferrite has formed as a number of α grains along the prior austenite grain boundaries. Comparing the microstructure at the right side of Fig. 3.4 to that at the bottom of Fig. 3.3, one sees similarities and differences. They are similar in that both contain a mixture of ferrite and austenite grains with the same volume fraction of each. But they are different in that the distribution of the ferrite grains is quite different. The microstructure of Fig. 3.3 will generally be formed upon heating the steel from room temperature up to 760 °C (1400 °F). Hence, this example illustrates one of the fascinating aspects of steels, the microstructure is controlled by heat treatment. As we will show later, the mechanical properties of steels are controlled by microstructure. The ***microstructure*** of a steel generally refers to the specific shape, size, distribution, and phase types of the grains in the steel. Remember, the phases present in Figs. 3.3 and 3.4 are only present at the high temperature of 760 °C (1400°F), not at room temperature. We will discuss room temperature phases later.

High Carbon Steels (Hypereutectoid Steels) As the %C dissolved in austenite increases the iron atoms are pushed further apart. This stretches the chemical bonds that hold the Fe atoms together generating a form of energy called strain energy. There is a limit to how much strain energy the austenite can stand. The amount of C dissolved in austenite when this limit is reached is called the solubility limit. Question: The solubility limit in austenite at 820 °C [1508 °F] is 1 wt. %C. If you make up an alloy containing 1.5 wt. % C and heat it to 820 °C, only 1% of this 1.5 %C will be dissolved in the austenite; what happens to the remaining 0.5 %C? This excess C becomes

incorporated into a new phase called cementite. The new phase, cementite, has one major difference from austenite or ferrite. It is a chemical compound that exists at only 1 composition. Chemical compounds are generally represented by their elemental formulas, such as NaCl, for sodium chloride table salt. The 1 composition for NaCl is 50 atomic percent sodium, which corresponds to 39.3 weight percent sodium. The chemical element formula for cementite is Fe_3C. For each atom of C in the compound there are 3 atoms of iron, giving an atomic composition of 25 at. % C. The corresponding weight percent carbon in cementite turns out to be 6.7 wt. %C. Other than this limitation to 1 composition, cementite has several similarities to austenite and ferrite. It is a crystal having its atoms arranged in regularly repeating geometrical arrays. The crystal structure is a bit more complex than either BCC of ferrite or the FCC of austenite, but it is well known. Also it is a separate phase and is present as discrete grains. So the excess 0.5 %C in our steel at 820 °C [1508 °F] will all be present as separate cementite grains mixed in with the austenite grains, i.e., the microstructure will be a 2-phase mixture of austenite and cementite.

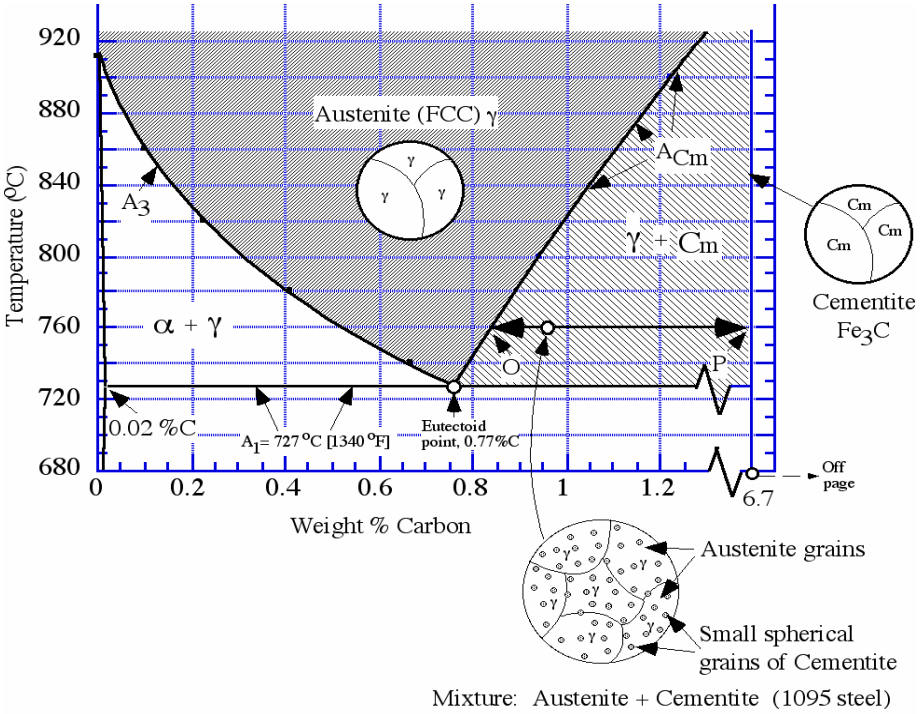

Figure 3.5 Extension of the Fe-C phase diagram to hypereutectoid alloys, (%C greater than 0.77 %).

The Fe-C phase diagram extended to higher carbon compositions where cementite becomes important is shown in Fig. 3.5. As before, the region on the temperature-composition map corresponding to austenite is shown as the central dark region. Because cementite exists at only 1 composition, it is shown on the phase diagram as a vertical line located at its 1 composition, 6.7 %C. Notice that the composition axis at the bottom of the diagram has a break in it just beyond 1.2 % and the value of 6.7 % is located next to the break. If the break were not inserted the 6.7 % composition would appear roughly 1 foot to the right. To envision the true diagram in your mind you simply need to extend the right portion over about 1 foot, which expands the shaded 2-phase region labeled γ + Cm into a much large area.

The line on the diagram labeled A_{cm} defines the solubility limit for C in austenite. Notice that at 820 °C this line gives a point at 1 wt. %C, which is the maximum amount of C that can be dissolved in austenite at 820 °C [1508 °F]. Alloys having % C values to the right of the A_{cm} line are in shaded 2-phase region labeled γ + Cm and must consist of a mixture of austenite and cementite grains. Consider a 1095 steel (0.95 wt. %C)

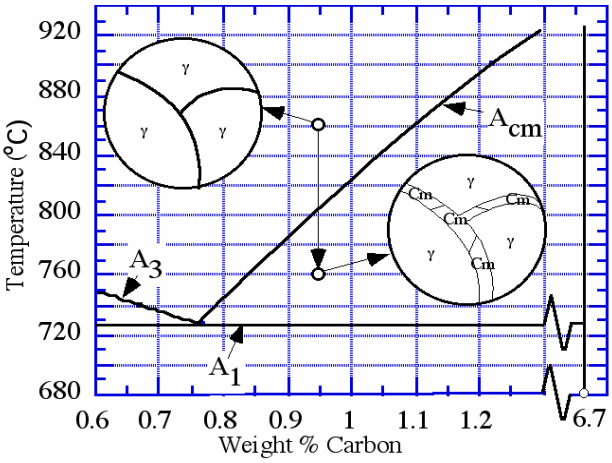

Figure 3.6 Change in microstructure on cooling a 1095 steel from 900 °C to 760 °C.

received from a steel mill. If this steel is heated to 760 °C [1400 °F] it will be at the open circle point located on the diagram with the horizontal arrowed line passing through it. Because the temperature-composition point now lies in the shaded 2-phase region labeled γ + Cm, we know that this steel must consist of a mixture of austenite having composition O (0.85 %C) and cementite of composition P (6.7 %C). The diagram does not tell us what the microstructure will look like. Experiments show that the microstructure will be as shown on the bottom of Fig. 3.5. All of the cementite is found to be present as small spherically shaped grains distributed fairly randomly over the austenite grains which have much larger sizes and are present with the typical curved grain boundaries.

To further illustrate the use of the phase diagram in understanding how microstructure changes during heat treatment, consider an experiment where the as-received 1095 steel is heated to 850 °C [1562 °F], and held for 20 minutes or so. As shown on the phase diagram of Fig. 3.6 this temperature-composition point corresponds to the single phase austenite region. Assuming we could observe the structure in a hot stage microscope the small region under observation at high magnification might consist of just 3 grains, which would have an appearance similar to that shown on Fig. 3.6. The temperature of the hot stage is now lowered to 760 °C [1400 °F] and this temperature-composition point lies in the 2-phase austenite + cementite region. This means that cementite grains must form on cooling. Just as is the case for hypoeutectoid steel of Fig. 3.3, where ferrite forms on the cooling austenite grain boundaries, here cementite forms on the austenite grain boundaries during cooling. As shown on Fig. 3.6, one ends up with a microstructure in which all of the prior austenite grain boundaries from the 850 °C structure are filled with thin plate shaped grains of cementite. Notice the dramatic difference in this microstructure from that shown on Fig. 3.5 where the 1095 steel was heated directly from room temperature to 760 °C . Both microstructures contain the same volume fraction of cementite and austenite but the distribution of the cementite is quite different. Unlike austenite and ferrite, cementite is very brittle. Consequently the 1095 structure of Fig. 3.6 with its interconnected Cm plates is not as tough as the Fig. 3.5 structure with its small isolated Cm grains. Again, this is an example of how heat treatment can change microstructure which in-turn changes mechanical properties.

Eutectoid Steel (Pearlite) In the previous 2 sections we considered steels having compositions on either side of the eutectoid composition of 0.77 wt. %C. It turns out that steels having the composition of 0.77 %C (a 1077 steel) generate a unique microstructure that is called pearlite. Figure 3.7 presents the Fe-C phase diagram on which the area below the A_1 line of 727 °C [1340 °F] is shaded dark. This entire area is a 2-phase region. Any steel cooled slowly into the temperature-composition coordinates of this area must consist of a mixture of the 2 phases: ferrite and cementite (α + Cm). The

microstructures of steels in this 2-phase region vary widely and pearlite is just one of many microstructures that can occur.

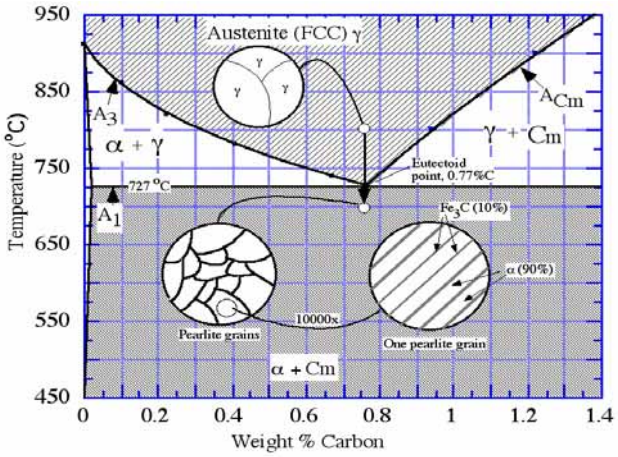

Figure 3.7 Formation of the pearlite microstructure on cooling a 1077 steel below the A_1 temperature of 727 °C [1340 °F].

To understand the pearlite microstructure consider a 1077 steel that is heated in a hot stage microscope to 800 °C [1472 °F]. As shown on Fig. 3.7 the steel will consist of all austenite grains after just a minute or two at 800 °C. After cooling to a temperature below A_1, and holding for 5 to 10 minutes or so, the austenite grains will be completely replaced by a new set of pearlite grains, as shown on the figure. Contrary to all the grains we have discussed up to this point, the pearlite grains are not a single phase. Rather, they consist of a mixture of 2 phases, α + Cm, having a unique microstructure. To observe the true details of the microstructure, one must blow up a small region within a pearlite grain to a very high magnification, as shown on the lower right of Fig. 3.7. The structure consists of alternating plates of ferrite and cementite. The ferrite plates are much fatter than the cementite plates, occupying 90 % of the volume compared to only 10 % for the cementite. At the pearlite grain boundaries one observe an abrupt change in the orientation of the plates as is shown for a real sample in Fig. 3.8, which is a transmission electron microscope picture at a magnification of 11000x. In this picture the cementite plates are the light phase and the ferrite plates are the dark phase. (Note that the Cm plates are only 0.1 μm thick, too thin to be resolved on an optical microscope. Although Cm is brittle pearlite is not, due largely to the fine size of the Cm plates.)

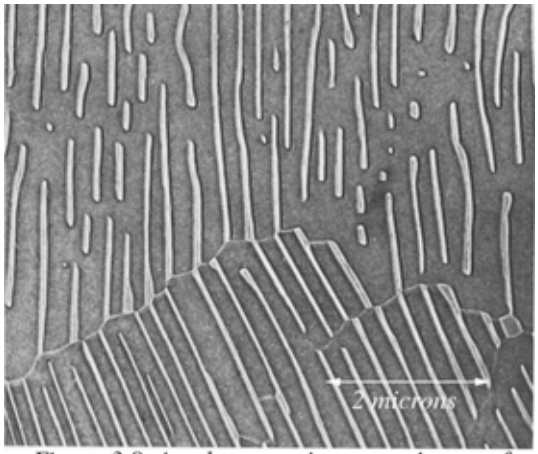

Figure 3.8 An electron microscope image of pearlite after polishing and etching in nital. Magnification = 11000x [3.1]

If the 1077 steel is now cooled from the 700 °C temperature shown on Fig. 3.7 to room temperature, the microstructure will not change significantly no matter how slow or fast the sample is cooled. The ferrite will remain a nearly pure BCC iron with less than 0.02 %C dissolved in it and the cementite will remain at 6.7 %C with an unchanged crystal structure. The phase diagram tells us that once austenite is cooled below the A_1 temperature and held for a short period, the austenite will be completely replaced by some form of α + C_m and on cooling to room temperature no further changes in the resulting α + C_m microstructure will occur. When we look at plain carbon steels at room temperature we never see austenite.• This means that microstructures containing austenite, such as those shown on Figs 3.2 to 3.5, can only be seen in a hot stage microscope, because the austenite will be replaced by other structures on cooling. At high cooling rates these include the martensite and bainite structures discussed below. At air cooling rates and slower the austenite will transform into some form of α + Cm.

• An exception to this rule is quenched high carbon steels, which contain mixtures of martensite and retained austenite.

The A_1, A_{e1}, A_{c1}, A_{r1} Nomenclature The Fe-C phase diagram shown in the above figures is called an ***equilibrium*** phase diagram. This means that the transformation temperatures given by the A lines were determined at extremely slow cooling or heating rates where equilibrium conditions are obtained. The A_3, A_{cm}, and A_1 lines that appear on equilibrium phase diagrams are often labeled the A_{e3}, A_{ecm} and A_{e1} lines respectively, where the e indicates equilibrium conditions. In this book the e will generally not be used. The absence of e implies equilibrium conditions.

Consider again the experiment illustrated on Fig. 3.7. The diagram predicts that when the austenite grains cool to 727 ^oC [1340 ^oF], pearlite will start to form from the austenite. This only occurs if one cools the austenite extremely slowly. At even modest cooling rates like 5 ^oF/min. (2.8 ^oC/min.) the transformation temperature is lowered by around 20 ^oC (36 ^oF). This means that the Fe-C diagram can only be used as a rough guide for estimating transformation temperatures. Not only is the transformation from austenite to pearlite on cooling shifted down in temperature, the reverse transformation from pearlite to austenite on heating is shifted up in temperature. To give you an idea of the magnitude of this shift on cooling and heating and how it can be measured, a simple experiment was run. A hole was drilled in a small piece of 1018 steel and a thermocouple secured in the hole. The output of the thermocouple was measured with a digital voltmeter every 2 seconds and sent to a pc where it was converted to a file of temperature versus time. The sample was placed in a small resistance furnace and heated to 870 ^oC [1598 ^oF] and then removed from the furnace. The output of the thermocouple for both the heating and cooling cycle is shown on Figs. 3.9 and 3.10.

As explained in Chapter 1, when austenite changes to ferrite on cooling heat is liberated and when ferrite changes to austenite on heating heat is absorbed. Consider first the heating curve of Fig. 3.10. As we will discuss in Chapters 5 and 7, the A_3 and the A_1 lines of the pure Fe-C diagram are shifted down in temperature by the 0.75 % Mn and 0.2 % Si present in 1018 steel to the values of A_1 = 725 ^oC, and A_3 = 824 ^oC. The heating data of Fig. 3.10 show that at around 737 ^oC the rate of temperature rise abruptly decreases. This is due to the heat absorbed by the sample as the pearlite part of the steel transforms to austenite. It means that the A_1 line has shifted up by 12 ^oC, from 725 to 737 ^oC. It is customary to label the actual temperature of the transformation on heating A_{c1}, as shown on the figure. The amount of the upward shift depends on the heating rate. If the heating rate were increased above the value of 40 ^oC/min. the value of A_{c1} would increase. On cooling an opposite effect occurs, the heat liberated when austenite transforms to ferrite or to pearlite slows down the rate of decrease in the sample temperature. Figure 3.9 illustrates this effect for both the austenite $\Rightarrow$ ferrite transformation below the A_3 temperature and the austenite $\Rightarrow$ pearlite transformation below the A_1 temperature. The former transformation begins to occur here at 762 ^oC, which is 62 ^oC below the A_3 temperature of 824 ^oC and the latter occurs at 652 ^oC which is 73 ^oC below the A_1 temperature of 725 ^oC. As shown on Fig. 3.9 it is customary to label the actual transformation temperatures that occur on cooling the A_{r3} and A_{r1} temperatures. Notice that the cooling rate for the data of Fig. 3.9 is 3 times larger than the heating rate for the data of Fig. 3.10. This larger rate accounts for the increased shift

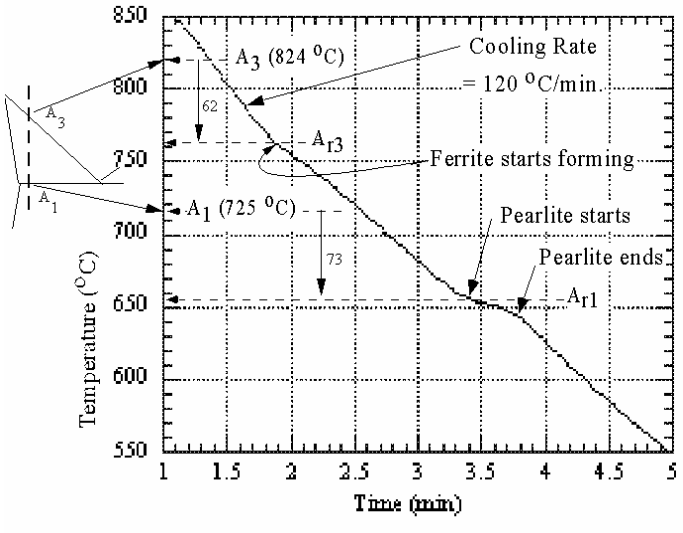

Figure 3.9 Cooling (refroidissement) curve for a 1018 steel.

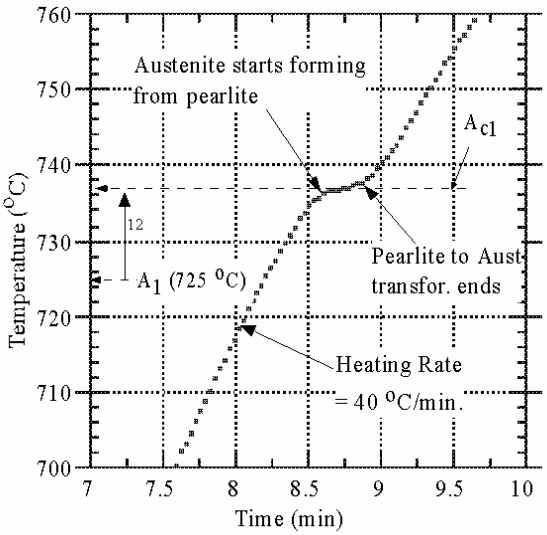

Figure 3.10 Heating (chauffage) curve for a 1018 steel.

in the A_1 temperature from - 73 °C on cooling to only + 12 °C on heating. (The temperature range of Fig. 3.10 did not extend high enough to measure the increased A_3 temperature, which is called the A_{c3} temperature.)

Historical Note: The same French scientist, Floris Osmond, who is responsible for the name of martensite is also responsible for the use of the letters r and c for the shift in the A lines on cooling and heating. At the end of the 19th century he was the first scientist to use thermocouples to measure the effect of heating and cooling rates. The letter r is from the French word for cooling, refroidissement, and the letter c is from the French word for heating, chauffage.

Figure 3.11 presents a graphical summary of the above ideas showing the shift up of the A lines on heating with labels having subscript c added, and the shift down on cooling with the labels have the subscript r added. These shifts in transformation temperatures can become important in operations involving rapid heating and cooling. An example is the shift up in transformation temperature with heating in processes such as flame and induction hardening.

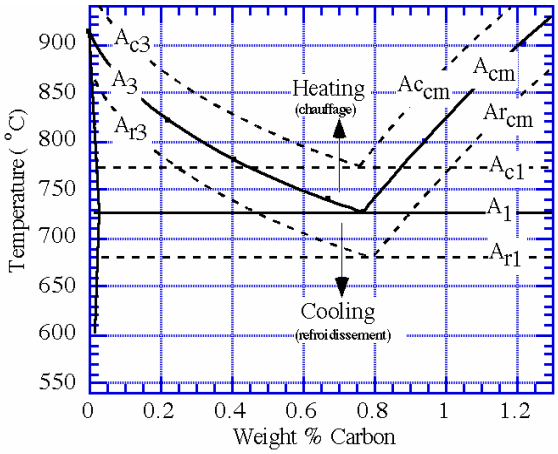

Figure 3.11 Nomenclature for the A lines shifted up on heating and down on cooling.

References

3.1 Metals Handbook, Vol. 7, 8th Edition, ASM, Metals Park, Ohio, (1972).

3.2 Heat Treaters Guide, 2nd Edition, ASM International, Materials Park, Ohio (1995).

Summary ideas of Chap. 3.

1 In the U.S.A. steels are specified with the AISI (American Iron and Steel) code. As shown in Table 3.1 the code tells us the carbon composition and if the steel is an alloy steel or a plain carbon steel. Ones needs to consult a reference, such as [3.2], to determine the full composition.

2. Steel is made by adding carbon to iron, and the main structures are the same as those of pure iron discussed in Chapter 1, ferrite and austenite. At low carbon compositions the carbon is dissolved into the iron forming solid solutions of ferrite (BCC) at low temperatures and austenite (FCC) at high temperatures. At high carbon compositions a compound of carbon with iron, cementite, Fe_3C, forms in the steel. These 3 structures are called phases and the iron-carbon phase diagram maps the temperature-composition values where the 3 different phases are stable.

3. The iron-carbon phase diagram is similar to the salt-water phase diagram of Chapter 2. As C is added the austenite-to-ferrite transformation drops from the 912 ^{o}C [1674 ^{o}F] value of pure iron and attains a minimum value at 727 ^{o}C [1340^{o}F]. Beyond the minimum the transformation temperature increases and cementite begins to form. The minimum occurs at a composition of 0.77 %C, which is called the eutectoid point

4. It is common to classify steels with carbon compositions less than the eutectoid value as hypoeutectoid steels and those with more than 0.77 %C as hypereutectoid steels.

5. As a hypoeutectoid steel cools from the austenite region, grains of ferrite will begin to form on the old austenite grain boundaries. At any specific temperature below which ferrite starts to form and above the eutectoid temperature, the phase diagram allows us to calculate: (1) the volume fraction of ferrite formed and (2) the composition of both the ferrite formed and the remaining austenite.

6. The microstructure of a steel refers to the size, shape and distribution of the phases that make up the steel. The microstructure is controlled by the history of the steel, i.e., how it was heated and cooled and any prior mechanical deformation.

7. As a hypereutectoid steel cools from the austenite region grains of cementite will begin to form on the old austenite grain boundaries. Cementite is a compound of iron and carbon having the chemical formula, Fe_3C. Like austenite and ferrite it is a phase in steel composed of small grains, but it is different in that it has only one chemical composition, 6.7 weight %C (25 atomic %C) and it is quite brittle. At any specific temperature below which cementite starts to form and above the eutectoid temperature, the phase diagram allows us to calculate: (1) the volume fraction of cementite formed and (2) the composition of the remaining austenite.

8. When steels having the eutectoid composition of 0.77 wt.%C are cooled below the eutectoid temperature of 727 ^{o}C [1340 ^{o}F] they transform into the pearlite structure.

Pearlite consists of 2-phase grains composed of alternating thin plates of cementite and fat plates of ferrite. The plate thickness depends on cooling rate, and in air cooled samples the cementite plates are so thin they cannot be seen in an optical microscope (thickness less than 0.2 microns).

9. The 3 important lines on the Fe-C phase diagram are labeled as follows: A_3 is the austenite $\Leftrightarrow$ ferrite transformation line, A_{cm} is the austenite $\Leftrightarrow$ cementite transformation line, and A_1 is the austenite $\Leftrightarrow$ pearlite transformation line. Only when heating or cooling is very slow do these transformations occur at the A_{cm}, A_3 and A_1 temperatures given by the equilibrium phase diagram. On cooling (refroidissement) the transformation lines shift down in temperature and the subscript r is added as, A_{r3}, A_{rcm}, and A_{r1}. On heating (chauffage) the transformation lines shift up in temperature and the subscript c is added as, A_{c3}, A_{ccm} and A_{c1}. The amount of the shift up or down scales with the heating or cooling rates, and is quite large even at modest rates, see Fig. 3.9.

4 - The Various Microstructures of Room Temperature Steel

The optical microscope is the principal tool used to characterize the internal grain structure of steels. It is traditional to call the structure revealed by the microscope the microstructure. The mechanical properties of a given steel are strongly influenced by the microstructure of the steel and this chapter reviews the common steel microstructures and how they are achieved by the heat treatment of the steel. The previous chapter discussed steel microstructures that occur at high temperatures where it is generally not possible to observe such structures clearly even in a hot stage microscope. This chapter discusses only the room temperature microstructures that we observe in optical and electron microscopes.

Optical Microscope Images of Steel Grains As discussed in Chapter 1, the grain structure of iron and steel samples is revealed by polishing the surface to a mirror quality, etching in an acid solution and then examining in an optical microscope. The etch removes atoms from the polished surface, and the rate of removal depends on both the crystal orientation of the grain and the type of grain, e.g., ferrite versus austenite. The gray level observed in the microscope for a given grain depends on the degree of smoothness of the grain surface after the etching. As shown in Fig. 4.1, grains that are single phase, like ferrite, austenite and cementite will have their atoms removed uniformly from point to point and so the original polished surface will remain smooth within a given grain after etching.

An optical microscope utilizes reflected light to generate an image. A beam of light is directed down onto the surface (open arrowheads in Fig. 4.1) and the image is generated either on film or at your eye by light reflected back up along the same direction. Figure 4.1 uses a symbol for your eye located directly above the sample surface showing the light path generating the image. The reflected light is shown by the dark arrows. For a smooth surface a very large fraction of the incoming light is reflected back up the image path, thereby forming a bright (white) appearance. Hence, the single phase grains of ferrite, austenite and cementite all appear at the white end of the gray level range in an optical image. Because they all appear white, it is often not possible to distinguish between them by their

Type of grain	Surface after etching	Appearance in the optical microscope
Ferrite	Smooth 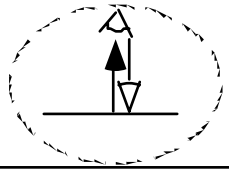	White
Austenite	Smooth	White
Cemenite	Smooth	White
Pearlite	Cm plates protrude 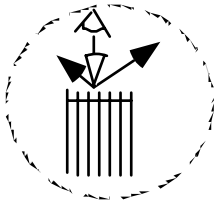	Dark
Martensite (Fresh)	Smooth 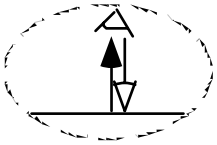	Mostly White
Bainite and Tempered Martensite	Cm particles protrude 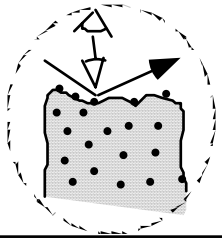	Dark

Figure 4.1 Appearance of various types of steel grains in an optical microscope.

appearance (gray levels) without further information.

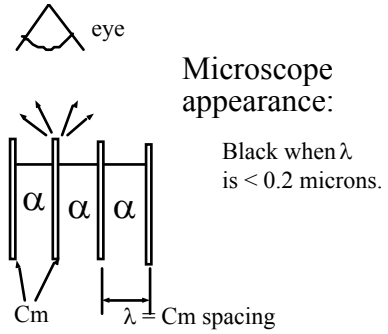

Figure 4.2 Light scattering at an etched pearlite surface.

Now consider pearlite. The common etches used for steels, nital (nitric acid in alcohol) and picral (picric acid in alcohol) etch the ferrite plates of pearlite much faster than the cementite plates. Hence, after etching the cementite plates protrude out from the ferrite plates. The cementite plates are very fine, and they scatter the incoming light away from the image path, see Fig. 4.2, thereby generating a low gray level (dark) image. So, pearlite will generally appear gray to black in an optical microscope, but not always. If the spacing of the cementite plates is large enough then one will observe the Cm plates as dark lines with white ferrite plates between them. The optical microscope can only resolve distances down to around 0.2 μm at the highest useful magnifications of around 1000x. Therefore when the spacing of pearlite is less than 0.2 μm the optical microscope image shows pearlite grains with a mottled dark/gray level as shown in Fig. 4.3. The spacing of the cementite plates in pearlite depend on how fast the sample was cooled from the austenite range down past the A_1 temperature; faster cooling gives finer spacings. Perhaps the most common way to do such cooling is simply to remove the sample from the furnace and allow it to cool in the air. The cooling rate then depends on how big the sample is. Even for fairly large samples, air cooling produces cementite spacings smaller than 0.2 μm. So, pearlite in samples that were air cooled virtually always appear with dark gray levels, similar to that seen in Fig. 4.3. The picral etch used in Fig. 4.3 dissolves ferrite more uniformly as its crystal orientation changes than does the nital etch. Therefore, picral gives a more uniform gray level than nital and is the preferred etch for pearlite

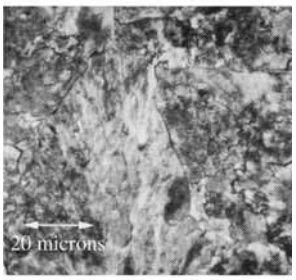

Figure 4.3 Optical micrograph of pearlite at 500x. Picral etch.

Room Temperature Microstructures of Hypo- and Hypereutectoid Steels

Reconsider the experiment shown on Fig. 3.4 where an 0.4 %C austenite is cooled from 850 °C to 760 °C. It was shown that the structure formed after such cooling will consist of thin sheets of ferrite grains lying on the prior austenite grain boundaries that originally formed at 850 °C. The question we want to consider now is what happens to the remaining austenite grains if the sample is cooled to room temperature.

To analyze this question consider a 3 step cooling process from 760 °C. The sample is 1st cooled to 740 °C, 2nd

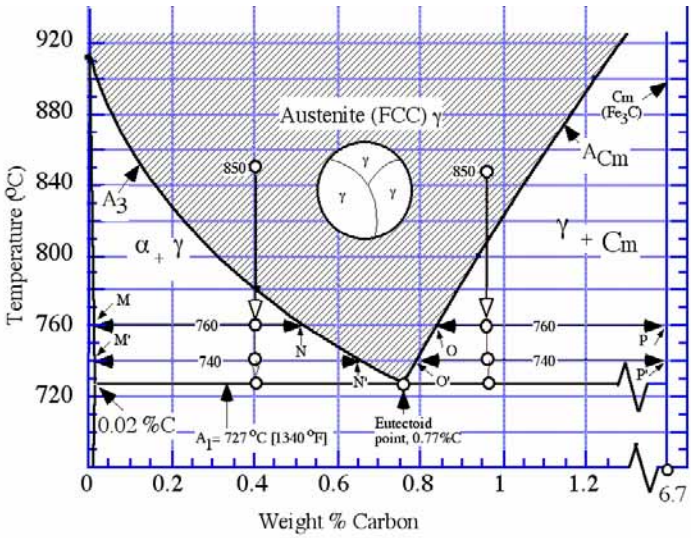

Figure 4.4 Phase diagram analysis of the decomposition of 0.4 % and 0.95 % austenite on cooling to the pearlite temperature.

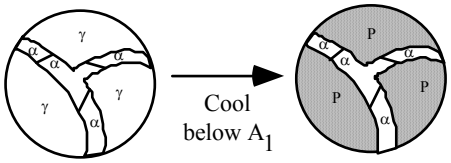

Figure 4.5 Austenite grains transform to pearlite on cooling below 727 ^{O}C [1340 ^{O}F].

cooled to 727 ^{o}C (the A_1 temperature), and 3rd cooled to room temperature. The previous analysis (Fig. 3.4) showed that the austenite present at 760 ^{o}C has a carbon composition of N, which is also shown on Fig. 4.4. After the 1st cooling from 760 ^{o}C to 740 ^{o}C, the phase diagram requires that the carbon composition of the austenite increase to the value of N', shown on Fig. 4.4. After the 2nd cooling to 727 ^{o}C the carbon composition of the austenite grains must increase further to exactly the eutectoid composition (also known as the pearlite composition) of 0.77 % C. At this point the microstructure of the steel will appear as shown on the left of Fig. 4.5. The only apparent difference between this structure and that shown on the lower right of Fig. 3.4 is that the thin ferrite grains are a bit thicker. But now the carbon composition of the austenite grains lies at the magic eutectoid point, 0.77 %C, so that on the final cooling to room temperature these austenite grains will transform into pearlite grains giving a microstructure similar to that shown on the right of Fig. 4.5. In the optical microscope the old austenite grains are now all dark because they have transformed to pearlite, and the ferrite grains will appear white and they will outline the pearlite grains. Figure 4.6 presents an actual micrograph of such a structure for a 1060 steel. Because the ferrite forms prior to the pearlite and because the pearlite forms at the 727 ^{o}C eutectoid temperature, the ferrite is often called **proeutectoid** ferrite. (It is possible to understand why the %C in austenite must increase on cooling if you remember that ferrite can dissolve almost no carbon. On cooling in the 2-phase region more ferrite must form, so when a small element of austenite transforms into ferrite virtually all the C atoms in that volume element must be ejected into any remaining austenite, thereby increasing its %C . This increase cannot exceed 0.77 %C because at this composition austenite decomposes to pearlite on further cooling; and pearlite has an average composition of 0.77%)

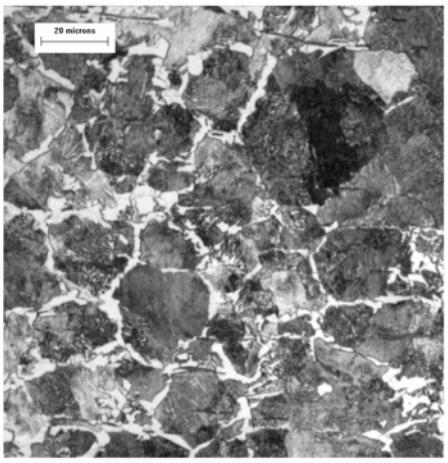

Figure 4.6 A 1060 steel air cooled from 850 C to room temperature.

Now consider a steel whose %C is greater than 0.77 %C, a hypereutectoid steel. A common such plain carbon steel is 1095 steel (also know as either drill rod, or W1 tool steel). After heating to 850 ^{o}C its temperature-composition coordinate is located on Fig. 4.4. It is now cooled following the same 3 step process that was considered above for the 0.40 %C steel. The action that occurs for the 1095 steel is very similar to that of the 1040 steel except that the new phase formed on the austenite grain boundaries is Cm and not α. At 760 ^{o}C thin plate shaped grains of Cm form on the prior austenite grain boundaries and the austenite grains must have the composition O shown on Fig. 4.4, around 0.85 %C. At 850 ^{o}C the austenite grains had the original composition of 0.95 %C. This composition is reduced to 0.85 %C after the Cm forms because the cementite, at 6.7 %C, must suck up carbon atoms as it forms. On cooling to 740 ^{o}C more Cm is formed and the austenite composition drops to point O'. On further cooling to the A_1 temperature of 727 ^{o}C the austenite composition will have dropped to the eutectoid composition of 0.77 %C. At this point the structure would appear in a hot stage microscope as shown on the left of Fig. 4.7, which is similar to Fig. 4.5 but with the prior austenite grain boundaries decorated with Cm grains rather than α grains. Cooling below 727 ^{o}C transforms the austenite grains to the pearlite structure as shown on the right of Fig. 4.7, and this structure will not change on cooling. So it would appear the same in a

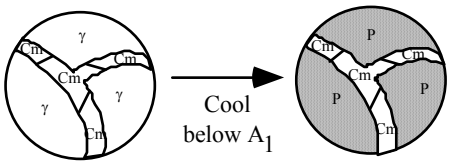

Figure 4.7 Austenite grains transform to pearlite on cooling below 727 °C [1340 °F].

hot stage microscope at temperatures just below 727 °C as it does to us at room temperature where we are able to view it easily. Figure 4.8 presents an optical micrograph of a real piece of 1095 steel that was given the heat treatment shown on Fig. 4.4, first held at 850 °C and then air cooled.

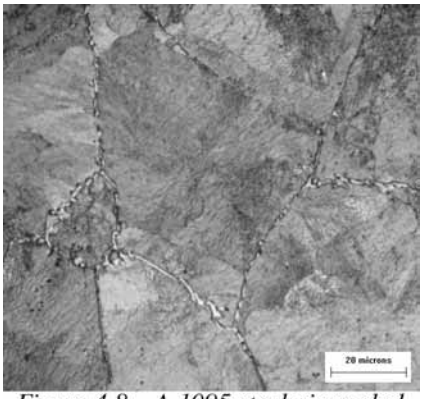

Figure 4.8 A 1095 steel air cooled from 850°C to room temperature (Nital etch, 500x)

Notice the similarities between the hypoeutectoid steel of Fig. 4.6 and the hypereutectoid steel of Fig. 4.8. In each case the set of prior austenite grain boundaries are filled with a proeutectoid phase, ferrite in the low C steel and cementite in the high carbon steel. The phase diagram provides information about the volume fraction of the proeutectoid phase that will be present between the pearlite grains. Suppose the steel were a 1075 steel. The 0.75 %C composition is very close to the pearlite composition of 0.77, and so this steel must be nearly 100 % pearlite. Similarly suppose one had a 1005 steel. Because the 0.05 %C is so close to the pure ferrite composition of 0.02 %C, this steel must be mostly ferrite with only a small percent pearlite. Hence, the volume fraction pearlite depends on where the overall composition lies between pure ferrite, 0.02 %C, and pure pearlite, 0.77 %C, along the A_1 temperature line. Let X = the overall composition of a hypoeutectoid steel. Then the volume fraction of ferrite in the steel is simply (0.77-X)/(0.77-0.02).* For our 1060 steel this works out to be 0.23 or 23%. For hypereutectoid steels the same type of rule applies with the volume fraction cementite measured by the relative position of the overall composition point along the A_1 line between pure pearlite at 0.77 %C and pure cementite at 6.7 %C. The formula now becomes, fraction cementite = (X-0.77)/(6.7-0.77), which for our 1095 steel gives a value of 0.03 or 3% cementite.

The room temperature microstructures of steel varies widely and those shown in Figs. 4.6 and 4.8 should be regarded as just 2 examples of many different possible structures. The following generalizations hold.

(1) If the steel has been cooled at rates of air cooling or slower its structure will be some mixture of ferrite and cementite. The cementite will usually be present as a component of the pearlite grains, but not always. By proper heat treatment it is possible to form the cementite as isolated grains such as shown for the microstructure at the bottom of Fig. 3.5. This structure is called "spheroidized" because the Cm is present as small spherical grains. A pearlitic steel is much stronger and more difficult to machine than a spheroidized steel. That is why steel mills generally supply hypereutectoid steels in the spheroidized condition. The microstructure of such steels consists of spherical Cm particles in a matrix of ferrite grains. (See pp. 32-33 for further discussion.)

The micrographs of Figs. 4.6 and 4.8 show the proeutectoid phases localized along prior austenite grain boundaries. As the steel composition moves further away

* Strictly speaking this formula gives weight fraction ferrite. However weight fraction is extremely close to volume fraction because the densities of cementite and ferrite are very nearly the same.

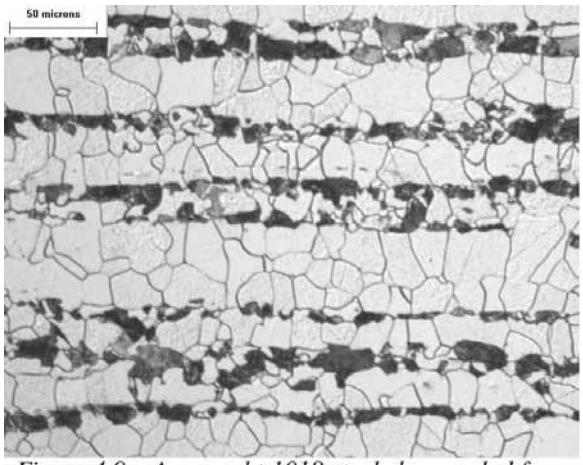

Figure 4.9 A wrought 1018 steel slow cooled from 900 °C to room temperature. Deformation direction is horizontal, (Nital etch, 240x)

from the eutectoid composition this morphology becomes less common. For example, Fig. 4.9 shows the microstructure of a 1018 steel that has been furnace cooled from the austenite region. Notice now that the dark pearlite has become a much smaller volume fraction than in the 1060 steel of Fig. 4.6. Now, the white ferrite grains dominate the structure and show no obvious alignment along the prior austenite grains where they first formed, The ferrite grains are simply too big to show traces of those old boundaries. Also, notice that the ferrite and pearlite appear to lie along alternating bands. This steel is called a "**banded**" steel. Virtually all hypoeutectoid steels show this pearlite/ferrite banding if the steel has been heavily deformed followed by slow cooling from the austenite range. All of our wrought steels are heavily deformed by some method, usually a mixture of hot and cold rolling. If such steels are slow cooled (usually just a bit slower than air cooling) and if they are sectioned parallel to the deformation direction, they will virtually always appear banded. Wrought steels having round cross sections will not show banding when sectioned at right angles to the deformation direction (the axis of the round), but they will show banding when sectioned along their axis.

(2) If the steel is cooled rapidly from the austenite region one can no longer estimate the type of phases, their relative amounts or their compositions from the phase diagram as has been done above. At the slower end of these faster cooling rates one still often ends up with mixtures of pearlite + ferrite for low C steels and pearlite + Cm for high carbon steels, but the amount of pearlite depends on the cooling rate. At increasing cooling rates one begins to form one of two new type of structures, bainite or martensite. These structures are the subject of the next section.

Microstructure of Quenched Steel Perhaps the most fascinating aspect of steel is that it may be strengthened to amazingly high levels by quenching. The strength levels are higher than the strongest commercial alloys of aluminum, copper and titanium by factors of roughly 4.7, 2.2 and 2.1. Steels are generally quenched by immersing the hot metal into liquid coolants, such as water, oil or liquid salts. Increased strengths do not occur unless the hot steel contains the austenite phase. The very rapid cooling prevents the austenite from transforming into the preferred ferrite + cementite structure. A new structure called ***martensite***[*] is formed instead, and this martensite phase is responsible for the very high strength levels.

Martensite As explained in Chapter 1, austenite has a face centered cubic (FCC) crystal structure and ferrite has a body center cubic (BCC) crystal structure. The

[*] Historical Note: The names ferrite, austenite, pearlite, eutectoid, and martensite all were suggested by two men, an American, Henry Marion Howe and a Frenchman, Floris Osmond, in the time period of 1890 - 1903. In the evolution of science the names suggested by researchers often fall by the wayside. An example of this is Howe's suggestion that martensite be called ***hardenite***. It seems unfortunate to this author that Osmond's preference for martensite was eventually adopted, as the term hardenite so aptly describes the outstanding property of the martensite phase.

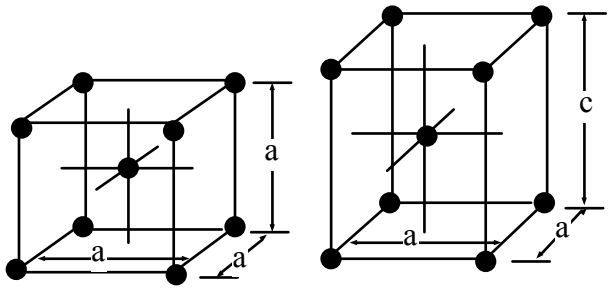

Figure 4.10 Comparison of the crystal structures of ferrite (BCC) and martensite (BCT).

steel phase diagram shows us that the FCC structure will dissolve way more carbon than the BCC structure. At the A_1 temperature the %C that can dissolve in FCC iron is higher than in BCC iron by the ratio of 0.77/0.02 = 38.5. As discussed above, carbon atoms are much smaller than Fe atoms and the dissolved C atoms lie in the interstices (holes) between the larger Fe atoms. The FCC structure dissolves more C atoms because some of the holes in this structure are larger than any of the holes in the BCC structure. The sketch at the right shows γ iron in a 1060 steel (0.6 %C) transforming to α iron as the interface (vertical line) moves to your right. After the interface has moved, say 1 inch, the %C in that 1 inch region must drop from 0.6 % to 0.02 %C. At slow cooling rates the carbon is able to move ahead of the interface into the γ iron along the direction of the dashed arrow by the diffusion process to be discussed in Chapter 7. However, If one forces this transformation to occur very rapidly by quenching, there is not enough time for the C atoms to get themselves rearranged and some or all of them get trapped in the ferrite causing its composition to rise well above 0.02 %, which makes its crystal structure become distorted from the BCC form. The resulting distorted crystal structure is martensite. Fig. 4.10 compares the unit cell of BCC ferrite to that of the distorted unit cell of martensite. What we find is that the unit cell of the martensite crystal is similar to the BCC unit cell in that it has an atom at its center and one atom at each of the 8 corners. However, the unit cell is no longer a cube. One of its edges, called the c axis in Fig. 4.10, is longer than the other two, called the a axes. So the structure is called body centered tetragonal, BCT.

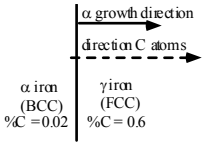

Using x-ray diffraction techniques we can measure the a and c lengths of the unit cell of martensite. As shown in Fig. 4.11 it is found that as the %C dissolved in the martensite increases the c axis becomes proportionately larger than the a axis. The increased carbon content in the martensite is obtained by quenching austenites of higher %C levels. The results of Fig. 4.11 show that as the %C goes up the resulting distortion from the cubic structure (c gets progressively bigger than a) increases due to the trapped carbon in the BCT martensite structure. The strength and hardness of the martensite is found to increase dramatically as the %C increases, as shown by the hardness data of Fig. 4.12. (If you are not familiar with hardness measurements, see p 38). One way to rationalize this increased hardness is to think of the chemical bonds holding the Fe atoms together as springs. As the %C increases the springs will be extended by larger amounts thereby making it more difficult to further extend them, i.e., making the structure harder.

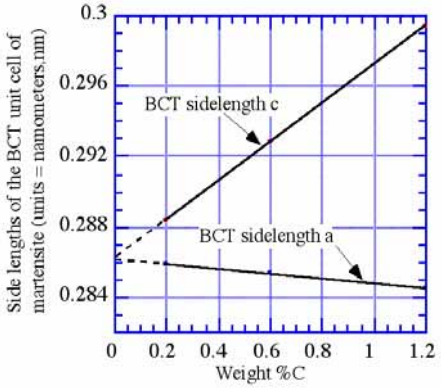

Figure 4.11 The actual a and c sidelengths of the BCT unit cell of martensite. (1 nm = 1000 μm)

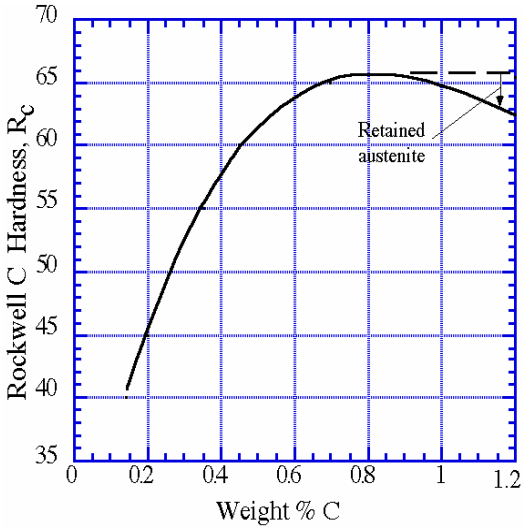

Figure 4.12 Hardness of fresh martensite vs %C.

Two Types of Martensite

The appearance of martensite in the optical microscope changes as the %C changes. It is illustrated schematically on the right of Fig. 4.13 that quenched pure austenite with compositions above or below the eutectoid value of 0.77 %C can produce structures that are all martensite. As shown on the left of this figure, it has become customary to partition the form of martensite into two types, depending on %C. For %C from 0 to 0.6 %C the martensite is called ***lath martensite*** and for %C above 1 %C it is called ***plate martensite***. At the intermediate %C levels from 0.6 to 1.0 % we have a mixture of these two types of martensite. The appearance of martensite in the optical microscope is a bit disappointing. Lath martensite has a somewhat fuzzy and non-distinct appearance as shown in Fig. 4.14(a) for a 1018 steel. In plate martensite it is possible to see the individual plates, but only if the %C becomes larger than around 1 %C, as is illustrated for a 1.4 %C martensite shown on Fig. 4.14(c). The reason you see the plates is because this structure is not 100 % martensite. The white regions surrounding the plates are grains of austenite that did not transform on quenching. It is customary to call these grains, retained austenite. This austenite is soft compared to the martensite and it is due to this austenite that the hardness is found to decrease at compositions above around 0.9 %C on Fig. 4.12. If a plate martensite contains little to no retained austenite, the individual plates do not stand out, see Fig. 4.14(b), although they can be imaged clearly in a type of microscope called a transmission electron microscope. Comparison of Figs. 4.14(a) and (b) illustrates that it is quite difficult (unless you are a steel metallographer) to distinguish between a pure lath martensite and a mixed lath + plate martensite based only on the appearance of the micrographs.

When martensite is removed from the quench bath it is called ***fresh martensite***. The hardness data of Fig. 4.12 refers only to fresh martensite. A big problem with fresh martensite is that if the carbon content is greater than around 0.2 to 0.3 %C it will be very brittle. This brittleness can be removed at the expense of a loss of some hardness if the quenched steel is heated slightly, a process known as ***tempering***. Therefore, quenched steels are almost always tempered to improve the toughness of the steel and the resulting martensite is called ***tempered martensite***. The

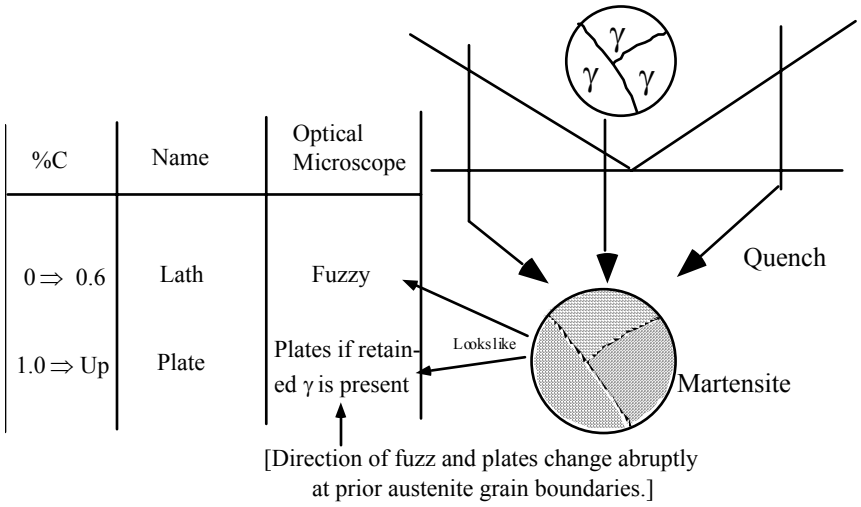

Figure 4.13 Martensite forms on quenching austenite of any %C. But it has a lath appearance or a plate appearance depending on %C level.

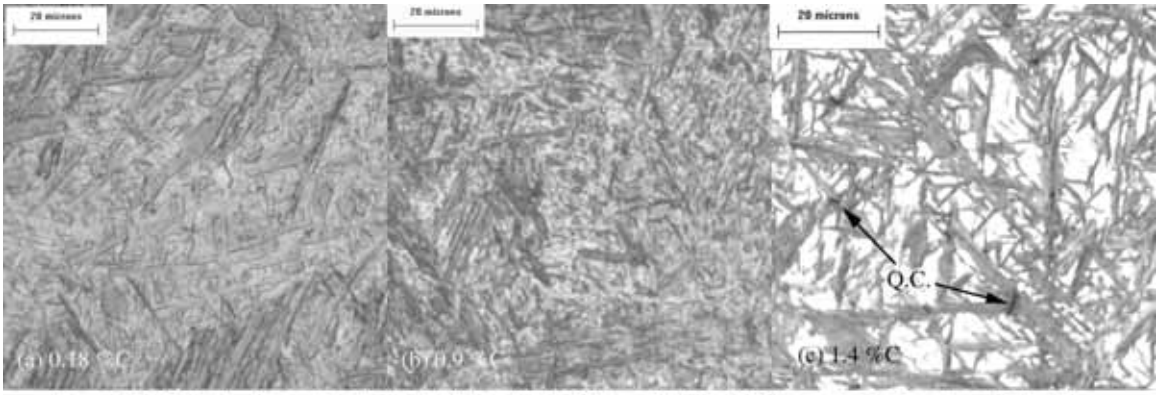

Figure 4.14 Optical micrographs of (a) lath-700x, (c) plate-700x, and (b) mixed-850x martensite structures (nital etch)

increased temperature of tempering allows the carbon atoms trapped in the BCT structure to move a bit. This atom motion does 2 things: (1) It allows the BCT structure to change to the BCC structure, and (2) It allows formation of very small particles of carbides (often having compositions of $Fe_{2.5}C$ and called epsilon carbide), too small to see in the optical microscope. Although too small to see individually, the carbides cause the etching process to roughen the surface so that tempered martensite appears dark in the optical microscope. As illustrated in Fig. 4.1, fresh martensite etches with a fairly smooth surface to give a mostly white appearance in contrast to the dark appearance of a tempered martensite. The tempering temperature needed to darken the martensite is fairly low, on the order of 150 ^{o}C [302 ^{o}F]. The martensites of Fig. 4.14 were lightly tempered.

The M_s and M_f Temperatures

There are two very important temperatures that must be understood when doing heat treatment processing that produces martensite: the ***martensite start temperature***, M_s, and the ***martensite finish temperature,*** M_f. When austenite transforms to another phase on cooling it is found that the new phase virtually always forms first (the books say: nucleates first) on the old austenite grain boundaries. For example, if a 1077 steel is converted to all austenite at 850 ^{o}C [1562 ^{o}F] and then air cooled to 650 ^{o}C [1202 ^{o}F], small grains of pearlite will nucleate on the old austenite grain boundaries shortly after the temperature falls below 727 ^{o}C. When the temperature reaches 650 ^{o}C, these grain will have grown, but there will still be some austenite trapped between them. If one just holds the sample at 650 ^{o}C the pearlite grains will continue to grow until all of the austenite is consumed. Now consider an alternate heat treatment where the sample is quenched from 850 ^{o}C into a hot liquid at 650 ^{o}C. This treatment will cause the temperature to drop much more rapidly down to 650 ^{o}C. The austenite decomposition sequence is the same, small pearlite grains nucleate on the old austenite grain boundaries and grow into the remaining austenite until it is gone. The faster cooling will produce 3 differences: (1) the pearlite grains will grow faster, (2) the Cm spacing of the pearlite will be much finer, and (3) the pearlite grains will be smaller because more of them will nucleate on the old austenite grain boundaries.

Now suppose that the 1077 steel is quenched into a bath at a much lower temperature, say a water bath at room temperature. At such a low quench temperature we expect martensite to form and harden the steel. There are similarities and differences between the formation of martensite at room temperature and pearlite at 650 ^{o}C. Like the

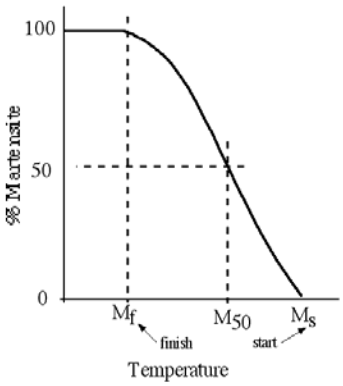

Figure 4.15 ·Quench temperature controls the amount martensite.

pearlite, the martensite will start to form (nucleate) along the old austenite grain boundaries. But, unlike the pearlite the martensite grows into the austenite at tremendously faster rates. Whereas the pearlite grows into the austenite at rates of around 50 microns/second (0.002 inches/s) at 650 ^{o}C, and slower at higher temperatures, the martensite grows at near the speed of sound into austenite, at whatever temperature it forms. Also, unlike the pearlite, which will completely replace the austenite if you simply hold the sample long enough at the reduced temperature, the martensite will not transform all of the austenite unless the quench temperature is below a temperature called the martensite finish temperature, M_f. Furthermore, martensite will not start to form at all unless the quench temperature lies below the martensite start temperature, M_s. If the quench temperature lies between M_s and M_f then only a fraction of the austenite will transform to martensite and the remaining austenite just sits there and is called retained austenite. Fig. 4.15 presents a graph which illustrates these ideas. Notice that an M_{50} temperature is defined as the temperature where 50 % martensite has formed. So, in a steel quenched to the M_{50} temperature, 50 % of the austenite would transform to martensite in a matter of milliseconds after the temperature reaches the M_{50} temperature. But the remaining 50 % of the austenite surrounding the martensite will remain as retained austenite so long as the temperature is not changed.

Notice that the steel phase diagram of Fig. 3.7 predicts that all austenite should disappear when the steel temperature goes below the A_1 temperature. Furthermore, it requires that the phases, α + Cm should be present below the A_1 temperature. But with quenched steels we violate both of these rules, as austenite is present and there is no α or Cm present. This illustrates that the phase diagram correctly maps the phases present at temperature-composition coordinates only if the steel is cooled at slow to moderate rates. At higher cooling rates we can find a new phase, martensite, not predicted by the phase diagram. Such phases are said to be metastable, i.e. not stable. If we heat martensite up, as in the tempering process, it converts to more stable phases. The stable phases are given on the phase diagram, so heating martensite structures up to temperatures below A_1 converts both the martensite and the retained austenite into α + Cm.

Martensite & Retained Austenite

It turns out that the M_s temperature of steels depends very strongly on the %C in the austenite. One may illustrate this fact with two different types of graphs shown as Figs 4.16 and 4.17. In Fig. 4.16 the M_s and M_f temperatures are plotted for increasing %C in plain carbon steels. The M_f temperature is not well established because experiments show a wide scatter in measured values. Notice the horizontal line labeled T(room) on Fig. 4.16. Most quenching is done to room temperature, so this line allows you to estimate what %C values are required to produce retained austenite in quenched plain carbon steels. It is seen that a room temperature quench will begin to lie above the M_f temperature at %C values exceeding around 0.3 to 0.4 %C. It is possible to measure the percent retained austenite in quenched steels fairly accurately using x-ray diffraction

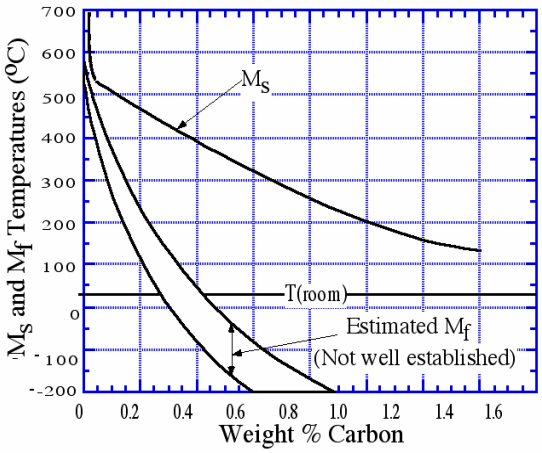

Figure 4.16 The M_S and M_f temperatures both fall rapidly as %C in austenite increases

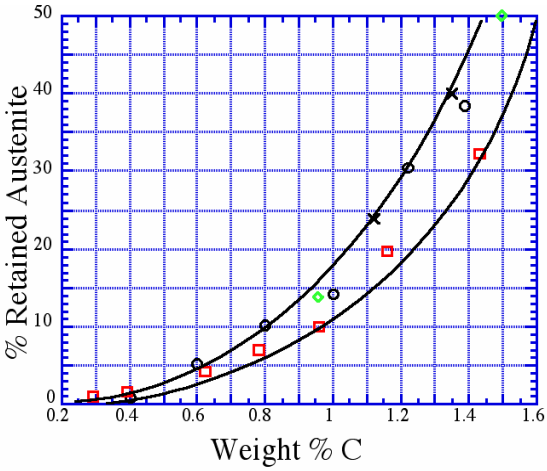

Figure 4.17 The % retained austenite versus carbon content in plain carbon steels quenched to room temp.

techniques. Figure 4.17 shows the results of the measurement of % retained austenite in quenched plain carbon steels as the carbon content increases. Similar to the M_f temperature there is a wide scatter in the data. For example in a 1.4 %C alloy the % retained martensite can be anywhere from 28 to 45 %. This figure can be used to note several things of interest: (1) Fully lath martensite steels (%C less than 0.6%C) will not have significant amounts of retained austenite in them. (2) Fully plate martensite steels (%C greater than 1 %C) will have significant and rapidly increasing amounts of retained austenite in them as %C increases. Notice that our 1077 steel quenched to room temperature is expected to have a mixed lath/plate structure and to have somewhere between 6 to 10 % retained austenite in it. It is generally difficult to see the retained austenite lying between the martensite plates in an optical microscope until the percentage becomes larger than around 10 % or so.

In the above discussion we have assumed that the quenching process would drop the temperature of the austenite down below the M_s temperature so rapidly that no ferrite, or pearlite or cementite would form prior to reaching the M_s. Consider a 1095 steel and note that its composition is fairly close to the pearlite composition. Figure 4.17 predicts that if quenched rapidly enough from the austenite region to room temperature to avoid pearlite formation, this steel will transform into martensite with around 13 % retained austenite. Now suppose that the steel is quenched a bit too slow to avoid formation of pearlite prior to reaching the M_s temperature. In this case it is possible that the austenite may begin to transform to pearlite before any martensite forms. If this happens the pearlite will begin to form along the old austenite grain boundaries, but once the temperature goes below M_s, the surrounding austenite transforms to the martensite + retained austenite in a matter of milliseconds. This rapid formation of martensite traps the first formed pearlite along the old austenite grain boundaries. One then ends up with a structure such as that shown in Fig. 4.18, with the dark pearlite surrounded by the white

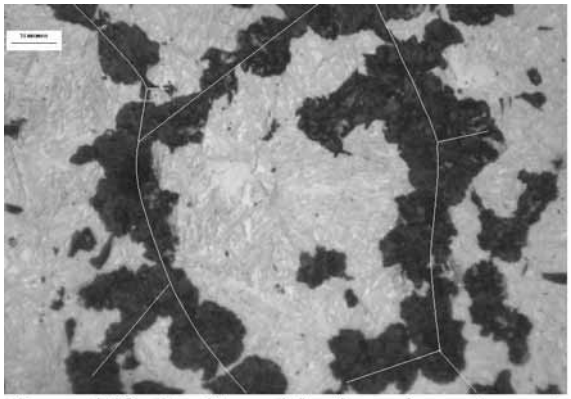

Figure 4.18 Pearlite nodules formed on prior austenite grain boundaries. Slow quenched 1095 steel. (Nital etch, 600x)

martensite+retained austenite. (The sample was not adequately tempered to darken the martensite. So the fresh martensite+retained austenite region appears white.) Thin white lines were superimposed on this micrograph to show the probable location of the prior austenite grain boundaries. Notice that the pearlite grains grow out from the austenite grain boundaries in little round-shaped structures. These are called pearlite nodules, and they are characterized by spherical shaped growth fronts.

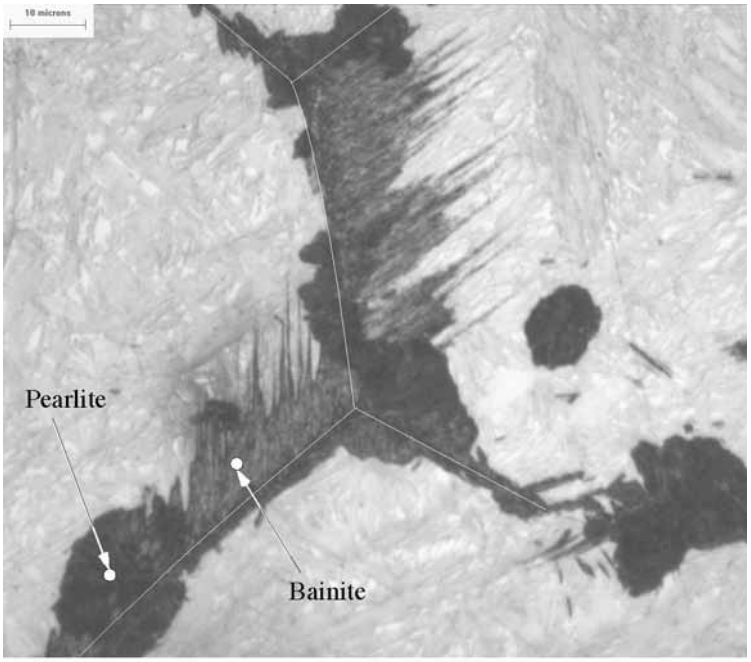

Figure 4.19 Mixed pearlite and bainite structures formed on prior austenite grain boundaries. Faster quenched 1095 steel. (mixed nital-picral etch, 1000x)

Bainite If one cools this steel from the austenite temperature a bit faster, it is possible to observe the formation of a new steel microstructure which is called bainite. Like pearlite, bainite forms from austenite and it also forms first along the old austenite grain boundaries. Consequently at fast cooling rates there will be a competition along the old austenite grain boundaries, with pearlite forming in some places and bainite forming in other places, as illustrated in Fig. 4.19. The bainite is the lighter constituent growing out from the prior austenite grain boundaries. Again, a thin white line was traced out along the old austenite grain boundaries on the micrograph. Similar to pearlite, bainite is a mixture of ferrite + cementite. However, the internal structure of bainite is very different from pearlite. Whereas the Cm is present in pearlite as plates lying between plates of ferrite, in bainite it is present as filaments and/or small particles lying in a ferrite matrix. Another difference in the two structures is illustrated in Fig. 4.19. The growth front of the pearlite is spherical, but that of the bainite appears to be needle like. Remember that Fig. 4.19 is a 2-dimensional cut through the structure. If the bainite growth front were really needle shaped you would only see the needle shape if the cut were to lie parallel to the needle axes, which

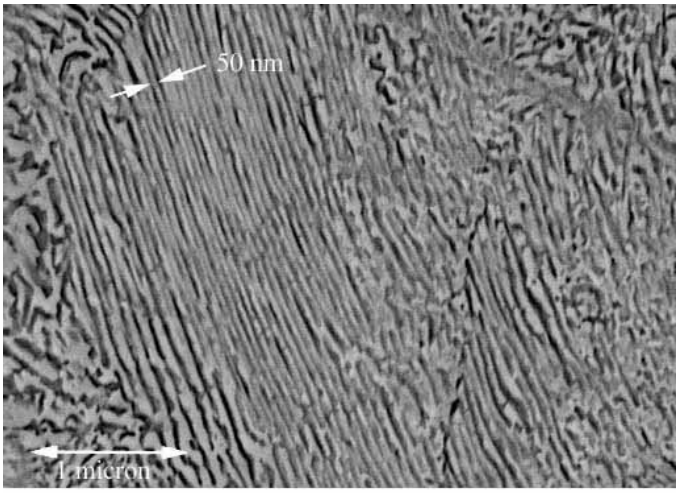

Figure 4.20 SEM micrograph of pearlite at location shown on Fig. 4.19 (21,000x).

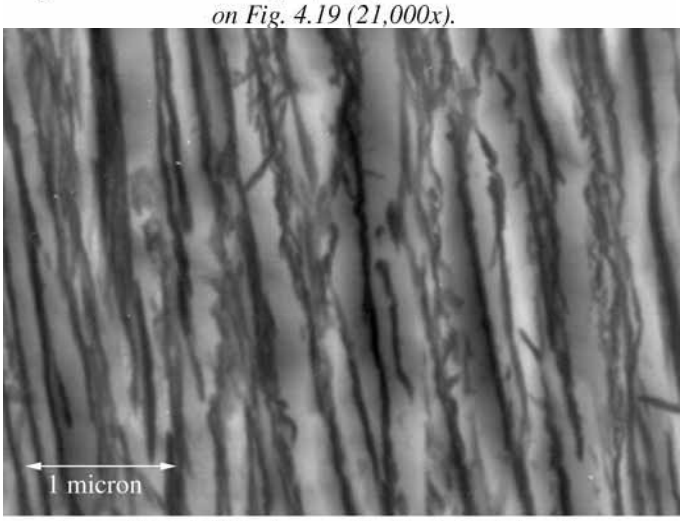

Figure 4.21 SEM micrograph of bainite at location shown on Fig. 4.19. (20,000x)

is unlikely, But if the growth front were plate shaped it would look like needles in the 2-dimensional view for many different orientations of the cut. Hence, the growth front of bainite is plate shaped here, as in most steel bainites.

The optical micrograph of Fig. 4.19 was taken at the highest useful magnification of 1000x. At higher magnifications, obtained by enlargement, one finds no new structural variation apparent because these magnifications are beyond the 0.2 μm (200 nm) resolution limit of the optical microscope. The plate and particle structure of the cementite in the pearlite and bainite regions of Fig. 4.19 are not seen because both features are too small to be resolved in the optical microscope. As mentioned above, the cementite particles are put into relief with the etch and they scatter the light making the image dark in the optical microscope. The pearlite appears darker than the bainite because the light scattering is more effective from the arrays of fine plates than from the small particle of the bainite. There is a type of electron microscope that became available in the late 1960's called a scanning electron microscope, SEM, which produces images of surfaces with resolution much higher, down to sizes of 2 nanometers (nm), where 2 nm = 0.002 μm. Figure 4.20 is an SEM micrograph of the pearlite at the point located on Fig. 4.19 and Fig. 4.21 is an SEM micrograph of the bainite at the point located in Fig. 4.19. In each micrograph the cementite is the dark phase. The difference in the two microstructures is clearly illustrated in these micrographs. As cooling rate is increased the spacing of the cementite plates in pearlite decreases. The plate spacing in Fig. 4.20 is 0.05 μm (50 nm), which is the smallest spacing ever formed by pearlite. As illustrated in Fig. 4.21, the cementite in bainite is generally in the form of ribbon shaped filaments and/or ribbon shaped particles. Both the ribbon axes of the bainite and the plane of the plates of pearlite are aligned close to the direction of growth of these structures.

In the late 1920's Edgar Bain initiated the study of quenched steels by a method called isothermal transformation. Isothermal means constant temperature. This method generally requires the use of thin pieces of steel. One first heats the thin steel to transform it to austenite and then quenches it into a liquid quench bath, usually molten salt, held at the desired isothermal temperature. Because the steel is thin, it will cool to the quench bath temperature throughout its volume before any of the austenite has decomposed. The steel is now held in the molten bath until the austenite is completely transformed, and it is then cooled to room temperature and examined in a microscope. With this method one may map out what structures form from austenite at all the temperature-composition coordinates on the phase diagram lying below the A_1 temperature, and the results are given as Fig. 4.22.

Using this technique Bain and his coworkers discovered that there exists a temperature range below which pearlite will not form, and above which martensite will not form, and in this range they discovered that a new structure forms, which after about 15 years, came to be called bainite. As shown on Fig. 4.22, bainite has two main forms which are termed upper bainite and lower bainite in reference to the temperature range in which they form. The bainite of Fig. 4.21 is upper bainite. The main difference between these two structures is that the carbide particles and filaments are much finer and more

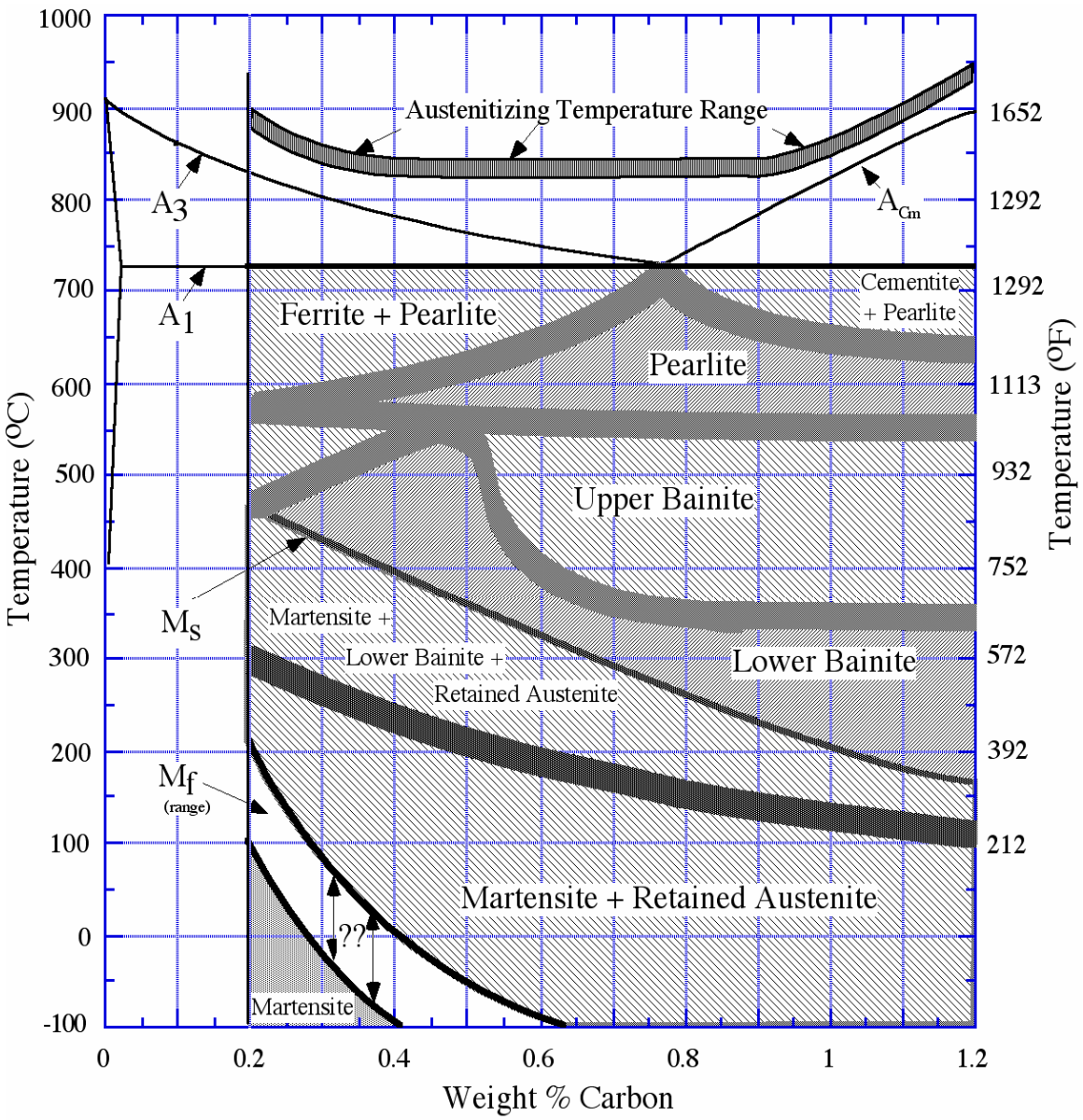

Figure 4.22 Austenite decomposition products for plain carbon steels quenched and held at various temperatures below A_1. (known as: isothemal transformation)

closely spaced in lower bainite. Pearlite never has any retained austenite in its structure. Bainite, however, may have significant amounts of retained austenite, particularly in certain alloy steels. When the element Si is added to steels at levels above the usual impurity level, it is found to have a significant effect on bainite. Silicon is present in higher levels in the spring steel, AISI 9260, and in all cast irons. It causes the bainites in

these metals to contain significant amounts of retained austenite, reduced amounts of carbides, and it changes the type of carbide in the lower bainite from Fe_3C (cementite) to $Fe_{2.5}C$ (epsilon carbide). Epsilon carbide does not appear on the Fe-C equilibrium phase diagram because it is not a stable phase. It is called a metastable phase and can only be formed in quenched steels. We will encounter it again in tempering.

Figure 4.22 can be used to illustrate an important aspect of pearlitic steels that is often not well understood. Just because a microstructure has the pearlite form does not

mean that the composition of the steel has the pearlite composition of 0.77 %C. Consider a 1095 steel. The diagram shows that if this steel is quenched into the temperature range of around 550 to 650 ^{o}C and held until all austenite has decomposed, it will become a 100% pearlitic structure. The difference between the structure of this steel and a 1077 pearlite is that the cementite plates of the 1095 pearlitic steel are slightly fatter than those of the 1077 pearlite. Similarly one can make a 1060 steel have a fully pearlitic structure by quenching to the 550 to 650 ^{o}C range, and here the difference is that the cementite plates are thinner than in the 1077 pearlite. In both cases the change in the plate widths are too small to be observed in the optical microscope and even in the scanning electron microscope.

Figure 4.22 does not tell us what structures will form on continuous cooling. Continuous cooling means the sample is cooled from the austenite temperature, not by quenching, but removal from the furnace and cooled at slower rates, such as air cooling, or simply a slow quench, such as perhaps oil quenching. Air cooling is often called ***normalizing***. As the name implies, continuous cooling means that the steel temperature falls in a continuous manner rather than abruptly plummeting, as happens in quenching. Experiments show that on fast air cooling a 1095 steel will end up being fully pearlitic, but a 1060 steel will not. The 1060 steel will have ferrite in the prior austenite grain boundaries surrounded by pearlite, similar to that of Fig. 4.6. As cooling rates are increased above that of fast air cooling, bainite will begin to appear and a great variety of microstructures are possible involving mixtures of ferrite, pearlite, bainite and eventually martensite.

Spheroidized Microstructures The cementite phase present in most steels is in the form of the fine plates of pearlite for hypoeutectoid steels and in this form plus thicker plates and globules formed on austenite grain boundaries in hypereutectoid steels. These cementite shapes result because they are the forms that cementite assumes when austenite transforms to pearlite at the A_{r1} temperature and when it nucleates on austenite grain boundaries in hypereutectoid steels at the A_{rcm} temperature. It is possible however to heat treat steels and change the shape of the cementite into a spherical form, sometimes called spheroidite. Cementite is very hard but very brittle, and by changing its form to isolated spheres in a matrix of, say, ferrite or tempered martensite, the mechanical properties of the steel comes closer to matching that of the matrix phase: soft and machinable with a ferrite matrix or strong and less brittle with a martensite matrix.

There are two heat treating processes that are effective for producing a spheroidized cementite structure. In the first process the steel is simply heated into the fully austenite region and then quenched to martensite. For both hypo and hyper eutectoid compositions the steel is then heated to a temperature just below the A_1 temperature for an hour or so and on cooling one has a microstructure of fine spheres of cementite in a ferrite matrix. The room temperature martensite is not a stable phase (it does not appear on the phase diagram) and at the elevated temperatures it decomposes into fine carbides (cementite) in a ferrite matrix. For hypereutectoid steels one can produce spheres of cementite in a martensite or bainite matrix by heating the quenched steel to temperatures between A_1 and A_{cm} for an hour or so where the martensite will decompose

into fine carbides in an austenite matrix. The martensite or bainite matrix is then formed from the austenite by quenching at the appropriate rate. The volume fraction of spherical cementite in the steel depends on the temperature of the one hour hold, going from a maximum amount for temperatures just above A_1 to near zero for temperatures just below A_{cm}.

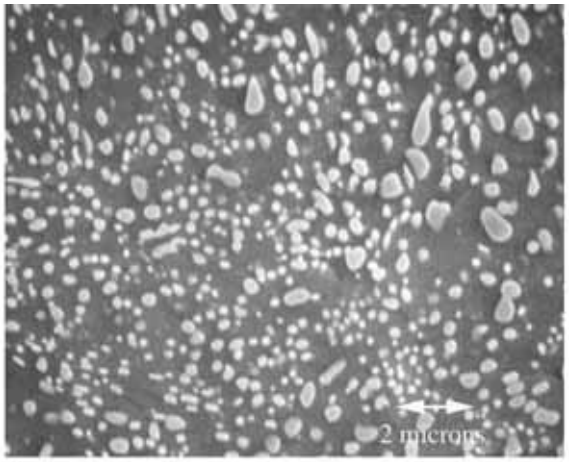

Figure 4.23 SEM micrograph (6000x) of a 52100 steel showing fine spherical Cm in a ferrite matrix.

The second method is most effective with hypereutectoid steels. It requires no quenching and is therefore used in industry to produce the spheroidized structures of cementite + ferrite in which these steels are supplied from the steel mill. In this method a trick is used which prevents pearlite from forming on cooling austenite below the A_1 temperature. The trick is to produce small particle of cementite in the austenite and then cool it below A_1 at a slow rate (usually a bit slower than air cooling). This treatment causes the austenite to transform directly into a spheroidized cementite+ferrite structure rather than into the plate shaped pearlite structure. (The transformation is sometimes called the divorced eutectoid transformation, DET.) Small particles of cementite are naturally formed in the austenite of a hypereutectoid steel when it is heated above A_1 and below A_{cm}. Experiments show that such is the case so long as the starting steel does not contain large particles of cementite (for example, if it consists of pearlite, bainite, martensite, or is already spheroidized as ferrite + cementite). In addition, the steel cannot be heated above around 800-840 ^{o}C [1472-1544 ^{o}F] during austenitization to have the DET dominate the pearlite transformation. The method will work with hypoeutectoid steels also, but requires more control. The reason is that when a hypoeutectoid steel is heated above A_1 the cementite plates of its pearlite are transformed completely into austenite after a time which becomes progressively shorter as the temperature is raised. Since the method requires particles of cementite to be present in the cooling austenite, hypoeutectoid steels cannot be held very long above the A_1 temperature before cooling. An effective way to achieve spheroidization with hypoeutectoid steels is to cycle the steel around 50 ^{o}C [90 ^{o}F] above and below A_1 a few times.

Figure 4.23 presents an example of a 52100 bearing steel produced by method 2 above. The steel was originally in a pearlitic condition with no cementite other than in the pearlite. It was then held at 795 ^{o}C [1463 ^{o}F] for 30 minutes and furnace cooled at 370 ^{o}C/h [666 ^{o}F/h] to 680 ^{o}C [1256 ^{o}F], where the DET had been completed, and then air cooled to room temperature. On cooling to 680 ^{o}C the pearlite transformation was completely replaced by the divorced eutectoid reaction producing the completely spheroidized structure of very fine cementite particles in a ferrite matrix.

Examples of spheroidized steels include most hypereutectoid steels, such as bearing steels and tool steels which are supplied from the mill with a spheroidized structure of cementite in a ferrite matrix to facilitate machining. Also, bearing steels and tool steels are often used in practice for applications in which the hard cementite particles

enhance wear resistance. Often these steels are heat treated to produce a spheroidized cementite structure in a matrix controlled by the final cooling, which might consist of fine pearlite, bainite or tempered martensite.

Summary of Ideas of Chapter 4

1 Mechanical properties of steels are strongly influenced by their microstructure. Microstructure is the distribution of the grains in the steel and its description includes such things as size, shape and identification of the phases present. Microstructure is determined mainly with the optical microscope by examination of polished and etched surfaces. All of the important microconstituents of steel (the phases: ferrite, austenite, cementite and fresh martensite, plus the phase mixtures: pearlite, bainite and tempered martensite) have characteristic appearances on a polished and etched surface, which allows evaluation of microstructure in the optical microscope.

2 The room temperature microstructure of slow cooled (non quenched) steels depends strongly on the carbon content of the steel. Eutectoid steels (0.77 %C) will usually be all pearlite, Fig. 4.3. Hypoeutectoid steels (%C less than 0.77) will often be arrays of pearlite grains with ferrite in their boundaries, Fig. 4.6. Hypereutectoid steels (%C greater 0.77) will often be arrays of pearlite grains with cementite in their boundaries, Fig. 4.8. At the low end of the hypoeutectoid steels (%C less than around 0.2%) ferrite grains become the dominant component with the pearlite distributed in various forms. Wrought steels often show a banded microstructure with alternating bands of ferrite grains and pearlite grains aligned in the direction of the prior mechanical flow, Fig. 4.9,

3 The cementite in slow cooled steels is generally contained as thin plates in the pearlite component. However it is possible to change the pearlitic cementite into arrays of small isolated spheres in a matrix of ferrite grains using special heat treatments described on pages 32-33. Such structures are referred to as spheroidized steels, Fig. 4.23, and are often the form in which high carbon steels are delivered from the mill because they are much easier to machine than when the cementite is in the pearlitic form.

4 When austenite is rapidly cooled by quenching two additional microstructures may appear, martensite and bainite.

5 Martensite is a non-equilibrium phase (it does not appear on the phase diagram). Martensite wants to be body centered cubic ferrite, but the C in the austenite distorts the crystal structure to bct (body centered tetragonal). The more C in the austenite the more the distortion and the harder (stronger) is the martensite, Fig. 4.12.

6 Martensite has two appearances in the optical microscope, lath and plate. Lath forms at %C from 0 to 0.6 %C and plate at 1%C and above, with a mixed structure in-between, Fig. 4.14.

7 The martensite formed in the quench bath is called fresh martensite. If %C is greater than around 0.3 %C it will be too brittle for most uses. Therefore most martensites are

tempered by heating to low temperatures. The tempering causes very small carbides to form in the martensite which reduces strength but enhances ductility. It also makes tempered martensite etch dark in the optical microscope.

8 To form martensite one must quench austenite to temperatures below the M_s temperature. As the quench temperature drops below M_s, progressively more martensite forms until the M_f temperature is reached where 100 % martensite forms. Between M_s and M_f a structure of martensite plus retained austenite is found, Figs. 4.15 and 4.14(c).

9 Both M_s and M_f drop as %C is increased and samples quenched to room temperature can contain appreciable amounts of retained austenite in higher C steels. The data of Figs. 4.16 and 4.17 show that significant amounts of retained austenite begin to form in plain carbon steels quenched to room temperature for carbon contents above around 0.4 %C.

10 At quench rates a bit slower than that required to form martensite a microstructure called bainite forms. Bainite is similar to pearlite in that it consists of ferrite plus carbides. The carbide component consists of aligned filaments or particles as opposed to the aligned plates in pearlite.

11 Bainite occurs in two forms, upper bainite and lower bainite depending on the temperature where it forms. The carbides are finer in lower bainite and it can obtain strengths approaching martensite with toughness often better than tempered martensite having the same hardness.

12 A unique property of martensite is that it forms much more rapidly than any of the other austenite products, ferrite, cementite, pearlite or bainite. Martensite grows at about half the speed of sound, so that once the austenite temperature gets below M_s, martensite forms in milliseconds.

13 When a steel is cooled from the austenite region the phase diagram tells us which austenite products want to form first: ferrite in hypoeutectoid steels, pearlite in eutectoid steels, and cementite in hypereutectoid steels. Experience shows us that these products form first on austenite grain boundaries. To form 100 % martensite a steel must be quenched so fast that these products do not form on the austenite grain boundaries. If one of these products does form on the austenite grain boundaries before the austenite reaches the M_s temperature, it will be trapped there by the martensite which forms in only milliseconds, and one finds structures like those of Figs 4.18 and 4.19.

13 If steels are quenched to a constant temperature in a salt bath so fast that the austenite has not yet decomposed, then the austenite will transform isothermally, at one temperature. Such isothermal transformation of steels has been studied extensively and it is found that the austenite product or products which form depends on the quench temperature and the %C in the steel, see Fig. 4.22.

5 Mechanical Properties

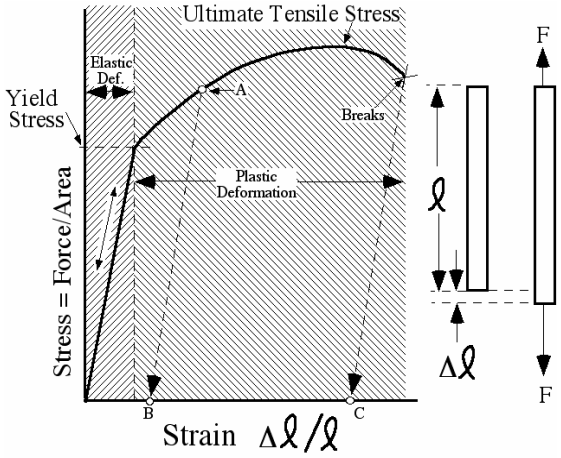

Figure 5.1 The stress-strain diagram.

The Tensile Test Consider the following simple experiment that many people may have actually performed when playing with springs. Take a small spring and pull it apart a fair amount and then release it. The spring will "spring back" into its original length. Now repeat the experiment except this time you pull on the spring an excessive amount. As the spring becomes overextended relative to its design, you can feel that the increasing force needed to continue extending the spring suddenly drops, the spring sort of "gives". And, when you release the spring you find that it does not collapse to its original length. Its rest length is now longer and you have probably ruined the spring, at least for its intended purpose.

Long ago engineers developed a test to evaluate the strength of metals that is related to this simple experiment. A length of the metal, usually a round cylindrical rod, is pulled apart in a machine that applies a known force, F. The machine has grips attached to the ends of the cylindrical metal rod and the force is applied parallel to the axis of the rod as shown schematically at the right of Fig. 5.1. As the force increases the rod gets longer and the change in length is represented as $\Delta\ell$ where the symbol Δ means "a change in" and the ℓ refers to the original length of the rod. Suppose you apply a force of 100 pounds to two rods of the same material, but one being thin and the other thick. The thin rod will elongate more. To make their measurements independent of rod diameter engineers define a term called ***stress***, which is simply the force divided by the area of the rod. When one applies the same stress to the thin and thick rods they elongate the same amount, because the actual force applied to the thick rod is now larger than that applied to the tin rod by an amount proportional to its larger area. Since stress is force per area it can have units of pounds per square inch, or psi.

When a metal is pulled along its axis the applied force is called a tensile force and the machine that applies the force is called a tensile test machine. Figure 5.1 presents a typical result obtained from a tensile test of a metal. The applied stress is plotted on the vertical axis. The change in length is plotted on the horizontal axis, but it is customary to plot the fractional change in length, as shown on Fig. 5.1. The fractional change in length $\Delta\ell/\ell$ is called the ***strain***, and the diagram of Fig. 5.1 is often called a stress-strain diagram.

The stress-strain diagram can be divided into regions as shown in Fig. 5.1, the ***elastic*** region, and the ***plastic*** region. As the stress on the metal rod increases the rod elongates, and just like the spring, as long as the stress is not too high, release of the stress returns the rod to its original length. This is called elastic deformation. However, if the applied stress reaches a critical level, called the ***yield stress***, YS, the metal "gives", just like in the spring experiment and now two things happen, (1) the increase in stress needed to produce a given small increase in strain becomes lower, and (2) upon release of

the stress the metal is found to have a permanent elongation, as shown by the arrowed line, A-B, of Fig. 5.1. In this case the rod was stressed to point A and after releasing the stress the rod had elongated from its original length by a percent given as B x 100. As shown on the figure, the increase in stress needed to continue elongating the rod reaches a maximum value in the plastic region and then drops a bit before the stress is able to break the rod in two. This maximum value is usually called the ***ultimate tensile strength***, UTS, or often just the tensile strength.

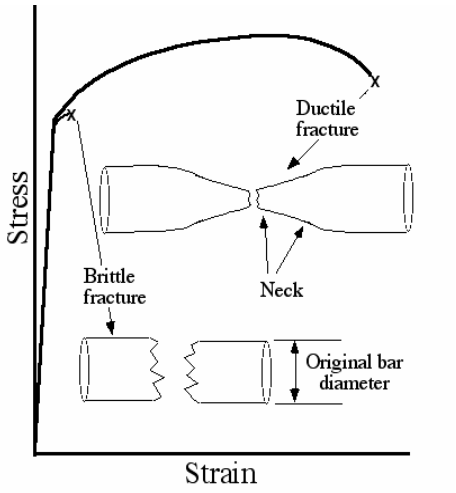

Figure 5.2 A brittle vs. ductile metal.

The stress-strain diagram also provides an additional measure of the mechanical properties of a metal, its ***ductility***. The amount of elongation that occurs after the stress increases beyond the yield stress and before the sample breaks is a measure of the ductility of the metal. This elongation is sometimes called permanent elongation because it remains in the sample after breakage and can be measured easily. The permanent elongation in the sample of Fig. 5.1 after the elastic strain is relaxed is given by point C. By simply multiplying the strain at C by 100 one obtains the ***% elongation*** of the metal. Figure 5.2 presents possible stress-strain diagrams for a ductile metal and a brittle metal. One sees that the breakage strain is much larger for the ductile metal and hence its % elongation is much larger. The figure also shows that the diameter of the bar at the fracture surface of a brittle failure remains close to its original value, while that of the ductile failure is reduced to smaller values. This reduction in diameter by plastic flow near the fracture surface is referred to as "necking" and one can observe it develop in ductile metals just before fracture. (In addition to % elongation, ductility is often characterized by percent reduction in area, which is simply the percent by which the original cross sectional area of the bar is reduced at the fractured neck.)The concept of ductile versus brittle behavior is fairly obvious. Put a metal rod in a vice and beat on the exposed end with a hammer. A brittle metal will break almost immediately, whereas a ductile metal can be bent severely by the hammer blows and may not break after bending 90 degrees or more.

When a bladesmith shapes a knife blade by forging, each blow of the forging hammer causes some permanent deformation of the metal. Hence, on each blow the stress produced in the metal is exceeding the yield stress. As anyone who has hand hammered a metal or bent a metal rod back-and-forth probably realizes, after the metal has been deformed a bit it becomes more difficult to deform. This effect is often called work hardening. It may be understood from the stress strain diagrams sketched in Fig. 5.3. The stress-strain diagram for the original metal is shown dashed. An original rod is now deformed to A and then the stress is released bringing it to point B. If this bar is now retested one finds that its Y.S. has increased from the original value up to the point A as shown on the diagram. This increase in yield strength is a measure of the work hardening resulting from the original defomation (work) put into the metal on the first deformation. Notice that although the metal is now stronger in the sense that it has to be stressed more before it will undergo

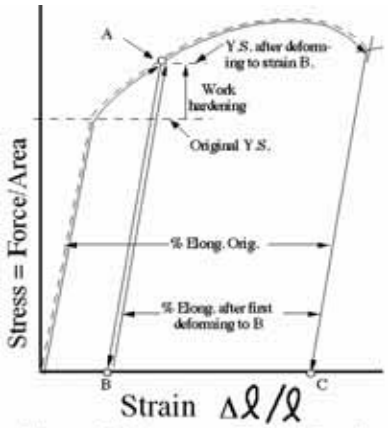

Figure 5.3 Increase of Y.S. after plastic deformation (work hardening).

Table 5.1 Mechanical properties of some steels.

Steel	Treatment	Yield Stress	Tensile Stress	Elonga-tion, %
1020	Normalized (air cooled)	50 ksi	64 ksi	36
1040		54	86	28
1095		73	147	9.5
1020	As -rolled	48	65	35
1040		60	90	25
1095		83	140	9

plastic deformation, its UTS is not changed significantly, and it is less ductile, i.e., its % elongation to failure has gone down. It is a general characteristic of metals that operations that increase their yield strength will decrease their ductility. People who have worked metals know this, as heavily work hardened metals often break easily. A familiar example of this behavior is the commonly used method of breaking a wire by bending it back and forth lots of times.

The mechanical properties of metals are often characterized by listing values of their yield strength, tensile strength and % elongation. The data of Table 5.1 illustrate such a characterization for some plain carbon steels. The units of stress in the table are ksi. The symbol k for kilo means 1000 times, so 1 ksi = 1000 psi or 1000 pounds per square inch. Therefore, 50 ksi is the same as 50,000 psi.

Note: Industry in the USA continues to be a holdout in the use of ksi or psi for the units of stress. The rest of the world has now pretty uniformly adopted an International System of units, called SI units. In this system stress is given in units of megapascals, MPa. One pascal is a stress of one newton per square meter, and a megapascal is a million pascals. The key to converting ksi to MPa is the number 7. Simply multiply stress in ksi by 7 and you obtain an excellent approximation of the stress in MPa, e.g., 50 ksi ≈ 350 MPa. (The correct multiplier is 6.895, so 50 ksi = 345 MPa).

The data on the normalized (air cooled) steels illustrates two general characteristics of steels. (1) Increasing the %C in steel increases both Y.S. and T.S. (2) Increasing %C drops the ductility, the % elongation. Comparing the as-rolled properties to the normalized properties illustrates the effects of work hardening: Yield strength goes up at higher C levels, tensile strength is changed only slightly, and % elongation drops a bit.

The Hardness Test A problem with the tensile test is that one must use a dedicated piece of metal which is then destroyed by the test. Another test that characterizes the strength of a metal, but does not destroy the metal part under test, is the hardness test. The hardness test is widely used because it is quick and it can be applied to parts which can then be placed into service. Over the years several different and useful hardness tests have evolved and the essential features of these tests may be explained by reference to Fig. 5.4. A hard material, often called the indenter, is forced into the metal surface with a fixed load (weight). The metal region located under the indenter point is deformed to strains well into the plastic region of Fig. 5.1, so that permanent deformation is generated. Therefore, after the test a crater (called an indent on Fig. 5.4) is left in the metal surface. The hardness is then defined by some number that is proportional to the size of the indent. In some techniques the size of the indent is measured from its diameter and in others it is measured from the depth of the indent.

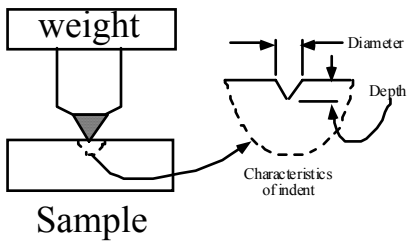

Figure 5.4 Schematic outline of essential features of hardness testing

Table 5.2 presents a comparison of various indentation hardness tests that are used for measuring the

Table 5.2 Comparison of Indentation Hardness Tests

Hardness Test	Weight*	Indenter	Measure	Use
Rockwell C	150 kg	120° diamond cone	Depth	med. to high hardness
Rockwell A	60 kg	120° diamond cone	Depth	hardened surfaces
Rockwell B	100 kg	1/16 in. ball	Depth	soft
Brinell	500 to 3000 kg	Large ball, 10 mm	Diameter	soft to med. hardness
Microhardness	1 g to 1 kg	136° diamond pyramid, DPH, or Knoop	Diagonal length	micro constituents
Vickers	10 to 120 kg	136° diamond pyramid	ditto	soft to high hardness

* g = 1 gram, kg = kilogram = 1000 gram

hardness of steels and other metals. The Rockwell hardness tester is probably the most widely used test in the USA. The table shows the 3 most common scales for the Rockwell test. The C and A scales both use a conical diamond indenter, with the only difference being that the A scale uses a lighter load. These testers provide a very quick and easy measurement with the machine measuring the depth of penetration automatically and providing the hardness value either on a dial or, on newer machines, as a digital readout. The smaller load for the A scale reduces the penetration depth and is often used to measure hardness on steel surfaces that have been case hardened, i.e., a thin hard layer has been produced only on the surface. The reported hardness values are referred to variously as R_C, or HRC, and similarly R_A or HRA. The indenter for the B scale is a 1/16 hardened ball and this scale is sometimes used for soft steels.

A more reliable hardness test for soft to medium hard steels is the Brinell test. It uses a larger ball, either hardened steel or tungsten carbide, and measures the diameter of the indent. This test is a 2-step test in that first the indent must be made and then the indent diameter measured optically. The size of the indent should run between 3 to 6 mm (0.12 to 0.24 in.) The Brinell hardness number (referred to variously as HB or BHN) is then determined either from a table or using an equation on a calculator. An advantage of the

Table 5.3 Approximate equivalent hardness numbers for several hardness tests on steels (a).

HRC	HV	HB(b)	HRA	UTS(ksi)
68	940	-	85.6	-
67	900		85	-
66	865	-	84.5	-
65	832	(739)	83.9	-
64	800	(722)	83.4	-
63	772	(705)	82.8	-
62	746	(688)	82.3	-
61	720	(670)	81.8	-
60	697	(654)	81.2	-
59	674	(634)	80.7	-
58	653	615	80.1	-
57	633	595	79.6	-
56	613	577	79.0	-
55	595	570	78.5	301
54	577	543	78.0	292
53	560	525	77.4	283
52	544	512	76.8	273
51	528	496	76.3	264
50	513	481	75.9	255
49	498	469	75.2	246
48	484	455	74.7	237
47	471	443	74.1	229
46	458	432	73.6	222
45	446	421	73.1	215
44	434	409	72.5	208
43	423	400	72.0	201
42	412	390	71.5	194
41	402	381	70.9	188
40	392	371	70.4	181
39	382	362	69.9	176
38	372	353	69.4	171
37	363	344	68.9	168

HRC	HV	HB(b)	HRA	HRB	UTS(ksi)
36	354	336	68.4	(109.0)	162
35	345	327	67.9	(108.5)	157
34	336	319	67.4	(108.0)	153
33	327	311	66.8	(107.5)	149
32	318	301	66.3	(107.0)	145
31	310	294	65.8	(106.0)	142
30	302	286	65.3	(105.5)	138
29	294	279	64.7	(104.5)`	135
28	286	271	64.3	(104.0)	132
27	279	264	63.8	(103.0)	128
26	272	258	63.3	(102.5)	125
25	266	253	62.8	(101.5)	122
24	260	247	62.5	(101.0)	120
23	254	243	62.0	100.0	117
22	248	237	61.5	99.0	114
21	243	231	61.0	98.5	112
20	238	226	60.5	97.8	110
(18)	230	219	-	97.8	106
(16)	222	212	-	95.5	102
(14)	213	203	-	93.9	98
(12)	204	194	-	92.3	94
(10)	196	187	-	90.7	90
(8)	188	179	-	89.5	87
(6)	180	171	-	85.5	84
(4)	173	165	-	85.5	80
(2)	166	158	-	83.5	77
(0)	160	152	-	81.7	75

(a) For carbon and alloy steels in the annealed, normalized and quenched and tempered condition and for austenitic steels. Values in parenthesis are beyond the normal range.
(b) 3000 kg load and tungsten carbide ball.

Brinell test is that it measures hardness over a much larger area than the Rockwell test which produces excellent averaging for materials with coarse microstructures, like cast irons. But this is also a disadvantage for application where the test piece must be small, such as the tooth on a gear. Another disadvantage is the test is not useful at the higher hardness ranges of steels. See references [5.1,5.2] for further discussion of hardness testing.

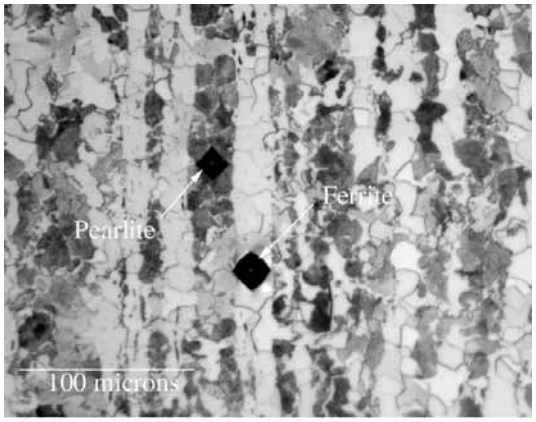

Figure 5.5 Diamond pyramid hardness indentations in ferrite and pearlite of banded 1045 steel. (230x)

Table 5.3 presents information form the American Society for Testing Materials listing HRC values measured on steel and the corresponding equivalent hardnesses of various other tests for steel. One needs to remember that these equivalent hardnesses apply to steels only, i.e., do not use them for aluminum and copper alloys.

There is another test, developed in England and generally used there in preference to the Rockwell test, which is called the Vickers hardness test. This test is similar to the Brinell test in that it is a 2-step test measuring the diameter of the indent, but with a diamond indenter shaped in the form of a pyramid. The pyramid geometry produces an indent having a square shape and the size is measured by the length of the diagonals of the square indent. The average diagonal length and the load used are plugged into a formula that calculates the Vickers hardness number, HV, also called the diamond pyramid hardness number, DPH. In Table 5.3, the range of hardnesses where the various tests are not applicable are shown either with blanks or using parenthesis. Notice that the Vickers test is the only one that applies at all hardness levels.

As shown in the second row from the bottom of Table 5.2, there is a microhardness test available. The test utilizes very light loads and makes indent diameters small enough to fit into micro-sized regions. It utilizes a microscope which allows one to position the indent at desired locations on a microstructure and then measure the size of the indent with the same microscope. There are two different indenters utilized in microhardness testers, the diamond pyramid indenter of the Vickers test and a special shaped indenter called a Knoop indenter. Figure 5.5 illustrates the use of the DPH test on a ferrite-pearlite banded 1045 steel. Indents have been placed in a ferrite band and in a pearlite band. Notice that the indent is smaller in the pearlite band telling us that the pearlite is harder than the ferrite. The weight used in this test had to be adjusted all the way down to 50 g to keep the indent small enough to fit inside the bands. Experiments have shown [2] that for steels the test results are independent of the weight for values down to just under 50 g. The test uses the same equation as the Vickers test to calculate hardness, HV, and the values

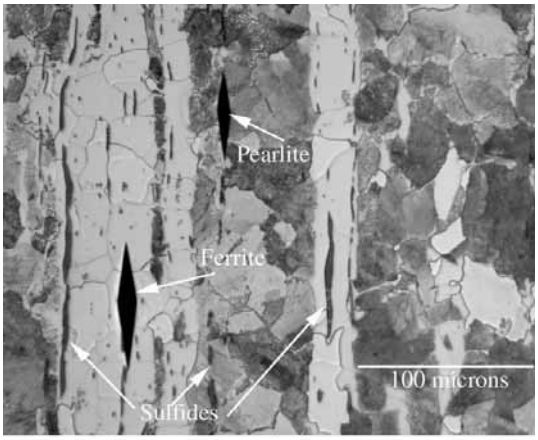

Figure 5.6 Knoop indentations in ferrite and pearlite of banded 1144 steel. (230x)

found here were HV = 260 in pearlite and 211 in ferrite. From Table 5.3 these correspond to HRC values of 24 in pearlite and 13.6 in ferrite.

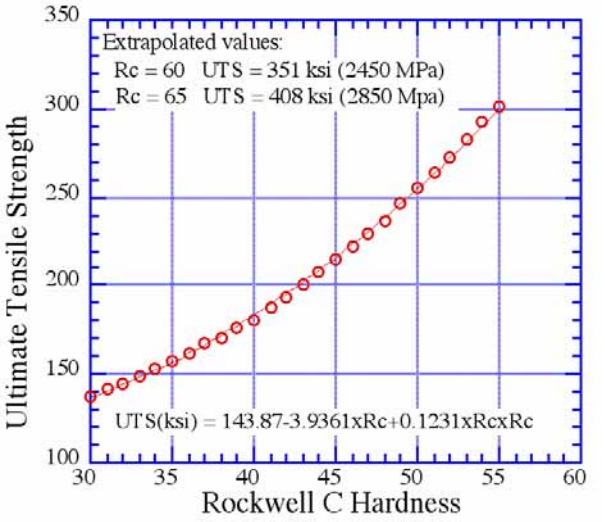

Figure 5.7 A plot of data of Table 4.3 showing the UTS of Q & T steels versus values of HRC.

Figure 5.6 presents results from a similar test on a ferrite-pearlite banded 1144 steel using the Knoop indenter. (Like a 1044 steel, 1144 contains 0.44%C, but it also contains elevated S levels, and as a result contains significant amounts of sulfides, as shown in the figure. The sulfides are ductile at the hot working temperature and become elongated during hot working. The sulfides make the steel machine more easily.) Notice that the Knoop indenter is quite oblong in shape. This allows one to fit it into thin layers more easily than a Vickers indent. Therefore it is particularly useful for microstructures in the shape of thin layers. It characterizes hardness with its own set of Knoop hardness numbers, which can be related to HRC values in tables similar to Table 5.3. (see reference [5.1])

It turns out that the indentation hardness numbers are found to correlate well with the UTS of steels that have been quenched and tempered. These data are given by the right hand column of Table 5.3 and they are plotted in Fig. 5.7. The correlation becomes less reliable at HRC values above 55, but the figure shows the UTS values that are obtained by extrapolating the curve to HRC values of 60 and 65. The results show that when one hardens a steel into the range of HRC = 60 to 65, the corresponding tensile strengths are extremely high. For comparison, the highest tensile strengths of commercial aluminum, copper and titanium alloys are approximately, 83 ksi, 177 ksi and 190 ksi, respectively. The highest of these strengths is exceeded by steels hardened to an HRC value of only around 43.

The previous chapter discussed the various microstructures that occur in steel. Table 5.4 presents estimates of the maximum hardness for the various microstructures. Notice that both ferrite and austenite are fairly soft. The hardness of pearlite is controlled by its spacing and the value of 41-43 given in Table 5.4 are for pearlite with the finest spacing that can be obtained on cooling, which was illustrated in Fig. 4.20. Finer spacing can be obtained in pearlitic steels by mechanically deforming this fine pearlite to thin wire form and winding into cable. Such pearlitic steel cable is used in wire rope which has tensile strengths to 320 ksi (2206 MPa). Quenched and tempered steel wire can easily be made to this strength level, but experience has found the pearlitic wire is tougher and for that reason it is the wire of choice for such industrial applications as bridges and crane cables. Lower bainite has hardnesses approaching that of martensite and also finds industrial uses because of slightly superior toughness to that of Q & T steels. Martensite has the highest strength and hardness of all, and as shown in Fig. 4.12, the hardness of fresh martensite depends on the %C in the steel. Fresh martensite is rarely used industrially because of its lack of toughness. It is tempered (heated to modest temperatures) which

Table 5.4 Hardness of various steel microstructures

Steel Microstructure	Maximum HRC values
Ferrite	10-15
Austenite	10-15
Pearlite	40-43
Upper Bainite	40-45
Lower Bainite	58-60
Martensite	65-66

lowers its strength but increases its toughness. Measurement of hardness is a major method of control of the tempering process.

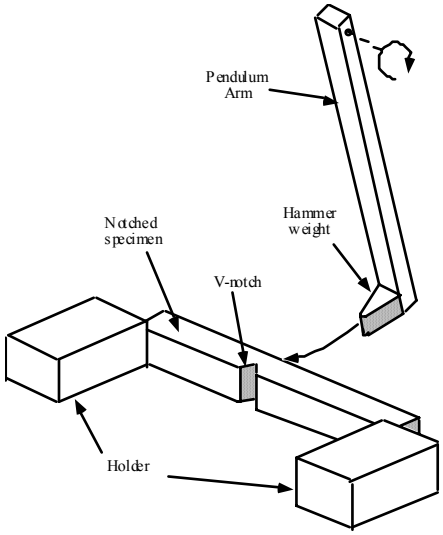

Figure 5.8 The Charpy Impact Test

The Notched Impact Test During the second world war the desire for higher production rates of ships led to construction utilizing welded steel plate, rather than the standard riveted construction. The ships were called "liberty ships" and brittle failure in the welded plates of these ships produced spectacular failures where the entire ship would break in half with catastrophic results. Cracks would begin at local points in the weld regions and propagate clear around the ship, passing from plate-to-plate causing failure by a brittle mode, i.e., little to no plastic flow. This brittle behavior was not detected by a sudden loss in ductility in the simple tensile test. Hence, these disasters led to a wide appreciation of the fact that ductility as measured by the tensile test was not a good measure of susceptibility to brittle behavior in complex steel parts.

Ferritic steel, as well as other BCC metals, suffer from the fact that at low enough temperatures they will break in a brittle fashion. What this means in terms of the ideas of the tensile test presented above, is that the % elongation to failure is close to zero. As the temperature is lowered one finds that over a small temperature range the BCC metals suddenly begin to fail in this brittle mode. An average temperature of the small range, called the DBTT (ductile brittle transition temperature), is often chosen to characterize the temperature where the transition occurs. The simple tensile test will detect this transition, but, unfortunately, it detects DBTT values well below those that occur in complex steel parts.

The tensile test applies stress in only one direction. In complex steel parts, the applied stress will act in all 3 possible directions, a situation called a triaxial stress state. The DBTT turns out to be raised by a triaxial stress state. A triaxial stress state will develop at the base of a notch when a notched sample is broken in a tensile machine, and such tests are called notched tensile tests. However, it is more useful to break the sample with an impact test, where the load is applied much more rapidly than in a tensile machine, as the combination of the notch geometry and the high load rate produces values of DBTT close to the temperature where brittle failure begins to occur in complex steel parts. In the USA the Charpy impact test, shown schematically in Fig. 5.8, is most often used for the impact test. A V-notch is machined into a square bar and placed in the holder. The specimen is broken cleanly in two with a weighted hammer attached to the arm of a pendulum. The pendulum arm is raised to a specified height and then released. It swings down through the sample and swings up on the opposite side. By comparing the rise after breaking the sample to the rise with no sample present one can calculate how much energy was absorbed by the specimen on breakage. This energy, usually given in units of foot-pounds, is called the Charpy impact energy, or CVN energy. (Note: The Izod impact test is similar to the Charpy. It is used mainly in Europe. The main difference in the Izod test is that the specimen is clamped at one end and the pendulum strikes the opposite end.)

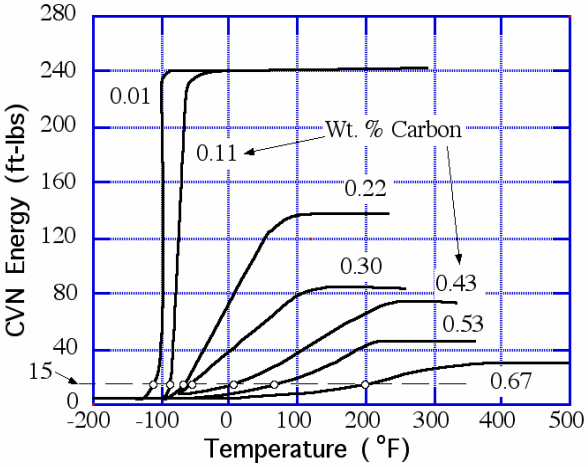

Figure 5.9 Charpy V notch data on plain carbon steels austenitized 1600 °F/4 hours and slow cooled [5.3].

Figure 5.9 presents Charpy impact data on plain carbon steels that were slow cooled from the austenite region so that the microstructures of these steels are mixtures of ferrite and pearlite. One sees that the behavior is very sensitive to %C in the steels. At all compositions there is a transition from ductile to brittle failure as the temperature drops, but at %C levels of 0.11 %C and below the transition is much sharper and the CVN energy is considerably higher for the high temperature ductile mode of fracture. For steels, a CVN energy value of 15 ft-lbs is often taken as the onset value for brittle failure. The line on Fig. 5.9 at 15 ft-lbs shows that for this criteria, steels with %C above around 0.5% would be considered brittle at room temperature. One needs to realize, however, that the DBTT predicted by the Charpy test is really only a guide to actual transition temperatures that will occur for a complex piece of steel used in the field. So the data of Fig. 5.9 do not mean that a 1060 steel will always fail by brittle fracture at room temperature. It is common to refer to the CVN energy as a measure of the notch toughness, or simply the toughness of the steel. This measure of toughness is much more useful than ductility measurements, such as % elongation, for evaluating a steel's potential for brittle failure in service. Toughness and ductility have related, but slightly different meanings and it is high toughness that one wants in steel parts. Experiments have shown that the toughness of steels can be improved by the following factors:

1 Minimizing the carbon content.
2 Maintaining the grain size as small as possible.
3 Eliminating inclusions, such as the sulfide stringers shown in Fig. 5.6. This is done by using steels with low impurity levels of S, P and other elements.
4 Using a microstructure of either quenched and tempered martensite or lower bainite rather than upper bainite or ferrite/pearlite

.

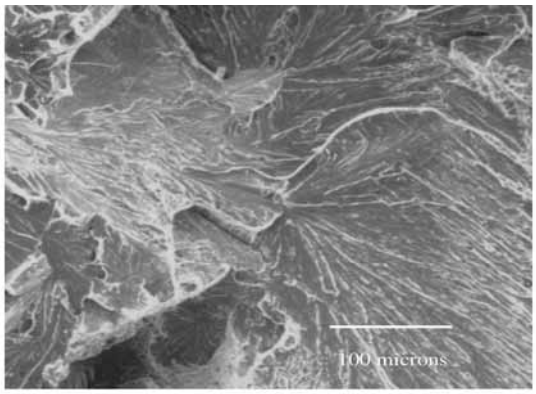

Figure 5.10 SEM picture of a cleavage fracture surface on a 1018 steel. (160x)

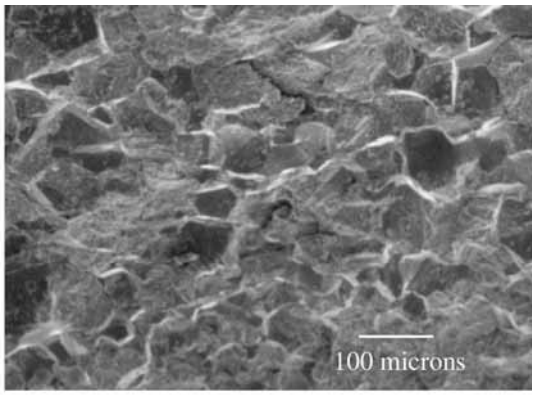

Figure 5.11 SEM picture of a mostly grain boundaryfracture surface on a 1086 steel. (95x)

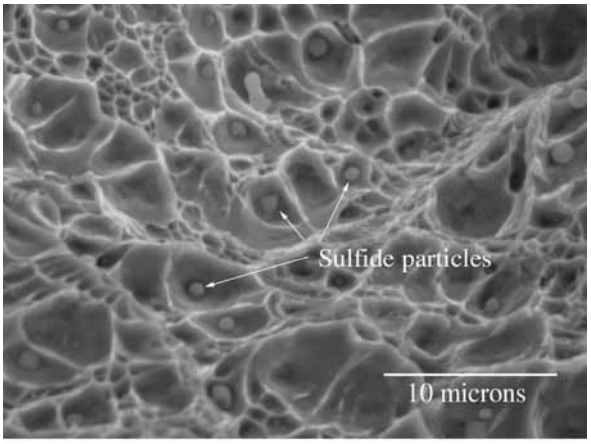

Figure 5.12 SEM picture of a ductile fracture surface on a 1018 steel. (2300x)

There is a large difference in the nature of the fracture mechanism when a steel fails in a brittle mode versus a ductile mode. In brittle failure there is little to no plastic flow of the metal prior to a crack forming and running through the metal causing it to break into pieces. The metal just sort of "pulls-apart" along the fracture surface. This sudden pulling-apart occurs in one of two ways: (1) The metal separates along grain boundaries, or (2) the metal grains are cleaved in half along certain planes of their crystal structure. These brittle fracture modes are called (1) grain boundary fracture and (2) cleavage fracture, and one can distinguish between them by looking at the fracture surface in either a low power microscope or an SEM. Figure 5.10 illustrates a cleavage fracture surface with an SEM micrograph. The characteristic parallel lines are often called a "river pattern" and they outline the paths of cleavage. Figure 5.11 presents an SEM image of a fracture surface which is roughly 60 % grain boundary fracture. Over 60 % of the surface one sees the 3-dimensional shape of individual grains revealed by failure along the old grain boundaries.

When a steel fails in a ductile mode there will be some plastic flow of the metal prior to breakage occurring along the fracture surface. This flow causes very tiny voids to form within the metal grains. As the flow continues these voids grow and coalesce until breakage occurs. SEM micrographs at fairly high magnifications, like that shown in Fig. 5.12, show remnants of the individual voids exposed on the fracture surface. The fracture is often called **microvoid coalescence** for obvious reasons. If the steel contains small foreign particles they will often be the site where the voids first formed and you end up seeing these particles at the bottom of the voids on one or the other of the fracture surfaces. The 1018 steel of Fig. 5.12 contained enough small sulfide particles distributed throughout its volume that many of the voids on the fracture surface reveal the sulfide particles that caused them to nucleate during the plastic flow leading to failure. Unfortunately, it is difficult to see the microvoids on fracture surfaces with optical microscopes because the depth of field is to shallow too image them at the high magnifications needed.

Grain boundary fracture surfaces virtually always indicate that brittle failure has occurred with little to no plastic flow before fracture. Cleavage fracture surfaces sometimes occur with significant plastic flow and by themselves do not indicate brittle failure. Microvoid coalescence fracture surfaces indicate a ductile fracture occurred.

The %C in structural steels that are subject to cold weather conditions is kept as low as possible to avoid embrittlement problems. A fascinating question is whether or not the steel plate used in the Titanic might have become embrittled at the 29 ^{o}F (-2 ^{o}C) temperature of the salt water when it struck the ice burg and sank. Studies of recently recovered pieces of Titanic steel plate have not completely settled this question. Charpy tests of the Titanic plate reveal CVN energies of only 3 ft-lbs at 29 ^{o}F, compared to values of 240 ft-lbs for modern ship plate [5.4]. Modern ship plate is superior due to lower levels of S, P, and silicate particles, along with smaller grain sizes. However, examination of

Titanic rivets [5.5] reveal a high level of slag inclusions and it is not possible to rule out failure due to popped rivets.

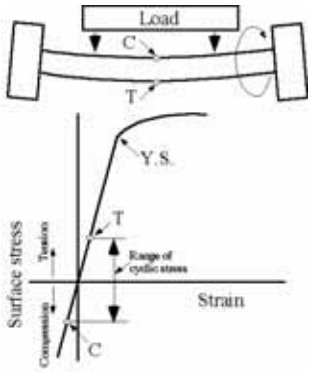

Figure 5.13 The stress state on the surface of a rotating axle.

Fatigue Failure and Residual Stresses A crude but quick way to break a steel rod in two is to make a small notch across the surface with a file or a cold chisel and then bend the rod at the notch. The rod will generally break with a single bend or maybe two. When the rod is bent away from the notch a tensile stress is developed at the base of the notch that is much higher than would be present if the notch were not there, and this leads to fracture starting at the notch. The small radius of curvature at the root of the notch causes a local rise in the stress there. The sharp radius is a stress concentrator, or alternately a stress intensifier. The smaller the radius the higher the stress concentration. Small surface scratches, even those too small to see by eye, can produce stress concentrations during bending, which are localized at the root of the scratch. If sufficiently high, the concentrated stress can exceed the yield stress locally and produce tiny cracks that have potential to lead to failure.

This idea can help us to understand a type of failure occurring in metals that is called fatigue failure. Consider an axle supporting a load heavy enough to cause it to bend down slightly at its center point between the wheels as shown schematically in Fig. 5.13. This bending will cause the metal to be pulled apart at the location T and also to be pushed together at the location C. This means the metal will undergo a tensile stress at T and a compressive stress at C. Therefore, as a point on the axle surface rotates it will undergo a cyclic stress, tension when it is down and compression when it is up. In a well designed axle the maximum tensile stress will be well below the yield stress and the strain experienced in the metal surface during rotation will all be in the elastic region of the stress strain diagram as shown at the bottom of Fig. 5.13. But suppose there is a very small scratch on the metal surface. If the stress is raised locally at the scratch root to a point above the yield stress, it may generate a crack there. Each time the axle rotates the crack grows and eventually the crack becomes large enough to break the axle and we have what is called a fatigue failure. Fatigue failures occur in metal parts subjected to cyclic stresses, as often occurs in rotating machinery, or valve and coil springs, or vibrating parts, such as airplane wings.

When we pull on a steel bar with a tensile stress we cause the atoms of the iron grains to be pulled away from each other so that, on average, the distance between atoms increases. Similarly, if we apply a compressive stress we will end up causing the average distance between atoms to decrease a bit. Hence, if the metal is stress-free, there is some average distance between atoms. When you see a metal rod lying on the bench you generally assume that it is stress free, that the atoms are spaced at their stress-free distance. Because the rod is just sitting there this must be true, but only for the average distance between atoms over the whole rod. It may be that in parts of the rod the atoms are sitting there with

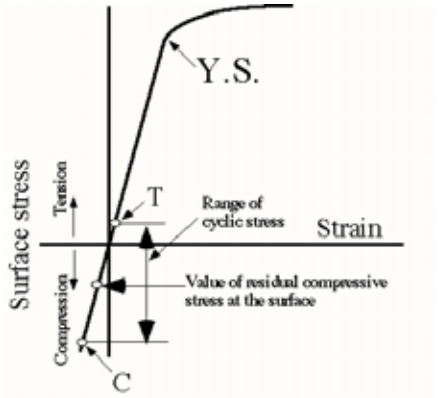

Figure 5.14 Range of cyclic stress shifted down by residual surface stress.

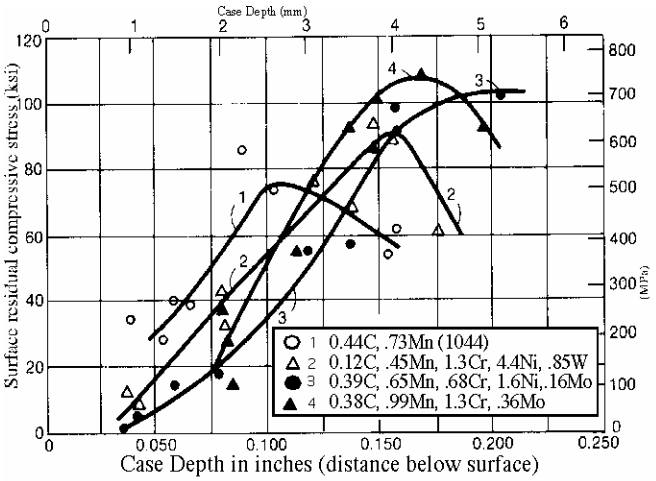
Case Depth (mm)
Surface residual compressive stress (ksi)
(MPa)
Case Depth in inches (distance below surface)
1 0.44C, .73Mn (1044)
2 0.12C, .45Mn, 1.3Cr, 4.4Ni, .85W
3 0.39C, .65Mn, .68Cr, 1.6Ni, .16Mo
4 0.38C, .99Mn, 1.3Cr, .36Mo

Figure 5.15 Longitudinal residual surface compressive stresses versus case depth in 4 induction hardened steels [5.6] (copyright 1963, Society Experimental Mechanics).

average distances between them greater than their stress free distance and in other parts less than this value. If this is the case we say that the rod contains residual stresses, some of them tensile and some of them compressive. Suppose, for example, that the outer millimeter of the rod is under compression. Then below this outer 1 mm thick cylindrical region there must be some region where the atoms are under tension. In this case we would have a residual stress on the surface which is compressive with residual tension below. It is on the surface where the scratches are that lead to fatigue failure. So, by producing residual compressive stresses on the surface it is possible to reduce the crack growth during cyclic loading. As shown on Fig. 5.14, the local residual compressive stress at the surface will cause the tensile stress on the rotating axle to decrease, because the cyclic stress produced by rotation now adds on starting at the value of the residual compressive surface stress. Hence, it is very desirable to have residual compressive stresses on metal parts.

There are several ways to produce residual compressive stresses in steels. These involve heat treating and/or mechanical deformation. Consider first the heat treating technique called flame hardening. The surface of a piece of steel is heated up much faster than its interior can follow by an intense flame directed at the surface. This causes a layer of the steel at the surface to become austenite while the interior remains ferrite + pearlite. On rapid cooling with a quench of some sort the surface layer will transform to martensite while the inner region remains ferrite + pearlite. Martensite has a lower density than the austenite from which it forms. Therefore the outer layer expands when martensite forms. The inner region resists this expansion causing the atoms in the outer layer to be forced closer together than they want to be. Hence a residual compressive stress is formed in the outer martensitic layer. An alternate way of heating the surface layer much faster than the interior is by induction heating. A copper coil is place at the surface of the steel and a high frequency current is passed through the coil. The magnetic field generated by this current induces currents in the steel surface causing localized surface heating. This technique is widely used in industry. It is so effective in enhancing the fatigue life of axles used in motor vehicles that axles are routinely induction hardening, not for increased surface wear resistance, but simply for improved fatigue life. Fig. 5.15 is presented to illustrate the magnitude of the surface stresses that are realized with this technique. It also shows the distribution of the residual stress below the surface.

The famous Japanese Samurai swords are a fascinating example where localized martensite formation on the surface of steel plays an important role. When these swords are quenched they cool faster on the thin cutting edge and form martensite locally along the cutting edge and not back from it. Not only does this produce a hard cutting edge, the expansion on martensite formation all along the cutting edge forces the blade to curve, the longer the blade the more the curve. This effect has been discussed in a recent paper [5.7].

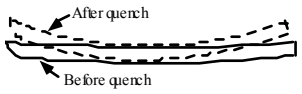

Residual compressive stresses can also be produced on heat treating due simply to thermal expansion/contraction effects that occur on heating and cooling. If a round bar is quenched the outer surface will thermally contract faster than the interior. The interior resists the contraction of the outer surface and pushes it into tension. If the tension is large enough to cause plastic flow in the outer surface, a stress reversal will occur on further cooling and one ends up with a residual compressive stress on the outer surface. As above then, the end result is a desirable residual compressive surface stress. However, if phase a transformation occurs on cooling, things become more complicated. So for steels, the compressive residual surface stress is assured if one does not heat the steel above the A_1 temperature before quenching. Heating above A_1 generates austenite which complicates matters due to the formation of martensite on quenching. If martensite forms only in an outer surface layer on quenching, then, as explained above, one again obtains a surface residual compressive stress. However, if martensite is obtained all the way to the center of the bar (a condition called through-hardening), one obtains a residual surface tensile stress, an undesirable situation.

There are many surface treatments that are given to steels. The two most common such treatments involve carburizing and nitriding. These treatments are usually done to produce hardened layers on the surface that reduce surface wear rates. It turns out that these treatments also enhance the formation of residual compressive stresses, which is a very fortuitous benefit accompanying the increased surface hardness.

Residual surface compressive stresses can also be generated by mechanical means. Perhaps the most common technique employed in industry is shot peening. The technique involves bombarding the steel surface with small steel balls (shot). This action cause localized plastic flow at the surface resulting in the desired residual surface compressive stress. Steel toughness is enhance by surface residual compressive stresses. An example involves the high strength pearlitic wire used in cables discussed above. It was pointed out in the section on impact testing that, in general, pearlitic steel is not as tough as quenched and tempered martensitic steels. Yet, the high strength pearlitic wire used in bridge and crane cables displays superior toughness to Q & T martensitic wires of the same hardness. The improved toughness of the pearlitic wire is thought to arise from the drawing operation used to refine the pearlite spacing which is necessary to achieve the high strength. Apparently the wire drawing operation produces residual surface compressive stresses that result in the improved toughness.

References

5.1 Hardness Testing, H.E. Boyer, ASM International, Metals Park, OH (1985).

5.2 Metallography, G.F. Vander Voort, McGraw Hill Book Co, New York, N.Y. (1984).

5.3 J.A. Rinebolt and W.J. Harris Jr, Effect of alloying elements on notch toughness of pearlitic steels, Trans. Amer. Soc. Metals, vol. 43, p. 1197 (1951).

5.4 B.L. Bramfitt, S.J. Lawrence and H.P. Leighly Jr., A Perspective on the Quality of Steel Plate from the RMS Titanic, Iron & Steelmaker, vol. 26, Sept. 29-40 (1999).

5.5 T. Foecke, Metallurgy of the RMS Titanic, NIST-IR 6118 (1998)

5.6 Handbook of Experimental Stress Analysis, Ed. M. Hetenyi, page 459, John Wiley, N.Y. (1963).

5.7 W.N. Weins and P. Bleed, Why is the Japanese Sword Curved?, Materials Research Society, pp 691-701 (1991).

Summary of the Major Ideas of Chapter 5

1 The mechanical properties of metals are often characterized with the tensile test. The test applies a stretching (tensile) force to a rod and measures the fractional length increase, Fig. 5.1. Results are shown as plots of ***stress*** (force per area of original rod) on the vertical axis against the ***strain*** (fractional length change) on the horizontal axis. At small strains the rod behaves elastically, it springs back to its original length when the applied stress is release. Beyond a stress called the ***yield stress***, the rod begins to deform plastically, meaning that upon release of the applied stress it has become permanently elongated. Stretching the rod to fracture, one finds a maximum stress on the diagram and this is called either the ***tensile stress*** or the ***ultimate tensile stress***.

2 In a simple bending test metals that bend a lot before fracturing are said to be ductile, as opposed to brittle metals which will fracture before significant bending occurs. Good ductility shows up in a tensile test by high values of ***% Elongation*** and/or ***% Reduction in Area.*** Percent elongation is simply 100 times the total fractional length change after fracture in the tensile test. Percent reduction in area is 100 times the fraction that the final area of fracture surface has dropped below the original cross sectional bar area.

3 Mechanical properties are often summarized by listing yield strength, tensile strength and elongation as in Table 5.1. The strength values in the U.S. are usually given as psi (pound per square inch) or ksi (thousands of pounds per square inch). The data of Table 5.1 show that as the carbon content of plain carbon steel, either air cooled (normalized) or as rolled, goes up from 0.2 to 0.95 %, the tensile strength increases from around 65 to 145 ksi and the % elongation decreases from around 35 to 9%. It is virtually always found that as one increases strength in a metal or alloy, a loss of ductility occurs.

4 Hardness tests evaluate mechanical properties by forcing an indenter material, often diamond, into the surface of a metal under a given load and measuring either the depth of penetration (the Rockwell test) or the size of the indent impression (Brinell and Vickers tests). Table 5.2 lists the various tests and the conditions for choosing between them.

5 In quenched and tempered steels there is a good correlation between the ultimate tensile test and hardness. Figure 5.7 presents a graph of this correlation for Rockwell C hardness, called HRC. It is common to heat treat steels to HRC values of 45 and above, which corresponds to tensile strengths of 215 ksi and above. Compare this to the strongest commercial alloys of Al, Cu and Ti, which are roughly 83, 177 and 190 ksi, respectively. Clearly, steels are much stronger than all of these alloys.

6 All BCC metals, such as ferritic steel, share the problem that at low temperatures they fracture in a brittle manner as opposed to their normal ductile fracture at higher temperatures. The ***DBTT*** (ductile brittle transition temperature) is defined as the temperature below which the brittle failure occurs. Values of the DBTT can be measured with the tensile test but they are much lower than where the transition is observed in complex steel parts. A V-notch impact test reveals a DBTT which does correspond fairly well with values experienced in the field. The Charpy V notch test measures the energy needed to

break the notched bar and data such as those of Fig. 5.9 show that the DBTT in carbon steels is increased as %C increases.

7. It is common to use the term toughness as a measure of a metal's ability to fracture in a non brittle manner. Pages 43-44 lists four important ways that a steel's toughness may be enhanced and also how the fracture surface can distinguish brittle failure from ductile failure.

8 The iron atoms in a ferritic steel are positioned on the corners and at the center of the little body centered cubes that make up its grains. There is some average distance of separation of atoms on the cubes that steel has before it is stressed. A ***tensile stress*** increases this distance and a ***compressive stress*** decreases it. Residual stresses occur in steels when there are regions in the steel part where the atoms lie, on average, closer together (compressive residual stress) or further apart (tensile residual stress) than in the unstressed state.

9 Residual stresses can be produced in steels during heat treatments that involve quenching, particularly when martensite forms only at the surface of a quenched steel. The density of martensite is less than that of the austenite from which it forms. This means that when a given volume of austenite transforms to martensite, the volume of the martensite needs to increase. When the martensite forms as a surface layer on a bar, the interior of the bar will restrain its expansion and pull its atoms into compression, thereby creating a residual compressive stress on the surface. It is common to generate surface layers of martensite by flame hardening or induction hardening by rapidly heating only the surface layers into the austenite temperature region prior to quenching. Figure 5.15 shows that very large surface compressive stresses (on the order of 70 to 100 ksi) can be produced in steels with induction hardening.

10 Surface compressive stresses are very beneficial to toughness, as they inhibit crack formation and growth at the surface. The compressive stress will subtract from any applied tensile stress and reduce the net tensile stress at crack tips. (The tempered glass in your automobile windows is an example of the benefits of producing materials with surface compressive stresses.)

11 Fatigue failure is a type of failure that occurs in metal parts subject to cyclic loading. The applied stress at the surface of a loaded axle will undergo alternating tension and compression on each rotation of the axle, see Fig. 5.13. The geometry of a crack tip leads to a concentration of applied stress right at the tip. Hence, the applied surface stress becomes increased locally at the tip of any crack lying on the surface and this can cause small enlargements of the crack size on each rotation until failure eventually occurs. Such fatigue failure can be reduced significantly by the presence of surface residual stresses, which subtract from applied tensile stresses at the surface of the part.

6 - The Low Alloy AISI Steels

There are many different chemical elements that occur in the various types of steel, either as a direct additive or as an impurity element. In order to understand the chemical symbols used for the various elements it is helpful to review the periodic table of elements that you learned about in your chemistry or science classes in school. Table 6.1 (page 57) presents the periodic table of elements that has been prepared to emphasize the crystal structures of the many different metal elements that occur in nature. The box in the lower left corner identifies the information for each element. For example, the element iron has chemical symbol, Fe, atomic number 26, atomic weight 55.85, density of 7.8 gms/cubic centimeter, melting temperature of 1538 ^{o}C, and a mixed crystal structure of BCC-FCC-BCC between room temperature and its melting temperature. Notice that the elements in the central columns of the table are grouped into 3 groups of columns with the elements having crystal structures of either (1) BCC, (2) some mixtures of structure like BCC and FCC for Fe, and (3) FCC. These groups of columns will be of most interest to us as they contain most of the alloying elements found in steels.

The discussion to this point has been restricted to plain carbon steels. The code for classifying these steels in the U.S. was developed by two professional organizations, the American Iron and Steel Institute (AISI) and the Society of Automotive Engineers (SAE). The code number of a particular steel is generally referred to as the AISI-SAE code number, but for the sake of simplicity it will be referred to here simply as the AISI code number. Table 6.2 presents a tabulation of the chemical compositions of a limited number of the plain carbon steels. You will notice that the first 2 digits of the code change from 10 to 11 for the free machining steels, and from 10 to either 13 or 15 for high Mn plain carbon steels. A complete list of the chemical compositions of all the plain carbon steels may be found in references [6.1 and 6.2]. In addition to the AISI specifications for steels in the U.S., the American Society for Testing Materials (ASTM) also specifies types of steels, as do the military. The ASTM specifications are generally preferred for applications of steels for uses where avoidance of failures is imperative, such as bridges and boilers, and the military specifications are used for military applications. Cross references between AISI and ASTM numbers as well as with the numbering system used in foreign countries can be found in [6.2 and 6.3]. Steel castings, such as those used in large valves, gears, machinery, etc., have their own codes, mostly set by ASTM. The AISI steel code is used for steel produced by steel mills and then sized by rolling or forging techniques, and called wrought steels.

Table 6.2 Selection of some plain carbon steels.

AISI No.	%C	%Mn	%Other
1018	0.18	0.75	-
1020	0.20	0.45	-
1044	0.44	0.45	-
1045	0.45	0.75	-
1060	0.60	0.75	-
1078	0.78	0.45	-
1080	0.80	0.75	-
1095	0.95	0.75	-
Free Machining Steels			
1141	0.41	1.45	0.11S
1144	0.44	1.45	0.26S
Plain Carbon Mn Steels			
1340	0.40	1.75	-
1518	0.18	1.25	-
1541	0.41	1.45	-

All steels contain a low level of impurity elements that result from the steel making process. These impurity elements can be eliminated from laboratory prepared steels where cost is not a problem. However, steel is an industrial metal produced in mega-tonnage quantities, and economic production processes result in a low level of certain impurity elements present in steel. These elements and their maximum levels traditionally found in steels are

shown in Table 6.3. These 4 elements appear next to each other in the 3rd row from the top of the periodic table where they have been cross hatched in Table 6.1 to highlight their importance. Improvements in steel processing techniques in the last two decades of the 1900's have allowed the industry to lower the residual level of S and P in steels, and present day steels often run levels of these elements at half or less than those given in Table 6.3.

Table 6.3 Impurity elements present in all steels.

Element	Maximum level
S	0.04 %
P	0.05 %
Si	0.2
Al	0.04

For reasons to be explained subsequently, it is often advantageous to add additional elements to steel, and the added elements are called alloying elements. If the % of these added elements is fairly low, like total additions of under 4 %, then the steels are called low alloy steels. Fortunately, the large bulk of alloy steels involve the addition of only 3 chemical elements over and above the elements in plain carbon steels, Cr, Mo and Ni, which are shown cross hatched in Table 6.1. There has been an evolution in the types of alloy steels used in industry, particularly the automotive industry, during the first part of the 20th century so that at the present time one can classify these alloy steels into 3 main categories, Mo steels, Cr steels and triple alloyed steels (Mo + Cr + Ni) steels. Table 6.4 lists a select number of the low alloy steels grouped into these 3 categories. A complete listing of the low alloy AISI steel compositions can be found in [6.1-6.3].

Table 6.4 Selection of some low alloy steels.

AISI No.	%C	%Mn	%Cr	%Mo	%Ni
Mo Steels (4xxx)					
4023 (Mo)	0-.23	0.80	-	0.25	-
4042	0.42	0.80	-	0.25	-
4130 (Mo-Cr)	0.30	050	0.95	0.20	-
4140	0.40	0.87	0.95	0.20	-
4320(Mo-Cr-Ni)	0.20	0.55	0.50	0.25	1.82
4340	0.40	0.70	0.80	0.25	1.82
4620 (Mo-Ni)	0.20	0.55	-	0.25	1.82
Cr Steels (5xxx)					
5046	0.46	0.87	0.27	-	-
5120	0.20	0.80	0.80	-	-
5160	0.60	0.87	0.80		-
52100	1.00	0.30	1.45	-	-
Triple Alloyed (8xxx)					
8620	0.20	0.80	0.50	0.20	0.55
8640	0.40	0.87	0.50	0.20	0.55

Following are some interesting points. Note that the Cr steels, 5xxx, are the simplest of the steels in that Cr is the only added alloying element in all of them. The Mo steels, 4xxx, are more complex in that they can contain various combinations of all 3 of the major alloying elements depending on the second digit of the code. For example the straight moly steels are coded 40xx and the moly-chrome steels are coded 41xx. Notice that there are no Ni steels. The Ni steels lost there popularity after the first half of the 20th century and large scale production of the 2xxx Ni steels, and the 3xxx Ni-Cr steels was discontinued around 1964.

There are 2 main reasons for the wide spread use of low alloy steels which will be discussed later. These are: (1) To improve the hardenability of the steel, and (2) To improve the toughness of tempered steels at a give level of strength.

Manganese in Steel The element S is present in all of our steels as an impurity element, as was illustrated in Table 6.3. There are 2 unique facts about S in Fe that lead to a potential for S impurities causing embrittlement of steel when present at even extremely low concentrations. (1) The solubility of S in both austenitic iron and ferritic iron is exceedingly low, being essentially zero. (2) S forms a chemical compound with iron, FeS, that melts at 2175 °F (1199 °C). To understand how these 2 facts combine to produce the embrittlement problem consider the following analysis. Suppose we have a steel containing only 0.04%S impurity. Because the solubility of S in the Fe grains of either austenite or ferrite is essentially zero, the S will virtually all be present as the compound FeS at all temperatures. Because hot rolling and forging temperatures are often above 2175 °F, the FeS will be present as a liquid at these temperatures. Because of the very low S level, only 0.04 %, one would not expect the corresponding very small amount of liquid to have any noticeable effect on the hot working of the steel. However, there is another unique factor that changes the picture. To understand this factor one must understand the concept of "wetting", which is well illustrated by the soldering process. A good solder joint at a fitting occurs when the molten solder metal runs into the thin joint between the copper pipe and the fitting being attached to it. If one just melts the solder at the joint region without applying a flux the molten solder metal will form a ball shape and not flow into the joint. Applying a flux causes the molten solder to flow into the joint. The liquid metal appears to get sucked into the joint and, in fact, it does get sucked in by a force called surface tension. Surface tension is a force acting along the plane of a surface. The flux removes an oxide from the copper surface and generates the desired surface tension force at the point where the clean surface contacts the molten solder, causing the solder to be pulled along the cleaned surface.

> To obtain a feel for the nature of the surface tension force consider the inflation of a rubber beach ball. The ball is inflated by increasing the pressure of air inside the ball above room pressure. This causes the rubber fabric to stretch into tension. This stretching tension means that there is a pulling (tensile) force acting in the surface plane of the rubber fabric. This surface tensile force is similar to the surface tension force that pulls the solder along the copper surfaces into the joint between pipe and fitting. It is an actual force that lies in the surface plane where the liquid solder contacts the copper.
>
> 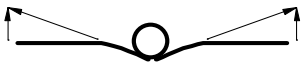
>
> You may also observe a surface tension force in action by gently floating a paper clip on the surface of the water in a glass. Note that the water surface is bent down a bit at the contact point. It is the surface tension force in the water/air surface that holds the clip up. The force acts at right angles to the axis of the clip wire along the bent-down water surface and is directed slightly upward as shown at the right. It is the upward component of this surface tension force that is holding up the clip. Addition of soap to water reduces this surface tension force. To illustrate dramatically, take a tooth pick and dip the tip into a liquid soap typically used in your kitchen. Now, gently touch the soap coated tip to the water surface well away from the clip. Try it and see what happens to the floating clip.

This sucking-in phenomena is often called "wetting" for obvious reasons. Now consider a small spherical ball of liquid FeS lying at a grain boundary in steel at the hot rolling temperature. The grain boundary is a type of surface similar to the surface on a copper pipe. We call the grain boundary a solid-solid surface compared to the solid-vapor-surface on the copper pipe. Just like there is a surface tension force where the liquid solder contacts the copper-vapor surface, there is a surface tension force where the

molten FeS contacts the grain boundary surfaces between austenite grains. This force causes the molten FeS to wet the austenite grain boundaries. The FeS is pulled into the grain boundaries generating a very thin film of liquid on the grain boundaries which destroys their strength. Because the thickness of the liquid film is extremely thin, the very small amount of FeS present is adequate to cover quite large fractions of the grain boundaries. Hence the steel will break apart by brittle failure (grain boundary fracture) in the rolling or forging operations. Such an embrittlement occurring during mechanical deformation at high temperatures is called ***Hot Shortness***. It almost always occurs when a liquid phase forms in metals, but only if the liquid wets the grain boundaries. The lead in leaded brasses becomes molten in the solid lead on heating. But the lead does not wet the grain boundaries, it forms small spheres in brass and does not embrittle the alloy. The impurity element P will also cause hot shortness in steels, but only at higher impurity levels than are found for S. The P forms a low melting liquid called steadite and can produce hot shortness at P levels of around 0.1 % and above.

A primary reason Mn is present in all of our steels is to control problems with S. Like Fe, Mn forms a chemical compound with Fe called manganese sulfide. It has the chemical formula of MnS and it melts much higher than FeS, at 3010 °F (1655°C). In steels, where both Fe and Mn are necessarily present, this compound will have chemical formula (MnFe)S and the melting point will be reduced somewhat. However, it is still higher than the hot rolling and forging temperature and it removes the hot shortness problem. It is customary to call the (MnFe)S particles present in steels manganese sulfide even though it often contains appreciable amounts of Fe. The sulfide particles highlighted in the 1144 steel of Fig. 5.6 are examples of such manganese sulfide.

Even though the Mn addition removes the problem of hot shortness, the presence of these particles (usually called inclusions) in steel can often lead to embrittlement problems in room temperature operations. Because the sulfide inclusions are often ductile at the hot working temperature, they elongate into stringers, as demonstrated in Fig. 5.6. This produces a type of embrittlement in sheet and rod which depends on the direction in which the load is applied. The embritllement often leads to failure problems in products made from steel plate. Both the longitudinal and transverse directions of the rolling operation are shown on a steel plate in Fig. 6.1, with the inclusions being elongated in the longitudinal direction. The orientations of two Charpy impact bars are also shown. Notice that in the transverse bar the elongated inclusions will run parallel to the base of the V-notch while in the longitudinal bars they will run at right angles to the base of the V-notch. Brittle failure occurs by cracks being opened up by the triaxial stresses generated at the base of the V-notch. Now consider the effects of the elongated inclusions. When the inclusions lie parallel to the V-notch base it is possible to have an inclusion lying along the entire base of the V-notch. But when the inclusions lie at right angles to the base of the V-notch an inclusion will pass the base of the notch at only one point. Hence, the inclusions will enhance crack formation much more effectively for the transverse bar orientations where they lie parallel to the base of the V-

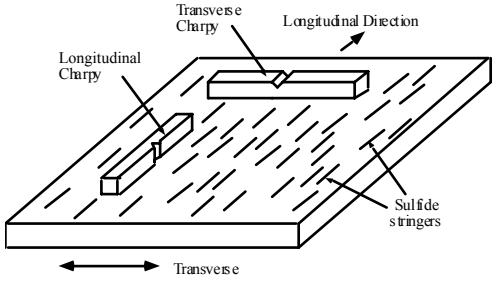

Figure 6.1 Orientation of the longitudinal and transverse Charpy specimens cut from sheet.

notch. Charpy data on rolled sheet containing elongated sulfide inclusions give impact energies of around 44 ft-lbs for longitudinal bars and only 15 ft-lbs for transverse bars. The data provide dramatic evidence illustrating how elongated inclusions reduce the transverse toughness of wrought steels.

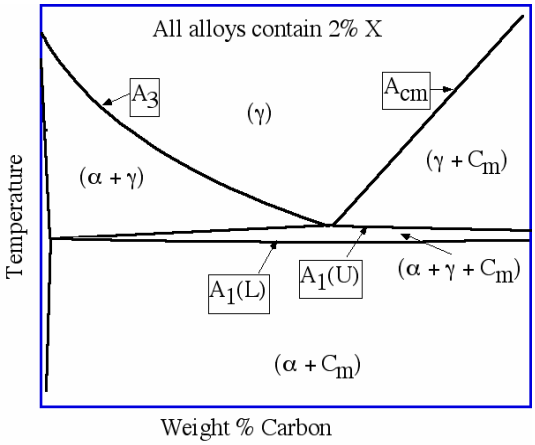

Figure 6.2 A ternary Fe-C-X phase diagram with %X held constant at 2%.

The Mn sulfides are called ***inclusions***. Inclusions are generally produced by impurities in the steel. Residual oxygen and nitrogen impurities generate inclusions of oxide and nitride particles. In general, these inclusions are brittle and do not elongate at the hot working temperature. Unless their volume fraction becomes excessive they do not lead to dramatic reductions of toughness.

Effect of Alloying Elements on Fe-C Phase Diagram The phase diagrams for steel presented in chapter 3, such as Fig. 3.5, are all pure Fe-C phase diagrams. When Mn and the various alloying elements are added to Fe+C alloys the 3 important lines on the phase diagram, A_3, A_1 and A_{cm} will all shift a bit. If one considers only one addition, such as the Fe-C-Mn compositions of plain carbon steels the phase diagrams is now called a ternary phase diagram. The study of ternary phase diagrams is considerably more complex than binary phase diagrams. The Fe-C diagram of Fig. 3.5 involves only 2 elements and is called a binary phase diagram. Details will not be presented here on ternary phase diagrams, but Fig. 6.2 is presented to give you a flavor of the complexity. This diagram is for a hypothetical ternary alloy of Fe+C+X, where X is the 3rd element addition. The diagram refers to alloys restricted to 2 % of the X element and it shows how the 3 important lines of the Fe-C diagram are shifted by addition of element X. The A_3 and A_{cm} lines are only shifted up or down relative to their position on the binary FeC diagram, but the A_1 lines is split into 2 lines labeled A_1(L) and A_1(U) on Fig. 6.2. For low alloy steels the temperature difference between these 2 lines is usually small and it can be neglected. In plain carbon steels the shift of the 3 important lines that occurs because of the Mn present is small enough that the pure Fe-C diagram presents a good approximation for these steels. However, for the low alloy steels one now has other elements present in addition to the Mn and the effects can become noticeable, although still fairly small. To simplify things we will ignore the split A_1 effect and characterize the shift of the lines by determining how the added elements shift (1) the temperature of the A_1 and (2) the composition of the pearlite point. The results are fairly simple: (1) The elements Mn and Ni both shift A_1 down and Cr and Mo shift it up. Reference [6.4] presents an equation for the A_1 temperature that illustrate these effects,

$$A_1 \text{ (in } ^oC) = 727 - 10.7(\%Mn) - 16.9(\%Ni) + 16.9(\%Cr) + 29.1(\%Si)$$

The equation is only valid for low levels of the elements shown, but applies to plain carbon and low alloy steels. The element Mo does not appear because it has no effect at levels below 0.5 %, see Table 6.4. To illustrate the use of the equation consider a 1018 steel which Tables 6.2 and 6.3 show contains 0.75 % Mn and 0.2 % Si. Plugging these

values into the equation gives an A_1 temperature of 725 ^oC, which was the value used on Figs. 3.9 and 3.10.

(2) All four elements shift the pearlite composition to values lower than 0.77 %. The various other elements that we will consider later with tool steels all raise A_1 and all also drop the pearlite composition.

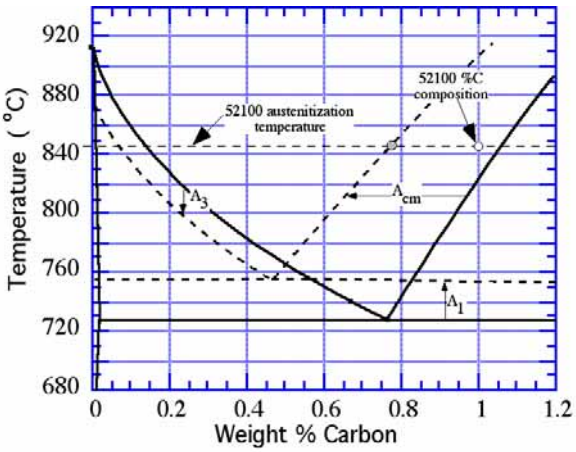

Figure 6.3 Dashed lines are estimates of new positions of the A_1, A_3 and A_{cm} lines in 52100 steel.

As a first example consider the steel 5160 which is the alloy of choice for most leaf springs used widely in motor vehicles. Comparing this steel to the plain carbon steel, 1060, in Tables 6.2 and 6.4, one sees that the main difference is the addition of 0.80% Cr. The added Cr shifts the pearlite composition down to around 0.66% for this alloy. Hence 5160 is closer to the pearlite composition than 1060 and the increase in the volume fraction pearlite formation as cooling rates are increased will be greater for 5160 than in 1060.

As a second example consider the widely used bearing steel, 52100, which has a carbon content of 1.0 % (larger than 0.77 %C and called hypereutectoid) and a Cr content of 1.45 %. The common heat treatment for this steel differs from that of most low alloy steels in that the austenitization temperature lies below the A_{cm} line. The solid lines of Fig. 6.3 shows the positions of the A_1, A_3 , and A_{cm} lines for the pure Fe-C diagram and the dashed lines are an estimate of their positions in 52100 steel. The recommended austenitization temperature for 52100 [6.1, p 429] is 845 ^oC (1555 ^oF) which is shown on the diagram. Notice that at this temperature a pure Fe + 1% C steel would be fully austenite because it would lie above the A_{cm} for pure Fe-C alloys. However, in 52100 steel the composition point lies well below it's A_{cm} line and, as such, the steel will contain particles of cementite at the austenitization temperature. On quenching these particles simply remain in the steel and when the austenite transforms to martensite the particles become surrounded by martensite rather than austenite. The cementite particles that are present in the 52100 bearing steel after quench and tempering are very small in size. Figure 6.4 presents a high magnification SEM micrograph showing a typical distribution of the particles. The small particles in this micrograph average a diameter of just under 0.2 microns and are too small to be resolved in an optical microscope. Smaller sized particles are preferred as some mechanical properties of 52100 are improved the smaller one can make these particles. We will return to 52100 steel in the chapter on austenitization.

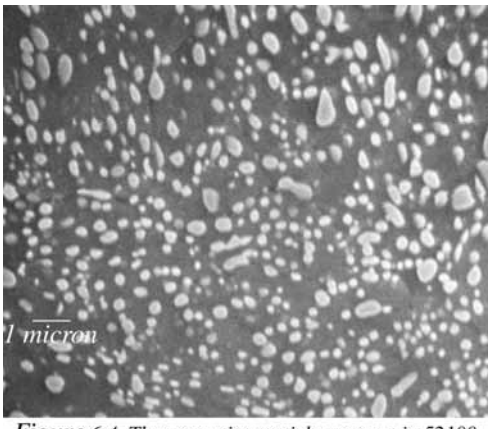

Figure 6.4 The cementite particles present in 52100 following the standard heat treatment. (5000x)

References

6.1 Metals Handbook, Vol. 1, 10th Edition, Properties and Selection: Irons, Steels, and High Performance Alloys, p.141, Classification and Designation of Carbon and Low Alloy Steels, ASM International, (1990).
6.2 Heat Treater's Guide, Practices and Procedures for Irons and Steels, ASM International (1995).
6.3 Worldwide Guide to Equivalent Iron and Steels, ASM, 2nd Ed. Nov. 1987, ASM International.
6.4 K.W. Andrews, Journal of the Iron and Steel Institute, London, volume 203, page 721, (1965).

Summary of the Major Ideas of Chapter 6

1 The major code used to classify the various steels in the U.S. was developed by the American Iron and Steel Institute and all the common wrought steels have compositions specified by their AISI number. As illustrated in Table 5.2 the AISI numbers of the plain carbon steels are of the form 1XXX where the last 2 digits tell you the carbon composition and the second digit tells you if excess sulfur or Manganese (Mn) has been added. Manganese is present in all steels. The amount of Mn present in a steel can only be found in a table of compositions as the AISI code does not contain this information.

2 Understanding the composition of steels requires a minimal familiarity with the chemical symbols used to represent the various alloying elements and impurity elements present in steels. The symbols of all the elements of nature are given on the periodic table of Table 6.1 (next page), which is taught in high school chemistry classes. The important alloying elements and impurity elements in steel are shown cross hatched on Table 6.1.

3 The common alloy steels have one or more of the 3 elements, Cr, Mo or Ni added, and these steels are referred to here as the low alloy AISI steels. Table 6.4 lists the composition of the most important of these steels. The steels may be grouped into 3 types: Mo steels, 4xxx, Cr steels, 5xxx and triple alloyed steels, 8xxx. Again the last 2 digits tell you the %C in the steel. As seen in Table 6.4 the meaning of the second digit varies in an irregular fashion.

4 Manganese is present in all steels to overcome problems with sulfur embrittlement. Sulfur is an impurity atom in steels that cannot be economically removed. It forms a compound with iron, FeS, that is molten at the hot rolling temperatures of steel. The molten FeS wets the austenite grain boundaries and leads to brittle grain boundary fracture during hot deformation, a phenomenon known as ***hot shortness.*** Addition of Mn replaces the iron sulfide compound, FeS, with a manganese sulfide compound, MnS, that is not molten at the hot rolling temperature and cheaply overcomes the hot shortness problem.

5 The small particles of MnS become elongated in wrought steels and form "stringers" lying in the direction of deformation, as illustrated in the resulfurized 1144 steel of Fig. 5.6. The "stringers" of MnS are a type of ***inclusion*** in the steel. They have little effect on the toughness of the steel for deformation in its longitudinal direction (the direction of the stringers), but can dramatically reduce toughness for deformation in the transverse direction, deformation at right angles to the stringers.

6 Addition of Mn and the Cr, Mo and Ni alloying additions change the position of the A_3, A_1 and A_{cm} transformation lines from their locations on the binary Fe-C phase diagram. The equation on page 55 shows that the A_1 line is lowered by Mn, raised by Cr and Ni, and not affected by Mo at its levels in the 4xxx steels. All of these additions reduce the composition of the pearlite point below 0.77%. In general these shifts are small and can often be ignored in designing heat treatments. However, as alloying content increases they can be significant as is illustrated for the heat treatment of 52100 steel on page 55.

Table 6.1 The periodic table of the elements

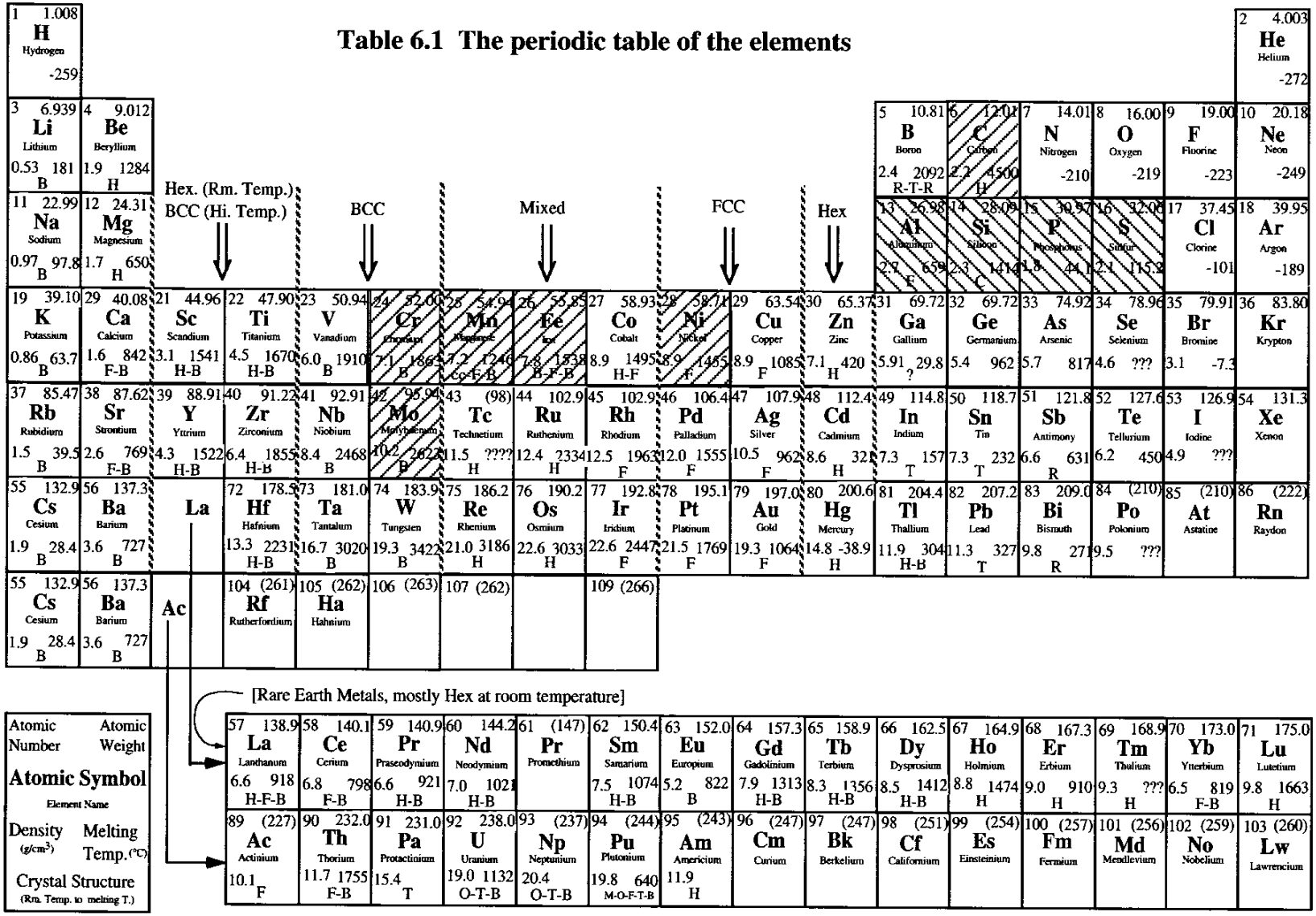

7 - Diffusion - A Mechanism for Atom Migration Within a Metal

Modern archeology teaches that our earliest ancestors evolved in East Africa and then spread to the rest of the world very slowly by a process called diffusion. Figure 7.1 indicates the direction of flow out of Africa into Europe, Asia and India. The lower right of the figure illustrates the 2 main requirements for diffusion. First, the direction of flow is from high density to low density, from peopled regions to no peopled regions. This results in what we call a gradient in the density of people, with the flow going from the dense end of the gradient to the less dense end. Second the moving species, in this case man, must have mobility that produces a back and forth movement. Because there are more people in the high density regions, on average more people will jump from high density regions to low density regions, which causes the net flow down the gradient.

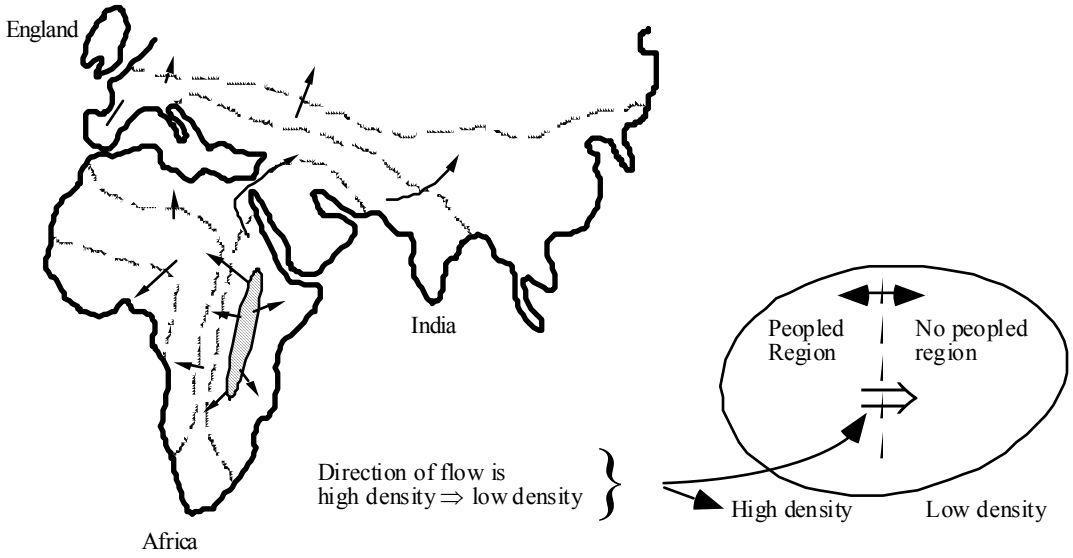

Figure 7.1 Spread of early man out of East Africa by diffusion (migration).

Now consider the experiment shown in Fig. 7.2. The end of a bar of pure iron is packed in charcoal and heated in a furnace to 1700 ^{o}F (925 ^{o}C). At this temperature the iron is austenite and the phase diagram shows us that it is capable of dissolving around 1.3 %C. But since the bar is pure iron it contains little to no carbon while the charcoal at its surface contains close to 100 % carbon. Hence, the carbon atoms are expected to move into the pure iron bar by the mechanism of diffusion if the atoms are able to jump

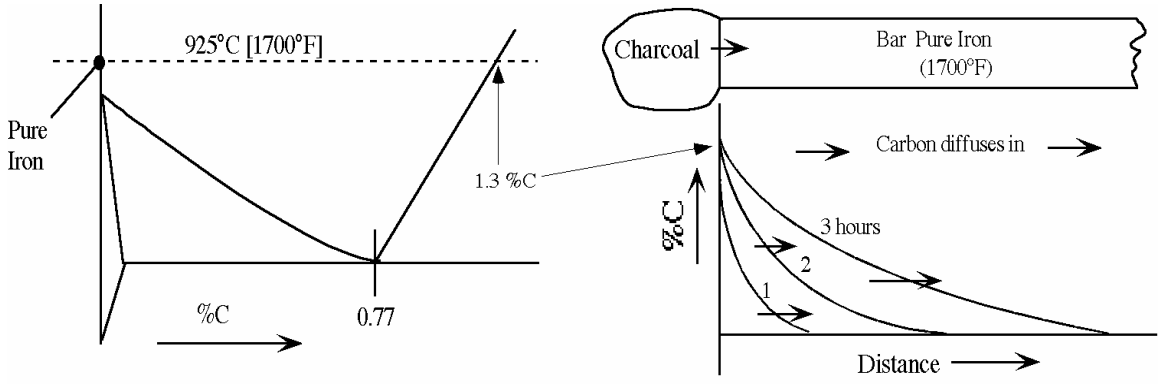

Figure 7.2 Diffusion of C into a pure iron bar at 1700 ^{O}F (925 ^{O}C).

back and forth fast enough. Notice in Table 6.1 that the atomic number of a C atom is much less than that of an Fe atom, only 12 versus 26. This means that the C atom is much smaller than an Fe atom. Mainly for this reason, a C atom dissolved in austenite will lie at holes in-between the Fe atoms. Figure 3.2 shows the iron atoms as spheres lying on the corners and face centers of the FCC cubes which make up the crystals of the austenite grains. The small circles locate the centers of the holes lying between the iron atoms. If a carbon atom wants to move it must jump from one hole (usually called a site) to another between the bigger iron atoms. Thermal energy associated with increased temperature causes atoms to vibrate back and forth. As temperature increases the magnitude of the thermal vibrations increases and it becomes increasingly probable that a given carbon atom will jump to a near empty site. Experiments show the following results. In austenite at room temperature, it takes years for a C atom to jump to a nearest site. But this changes tremendously on heating. At 1700 ^{o}F (926 ^{o}C), a carbon atoms in an austenite iron grain will jump back and forth between neighboring holes between the Fe atoms of the FCC crystal at nearly unimaginably high rates, around 1.8 billion times per second. So for this reason diffusion of the carbon atoms will occur out of the graphite into the pure iron at rates that are extremely sensitive to the temperature. At the temperature of 1700 ^{o}F it becomes possible to diffuse the carbon atoms well into the pure iron bar. The carbon concentration increases to the maximum possible value in austenite, 1.3 %, at the charcoal interface and, as shown on Fig. 7.2, with increasing time more C diffuses into the interior. In the C-Fe case the 2 basic requirements for diffusion are also met: 1) The C atoms have a high mobility, they rapidly jump back and forth, and 2) The C atoms move from high compositions on the left to low compositions on the right. Here the flow is down a concentration gradient, which is similar to the density gradient.

Figure 7.3 illustrates that it is also possible to remove carbon atoms from steel by the process of diffusion. The figure shows a bar of 1095 steel heated to 1700 ^{o}F with only its left end exposed to air. The oxygen in the air will react with the carbon atoms at the surface and form gaseous molecules of carbon dioxide, CO_2, which will then float away from the surface removing carbon from the left end of the bar. This will cause the %C at the left end of the bar to drop down and as the carbon diffuses out of the bar the %C is reduced in the bar as shown in the figure. This process is called decarburization, It can be a big problem for steels heated in air. To avoid the problem one must control the composition of the gas surrounding the steel during heating. Methods of doing this will be discussed later.

The rate at which diffusion occurs is characterized by a parameter, D, called the diffusion coefficient. To a good approximation one may calculate how long it will take a C atom to diffuse a distance d by dividing the distance squared by 6 times D,

$$\text{time(sec)} = \frac{dxd}{6xD} \qquad \text{Equation 7.1}$$

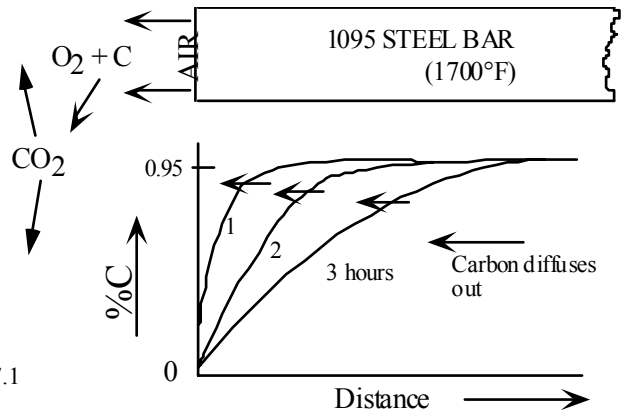

Fgiure 7.3 Decarburization removes carbon from a 1095 steel bar by diffusion.

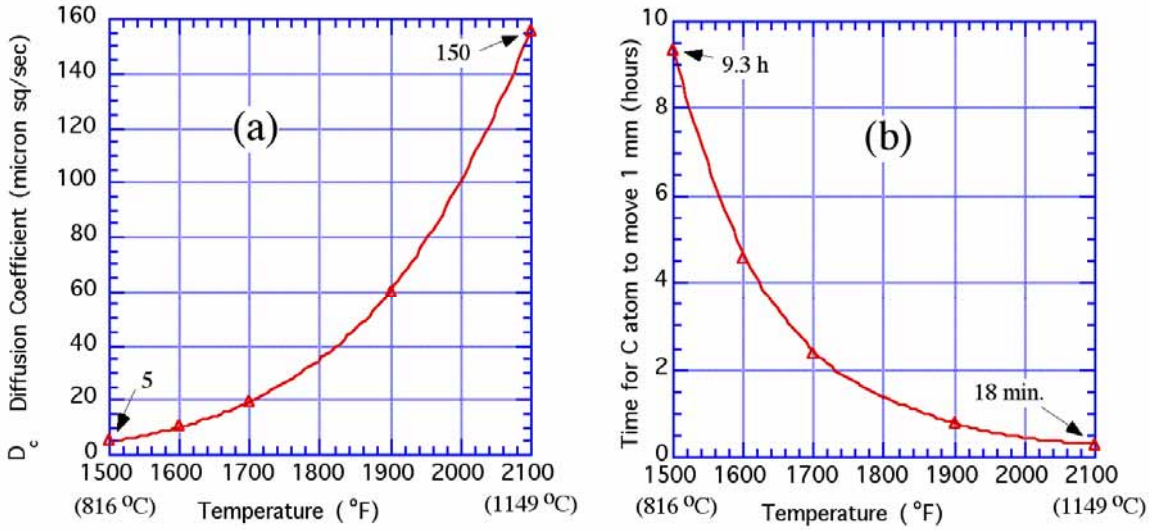

Figure 7.4 Temperature dependence of: (a) the diffusion coefficient of C in austenite, and (b) the time for a carbon atom to diffuse a distance of 1 mm in austenite.

The units of D used here will be microns squared per second. So to calculate the time in seconds one needs to convert the distance of interest, d, to microns, then square it and divide by 6 times D. To illustrate the very strong effect of temperature on diffusion the two plots in Fig. 7.4 are presented. Figure 7.4(a) is a plot showing how much the diffusion coefficient of carbon in austenite, D_c, changes as the temperature rises from 1500 to 2100 ^oF. This 600 ^oF (333 ^oC) increase in temperature raises D_c from approximately 5 to 150 (microns^2/sec), a factor of 30 (or alternately by 2900% ! - a very large change). Figure 7.4(b) uses equation 7.1 to calculate how long it will take a C atom to diffuse a distance of 1 mm in austenite (1mm = 1000 microns). Again the strong temperature dependence is obvious, as the time drops from 9.3 hours at 1500 ^oF to only 18 minutes at 2100 ^oF. Most heat treating is done in the 1500 - 1600 ^oF temperature range while most forging is done in the 2000-2200 ^oF range.

In addition to being very sensitive to temperature, the time to diffuse a distance d is surprisingly sensitive to the length of the diffusion distance, d. Equation 7.1 shows that if you reduce the distance d to 1/2 of the original value, the time goes down by a factor of 4, and for a reduction to 1/4 of the distance it goes down by a factor of 16. Hence, if you are forging steel at 2100^{o}F the time to diffuse a C atom 1/4 mm (250 microns) is 18/16 min. or roughly only 1 minute, compared to the 18 min. needed to diffuse 1 mm.

> The alternating layers in a pattern welded Damascus blade are spaced at distances on the order of 50-100 microns (2-4 mils). Blacksmiths often assume that if one of the original layers is a high carbon steel and the other a low carbon steel the final blade will consist of high and low carbon layers. Suppose the forging is being done at 2100 ^oF, a typical value. Figure 7.4(a) shows that the value of D is 150 microns squared per second and Equation 7.1 gives the time to diffuse the C atoms over a spacing of 100 microns as, t = (100 x 100)/(6 x 150) = 11 seconds. This result shows that diffusion will homogenize the steel during the forging operation so that both layers have the same carbon composition. For more on this topic see reference [7.1].

Notice in Table 6.1 that the size of the 3 major alloying elements, as well as the element Mn are about the same size as an Fe atom or larger (compare their atomic numbers). This means that they will have a difficult time dissolving in austenite because they are too big to fit in-between the iron atoms. When these atoms dissolve in austenite they do

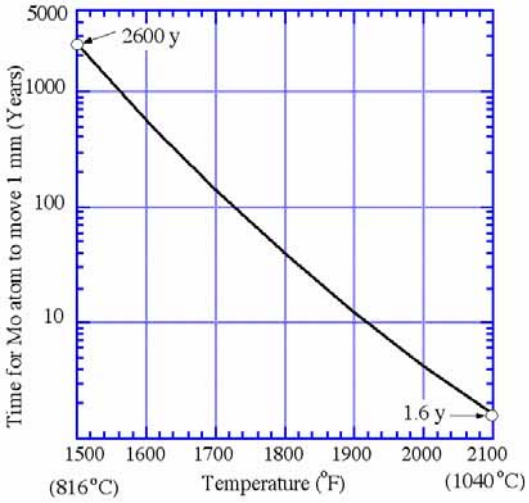

Figure 7.5 Temperature dependence of time for a Mo atom to diffuse 1 mm in austenite

so by replacing the Fe atoms on the corners or faces of the FCC crystals. Now ask yourself how one of these alloying atoms can diffuse in the FCC austenite grains. A carbon atom has an easy time diffusing because all it has to do is jump into one of the neighboring holes between the iron atoms that is not occupied by another C atoms, and there are many such empty holes available. But an alloying element lying in a face center of a given cube cannot jump into one of the holes between the iron atoms because the holes are too small. Also they will not generally be able to jump into a nearby corner sites of the cube because those sites will generally have Fe atoms on them. However, not all of those sites are occupied by iron atoms and if there is not an atom on a corner site we call it a vacancy site. It turns out that a very small fraction of the corner sites will be vacant and this fraction increases very rapidly as temperature increases. Consequently, the alloying elements are able to diffuse in austenite by jumping between vacant sites, and the diffusion rates increase rapidly with temperature. The rates of diffusion, however, are very much lower than the rates for C diffusion. The diffusion coefficients of Mn and the 3 major alloying elements have all been measured in austenite and they are all roughly the same and 1000s to millions of times smaller (depending on temperature) than the C diffusion coefficient [7.2]. To illustrate how very small their diffusion rates are compared to C, Fig. 7.5 presents data for diffusion times of Mo atoms in austenite. The times needed to diffuse a 1 mm distance at 1500 ^{o}F and 2100 ^{o}F are 2600 years and 1.6 years, respectively. As seen in Fig. 7.4 for C the times are only 9.3 h and 18 min. What these results show is that when steel is heat treated the Mn and the 3 major alloying elements will not move significantly, whereas the C atoms will move significantly. It is possible to make the larger atoms move smaller distances, in reasonably short times, but only by heating them very hot for long times. For example a Mo atom will diffuse 50 microns when austenite is held at 2200^{o}F for 8 hours. But the corresponding diffusion time for a carbon atom is only 1.7 seconds.

Carburizing and Decarburizing The carburizing process is shown in Fig. 7.2. Since charcoal is a solid form of carbon, one might expect that the C atoms get transported from the charcoal to the iron surface at the points where the charcoal makes contact with that surface. But such is not the case. If one does not have a gas in the porous charcoal no carbon transport into the iron occurs. If one uses pure carbon powder instead of charcoal no carburization occurs. Charcoal, being the remains of burned wood, contains hydrocarbons that vaporize and produce a gas containing carbon monoxide, CO. The transport of the C atoms to the iron surface is carried by gas molecules of carbon monoxide.

Suppose one is heating a piece of steel in a charcoal fire (forge) like blacksmiths have done for centuries. Air is a mixture of about 20 % oxygen (molecules of O_2) and 80 % nitrogen (molecules of N_2). When air is pumped into the charcoal the oxygen burns and

makes the fire hot. The reaction of the O_2 in the air with the C in the charcoal can be written as.

$$2O_2 + 3C \Rightarrow CO_2 \text{ (carbon dioxide)} + 2CO \text{ (carbon monoxide)} \qquad \text{Equation 7.2}$$

This chemical reaction formula is telling us that 2 molecules of oxygen react with 3 atoms of C to produce two different gases: 1 molecule of carbon dioxide and 2 molecules of carbon monoxide. The nitrogen of the air does not change form during the burning so that after the reaction the gases in the charcoal bed still contains mostly N_2, around 72 %. The remaining 28 % is a mixture of CO_2 + CO. In general, if the mixture contains a lot of CO_2 the surface of the steel bar will be decarburized and maybe even oxidized. Being oxidized means that a layer of iron oxide (FeO) will form on the surface, i.e., an oxide scale will form on the surface. But, if the mixture contains a lot of CO the steel may be carburized and you might even form cementite or graphite on the surface. These ideas may be understood by consideration of the chemical reaction equation,

$$CO_2 + [C]_S \underset{\text{decarburize}}{\overset{\text{carburize}}{\rightleftharpoons}} 2CO \qquad \text{Equation 7.3}$$

The symbol $[C]_S$ refers to a carbon atom dissolved in the steel. If the reaction proceeds to the right the equation is telling us that one molecule of carbon dioxide will react with an atom of C dissolved in the iron, lying at the surface, and 2 molecules of carbon monoxide will be generated. These CO molecules then drift off and the net result is removal of C from the steel surface, decarburization. But if the reaction proceeds to the left the equation tells us that 2 molecules of carbon monoxide decompose at the steel surface dissolving an atom of C into the steel and generating a CO_2 molecule that will float off, carburization. Hence, the relative amount of CO versus CO_2 in the gas determines whether the steel will be carburized or decarburized or oxidized. As the CO_2 content increases the reaction is biased to the right and chances of decarburization and oxide scale formation are increased.

There is a branch of science called thermodynamics that evolved around the end of the nineteenth century that allows one to calculate the actual percentages of CO_2 needed to promote decarburization. The calculations require measurements of what are known as equilibrium constants of reactions, such as Equation 7.3, and activity coefficients of the alloying elements in steel. Using these measurements, Fig. 7.6 was determined for the 3 steels, 1020, 1060 and 1095 assuming they contained 0.75% Mn. The figure allows us to predict the $\%CO_2$ on these steels that produces either carburization or decarburization. For example suppose a 1095 steel is heated to 1832 ^oF (1000 ^oC). The 1095 curve of Fig. 7.6 intersects the 1832 ^oF temperature line at around 0.068 % CO_2. This predicts that if the % CO_2 in the

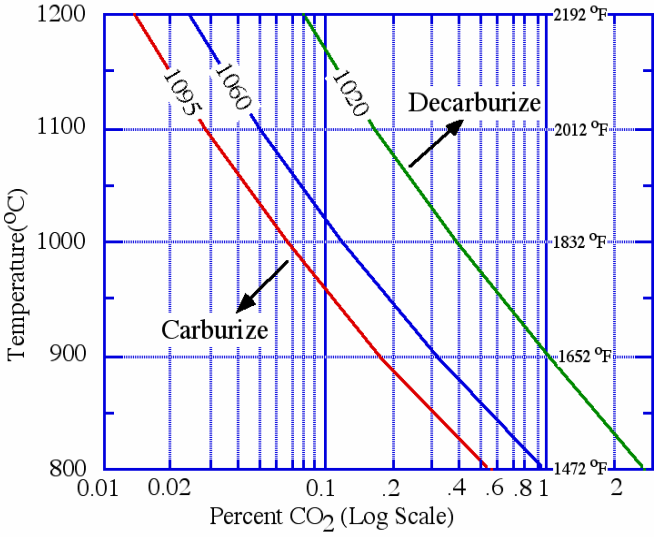

Figure 7.6 The % CO_2 above which decarburizing occurs and below which carburizing occurs.

gas surrounding the 1095 steel is less than 0.068 % the steel will carburize, but if it is above this value it will decarburize. If the gas contains exactly 0.068 % CO_2 there will be no addition or depletion of C from its surface. We will call such a gas a neutral gas and we will call the 0.068 %CO_2 value the neutral CO_2 composition for a 1095 steel at 1832 ^oF. Figure 7.6 shows that the neutral CO_2 composition increases as the carbon content of the steel decreases, going from 0.068 % for a 0.95 %C steel (1095) to 0.4 % CO_2 for a 0.2%C steel (1020) at 1832 ^oF. For any of the steels, as the % CO_2 value exceeds the neutral value by large amounts, an oxide scale (FeO) will eventually form on the steel surface. The curve for the formation of FeO scale lies well to the right boundary of the diagram shown on Fig. 7.6 and is on the order of 5 % CO_2 at 1832 ^oF.

The heat treat industry in the U.S. utilizes a gas called endothermic gas (often just endo gas) to control the CO_2 levels in furnaces to produce either neutral or carburizing gases for steel heat treating and carburizing. The gas is generated by burning natural gas (methane, CH_4) in a very hot catalytic converter. The endo gas contains close to a 20 % mixture of CO and CO_2 and the curves of Fig. 7.6 apply to its use. The % CO_2 in the gas is controlled by changing the ratio of air to natural gas fed to the gas generator, which allows the gas to easily switch from a neutral gas for heat treatments to a carburizing gas for carburizing treatments. The rest of endo gas contains 40 % hydrogen (H_2) + 40% nitrogen (N_2). The presence of the H_2 does two notable things. (1) It makes the gas explosive at lower temperatures so great care is needed with its use. (2) It speeds up the rate of C transport from gas-to-steel surface so that carburizing rates are increased, particularly at short times.

Many bladesmiths utilize furnaces that are heated by combustion of air-natural gas or by air-propane. Both natural gas (CH_4) and propane (C_3H_8) are hydrocarbon gases containing both hydrogen and carbon. Combustion with air will produce gas mixtures of CO, CO_2 and H_2, and the % CO_2 in the combustion gas will control whether or not decarburization and/or oxide scale will form on the steel being heated. Proper design of the combustion chamber combined with control of the air/gas ratio can minimize these problems.

Although present day bladesmiths generally use gas fired furnaces (forges), some still use the forges of our ancestors, which produce heat by air flowing through a bed of hot charcoal. In a charcoal forge the CO_2/CO ratio is controlled by the air flow rate through the hot bed. High flow rates produce a higher temperature but increase the CO_2/CO ratio, which can decarburize or even oxidize the steel. Lower air flow rates drop the temperature, but can carburize iron and steel. These facts explain why only the more clever blacksmiths of old were able to consistently carburize bloomery iron to levels that produced strong steels. (See historical note on page 9.)

References

7.1 J.D. Verhoeven and H.F. Clark, Carbon Diffusion Between the Layers in Modern Pattern Welded Damascus Blades, Materials Characterization, 41, 183-191 (1998).

7.2 J. Fridberg, L.E. Torndahl and M. Hillert, Diffusion in Iron, Jernkont. Ann. vol. 153, pp 263-76 (1969).

This paper summarizes diffusion coefficient measurements of the important alloying elements in steel in graphical form. For each alloying element one can determine the equations for the temperature dependence. For Cr: D = 1.7 exp(61300/RT), Mo: D = 1.8 exp(68200/RT), Mn: D = 1.1 exp(68200/RT) and for Ni: D = 0.51 exp(68200/RT), where R = 1.987, T is temperature in degrees Kelvin and the units of D are cm squared per second. A good approximation for the diffusion coefficient of C in austenite is: D=0.12 exp (32000/RT) cm^2/s. From these equations one can calculate how many times bigger the diffusion coefficient of C is than the alloying elements at any temperature and some results are given in the following table.

Number of times larger D is for C in austenite over 4 major alloying elements at 3 temperature.

Element	800 ^oC (1472 ^oF)	1000 ^oC (1832 ^oF)	1200 ^oC (2192 ^oF)
Cr	72,400	8,200	1,690
Mo	1,400,000	119,000	16,800
Mn	2,840,000	194,000	27,500
Ni	6,140,000	419,000	59,400

Summary of Major Ideas of Chapter 7

1 Diffusion is a process that allows carbon atoms to migrate into solid iron. A carbon atom dissolves in iron by fitting into the holes (interstities) lying between the much larger iron atoms. As the temperature is raised the carbon atoms begin to vibrate so much that they will often jump to the nearest empty hole. If there are more empty holes to the right than to the left, the carbon atoms will produce a net migration to the right. Hence, diffusion causes atom migration from high composition regions into low composition regions.

2 Any foreign atom dissolved in iron can move by diffusion. Because migration is always directed from high concentrations of the foreign atoms to low concentration, if you place charcoal on the surface of an iron bar and heat it the carbon atoms of the charcoal will diffuse into the iron bar since that is the direction from high carbon to low carbon concentrations. Similarly, if you heat a steel bar in air and carbon atoms are removed from its surface by oxidation to form carbon dioxide molecules, the concentration of C near the surface drops and more carbon atoms will diffuse toward the surface and be removed, thus resulting in a decarburized layer near the surface.

3 The rate of diffusion is characterized by a number called the diffusion coefficient, D. Using Equation 7.1 on p. 60 it is possible to estimate how long it will take an atom to diffuse an arbitrary distance d.

4. Rates of diffusion are very strongly dependent on temperature,. Experiments have measured how much D increases as the temperature is raised. Figure 7.4 gives results for the diffusion of C in iron. It takes a C atom 9.3 hours to diffuse a distance of 1 mm at 1500 ^oF, but only 18 minutes at 2100 ^oF. To move a C atom the distance between the bands of a forged Damascus blade (a distance of around 100 microns, about 0.004 inches or 4 mils) at a forging temperature of 2100 ^oF takes only 11 seconds.

5 The important alloying elements in steel, Cr, Mo and Ni as well as the Mn present in all steels have sizes very similar to Fe atoms. Their large size prevents them from fitting into the small intersticies (holes) between the atoms of solid Fe. Hence, it is much more difficult for these atoms to migrate by diffusion in steels and this is reflected in their much lower values of D. For example, Fig. 7.5 shows that it takes a Cr atom around 1000 years to migrate 1 mm in austenite at 1500 ^{o}F (816 ^{o}C), compared to only 9.3 hours for a C atom. See also the above table.

6 This large difference in diffusion rates for C versus the common alloying elements is important in the heat treatment of steel. It allows one to move the C atoms around without significantly changing the distribution of the alloying elements.

7 Two important processes in the heat treating of steel that are dependent upon diffusion of C atoms in iron are ***carburizing*** and ***decarburizing.*** Carburizing requires adding C atoms to the surface of an iron or steel bar, and decarburizing requires removing C atoms from the surface of a steel bar. The addition and removal of C at the bar surface is accomplished by a gas reaction involving carbon monoxide, CO, and carbon dioxide, CO_2. As C atoms are added to the surface on carburizing they then diffuse into the bar, and as they are removed from the surface on decarburizing additional atoms diffuse out from the interior of the bar.

8 When charcoal burns a mixture of CO and CO_2 gases is produced as shown by the chemical reaction Equation 7.2, p. 63. These 2 gases are also produced as reaction products in a methane (natural gas) or propane fired furnace. If the fraction of the CO_2 becomes larger than around 1 percent the hot gas will decarburize steel. But if the percent CO_2 is reduced adequately the hot gases will carburize the steel, It is possible to calculate the percent CO_2 that will give a neutral gas, no carburizing or decarburizing. As shown in Fig. 7.6, values of the neutral % CO_2 depend on both the temperature and the amount of C in the steel.

9 Many industrial steel parts, such as gear teeth and axle journals are given a carburization heat treatment which locally increases the hardness near the surface over a small distance of around 1 mm (0.04 inches). Low carbon steels, such as 1020 or 8620, are often used. After quench and tempering one ends up with a high C martensite on the surface and either a low carbon martensite or a bainitic/pearlitic interior. As shown in Fig. 4.12, the high C surface will be much harder than the low carbon interior. Hence, one produces a part with a very high hardness having excellent wear resistance combined with an interior of high toughness.

8 Control of Grain Size by Heat Treatment and Forging

Figure 8.1(a) Soap grains simulate metal grains.

As mentioned on p. 43 it is important to keep the grain size of steels as small as possible in order to improve the toughness of the steel. Wrought or cast steels will arrive with a certain grain size. This grain size can be changed significantly by further heat treatment or forging operations and it is important to understand what controls these changes.

The shape and some of the properties of grains in steel and other metals can be modeled surprisingly well with soap bubbles. You can carry out a very simple experiment in your kitchen to obtain a feel for the geometry of grains in metals. In the bottom of a clear glass, preferably of small diameter, place several drops of a liquid dishwashing soap and then add enough water to make a layer about 1/8 inch deep. After gently homogenizing with the end of a straw, blow vigorously through the straw until you have generated an array of soap bubbles that fills the entire glass. The surface tension forces in the liquid soap film are similar to the surface tension forces in the solid-solid surfaces of metal grain boundaries. This causes the shapes of the soap grains that you see and the growth of these grains to simulate metal grains very well. The soap grains show you an excellent model of the 3-dimension shape of metal grains. For example, there is a 7 sided soap grain contacting the glass surface at the lower right of the Fig. 8.1(a), and by studying the picture you can see the 3rd dimension of this grain below the glass surface. Metallographic pictures of grains, such as Fig. 1.1, only show a 2 dimensional section of the grain and the soap grains help to visualize how these grains generally extend below the surface. You may model grain growth by placing the tip of the straw at the center of the glass and gently blowing inward to expand the bubble positioned at the end of the straw. Perhaps a more pleasant way to model metal grains is to empty a glass of beer rapidly as is illustrated in Fig. 8.1(b)

Figure 8.1(b) Beer bubbles model metal grains

Grain Size As seen in the Fig 8.1 bubble models of grains, the grains are irregularly shaped structures which makes it difficult to easily characterize their size. The ASTM adapted a method for measuring grain size in 1947 that is widely used for characterizing grain size in steels. See Ref. [8.1] for a discussion of the evolution of the method and for more details. A grain size number G is defined by the equation,

Table 8.1 ASTM Grain Size Numbers

ASTM No.	Average Diameter (microns)	Relative Size
-1	510	Very coarse
0	360	
1	250	Coarse
2	180	
3	125	
4	90	Medium
5	65	
6	45	
7	32	Fine
8	22	
9	16	
10	11	Very Fine
11	8.0	
12	5.6	
13	4.0	Ultrafine
14	2.8	
15	2.0	

$$n = 2^{G-1} \quad \text{or} \quad G = 1 + \text{Log } n/\text{Log } 2 \qquad \text{Eqn. 8.1}$$

where n is defined as the number of grains per square inch on a micrograph having a magnification of 100x. Figure 1.1 is at a magnification of 100x, so that if one counts the number of grains shown and measures the area of the circular micrograph one can calculate the grain size number G from Equation 8.1. Because a large fraction of the grains in this micrograph contact the edge and are therefore not fully represented, some error will be introduced. Corrections for such problems are discussed in [8.1]. Table 8.1 presents a list of the ASTM grain size number G along with a corresponding average grain diameter given in microns (1 μm = 0.001 mm). The right hand column of the table indicates general guidelines for characterizing sizes. The very coarse sizes are only encountered in large ingots or steels held near their melting points for long times. The finest sizes are only encountered in steels given special treatments that inhibit grain growth, and some of these treatments will be discussed later.

Grain Growth As austenite is heated to higher temperatures or held for longer times at temperature the average grain size is found to increase. This process of grain growth occurs by smaller grains shrinking in size until they disappear and larger grains growing in size; the net effect being an increase in the size of the average grain. It is the surface tension force in the austenite/austenite grain boundaries that causes grain growth. The process may be understood by considering the soap bubble grains of Fig. 8.1, which also grow by the same mechanism. Figure 8.2 presents an analysis of a force balance on a short segments of grain boundaries snipped out of a small and a large grain. The magnitude of the surface tension force is represented by the length of the arrow labeled T and this force is pulling out from both ends of the segments as shown. (The grain boundary is like a piece of stretched rubber, so a segment must have a force pulling out from each end.) This surface tension force always acts in the plane of the boundary. Therefore the lower curvature of the big grain results in the T force being directed more vertically on Fig. 8.2. The arrow labeled T_h is the horizontal component of the T force. This is the fraction of the T force that is directed in the horizontal direction. Note that there are two such forces acting to the right on each segment. But, movements of the soap grain boundaries caused by the forces are too slow to be visible. This tells us that the force of $2T_h$ is not able to pull the grain boundary segment to the right. The reason is that a pressure difference develops across the boundary that balances this

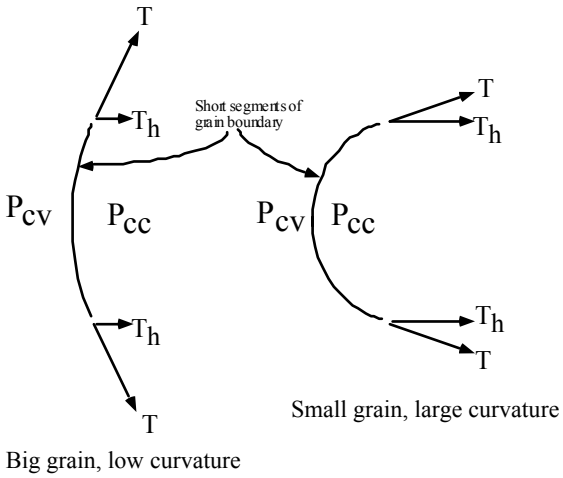

Figure 8.2 How surface tension on a segment of grain bourndary produces pressure difference across boundary.

force. The air pressure on the concave side of the boundary is called, P_{cc} and on the convex side, P_{cv}. The air pressure on the concave side increases over that on the convex side by the amount needed to balance the surface tension force to the right, $2T_h$. (This pressure increase is similar to the air pressure causing a balloon to blow up, it is higher on the convex side (inside) of the balloon.) Remember, pressure is force per unit area, so the pressure difference, P_{cc} - P_{cv} is a force per area to the left and it adjusts to balance the surface tension force going to the right. What this means is that the pressure is always higher on the concave side of curved boundaries. In soap bubble grains this higher pressure on the concave side causes the air molecules to diffuse through the soap to the low pressure convex side. So the soap bubble grain boundaries always move slowly toward the concave side as the air diffuses to the convex side. Note that the force, $2T_h$ is larger for the smaller grains. This means that the small grains will shrink faster due to a larger pressure difference across them. In fact very large grains will be convex-out and will always tend to eat-up their neighbors by grain growth. Note that side 2 of the labeled 7 sided grain of Fig. 8.1(a) is concave toward the neighboring 5 sided grain to its left. Hence, boundary 2 will tend to move into the 5 sided grain causing it to shrink and the larger 7 sided grain to grow. The 4 sided grain labeled at the top right of Fig. 8.1(a) illustrates the concave-in geometry that causes the smaller grains to shrink.

This same type of action occurs in the grain growth of austenite. It is a bit unusual to talk about a pressure in a solid, but the analogy holds. The higher pressures on the concave side of the austenite grain boundaries cause the iron atoms to jump across the boundaries from concave to convex sides, thereby causing large grains to grow at the expense of small grains. This motion of the iron atoms occurs by a jumping process similar to the impurity diffusion discussed above. Like that diffusion, the process is very very sensitive to temperature, going faster at higher temperatures where thermal energy is causing larger vibrations of the atoms. Hence, the grain growth of austenite is very sensitive to the austenitizing temperature, and that is why it is important not to austenitize at temperatures any higher than needed to homogenize the austenite. Figure 8.3 presents data on austenite grain size of 1060 steels held for 6 minutes and 2 hours at increasing austenitization temperatures. Note that raising the temperature of the 6 min. hold from 1400 to 1700 ^{o}F nearly triples the grain size, from 33 to 94 microns. Like most metallurgy rate processes, grain growth is more sensitive to temperature than time. For example, increasing the austenitization hold time at 1700 ^{o}F from 6 to 120 minutes, a factor of 20, increases the grain size from only 94 to 174 microns, a factor of 1.85.

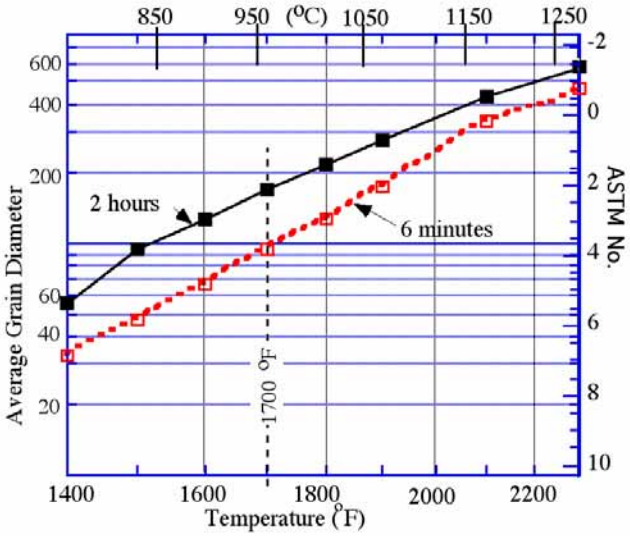

Figure 8.3 Average grain diameter versus austenitizatoion temperature. 1060 steels austenitized for 6 min. and 2 hours [8.2].

New Grains formed by Phase Transformation

For simplicity consider first a pearlitic steel. At room temperature there will be some average pearlite grain size. When this steel is heated above its A_{c1} temperature

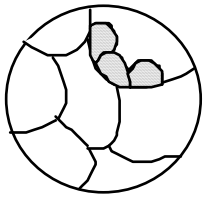

Figure 8.4 Three new grains form along an old grain boundary.

austenite grains will begin to form. The new austenite grains start to form on the old pearlite grain boundaries as shown schematically in Fig. 8.4. After a short time all the old pearlite grains are replaced with a completely new set of austenite grains. The new austenite grains have their smallest size immediately after the pearlite is consumed, before significant grain growth occurs as the temperature rises and time proceeds. Following are two factors that enhance the formation of the smallest possible initial austenite grain size.

(1) Faster heating rates cause the austenite grains to nucleate closer together and enhance small grain size.

(2) Smaller original pearlite grains produce smaller austenite grains.

When the austenite is cooled back down below the A_{r1} temperature a whole new set of pearlite grains is formed and the same two factors: rate of transformation and size of the prior grains, control the size of the new grains. Hence, on simply heating and cooling through the transformation temperature three different sets of grains are involved. When dealing with hypoeutectoid steels the same ideas apply only now one must heat above the A_{c3} temperature before 100 % austenite is formed. If one wants to reduce the grain size of a ferrite/pearlite steel, a simple technique is to heat into the austenite region holding the maximum temperature as low as possible and the time as short as possible and then rapidly cooling back to room temperature as fast as possible without forming bainite, assuming it is not desired. Since smaller initial grain size promotes smaller final grain size, repeating this cycles several times will enhance fine grain size.

When heat treating to form martensite, toughness is also enhanced by fine grained austenite because it results in a finer lath or plate size in the martensite. Again the same ideas apply. Rapid heating and repeated cycling produce smaller martensite microstructures. Grange [8.3] has presented a study showing the beneficial effect of small austenite grain size on the mechanical properties of 8640 steel. He achieved grain sizes in the ultrafine range of ASTM No. 13 to 15 by a 4 cycle process where the steel was austenitized in molten lead for around 10 s, cooled to room temperature, cold worked and then cycled again. A series of similar experiments was performed here on 3 steels to examine the effectiveness of thermal cycling alone, no cold working was employed. The steels were heated by immersion in a salt pot. Initially the steels were austenitized for 15 min. at 1650 ^{o}F and oil quenched in rapidly stirred oil. Then the steels were given 3 thermal cycles consisting of a 4 minute austenitization in 1450 ^{o}F salt and a quench in rapidly stirred oil. The grain sizes were measured with the same technique described by Grange [8.3] and the ASTM numbers before and after the 3 cycle treatment are given in Table 8.2. It is seen that ultrafine grain sizes were obtained. Figure 8.5 presents photomicrographs of the martensite structures found in the 1086 steel before and after the cycling. The composition of this steel is in the range where we expect the martensite to be a mixture of lath and plate morphologies, and in the uncycled coarser grained sample Fig. 8.5 (A), one can see dark plates in a matrix of the lath structure. However, in the finer grained austenite produced by thermal cycling, Fig. 7(B), the martensite structure is clearly finer and the plates are not easily identified.

Table 8.2 ASTM grain size no. of austenite before and after the 3 cycle treatment done here.

Steel	ASTM Number	
	Initial	After cycling
1045	9	14
1086	11	15
5150	8.5	14

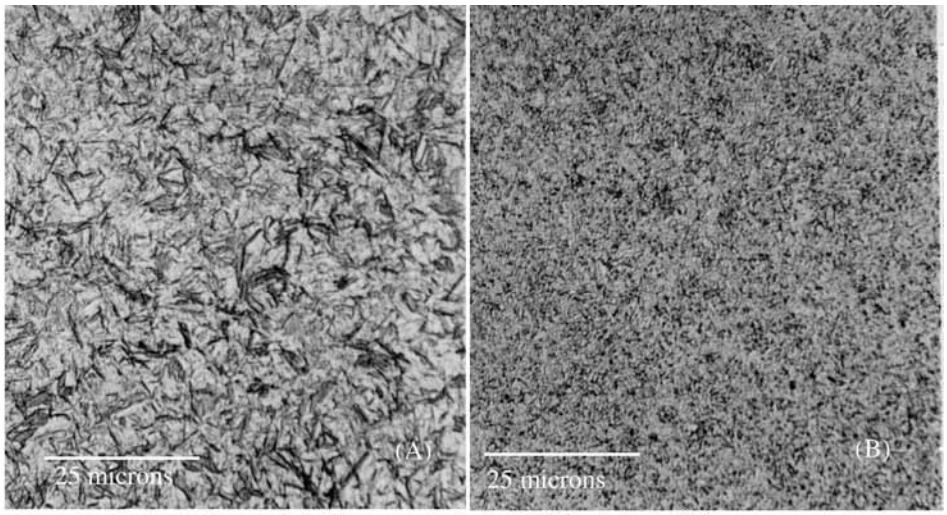

Figure 8.5 The martensite in 1086 steels at 800 x.
(A) Uncycled sample (ASTM No. 11). (B) Cycled sample (ASTM No. 15).

New Grains formed by Recrystallization When a metal is plastically deformed the flow of the metal matrix generates defects in the crystal structure. These defects (called dislocations) are planes of atoms that are shifted off of the sites they occupied prior to the flow and they are locations where the energy of the crystal is increased. This means that as the metal is made to plastically flow, energy is being stored in the crystals, in the form of defects, and the more flow the higher the defect density and the more the stored energy. If one plastically deforms a metal by forging or rolling, the grains in the metal will deform into elongated pancaked shapes lining up in the direction of the metal flow. The thinner grains of Fig. 8.6(a) are such elongated grains in a 1010 steel that was cold rolled 90 %. This terminology of 90% cold work means that the cross sectional area of the metal was reduced 90 % by mechanical deformation at room temperature. In rolling deformation the slab width changes little during reduction, so a 90 % reduction in area is the same as a 90 % reduction in thickness. These elongated grains now contain a high defect density and upon heating a new set of grains will form that contain a low defect density because they have a lowered energy content. Figure 8.6(b) shows the new grain set after about 80 % of the original structure has been replaced, and Fig. 8.6(a) shows the new grain set after about 10% replacement. The formation of this new set of low defect density grains is called ***recrystallization***. The new grains are all individual crystals and the name conveys the idea of an old set of crystals (the deformed grains) transforming into a new set.

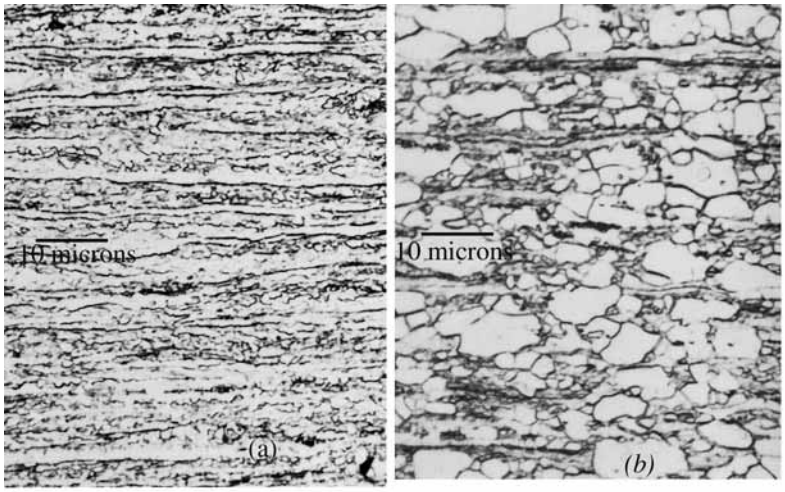

Figure 8.6 A 1010 steel cold rolled 90 % and then annealed at 1025°F (552 °C).
(a) 2 min.-10% recrystallized. (b) 15 min.-80 % recrystallize [8.4].

In metals like steel it is possible to obtain new sets of grains by the 2 different techniques described here: (1) Heating to produce a phase transformation, or (2) deforming and heating to produce recrystallization. The first technique works for steel because of the BCC to FCC crystal structure change

that occurs in iron at the A temperature. In metals and alloys of copper and aluminum, however, there are usually no A type transformation possible because these metals retain the FCC crystal structure all the way from room temperature to the melting point. Therefore in these metals recrystallization is the only way to produce a new sets of grains.

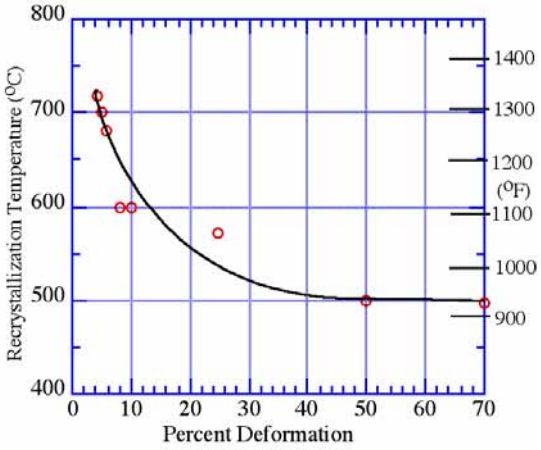

Figure 8.7 Data on recrystallization temperature of low carbon steels as a function of the amount of prior cold work [8.5].

To produce recrystallization one must heat the cold worked metal up to a temperature called the ***recrystallization temperature***. The recrystallization temperature depends on the amount of prior deformation that was used. More deformation increases the defect density and lowers the recrystallization temperature. However, as shown in Fig. 8.7, the drop in recrystallization temperature stops after around a 50 % reduction. This results because the increase in defect density saturates at a maximum value for deformations larger than around 50 %. Therefore, if one talks about the recrystallization temperature of a given alloy, it is assumed that the deformation used is roughly 50% or more. Another complication is the time for recrystallization. Recrystallization will occur faster at higher temperatures. So data such as that of Fig. 8.7 are generally presented for the 1 hour recrystallization temperature. That temperature is defined as the temperature where recrystallization is complete in roughly 1 hour. An important practical question when trying to produce recrystallization is how much cold work is needed to cause recrystallization to occur. The data of Fig. 8.7 show that in low carbon steels recrystallization will occur with only around 5% cold work, but the temperature needed is significantly higher than required with larger amounts of cold work. And as suggested by Fig. 8.6 recrystallization will start at relatively short times in low carbon steels, but will take 30 to 60 minutes to complete at the temperatures defined by Fig. 8.7.

When forging austenite the sample is necessarily at a high temperature. Because the deformation is being applied rapidly in the forging operation the defect density can accumulate in the deformed austenite grains and cause recrystallization to occur during the reduction that occurs on forging. The same is true of hot rolling. This type of recrystallization is often called dynamic recrystallization, in contrast to static recrystallization which occurs after mechanical flow has stopped. Dynamic recrystallization of austenite does several things. The reasons metals work harden at low temperatures is because the increased defect density makes the metal stronger. In dynamic recrystallization work hardening does not occur because the new recrystallized grains have a low defect density. Hence, the worked metal remains soft and pliable due in large part to the dynamic recrystallization. Also, the dynamic recrystallization in hot forging allows the continuous generation of new sets of austenite grains with each forging cycle, which prevents excessive grain growth at the high temperatures where forging and rolling of austenite is usually done, around 2200 ^{o}F (1200 ^{o}C).

The temperature at which a metal recrystallizes depends on its melting point. Tin melts at a low temperature, 232 ^{o}C (450 ^{o}F), and therefore in alloys such as soft solder recrystallization can occur at room temperature. Take a thick copper wire and bend it back and forth and it will harden at the bend and break there. Do the same for the wire from a roll of soft solder and you find you can

continue to bend it almost indefinitely with no hardening or breaking. The soft solder is recrystallizing in your hands at room temperature, producing new low defect grains that are soft, while the copper retains its original grains and they progressively become harder and brittle as the defect density increases on bending.

Effect of Alloying Elements

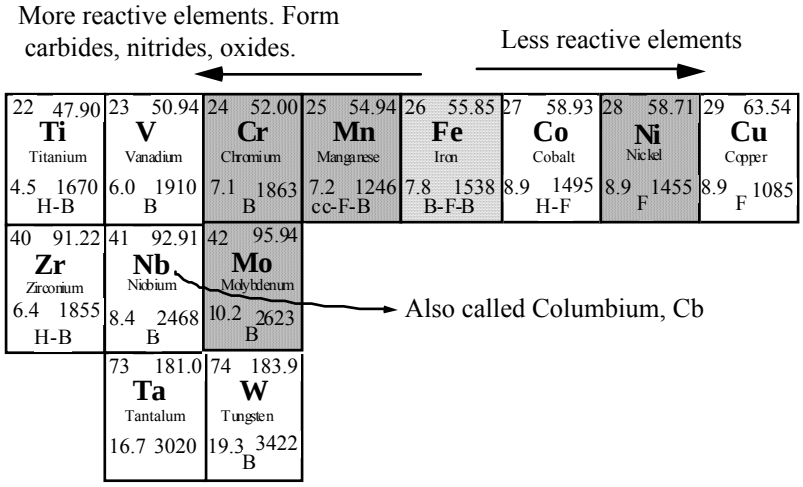
More reactive elements. Form carbides, nitrides, oxides.
Less reactive elements
22 47.90 Ti Titanium 4.5 1670 H-B
23 50.94 V Vanadium 6.0 1910 B
24 52.00 Cr Chromium 7.1 1863 B
25 54.94 Mn Manganese 7.2 1246 cc-F-B
26 55.85 Fe Iron 7.8 1538 B-F-B
27 58.93 Co Cobalt 8.9 1495 H-F
28 58.71 Ni Nickel 8.9 1455 F
29 63.54 Cu Copper 8.9 1085 F
40 91.22 Zr Zirconium 6.4 1855 H-B
41 92.91 Nb Niobium 8.4 2468 B
42 95.94 Mo Molybdenum 10.2 2623 B
Also called Columbium, Cb
73 181.0 Ta Tantalum 16.7 3020
74 183.9 W Tungsten 19.3 3422 B

Figure 8.8 General reactivity of the important elements in steels.

Figure 8.8 presents a portion of the periodic table of Table 6.1 that surrounds Fe and contains several elements sometimes added to steels in addition to the 4 major alloying elements of Mn, Cr, Mo and Ni. Some elements tend to be much more reactive than other elements. Such reactive elements will combine with the elements C, N, O and S to form carbides, nitrides oxides and sulfides. In addition to carbon steels always contain a low level of N, O and S. Consequently, it is common to have carbides, nitrides, oxides and sulfides present in steel. These are all chemical compounds that tend to melt at very high temperatures and to be very hard and brittle. Cementite is an iron carbide (chemical formula Fe_3C) and it is hard and brittle. The cementite in steel is in a form that is generally not brittle because of its very small size and because it is surrounded by ductile ferrite. This is true for the cementite in pearlite (remember, pearlite contains only around 11 % cementite and it is present as very thin plates), and it is true for the very small cementite particles in hypereutectoid steels, such as those shown in Fig. 6.4 in 52100 steel.* The arrows at the top of Fig.8.8 show that the elements to the left of Fe tend to be chemically reactive elements, while those to the right are less reactive. Of the 4 common alloying elements, Cr and Mo are carbide forming elements and, in general, will prefer to segregate into the cementite constituents of steel, while Ni is not a carbide forming element and will prefer to segregate into the ferrite, and Mn tends to be sort of in-between these groups. The elements on the left, Ti, Zr, V, Nb, Ta and W all form very stable carbides (tantalum carbide is the highest melting solid in the universe[melting point = 4000 ^oC (7100 ^oF)], besides solid carbon). There are 3 other important reactive elements in steel, Si, Al and B. The steel making process produces low levels of Si and Al in all steels and B is sometimes an additive. The oxides, nitrides and sulfides formed by all of the reactive elements in steel are generally present as small particles that are called ***inclusions***. These inclusions are usually present at very small volume percentages and in some cases are detrimental to toughness as was discussed on pp. 53 for sulfide inclusions. At other times, however, the

* Note: The term nanomaterial has become a current buzzword in the world of science for possible exciting new materials. The pearlite spacing in an air cooled 52100 steel runs around 0.075 microns, which is 75 nanometers (nm). The cementite plate thickness is just 11 % of this value which shows that these plates are only around 8 nm thick. In the drawn pearlitic wire used for cables and discussed on p. 41 the pearlite spacing is reduced by the drawing operation and cementite plate thicknesses of 1 nm are obtained for maximum drawing. Hence it is clear that pearlite is an example of a nanomaterial that has been widely used long before this buzzword came along.

inclusions can offer beneficial effects, as will be discussed here in considering their effect on grain growth of austenite.

Adding alloying elements to steel can produce a very significant reduction in the rate of grain growth of austenite. The alloying elements produce this reduction in grain growth rates by two different mechanisms, which we will call, (1) Particle drag and (2) Solute drag.

1. Particle Drag To understand how the importance of particle drag was discovered one needs to understand an aspect of steel ingot making practice. Until only about 2 decades ago steel in the US was produced predominately by solidification of molten steel in large individual ingots. (The major tonnage of steel is now produced by continuous casting. It is often referred to as strand cast steel, as the production line facility is called a strand.) The oxygen content in the molten steel was generally high enough that upon cooling in the ingot mold, the oxygen would combine with the C in the steel to form bubbles of carbon monoxide (CO) gas. This hot gas would boil up out of the surface of the ingot producing a fire-works type display and the ingots so produced were called ***rimming ingot***s because they had a soft ferrite rim at their surface. Rimming ingots were only useful for low carbon non-alloy steels which, incidentally, represented a large fraction of steel production because rimming ingots were used for the sheet material in such items as car bodies and appliance bodies. With alloy steels, to avoid oxidation of the alloying elements, one needed to reduce the oxygen level in the ingot to the point where the CO boil did not occur, and these ingots were call ***killed ingots***. The method used to reduce the oxygen content of killed ingots was to add small amounts of either Si and/or Al to the ingot. These reactive elements would tie up the oxygen as Si and Al oxides thereby lowering the amount of oxygen dissolved in the molten steel and stopping the CO boil. In the first half of the 20th century it was realized that steels that were Al killed had a much superior resistance to grain growth than steels that were Si killed . The grain growth data of Fig. 8.3 were taken on a Si killed 1060 steel. These data are replotted in Fig. 8.9 and compared to grain growth data for an Al + Si killed 1060 steel. Note the dramatic reduction in grain growth produced by the increase of the aluminum content from only 0.006 % to 0.02 % Al. Modern strand cast steels are all Al killed steels, sometimes referred to as AK steels.

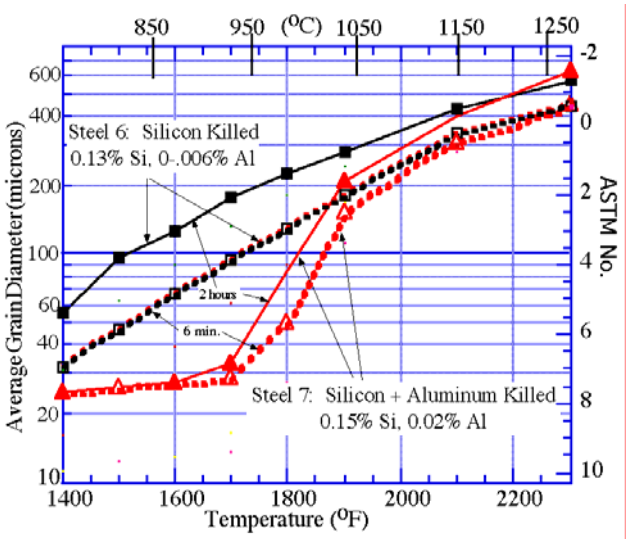

Figure 8.9 Average grain diameter of austenite versus temperature in two 1060 steels austenitized for 6 min. and 2 hours [8.2].

For many decades it was not known what caused this dramatic difference. Finally, in the 1960's it was shown that the effect was produced by the formation of very small particles of aluminum nitride that formed in the steel as it cooled down. The small particles exert a drag force on the growing grain boundaries which is called "particle drag" here. The small AlN particles have sizes on the order of 0.01 microns (requiring electron microscopes to see) and upon heating they coarsen in size and when they

become larger than some critical value they are no longer able to pin the austenite grain boundaries. In steel 7 of Fig. 8.9 the critical size was achieved at a temperature of around 1700°F and above this temperature grain growth accelerated up to the value found for steels free of particles. Experiments have shown that particle drag is optimized by:

(1) minimizing the size of the particles.
(2) choosing particles that resist coarsening or dissolving to high temperatures.
(3) maximizing the volume fraction of particles.

Generally, coarsening of a particle is lower for higher melting particles. The reactive elements in Fig.8.8 are ideal for forming particles and since the highest melting point metals such as Nb (also called Cb in U.S.), Ta and W produce the highest melting carbides, we expect them to resist coarsening to high temperatures. Figure 8.10 presents data showing the effectiveness of very small additions of Nb on grain growth of a 1040 steel. Note that the onset of accelerated grain growth is increased from the 1700 °F value for the aluminum nitride particles of Fig. 8.9 to temperatures of just over 2000 °F. The Nb is found to react with both the carbon and nitrogen in the steel and form particles that are called niobium carbonitrides. As the figure shows, these particles are able to effectively pin the austenite grain boundaries at temperatures up to 2000 °F.

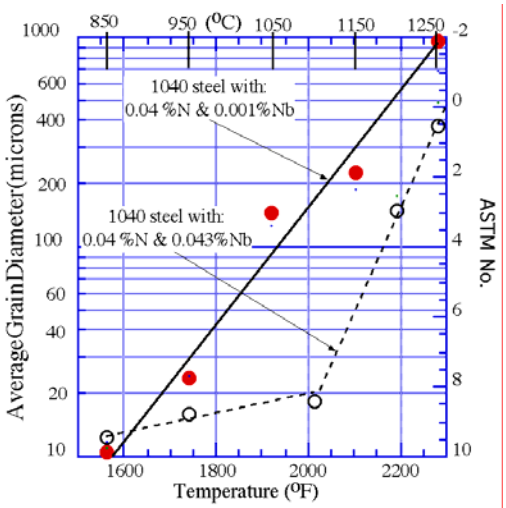

Figure 8.10 Effect of adding a pinch of Nb on one hour grain growth of a 1040 steel [8.6].

The discovery that particle drag would inhibit grain growth played a big role in the development of a new class of steels. These are structural steels called HSLA (high strength low alloy) steels, that are non-heat-treated low carbon steels. The C level is around 0.15 to 0.25 %C and for this low level they produce relatively high strengths in the hot-rolled condition, tensile strengths of 415-700 MPa (60-100 ksi). Grain refinement is aided by the addition of one or more of the reactive metals, Nb, V, Ti or Al. Because these elements are added at very low percentages, on the order of 0.04 to 0.1 %, the steels are sometimes called microalloyed steels. The small particles reduce austenite grain growth and also increase the recrystallization temperature of austenite. This combination allows the steel mill to produce a fine final ferrite grain size by a process called controlled rolling. The process first generates a fine austenite grain size and then rolls it at a relatively low temperature with the highest reduction that will not recrystallize the austenite. The high density defect structure remaining in the deformed austenite grains causes the ferrite grains that form in them on cooling below A_{r1} to be very fine. The resulting ferrite/pearlite or ferrite/bainite steels have very fine grain sizes and higher levels of strength and toughness than plain carbon structural steels.

2 Solute Drag Any element that is dissolved in a phase, such as C dissolved in FCC iron or N dissolved in BCC iron, is called a ***solute***. As explained on pp. 61-2, when alloying elements such as Cr, Ni and Mo are dissolved in iron they are too big to fit into the holes between the iron atoms and they must replace the iron atoms from their preferred sites on the FCC lattice sites or the BCC lattice sites. These solute atoms will

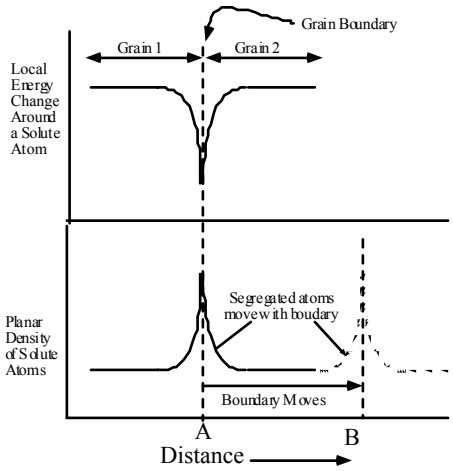

Figure 8.11 Segregation of solute atoms to grain boundaries.

not be the correct size to fit in the vacant Fe lattice sites easily and therefore they will introduce a local energy increase by pushing or pulling on the neighboring iron atoms. However, if a solute atom is near a grain boundary it can reduce this energy increase significantly by hopping onto the grain boundary surface. The reason for this is that the grain boundary surface is a region where the iron atoms do not match up very well from one side to the other of the surface. Hence, there is more open space along this boundary than elsewhere and so the solute atoms will fit in there with less pushing or pulling of neighboring iron atoms. Consequently the localized energy increase around the solute atoms will go down if the atom sits on the grain boundary, as is shown schematically at the top of Fig. 8.11. Because of this energy decrease the solute atoms will prefer to lie on the grain boundary and if one plots the planar concentration of solute atoms (solute atoms per area parallel to the grain boundary) the solute concentration will be highest on the grain boundary, as shown at the bottom of Fig. 8.11. This phenomena is call grain boundary segregation and it is largest for the atoms that do not fit well into the vacant lattice sites.

Now consider what must happen when one of these grain boundaries with atoms segregated on them tries to move. The sketch at the bottom of Fig. 8.11 shows that when a boundary moves from location A to location B, the atoms that have segregated onto the boundary must move along with the boundary as it migrates from A to B. But these atoms can only move from position A to B by the process of diffusion. And since these atoms are too large to fit into the holes between the iron atoms of the BCC or FCC lattice sites they will have very low diffusion coefficients, as was shown on Fig. 7.5 versus Fig. 7.4(b). Therefore as the grain boundary moves it must drag the solute atoms along with it and hence the solute atoms will exert a drag force on the boundary and slow down its migration rate. This is the effect known as grain boundary drag. The 4 major alloying elements, Mn, Cr, Mo and Ni are not particularly effective at forming fine particles that will give a strong particle drag effect as do Nb, Ti, V and Al. But they will produce a grain boundary drag effect and can therefore reduce the rates of grain growth. To illustrate this effect the data of Fig. 8.12 are presented. The data show that that grain growth in an 8620 steel is significantly lower than in a 1018 steel. Table 6.4 shows that 8620 steel is a triple alloyed steel containing low levels of Cr, Mo, and Ni. It is a commonly selected alloy for applications requiring carburization. To reduce carburizing times and save energy costs, it is desirable to carburize at as high a temperature as possible. A problem in doing this with plain carbon steels, such as 1018, is that excessive austenite grain growth may occur. The data of Fig. 8.12 show that an advantage of 8620 steel is a

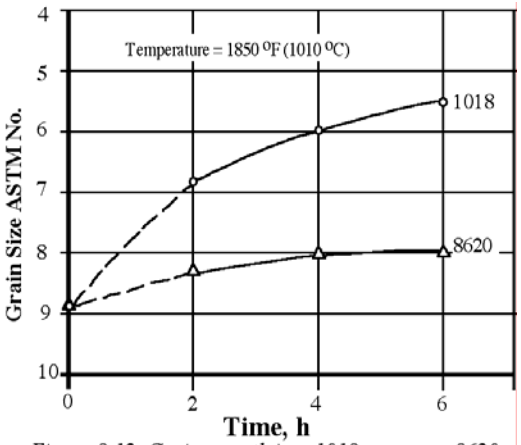

Figure 8.12 Grain growth in a 1018 versus an 8620 steel at 1850 °F [8.7].

reduced rate of grain growth.

References

8.1 G. F. Vandervoort, Metallography, Principles and Practice, McGraw-Hill, New York, N.Y. (1984).
8.2 O.O. Miller, Influence of Austenitizing Time and Temperature on Austenite Grain Size of Steel, Transactions American Society for Metals, vol. 43, pp. 261-287 (1951).
8.3 R.A. Grange, Strengthening Steel by Austenite Grain Refinement, Transactions American Society for Metals, vol. 59, pp. 26-48 (1966).
8.4 Metals Handbook, 8th Edition, vol. 7, p. 10 (1972).
8.5 H.F. Kaiser and H.F. Taylor, Transactions American Society for Metals, vol. 27, p. 256 (1939).
8.6 R. Coladas et. al., Austenite Grain Growth in Medium and High Carbon Steels Microalloyed with Niobium, Metals Science, pp. 509-516 (November 1977).
8.7 G.O. Ratliff and W.H. Samuelson, High Temperature Carburization is Routine Process at Shore Metal, Metal Progress, vol. 108, 75-78 (September 1975).

Summary of Major Ideas of Chapter 8

1 The grains of steel, first discussed with Fig. 1.2, have 3-dimensional shapes that are well modeled by soap bubbles, as shown in Fig. 8.1(a). Similarly, they are modeled by the bubbles that form in a beer bottle after rapidly emptying the bottle, Fig. 8.1(b).

2 Grain size is characterized by the **ASTM grain size number**. Large numbers, like around 10, indicate small grains, and small numbers, like around 2 indicate large grains. See Table 8.1 for details.

3 As austenite is heated to higher temperatures the grain size increases, a process called **grain growth**. It is produced by the surface tension forces acting in the grain boundaries which cause small grains to shrink and large ones to grow. It is well modeled by water bubbles and may be visualized well by studying the growth of the bubbles in a beer bottle after rapidly emptying its contents. Grain growth increases very rapidly as you raise the temperature and less rapidly with time held at a temperature, see Fig. 8.3.

4 The toughness of steel is improved as grain size becomes smaller. For this reason it is important to do heat treatments at as low a temperature as possible to reduce grain growth of the austenite.

5 In a steel, the grain size may be dramatically reduced by a cyclic heat treatment where the temperature cycles above the A_{c3} (and/or the A_{c1}) and below the A_{r1} values. With each heating ramp a whole new set of austenite grains form and in each cooling ramp a new set of ferrite/pearlite grains form. The reduction in grain size is enhanced by using rapid heating and cooling rates such as is possible with salt pot quenching, It is also enhanced by keeping the maximum temperature as low as possible. Ultrafine steel grain sizes are easily obtained, compare the data of Table 8.2 to Table 8.1.

6 A new set of grains may also be formed by the process of **recrystallization**. The steel must be fairly heavily deformed and then heated. The deformation introduces defects (planes of atoms displaced from their low energy positions) into the grains which raises their energy level. Subsequent heating produces a new set of defect free grains because they

have a lower energy content. The new strain free grains form at a temperature called the recrystallization temperature. The recrystallization temperature depends on the amount of prior deformation for steel as shown on Fig. 8.7.

7 When forging austenite at high temperatures, recrystallization often occurs during forging as the metal is deformed in the forging dies. The process is called **dynamic recrystallization**. The defects which form in steel grains on deformation cause the grains to become harder, stronger and brittle. The new strain free grains formed in recrystallization are softer and ductile. Hence, dynamic recrystallization allows the austenite to be deformed large amounts without becoming brittle, and at the same time refines grain size.

8 Alloying elements in steel can be subdivided into chemically reactive elements, those to the left of Fe in the periodic table, Fig. 8.8, and non-reactive elements to the right of Fe in the table. The reactive elements will form compounds, which appear as discrete particles in the steel. These elements react with C, N, O, and S in the steel to form carbides, nitrides, oxides and sulfides that are sometimes called inclusions.

9 Addition of alloying elements can produce dramatic reductions in the grain growth of austenite. This reduction is produced by different effects in the reactive versus non reactive alloying elements.

10 If the particles formed by the reactive elements can be made very small they will reduce austenite grain growth until the temperature becomes high enough to either dissolve them or make them grow to larger sizes (coarsen). Addition of minute quantities (like 0.04 %) of the reactive elements lying in the left 2 columns of Table 8.8 are very effective in reducing grain growth and are the basis of the relatively new HSLA (High Strength Low Alloy) steels, see Fig. 8.10 and discussion.

11 The less reactive elements, such as the common alloying elements, Ni, Mn, Cr and Mo produce a reduction in grain growth by segregating to the austenite grain boundaries. They become trapped in the grain boundaries and are dragged along with them as they move, thereby slowing grain growth. Fig. 8.12 presents data for this effect by comparing grain growth at 1850 ^{o}F in a plain carbon steel and a Cr-Mo-Ni low alloy steel, both having around 0.2 %C.

9 - Hardenability of Steel

The professional metallurgy organization, ASM International (formally the American Society for Metals) has published an excellent handbook [9.3] on the heat treating of steels. This handbook which will be referred to fairly extensively in this chapter and the next.

The subject of this chapter, hardenability, is often confused with hardness and, hopefully, the difference in these two concepts will be made clear. Suppose you want to harden a round bar of steel. Generally the process involves 3 steps:

1) *Austenitization step* Heat the steel to form austenite (usually 100 % austenite, but not always). The recommended austenitization temperatures vary with the carbon composition of the steel and are shown roughly on Fig. 4.22. Various aspects of austenitization will be discussed in Chapter 11.

2) *Quenching step* Rapidly cool the steel by immersion in water or oil. Quenching techniques will be discussed further in Chapter 12.

3) *Tempering step* Heat the steel to a low temperature to remove brittleness. The tempering process will be discussed further in Chapter 10.

The steel will be hardened after the second step but the tempering step is included in the list because it is virtually always employed in the heat treatment of hardened steels.

In order to fully harden the steel bar the austenite must transform to martensite at all points from the surface to the center of the bar. Consider again the microstructures of the quenched steels shown in Figs 4.18 and 4.19. As explained in Chapter 3, the reason that pearlite and bainite have formed on the old austenite grain boundaries is that the temperature of the austenite did not fall below the M_s temperature fast enough to avoid their formation. And once pearlite or bainite form in austenite the volume they occupy cannot transform to martensite. To fully transform austenite to martensite the cooling rate on quenching must be above some critical value throughout the austenite. Now think about how the temperature will drop in a round bar that is quenched in water. The rate at which the temperature drops will be fastest at the bar surface and slowest at the bar center. Hence it is possible that the outer regions of the bar will be fully martensitic, but the central regions will have pearlite and bainite mixed in with the martensite. If this happens the hardness of the bar will be lower in the central regions. Such a situation is shown for the 1060 bar on Fig. 9.1. The figure shows the hardness of an oil quenched 1 inch diameter bar at positions from the center (r = 0) to the surface (r= 1/2 inch, or r/R = 1, where r is any radial position and R is the outside radius of the bar).

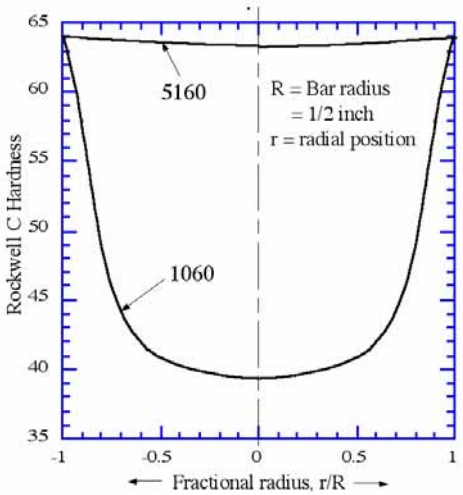

Figure 9.1 Hardness versus radius in 1 inch diameter bars of oil quenched 1060 and 5160 steels.

Now consider a 5160 steel. From Tables 6.2 and 6.4 one sees that the only significant difference in the composition of the 1060 and 5160 is the addition of 0.8 % Cr in 5160. Figure 9.1 shows that the as-quenched

hardness of the 5160 steel does not decrease significantly below the surface of the bar. We say that the bar has been "through hardened". The 5160 steel has martensite all the way to its center, but the 1060 has pearlite and bainite in the central regions causing the drop in hardness. Both bars were cooled at the same rate. This means that the Cr present in 5160 must have made the formation of pearlite and bainite more difficult. The results also illustrate another important point regarding the effect of alloying elements. At the surface both bars are fully martensitic and both bars have the same hardness. This means that the Cr addition in 5160 has not changed the hardness of the fresh martensite. Figure 4.12 presents the hardness of fresh martensite versus the %C in steel. This curve is found to apply to both plain carbon and alloy steels, which means that alloying elements do not affect the hardness of martensite. So alloy steels are not harder because the alloying elements make the martensite harder. When as-quenched alloy steels are harder than plain carbon steels of the same C composition, it is because the alloying elements are preventing formation of the softer pearlite and bainite. Comparing the hardness profiles of 1060 and 5160 in Fig. 8.1 we say that the Cr addition has improved the ***hardenability*** of the steel. So, hardenability is a measure of how deep below the surface a quenched steel can be made fully martensitic. On the other hand, hardness is a measure of the resistance to penetration that the steel offers to an indenter point forced into its surface under a given load.

From the above discussion it should be clear that to improve the hardenability of a steel we need to slow down the formation of the constituents that can form in austenite prior to martensite and prevent its formation. These product constituents can be any of the 3 shown on Fig. 4.22 at temperatures above the M_s temperature: ferrite or pearlite or bainite. Two experimental techniques have evolved for characterizing the rate of formation of these constituents: IT - Isothermal Transformation and CT - Continuous Transformation. Each technique generates a diagram which will be called IT diagrams and CT diagrams. We will first discuss the IT technique. (Note: some people continue to prefer the use of the older names, TTT in place of IT and CCT in place of CT.)

IT Diagrams As previously discussed on page 30, the IT technique involves the use of thin samples which are quenched from the austenitizing temperature to a temperature of interest and the transformation of the austenite is allowed to occur isothermally at this temperature. Figure 9.2 will be used to explain how an IT diagram is constructed. After the quenched sample rapidly cools to the isothermal temperature the austenite will eventually begin to transform to one of the 3 product constituents. Consider a pearlite steel, composition (A) on Fig. 9.2. After the sample has been quenched to the temperature labeled T_{nose} for the time labeled 1 on the IT diagram at the left, the austenite will start to form pearlite. This point is therefore labeled P_s, for pearlite start. After the time 3, the austenite has completely transformed to pearlite and so this point is labeled P_f, for pearlite finish. The point 2, not always shown on IT diagrams, gives the time when 50 % of the austenite has transformed. The experimental determinations of these times is often made using a device called a dilatometer. It measures the length change of the sample during the hold time. Austenite has a smaller volume per atom than any of the 3 product constituents. Hence, a sample expansion will begin to occur at P_s and will stop occurring at P_f. By quenching to different temperatures one can determine the P_s and P_f times at a bunch of temperatures and then draw lines

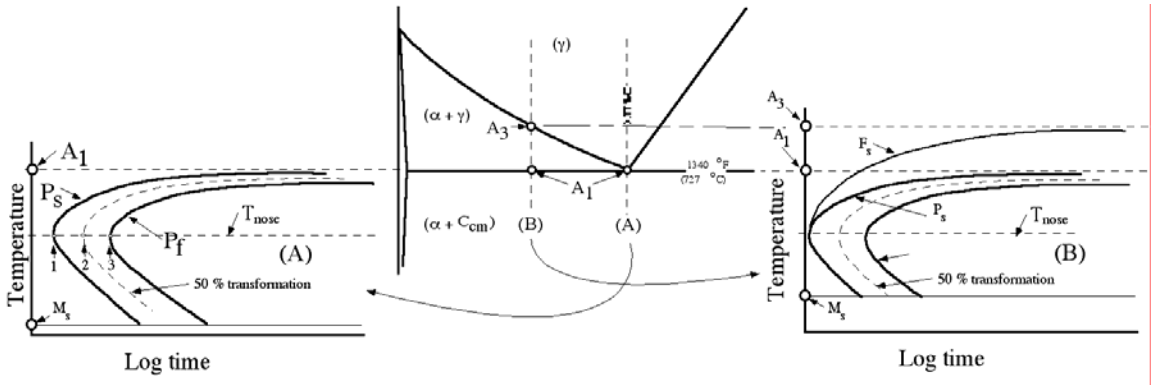

Figure 9.2 The Fe-C diagram at the center locates 2 alloys at %C compositions of (A) and (B). The IT diagrams for the two alloys are shown at the sides.

along them thereby constructing the IT diagram. Consider the P_s curve and notice that it has a minimum time value at the temperature labeled T_{nose} on the diagram. This point is often called the "nose" of the P_s curve for obvious reasons. If it has values of less than a few seconds we know immediately that the steel will have poor hardenability, because it will be very difficult to cool the interior of a bar fast enough to avoid pearlite formation.

Pearlite cannot form unless austenite is cooled below A_1. So, one might expect that the more you undercool the austenite below A_1 the faster the pearlite will form. The IT diagram for the pearlite steel (A) shows that, initially, such is the case. However, this changes once one cools below the T_{nose} temperature. Now it begins to take longer for the pearlite to form as the undercooling below A_1 is increased. The reason for this result is diffusion. In order for pearlite to form in austenite the C atoms have to rearrange themselves from the random distribution in austenite to the special distribution in pearlite. As discussed on pp. 13-14 and shown in Figs. 3.7 & 3.8, pearlite consists of plates of ferrite (%C = 0.02) and plates of cementite (%C = 6.67). The mechanism that redistributes the carbon from the uniform composition of 0.77% in austenite to the 0.02%/6.67% mixture of plates in pearlite involves diffusion. But, as discussed on p.60, diffusion is very sensitive to temperature. It is the rapid decrease in the C diffusion coefficient as the temperature drops that eventually wins out and begins to increase pearlite formation times as the temperature drops below T_{nose}.

The IT diagrams always show the A_1 and the A_3 or A_{cm} temperatures on the temperature axis (except for pearlitic steels where only A_1 is needed). Steel B is a hypoeutectoid steel because its composition is below the 0.77 % eutectoid (pearlite) value. Hypoeutectoid steels will have A_3 values lying above the pearlite temperature, A_1, by increasing amounts as %C drops. Therefore, these steels will have a temperature range on the IT diagram that lies between A_3 and A_1 as shown on the IT diagram for the B steel at the right of Fig. 9.2. If you look at the phase diagram at the center of Fig. 9.2 it is clear that in this A_1 - A_3 temperature region you will only have ferrite (α) forming from the austenite (γ). On the IT diagram then, you will find a line labeled F_s which locates the times where ferrite begins to form from the austenite, the ferrite start line. This line never extends above the A_3 temperature because ferrite cannot form above that temperature. But ferrite can form below the A_1 temperature and the curve illustrates that for this example it can form at temperatures nearly down to the nose temperature. If you look on Fig. 4.22 you will see that the lowest temperature where ferrite can form drops as the %C moves away from the 0.77% pearlite composition in hypoeutectoid steels.

The actual IT diagrams for 3 different AISI plain carbon steels that appear in reference [9.1] and other ASM handbooks are shown in Fig. 9.3. The diagrams illustrate several points. First, most published diagrams do not label the F_s, P_s or B_s curves (the start curves for ferrite, pearlite and bainite). Nor do they usually tell you where pearlite and bainite form. They include the labels, A, F and C for austenite, ferrite and cementite (or carbide). The dilatometer that locates the lines on these diagrams cannot distinguish between the 3 product constituents and so it is left to the reader to figure out whether a given line is a F_s, P_s or B_s line. For plain carbon steels, one can make a reasonable estimate using the information of Fig. 4.22. For example, this figure predicts that in a 1080 steel pearlite will form from A_1 down to around 550 ^oC and bainite from there down to the M_s temperature. Hence on the IT diagram for 1080 at the bottom of Fig. 9.3 the start curve would be the P_s for temperatures from A_1 down to around 550 ^oC and below that temperature it would be the B_s down to the M_s temperature.

Note (1) The ASM diagrams label the A_3 temperature A_f, and the A_1 temperature is labeled A_s. This nomenclature was suggested by R.A. Grange in 1961 for its similarity to the M_s and M_f nomenclature [9.2]. It is used in the various ASM publications, but virtually no one else has adopted this nomenclature and it will not be used here except on copied ASM diagrams. Andrews [6.4] has shown that $A_f = A_3$ and that $A_s = A_1$. (2) It is not uncommon to encounter IT and CT diagrams that use the labels A_{c1} and A_{c3} instead of A_1 and A_3. This is done because the A_1 and A_3 temperatures have been measured in heating experiments done at very low heating rates and resultant values are estimates of A_1 and A_3 measured in heating experiments, and hence the use of the c subscript (see pp. 15-16). Many authors use the nomenclature A_{e1} and A_{e3} , but as noted on p. 15, in this book the e is understood, so that $A_{e1} = A_1$, $A_{e3} = A_3$.

There are 3 important effects that occur as the %C is increased in plain carbon steels that can be illustrated with Fig. 9.3.

(1) As the %C increases the curves shift to the right, to longer times. Notice that the nose time for the start curves rises from below 0.5 sec. on the two lower carbon steels to 0.8 sec. on the 1080 steel. This shifting of the start curves to longer times with increased %C means that the hardenability of plain carbon steels increases as the %C increases, at least up to the pearlite composition, 0.77 %C. The 1060 curve illustrates why the hardness drops so fast below the surface in Fig. 9.1. To avoid pearlite formation and obtain 100 % martensite in this steel, Fig. 9.3 shows that the temperature must fall below 1000 ^oF in roughly 0.3 seconds. Clearly, it is only near the quench surface that the temperature can fall fast enough to avoid pearlite formation.

(2) As the %C increases the M_s temperature decreases as was illustrated with Figs. 4.16 and 4.22. The IT diagrams show this effect because they give the M_s temperatures next to the temperature axis. Note that they also list the M_{50} and the M_{90} temperatures. These are the temperatures at which 50 % and 90 % martensite has formed.

(3) As the %C increases the size of the A + F region decreases and vanishes for the 1080 steel were A_3 has collapsed to A_1. This effect was explained with the hypothetical IT diagrams of Fig. 9.2. The Fig. 9.2 diagrams also show both effects (1) and (2).

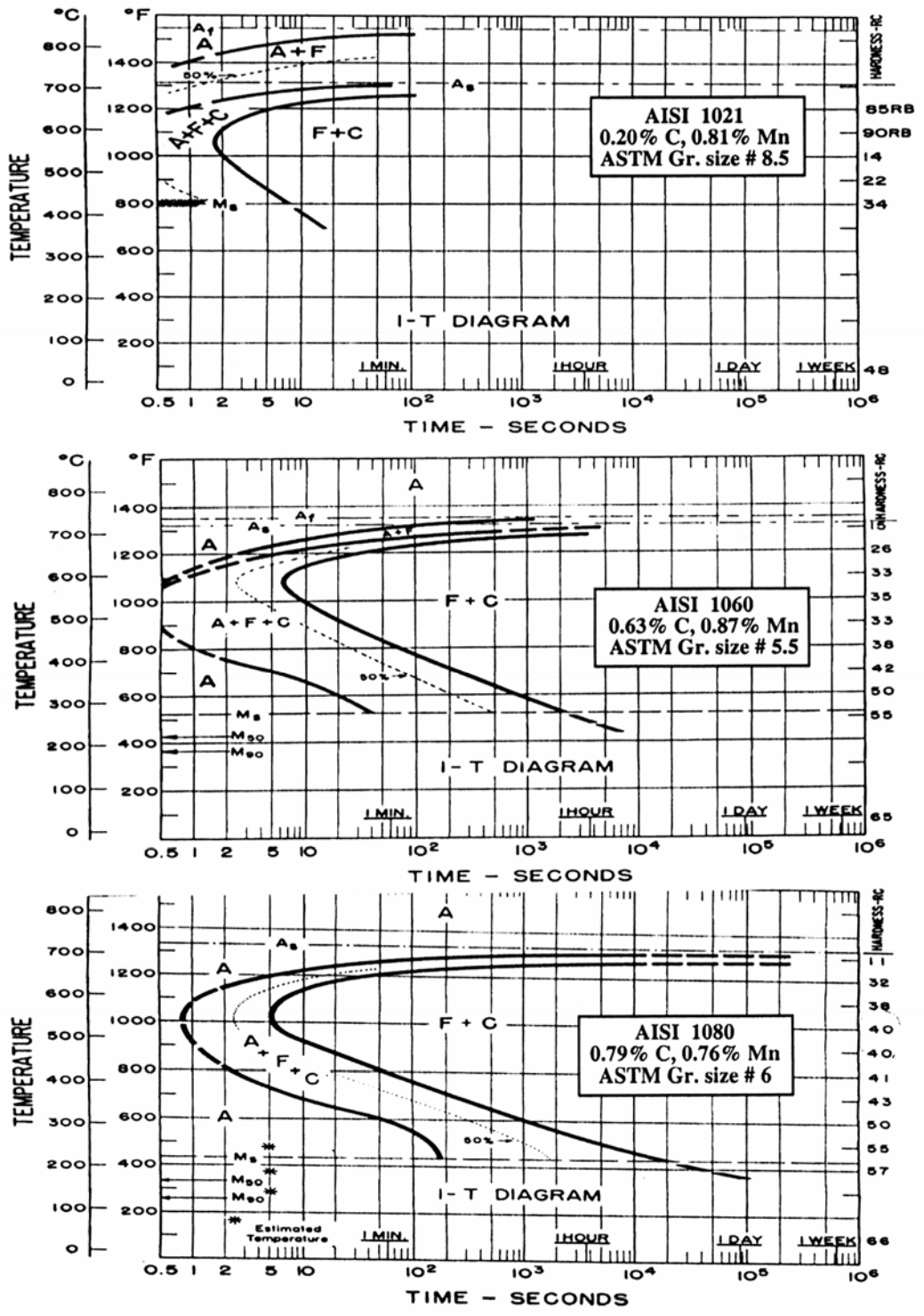

Figure 9.3 The IT diagrams for 3 plain carbon steels showing the effects of increasing %C [9.1].

To improve hardenability one needs to force the various start curves that appear on the IT diagrams to longer times. Physically this means that one must make it more difficult for the 3 product constituents, ferrite, pearlite and bainite to form in the austenite. There are 2 principal ways in which this can be effected: (1) increasing grain size, and (2) adding alloying elements.

(1) Effect of grain size on Hardenabiltiy It was pointed out above that the product constituents virtually always form on the austenite grain boundaries. The amount of grain boundary area depends on grain size. A larger grain size will reduce the amount of grain boundary area per unit volume, which will shift the start curves to longer times and improve hardenability. Hence, the position of the curves on IT diagrams depend on the austenite grain size. For this reason, as shown on Fig. 9.3, published IT diagrams always specify the grain size.

(2) Effect of alloying elements on Hardenabiltiy As discussed on p 72, reactive alloying elements such as Cr and Mo will form carbides. Consequently these elements will prefer to go into the cementite (carbide) part of pearlite or bainite when they form. Hence, when pearlite, for example, forms from austenite these elements have the same problem that C has: They want to rearrange from a uniform distribution in the austenite to a distribution in pearlite where they have higher composition in the cementite plates than in the ferrite plates. This rearrangement is accomplished by diffusion. But the diffusional rearrangement of the alloying elements is more difficult than it is for C because of their tremendously smaller diffusion coefficients. Hence, their presence makes it more difficult for pearlite and bainite to form and the P_s and B_s curves are shifted to the right (longer times) on the IT diagram. All elemental additions to steel, except Co, shift the start curves for ferrite, pearlite and bainite to longer times. The reason that non reactive elements such as Ni slow the formation rates of pearlite and bainite is a bit too complicated to be explained easily. But the net result is simple to remember: virtually all alloying additions in steel slow the formation of the constituents that form on cooling austenite. Figure 9.4 presents a comparison of the IT diagrams for 1060 and 5160 steels which shows the effect of the alloying addition of Cr. Note from Tables 6.2 and 6.4 that 5160 is basically a 1060 steel with 0.8 %Cr added. Figure 9.4 shows that the addition of this small amount of Cr has a significant effect on the position of the start curves on the IT diagram. Even though the grain size of the 5160 steel is smaller, the nose of the IT diagram is shifted to around 5 seconds on the 5160 steel versus less than 0.5 seconds on the 1060 steel.

Hardenability Demonstration Experiment A simple and instructive experiment will be presented which illustrates the dependence of hardenability on both grain size and composition. Two steels, 1086 and 5150, were forged into the tapered shape of a knife blade as shown in Fig. 9.5. The 1 inch wide blades tapered from a thickness of 1/4 inch to 1/32 inch. Samples of each steel were prepared with a fine and course grain size using the cyclic heat treatment discussed on p. 70 to give the grain sizes shown in Table 8.2. The steels were quenched into agitated room temperature oil, sectioned in half, polished, etched and examined in a microscope. Three samples were 100 % martensite, both the large and small grained 5150 steels and the large grained 1086 steel. However, the small

grained 1086 steel was a mixture of martensite and fine pearlite. The distribution of the martensite was quite interesting. Because the cooling rate should be fastest right at the surface one might expect the martensite to form first along the surface as shown in Fig. 9.5(A). However, it was found to form at the thin end with a bit at the back corners, as shown in Fig. 9.5(B). The fact that it does not form preferentially along the surface means that for this tapered knife blade geometry quenched in agitated oil, the cooling rate at the centerline of the blade is nearly the same as at the surface for thicknesses up to 1/4 inch. (Such behavior is predicted for thin samples and is explained by what is called film heat transfer control.)

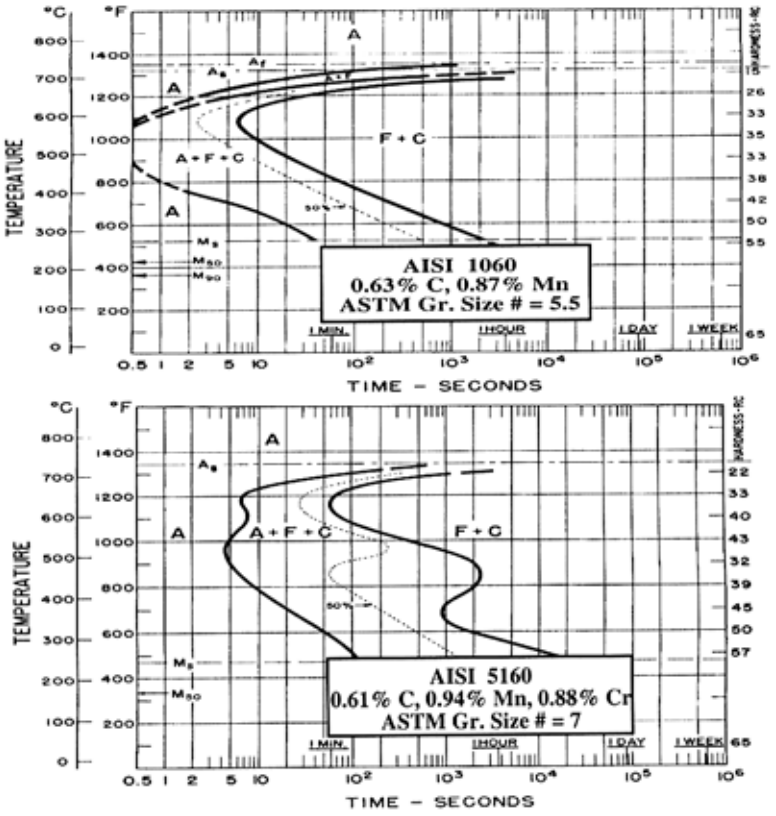

Figure 9.4 Comparison of the IT diagrams for 1086 and 5160 steels [9.1].

The samples were further studied by making HRC hardness measurements at 1/16 intervals on the transverse blade sections starting at the thin edge and progressing toward the spine (fat edge). The results of these measurements are plotted versus the blade thickness in Fig. 9.6. (Hardness measurements were not made on blade thicknesses less than 0.08 inches due to end effects. Microhardness tests confirmed, however, that the hardness remained constant at blade thickness from 0.08 inches to the thin end of the blades, where the thickness was about 0.03 inches.) The results for the 1086 blade dramatically show the effect of grain size. In the large grained sample (1086, G.S. = 11) the blade is fully martensitic (HRC = 65) at all thicknesses. However in the fine grained cycled blade (1086, G.S. = 15), 100 % martensite is only able to form out to blade thickness of around 0.09 inches and beyond thicknesses of around 0.15 inches the blade has no martensite and consists of all bainite or pearlite. On the other hand the 5160 steel is much less affected by grain size variation. It appears that there is a small loss of martensite due to the fine grains only at thicknesses of greater than around 0.18 inches. These results illustrate why the low alloy AISI steels are desirable for heat treated samples of industrial sizes. Fine grained samples are needed for improved toughness and the increased hardenability of the alloy steels allows much deeper hardening than is possible with fine grained plain carbon steels.

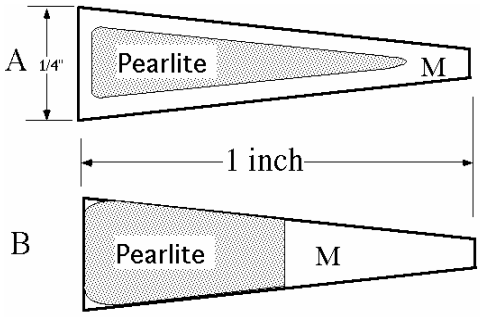

Figure 9.5 Two possible martensite/pearlite configurations of quenched blades.

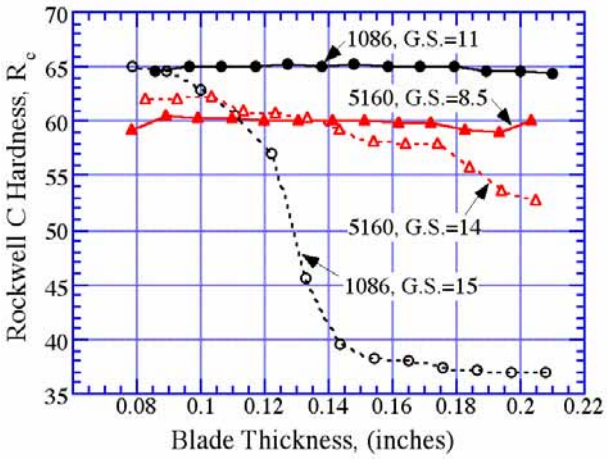

Figure 9.6 Rockwell C hardness versus thickness along blade

It is possible to present a detailed explanation for the martensite formation in the 1086 steel using the IT diagram for 1080 steel given on Fig. 9.3 and replotted in Fig. 9.7. Assume the IT curves apply to the small grained 1086, G.S.15 steel. Hypothetical cooling curves are shown as the dashed lines for positions in the blade at thicknesses of 0.09, 0.125 and 0.15 inches. Because the thickness at 0.09 is the largest thickness showing 100 % martensite its cooling curve must be just to the left of the nose of the P_s curve. Because the thickness of the 0.15 is the smallest thickness showing no martensite its cooling curve must be just to the right of the nose of the P_f curve. And since the thickness at 0.125 corresponds to a hardness 50% of the way between no martensite and all martensite (midway between Rc = 65 & 38 on Fig. 9.6), its cooling curve should pass through the nose of the 50 % transformation curve. Now what happens when we go to the course grained pearlite? The cooling curves will not change their shapes or positions as cooling rate is not affected by grain size. But the position of the P_s and P_f curves depend on grain size and the larger grain size must shift the nose of the pearlite start curve to the right of the cooling curve for the thickest part of the bar, because no pearlite formed in the large grained 1086 steel.

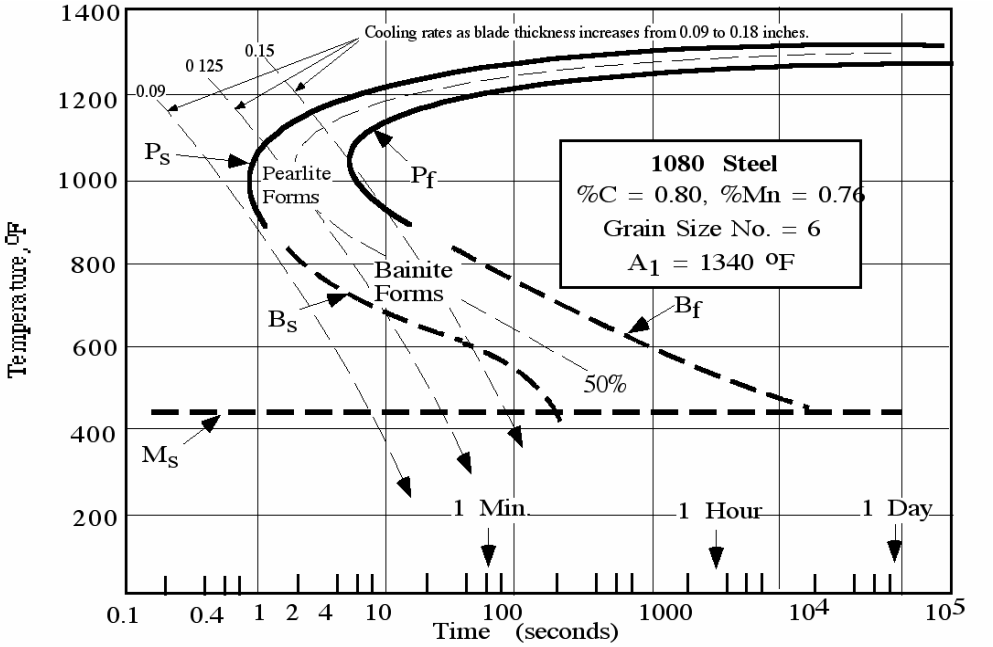

Figure 9.7 Using the 1080 IT diagraam of Fig. 9.3 to explain the structure variation found in the 1086 blade.

CT Diagrams The above analysis using the IT curve of Fig. 9.7 explains the fundamental ideas behind the variation of martensite formation in the 1086 blades, but it can only serve as a qualitative guide. The reason is that IT curves only apply to

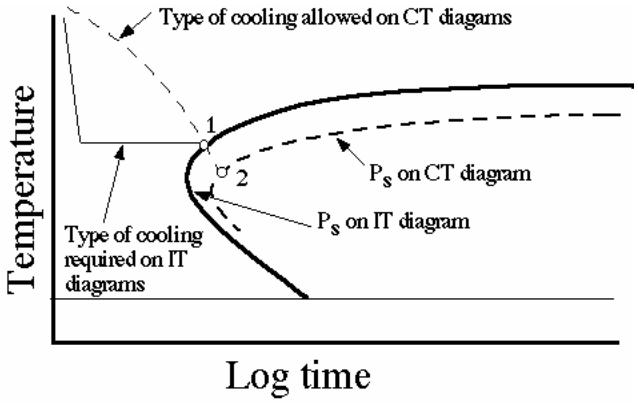

Figure 9.8 Differences between IT CT diagrams.

isothermally cooled steels. In other words, they apply only to steels that are quenched so fast that they remain fully austenite at the temperatures shown on the diagram until the first product constituent (ferrite, pearlite or bainite) forms in the austenite. Figure 9.8 presents a sketch of the P_s curve for the 1080 steel and shows the cooling path that must be followed for the use of an IT diagram. It is a very rapid drop followed by an isothermal hold. In our blade experiment this did not happen because of a combination of the size of the sample and the slowness of the oil quench. Hence, the cooling curve for this experiment would correspond to the dashed line of Fig. 9.8. Experiments have shown that when a sample is cooled along a continuous cooling curve, such as the dashed line of Fig. 9.8, the first pearlite will not form at point 1, but will be delayed and will form later at point 2. Hence, the P_s curve on a CT diagram will not have the same position as on an IT diagram. The CT curves are shifted down and to the right.

Unless you are working with very thin samples and very fast quench conditions the transformation rates of steels require the use of CT rather than IT diagrams. Examples of CT diagrams are presented in Fig. 9.9 for two steels having compositions close to 0.4 %C. CT diagrams show cooling curves directly upon them. The downward sloped lines with fractions like 1/4 and 1/2 are the cooling curves on Fig. 9.9. The shape of the cooling curves depends on how the sample was cooled and will, in general, vary depending on the source of the CT diagram. The curves in Fig. 9.9 are for samples cooled in the Jominy technique which will be described in the next section, and the fractions in inches on the cooling curves refer to the position on the Jominy bars. Notice that on the 5140 diagram the F_s, P_s, B_s, and M_s curves are

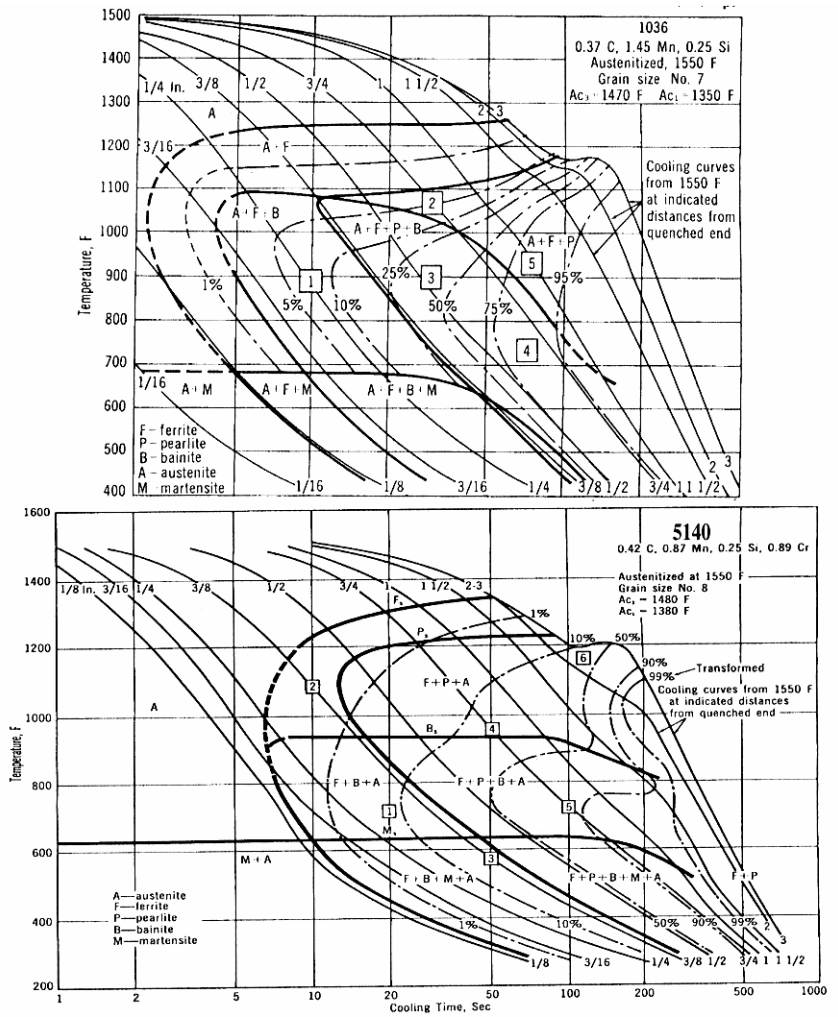

Figure 9.9 CT curves for two steels having around 0.4 %C, 1036 and 5140 [9.1].

all labeled. By comparing the two diagrams you may also identify these same curves for the 1036 steel. Even though the 1036 steel has considerably more Mn in it than most plain carbon steels (see composition in upper right corner and compare to Table 6.2), its hardenability is quite a bit lower than the 5140 steel. The nose of the F_s curves is only around 2 s in the 1036 compared to around 7 s in 5140. Notice that the diagrams show dashed lines with percentage numbers labeled on them. These lines allow you to make rough estimates of the percentage of the various constituents that will be contained in a steel cooled along one of the cooling curves. Consider the cooling curve marked 3/4 on the 5140 diagram. This cooling curve crosses the 1% line just below the P_s line at around 30 seconds. Notice that the cooling curve had crossed the F_s curve at around 20 seconds. Hence at this cooling rate the steel started to form pearlite after a bit under 1% ferrite had formed. The cooling curve crosses the B_s curve about midway between the 10 % and 50% line so bainite started to form after roughly (50-10)/2 = 20% pearlite had formed. It crosses the M_s line just beyond the 99 % line, so we expect that the remainder of this steel will be bainite and there will be little to no martensite in it. Hence, the steel cooled at this rate will end up with at least around 1 % ferrite, 20 % pearlite and remainder bainite. By similar reasoning you may show yourself that a steel cooled along the curve labeled 3/8 will end up with roughly at least 3 % ferrite, no pearlite, at least 20 % bainite and the remainder martensite.

There are many sources of IT and CT diagrams available in the literature. The ASM has published a book which brings most all of these together [9.1]. In the reference list a short explanation is presented of the various sources used in this book. The presentation of CT diagrams varies more widely than the IT diagrams. To illustrate this idea Fig. 9.10 presents an alternate type of CT diagram for an 0.38 %C steel whose composition is given at the top of the diagram. The cooling curves for this diagram do not correspond to positions on the Jominy bar but are those utilized in the specimen from which this particular diagram was made. The circled number is the room temperature hardness found for that cooling curve in units of DPH (diamond pyramid hardness). The dashed lines give the estimated percent of the austenite that has transformed. The start curves are not labeled on the original diagram but labels have been included here after consulting the original reference. No distinction was made between the ferrite and pearlite start so that the upper start curve is a combined F_s- P_s curve.

There is a third style of CT diagram that is presented in ref. [9.3] without explanation. These diagrams were produced by the British Steel Corporation and an example is presented in Fig. 9.11 for a 4130 steel. With these diagrams it is possible to determine the

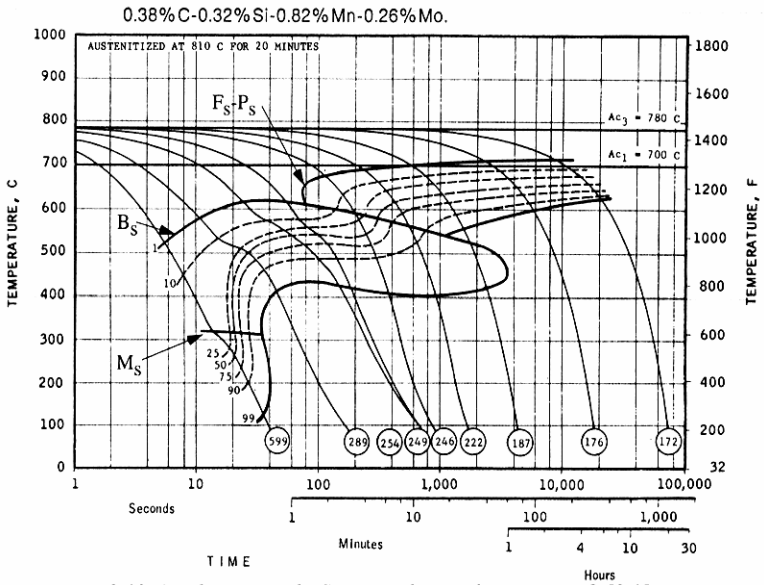

Figue 9.10 An alternate style CT curve that is often presented. [9.1]

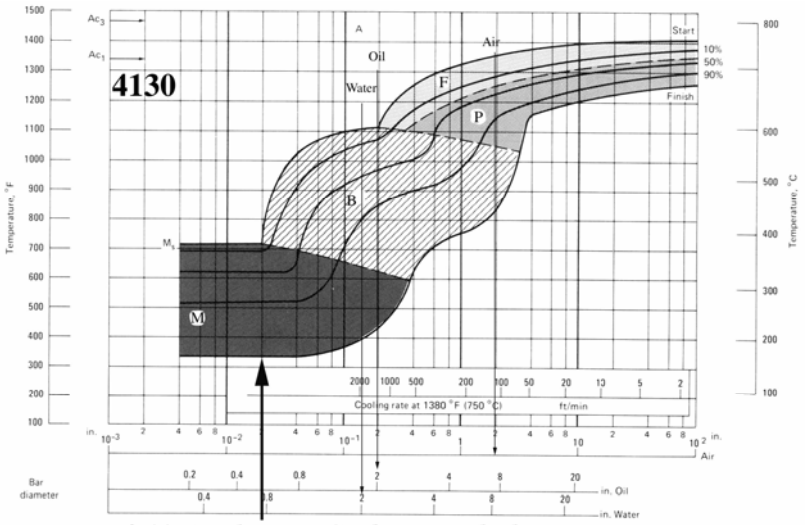

Figure 9.11 An alternate CT diagram which gives microstructures at the center of various diameter bars for air, oil and water cooling. [9.5]

microstructures that will be present only at the center of round bars of various diameters for 3 types of quenches, water, oil and air. To illustrate the use of the diagram consider 3 bars, each of 2 inch diameter. There are vertical downward pointing arrows at the 2 inch diameter positions on the bottom horizontal scales for the water, oil and air quenches. By simply following up these lines one can determine the predicted microstructures for the center position of the bars. Consider the water quenched arrow. It passes through the bainite/martensite transition just below the 90% transformation line. Hence this steel would be predicted to contain around 93% bainite and 7% martensite at its center. Similarly, the structure at the center of a 2 inch air cooled bar is estimated to be around 30% ferrite, 63% pearlite and 7% bainite. The diagrams allow one to easily determine the maximum bar diameter that can be through-hardened (100% martensite at the center, see bold upward pointing arrow, smallest diameter with no bainite). For a water quench the maximum diameter would be just under 0.8 inches, while for an oil quench it would be just under 0.6 inches. The diagram also specifies equivalent cooling rates at the center after its temperature has dropped to 1380 ^{o}F (750 ^{o}C). This information allows application to any arbitrary quench if the 1380 ^{o}F cooling rate is known. For example, the 1380 ^{o}F cooling rate at the center of the 2 inch water quenched sample corresponds to a value of just under 2000 ^{o}C/min. (Note refs. [9.5 & 9.3] have mislabeled the cooling rate ft/min.)

The Jominy End Quench Walter Jominy, a University of Michigan graduate working at Chrysler in the 1930s, developed a test that has become widely adopted for evaluating the hardenability of steels. The test is basically a controlled heat transfer experiment in which a 1 inch diameter round bar by 4 inch length is heated to a temperature in the austenite range and placed in a jig that sprays water on one end thereby cooling the bar directionally from the quenched end, see Fig. 9.12(a). The test has been standardized by the American Society for Testing Materials as ASTM A 255, which may be found in the ASTM book of standards available in most technical libraries. To insure consistency, the test is conducted with a specified bar temperature depending on %C level, a specified rate of water flow and diameter of the water stream. After cooling, small flats are machined onto opposite sides of the bar with a surface grinder in the geometry shown on Fig. 9.12(b). The bar is then placed

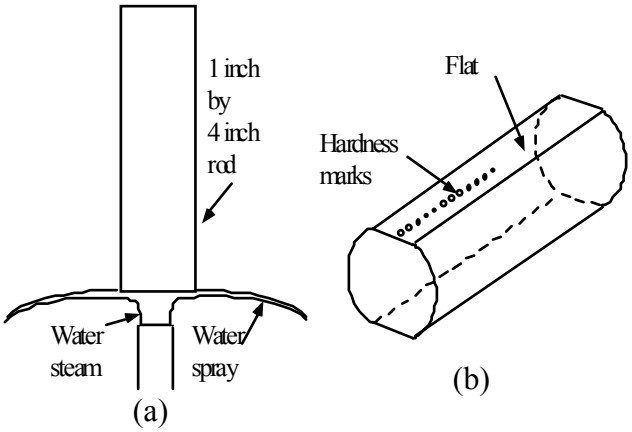

Figure 9.12 (a) The Jominy setup. (b) Flats and hardness measurements on quenched bar.

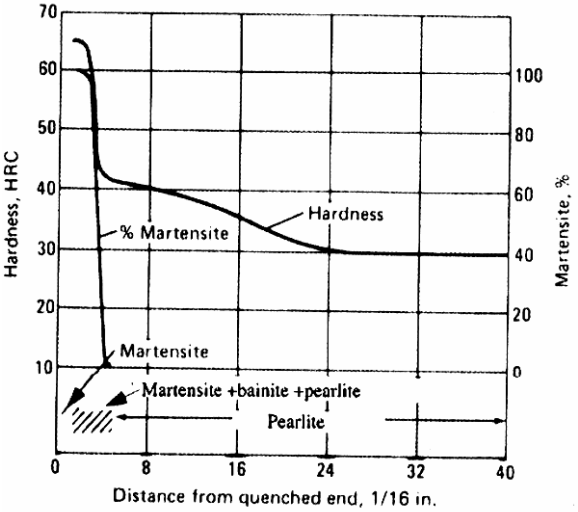

Figure 9.13 Jominy data of 1080 steel [9.3]

in a hardness tester and HRC measurements are made at 1/16 inch intervals along the bar starting at the quenched end and extending to the opposite end. Measurements are made on both sides and the average at each location is used to generate a hardness profile such as that shown in Fig. 9.13 for a 1080 steel. The distance along the bar is often called the J_D position and in the U.S., a value of $J_D = 1$ indicates a position of 1/16 inch, but one must be careful of the particular units any given author uses. In non U.S. countries distance is generally in mm units. The cooling curves that are superimposed on the CT diagram of Fig. 9.9 refer to specific J_D values. For example, the curve labeled 3/4 gives the cooling curve for a position located 3/4 inches from the quenched end of the J-bar, i.e., $J_D = 12$. One of the things that makes the Jominy test useful is the fact that cooling rates of the low alloy AISI steels with different chemical compositions as well as different grain sizes are essentially the same. This results because the alloying element additions do not change the thermal conductivity significantly in these steels, nor does grain size variation. Consequently, all the different cooling curves shown on Fig. 9.9 will be the same for different steels. The only thing that changes from steel-to-steel is the position of the various start curves. As the alloy composition is increased and the grain size is increased those curves shift to the right.

The Jominy bar provides a map of all the microstructures that appear in a continuously cooled sample. Right at the quenched end the structure will virtually always be 100 % martensite. Moving in from the quenched end the cooling rates decrease and at some point non-martensitic constituents such as ferrite, pearlite or bainite will appear and the hardness will start to drop. This effect is shown on Fig. 9.13 for the case of a 1080 steel. The Jominy data is given by the curve marked hardness. The % martensite curve shows the amount of martensite going from 100 % at around $J_D = 3$ to zero at around $J_D = 6$. (% martensite is given on the right axis and HRC on left axis.) It is shown at the bottom that in the $J_D = 3$ to 6 region the bar contains a mixture of martensite, bainite and pearlite, but beyond $J_D = 6$ the bar is all pearlite. The continued drop in hardness in the pearlite is due to the increased spacing of the plates of the pearlite at the lower cooling rates, which saturates at distances beyond $J_D = 24$.

Figure 9.1 illustrated the concept of hardenability by showing the hardness as a function of radius for a 5160 versus a 1060 steel. The Jominy data for these 2 steels also illustrates the superior hardenability of 5160 as shown in Figure 9.14, which superimposes the data for the two steels found in refs. [9.3&9.6]. The increased depth to which the 5160 steel hardens is clearly seen in the comparison of the Jominy data. In the

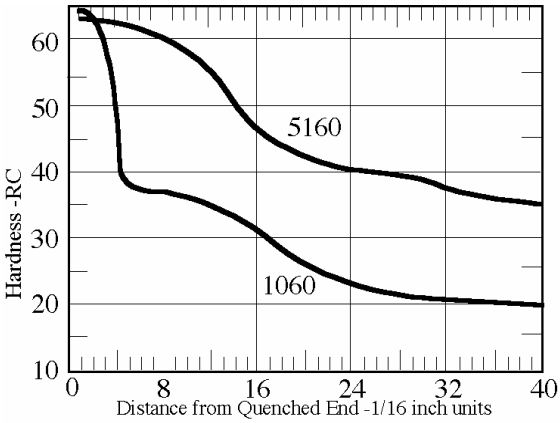

Figure 9.14 Jominy data for 5160 and 1060 steels [9.3&9.6].

1060 steel the depth of 100% martensite extends to a J_D value of only around 1 to 2, whereas in the 5160 it extends to a J_D value of around 6 to 7. In the 1060 steel all of the martensite is gone at J_D of around 6, whereas in the 5160 the significant increase in hardness over 1060 at J_D =40 shows that some martensite is present even at this large distance from the quenched end.

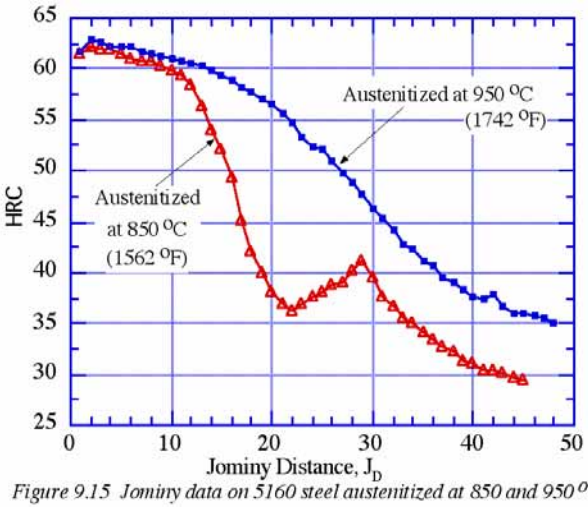

Figure 9.15 Jominy data on 5160 steel austenitized at 850 and 950 °C.

The Jominy test is able to detect changes in hardenability produced by small changes in the heat treating operation. Figure 9.15 presents data from Jominy tests on 5160 steel where the steel was austenitized at two different temperatures for the same time of 1 hour. It is clear that the higher temperature austenitization has produced a dramatic increase in hardenability. This could be due to either (1) an increase in grain size at the higher temperature or (2) a change in the composition of the austenite at the higher temperature. The grain size of both steels was found to be the same within the scatter of the measurement, at around ASTM size No. 10. The carbides in 5160 will contain significant amounts of Cr. Apparently the 850 °C austenitization for 1 hour is not adequate to dissolve all of the carbides and then fully homogenize the Cr in the austenite grains of the steel. This is another example of the slow rates of diffusion of the alloying elements contained in low alloy AISI steels.

The Jominy data for a given steel provides quantitative information about the cooling rate needed to produce a given amount of martensite, like 50 % or 99+ %. As will be discussed in Chapter 12 on quenching, the cooling rate within the steel depends on the quenching method. For example, oil quenching produces lower cooling rates than water quenching. The cooling rates corresponding to the different types of quenchants have been analyzed and it is possible to use the Jominy data to determine the % martensite at the center and various radii of bars for the different quenchants. Knowing the % martensite one can then estimate the hardness versus the radius for various quenchants. The analysis is fairly complicated and will not be presented here. However, the results of these analyses are presented graphically in reference [9.3]

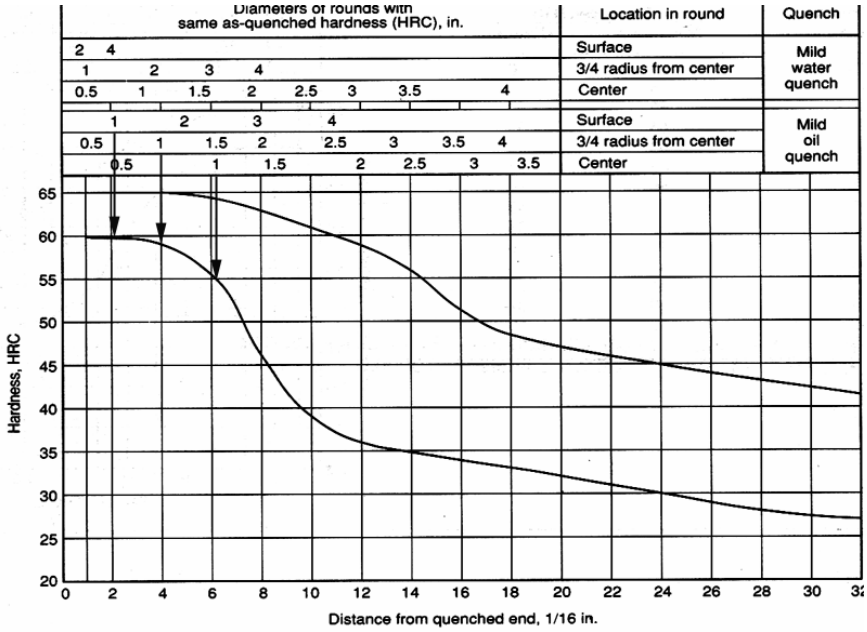

Figure 9.16 Hardenability band for 5160H and equivalent Jominy positions for mild water and oil quenches.[9.3]

Table 9.2 Oil quenched hardness of 1060 & 5160[9.1].

Bar Diam	Surface		1/2 radius		Center	
	1060	5160	1060	5160	1060	5160
1/2 inch	59	63	37	62	35	63
1 inch	25	62	32	62	30	60
2 inch	30	53	27	46	25	43
4 inch	29	40	26	32	24	29

for the special cases of mild water quenches and mild oil quenches. Data such as that at the top of Fig. 9.16 are provided for many steels. These data give the equivalent Jominy position for 3 locations along the radius (center, 3/4 out and surface) for mild oil and mild water quenches. For example, with a mild oil quench and 1 inch diameter bars the equivalent Jominy positions are shown by the downward pointing arrows at J_D = 2.2, 4 and 6.2, for surface, 3/4 radius and center positions, respectively. Knowing the equivalent Jominy positions, one can then go to the Jominy data for the steel and determine the corresponding hardness predicted for that position. For example, if the steel produced the Jominy data on a mild oil quench given by the lower curve, the HRC hardness for a 1 inch bar would be 60 at its surface, 59 at its 3/4 radius and 55 at its center. Similarly, if the Jominy data followed the upper curve the hardnesses would be 65, 65, 64 at surface, 3/4 radius and center.

Reference [9.3] also provides simple straight forward data on hardness at different radii for oil quenched samples in table form. The results given for 1060 and 5160 are presented in Table 9.2 as an illustration. The table gives the HRC values for the 3 locations, center, 1/2 radius and surface for the two steels after an oil quench of 4 different bar diameters. The data show that an oil quench will through harden 5160 bars of 1 inch diameter or lower, but will not through harden a 1060 steel of 1/2 inch diameter.

Hardenability Bands The hardenability is strongly controlled by composition of the low alloy steels. The composition of the steel is set at the mill that produced the steel and there is always going to be some variation of composition from that of the standard target values given in Table 6.4. Also there can be grain size variation in the as-received steels. These composition and grain size variations will shift the Jominy data to the right or left as discussed above. To limit such variations to a minimum, steel companies supply steels that are guaranteed to produce a Jominy curve that falls inside a so-called "hardenability band". Such steels are designated with an H at the end of their AISI name. For example, the hardenability band for 5160H is presented as Fig. 9.16 The steel company will guarantee that the Jominy data for their 5160H steel will lie somewhere between the two lines given on the Hardenability band. The hardenability bands are presented in many different references in addition to [9.3]. A particularly good reference is the SAE Handbook [9.4], which also presents other useful information on hardenability and the general heat treatment of steels.

References

9.1. G. Vander Voort, Atlas of Time-Temperature Diagrams for Irons and Steels, ASM International, Materials Park, OH (1991). This is the most complete source of IT and CT diagrams. Table below is summary of contents.

9.2 R.A. Grange, Estimating Critical Ranges in Heat Treatment of Steels, Metals Progress, vol. 79, pp73-75 (April 1961).

9.3 Heat Treater's Guide Practices and Procedures for Irons and Steels, ASM International, 2nd Edition (1995).

9.4 SAE Handbook, Volume 1, Materials, SAE, Warrendale, PA.

9.5 M. Atkins, Atlas of Continuous Cooling Transformation Diagrams for Engineering Steels, British Steel Corp., Sheffield (1977). See also pp 297-452 of [9.1] and p 309 of [9.3].
9.6 Atlas of Isothermal and Continuous Cooling Diagrams, ASM, Metals Park, OH (1977).

Summary of the IT and CT diagrams in reference 9.1		
Steels	Pages	Type of Diagram
U. S.	3-51	IT
British	53-113	IT
German	115-161	IT and CT
French	163-220	IT and CT
Mo steels	243-296	CT(Climax Moly-Cias work)
V steels	297-369	CT (M. Atkins, Atlas CT Diagrams, ASM 1980)
British Engr steels	373-452	CT (ditto)
Other steels	453-520	IT
Additional steels	521-607	CT in old 1977 ASM book [9.6]

Summary of the Major Ideas of Chapter 9

1 Quenched steels harden because martensite forms from the austenite. The hardness of the martensite depends on the carbon content, the higher the %C, up to around 0.8%, the harder the steel, see Fig. 4.12.

2 Adding alloying elements, such as Mo, Cr, Ni, and Mn does NOT increase the hardness of the martensite. But it does increase the **hardenability** of the steel.

3 If any of the 3 austenite quench products (ferrite, pearlite or bainite) form before martensite forms, then martensite cannot form and the hardness of the steel is decreased. The alloying elements slow down the formation of all 3 quench products. Hence, they allow martensite to form at slower cooling rates.

4 Cooling rates are always slower at the center of quenched bars. Because alloying elements allow martensite to form at slower cooling rates they increase the depth below the surface of a quenched bar where 100% martensite forms. This is what we mean when we say alloying elements increase hardenability. Figure 9.1 illustrates the effect of adding 0.8 %Cr on the hardenability of a steel containing 0.6 %C.

5 How much an alloying element improves hardenability is measured by how much it slows down formation of the 3 quench products, ferrite, pearlite or bainite. Isothermal transformation (IT) diagrams provide curves giving the time lapse after a quench needed to start formation of ferrite, (the F_s curve), of pearlite, (the P_s curve), and of bainite, (the B_s curve) versus the temperature of the quench. The longer the times the more the improvement in hardenability.

6 The start time curves are shifted to longer times (hardenability increased) by: (1) increasing the %C in hypoeutectoid steels, (2) increasing the % of the alloying elements added and (3) increasing the grain size of the austenite. Because fine grain size is critical for improved toughness, it is important to use alloying elements in fine grained steels to

restore the hardenability loss due to the finer grains. The experiment of Fig. 9.6 illustrates the lack of hardenability in a fine grained plain carbon 1086 steel versus a fine grained alloy steel, 5160.

7 The isothermal transformation (IT) curves require that the steel be quenched so fast that even at its center the temperature has dropped to the isothermal value before any of the 3 quench products form in the austenite. Hence, IT diagrams are only useful for thin samples. A second type of cooling diagram, the continuous cooling (CT) diagram, applies to steels cooled at slower rates, which occur near the center of steel samples that are not thin in section size.

8 Similar to the IT curves, the CT curves also show the start curves for ferrite, pearlite and bainite. But, in addition, they show cooling curve lines for steels cooled at increasing cooling rates. By measuring the cooling rate of a steel and then finding the corresponding cooling rate on the diagram one may estimate the start times for the onset of formation of the 3 quench products, ferrite, pearlite or bainite.

9 Most published IT diagrams, such as those of Fig. 9.3, and many published CT diagrams, present the start curves without labeling which quench product is forming. For IT diagrams of plain carbon steels, one may make a good estimate of the temperature regions of the curves which are specifying the start time of ferrite or pearlite or bainite from the information of Fig. 4.22. As an example the unlabelled IT diagram of 1080 steel in Fig. 9.3 has been given the appropriate P_s and B_s labels in Fig. 9.7.

10 The IT diagrams also supply curves identifying the times when the quench products have finished forming. This tells us the times at which all of the original austenite has transformed into the quench products of ferrite, pearlite, bainite or combinations thereof. These lines are often labeled with a subscript f, as has been shown for the pearlite finish, P_f, and the bainite finish, B_f, on Fig. 9.7. In addition it is common for IT diagrams to include a dashed line showing when 50% of the austenite has transformed into one of more of the 3 quench products.

11 The CT diagrams show a series of dashed lines that identify the extent of the austenite transformation. For example, the 5140 diagram of Fig. 9.9 presents dashed lines showing when 1%, 10%, 50%, 90% and 99% of the austenite is gone.

12 An alternate form of CT diagram telling the transformation progress only at the center of bars of known diameters has been developed in Britain, and you may encounter such diagrams in ref. [9.3]. Figure 9.11 presents such a diagram and the text tells you how to read these diagrams.

13 The Jominy End Quench is a test that measures the hardness at 1/16 inch intervals from the quenched end of a controlled heat transfer experiment. Martensite forms at the quenched end. Progressing away from the end the 3 quench products bainite, pearlite and ferrite form as the cooling rate is reduced. The order in which they form depends on the composition of the steel. The test provides a qualitative measure of the hardenability of a

steel. High hardenability steels will maintain 100% martensite to larger distances from the quenched end and will therefore remain harder to larger distances below a quenched surface. Figure 9.14 illustrates this effect by showing the Jominy hardness data for a 1060 and a 5160 steel. The 5160 steel is the same as a 1060 steel with the addition of 0.8% Cr.

14 The Jominy end quench experiment can reveal useful information on the effect of austenitizing conditions on hardenability. For example Fig. 9.15 illustrates the dramatic effect of increasing the austenitizing temperature from 850 to 950 ^{o}C (1562 to 1742 ^{o}F) in 5160 steel, an effect resulting from the slow homogenization of Cr into the austenite after the carbides with their high Cr content have dissolved. The slow homogenization is due to the low diffusion coefficient of Cr in austenite.

15 It is possible to use the Jominy end quench data to make theoretical predictions of the hardness of bars at various radial depths below the surface for different types of quenches, like a water quench (a fast quench rate) or an oil quench (a slower quench rate). Results of such calculations are available in graphical form for many steels in reference [9.3], such as that shown for 5160 steel on Fig. 9.16. By plotting the Jominy data for a 5160 bar on this graph and drawing lines down to a given hardness from the locations of its bar diameter found at the chart top, the chart predicts 3 radial locations (center, surface and 3/4 out from center) where this hardness will occur for either a mild oil quench or a mild water quench. An example use would be to determine the maximum bar diameter than can be "though-hardened", 100 % martensite to the bar center. The lower Jominy curve shows an HRC 60 hardness at the quenched end, where one has 100 % martensite. It also shows that this hardness is maintained to a maximum Jominy distance of $J_D = 3$ (which means 3/16 inches). Running a line up to the top at $J_D = 3$, and reading off the diameters on the rows labeled center, one sees that 100 % martensite should be obtained at the center of an 0.6 inch bar in a mild oil quench and an 0.95 inch bar in a mild water quench. This result predicts that changing from an oil to a water quench should increase the maximum through hardening diameter from 0.6 to 0.95 inches.

16 If the AISI code label for a steel has an H at the end, like the 5160H of Fig. 9.16, it means that the steel company guarantees that the composition and grain size of the steel is such that the Jominy data for the steel will fall within the published H-band width for this steel. The two lines on Fig. 9.16 give the H band width for 5160H. Graphs of the H band widths for the various AISI steels are available in references [9.3 and 9.4], and many other sources.

10 Tempering

The importance of tempering will be illustrated by describing a simple experiment that can be done if one wants to obtain a hands-on appreciation of heat treatment. The experiment is done with two lengths (each around 6 to 12 inches) of drill rod having a diameter of 1/8 inches. Drill rod is either 1095 steel or W1 tool steel, which have essentially the same composition. One inch long sections of the two rods are simultaneously heated with a propane torch to an orange color for around 20 seconds and then immediately quenched in a glass of water. The temperature produces austenite over a short length of the rods and the quench converts it to martensite + retained austenite. The first rod is placed in a vice with the discolored heated section about 1/2 inch from the grips and struck firmly with a hammer. The piece will break across the center of the heated section in a brittle manner, just like a piece of glass. The discolored heated section of the second rod is polished shinny with a fine emery or sand paper. It is now gently heated with the torch until it turns a deep blue color, this is the tempering step. Bending this rod in the vice or with a set of pliers produces the result shown in Fig. 10.1 Martensite has formed in the heated zone, and if you look carefully at a severely bent rod you will be able to see the boundary between the martensite and non martensite, as shown at the arrows in Fig. 10.1. The non martensite region has the as-received spheroidized structure of Fig. 4.23. This structure is soft and the metal flow within it on bending produces a surface distortion that terminates at the hard martensite zone and reveals the transition boundary.

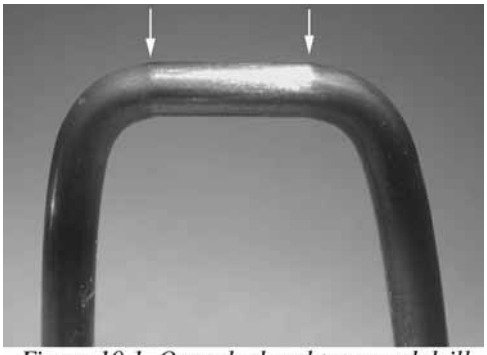

Figure 10.1 Quenched and tempered drill rod after bending.

If the tempering temperature is hot enough, the rod will not break through the martensite region even when this region is bent to over 90 degrees by hammering in the vice. If it is too hot the martensite region will become softer than one might like. Upon heating the polished steel rod, an oxide layer forms on its surface and the thickness of the oxide layer produces various colors due to an interference effect of light rays bouncing off the bottom and top of the oxide layer. The oxide thickness is controlled by the temperature of the steel and hence a series of different colors occurs at the relatively low temperatures used for tempering. The temperatures corresponding to the various colors are know as temper colors and Table 10.1 presents the correlation between colors and temperatures. The color temperature has been used for millennia by blacksmiths when tempering steels.

Table 10.1 Temper Colors

Color	^{o}C	^{o}F
Pale yellow	430	220
Golden yellow	470	240
Brown	490	255
Purple	530	280
Bright blue	550	290
Dark blue	600	315

The experiment shows that in the as-quenched condition the steel is way too brittle to be useful for applications other than those which require extreme hardness with no bending, such as files. Hence, virtually all quenched steels are tempered. Figure 10.2 shows qualitatively how the quenching and tempering operation changes the stress-strain characteristics of the steel. The tempering operation sacrifices the high strength of the steel to gain back improvements in ductility and toughness. Figure 10.3 presents actual

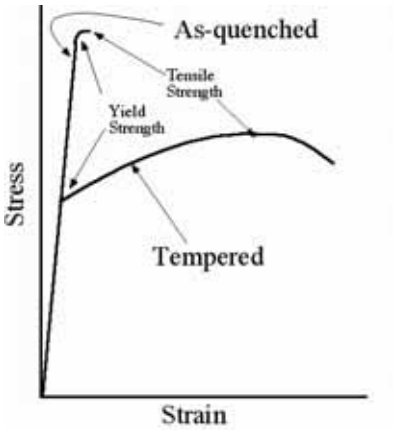

Figure 10.2 Effect of tempering on stress-strain relationship.

data for an oil quenched 4340 steel that has been tempered at increasing temperatures. One sees that both the tensile and yield strengths fall as the tempering temperature is increased but the % elongation, which measure ductility, increases. The reference of Fig. 10.3 shows similar curves for several other steels, and the trend is the same.

Several things are going on in the steel during the tempering process that result in the loss of strength and the gain in ductility and toughness. The first thing that happens is the relief of the high degree of volume strain in the steel produced by the formation of the higher volume per atom martensite phase. Then a series of internal structure changes occurs which is generally partitioned into the 3 stages of tempering. Stage 1: This first stage consists of the formation of very small carbides in the martensite, so small (around 10 nm) they can only be seen in an electron microscope. These first formed carbides are metastable carbides (do not appear on the equilibrium phase diagram), epsilon carbide ($Fe_{2.4}C$) in hypoeutectoid steels and Hagg ($Fe_{2.2}C$) and eta (Fe_2C) carbides in hypereutectoid steels. Stage 2: This stage is simply the decomposition of any retained austenite into carbides and ferrite. It is only important in high carbon steels where % retained austenite is significant. Stage 3: This stage occurs at the highest tempering temperatures and here the metastable carbides are replaced with small particle of cementite, the stable carbide of steels.*

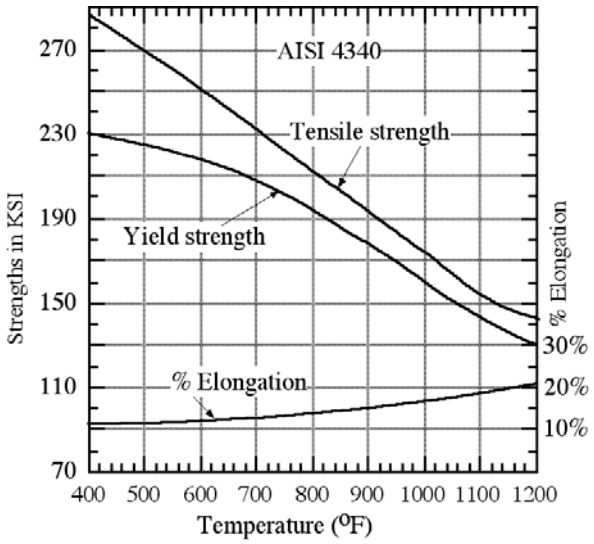

Figure 10.3 Change in mechanical properties of 4340 steel vs. tempering temperature [10.1]

As explained in Chapter 4, toughness is a better measure of the ability of a steel to avoid failure in practice than is ductility; and, toughness is evaluated with impact tests, such as the Charpy test. The Izod test is similar to the Charpy test and Fig. 10.4 presents a summary of scatter bands of data from such tests on steels of two different levels of %C. These curves illustrate two important characteristics of heat treated steels:

1) Tempered martensite embrittlement (TME)

Note that the impact energy drops significantly in the tempering range of 500-550 °F. It is now customary to call this loss of toughness, tempered martensite embrittlement, TME. (An old name for it is 500 °F embrittlement.) Because of this problem steels intended for use at high strength levels are not tempered above around 400°F (205 °C). For applications requiring high toughness with less strength required, tempering is done at temperatures above

* Strictly speaking, cementite should not be called a stable phase. In steel held in the 600 °C range for extended times, the cementite will sometimes be replaced by graphite. This shows that graphite is the stable phase in the Fe-C system, and the Fe-C phase diagram of Chapter 3 is really not an equilibrium diagram. But, because graphitization of steels is rare, this point is mainly of academic interest.

around 700 °F (370 °C). Notice that at temperatures of 1000-1200 °F excellent toughness is obtained. Of course the hardness goes way down and one might think that air cooled pearlitic steels would be cheaper for applications in this range of hardness. However, tempered martensite structures are generally tougher than pearlitic structures of the same hardness.

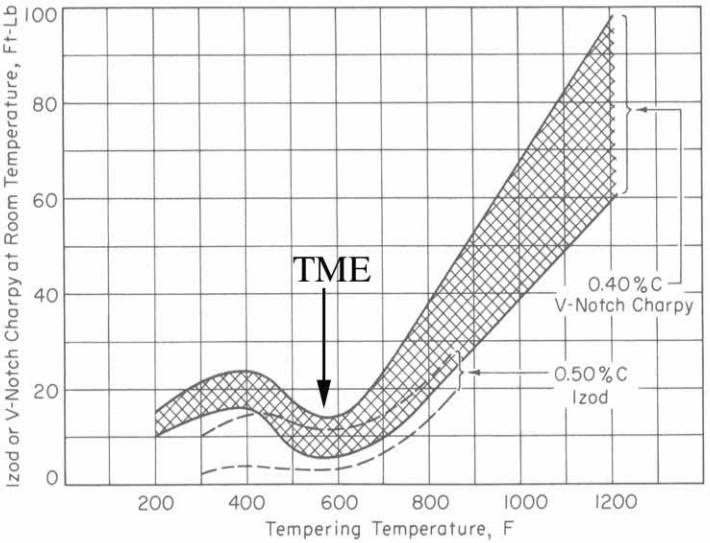

Figure 10.4 Notched impact energy versus tempering temperature for steels of 0.4 and 0.5 %C [10.2].

Temper Embrittlement, TE

There is a second type of embrittlement that occurs on tempering at high temperatures which is known as temper embrittlement, TE. Note the similarity of names and avoid confusing the two types of embrittlement. (An older name for TE is, temper brittleness.) Temper embrittlement occurs for tempering in the high temperature range of around 1100 °F (~600°C). It is not a big problem because it may be simply avoided by quenching from the tempering temperature. As illustrated in Fig. 10.4, TE is not detected by simple plots of impact energy versus temperature. However, it is detected by more extensive impact testing that measures variation of the DBTT (ductile brittle transition temperature- see p. 42) with the tempering temperature.

It is often possible to tell if a steel has failed because of one of these embrittlement problems by examining the fracture surface. A grain boundary fracture mode is characteristic of both types of embrittlement. However, in steels with extremely low levels of P and S tempered martensite embrittlement can display a cleavage surface. (See Chapter 5, pp. 42-44 for a discussion of fracture surfaces.)

2) Effect of %C on toughness

Figure 10.4 illustrates that increasing the %C from 0.4 to 0.5% produces a significant loss of fracture energy. Fracture energy values of less than 10-15 ft-lb (foot-pounds) are dangerously low for protection from brittle failures. If you go through all the steels used in an automobile you will find that the maximum %C is only 0.4% in all parts except the springs, where %C is 0.6% (often 5160 in the leaf springs and 9260 in the coil springs) and the bearings, %C = 1% (often 52100). This fact is directly related to the loss of toughness as %C increases. Figure 4.12 shows that one does not really gain too much in strength by increasing the %C above roughly 0.4 %C. The strength level possible at 0.4 %C (HRC = 57) corresponds to a tensile strength of 320 ksi (2210 Mpa), which is adequate after the reduction on tempering for most applications. Springs utilize a higher strength level because springs are subject to fatigue failure and high fatigue life is promoted by high strength. Probably the main reason for the use of high carbon steels at all is because of improved wear resistance. The wear resistance of a 0.8-0.9%C steel tempered to the same hardness as a 0.5-0.6% C steel is improved significantly. The improved wear

resistance results from the increased volume percent of carbides in the tempered higher carbon steels. The farm equipment industry utilizes high carbon steels, such as 1077-1086 for the many implements that experience wear by dragging through dirt. High carbon levels are also an advantage for increasing wear resistance of knives made by bladesmiths. As in most applications one desires the highest combination of hardness and toughness and a continuous battle of compromise occurs because the two properties vary inversely, as illustrated in Fig. 10.3. The presence of carbides within the martensite matrix of bearing steels, such as 52100, produces increased wear resistance because the carbides are even harder than the martensite. But the presence of large carbides are detrimental to toughness. It is important in such steels to keep the carbides as small as possible and to realize that, even then, toughness will be inherently low and therefore the steels should be used in applications not subject to tensile stresses, which is the case for most bearing applications. Another inherent problem contributing to the loss of toughness in high carbon martensite is the formation of cracks in the plate martensite formed on quenching, as illustrated in Fig. 4.14(c). An enlargement of the region labeled Q.C. (Quench Crack) is shown at the right. Such cracks often occur where plates impinge upon each other, and they lead to a severe loss in toughness. So, lath martensite is inherently a better form of martensite than plate martensite when toughness is important.

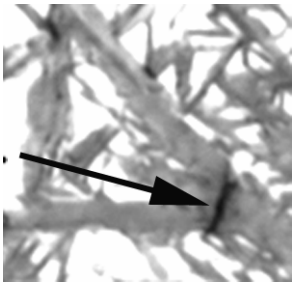

Effects of Alloying Elements In addition to improving hardenability, the most important reason for adding alloying elements to plain carbon steels is to improve their tempering response. The effect of alloying elements in general is illustrated in Figs. 10.5 and 10.6. The upper curve of Fig. 10.5 presents the same data for the hardness of fresh martensite that was presented in Fig. 4.12. Note that this curve applies to both plain carbon and alloy steel. Tempering causes the hardness to drop and the lower two curves show the hardness vs. %C after tempering at the same temperature for the plain carbon and the alloy steel. The main thing to see is that the alloy addition allows one to achieve a higher tempered hardness. The increased hardness is shown by the vertical arrowed line labeled ΔH, where the symbol Δ means change and H means hardness. The lower curve on Fig. 10.6 presents actual data showing how the hardness of a 1040 steel drops with tempering temperature, and the upper curve shows how the

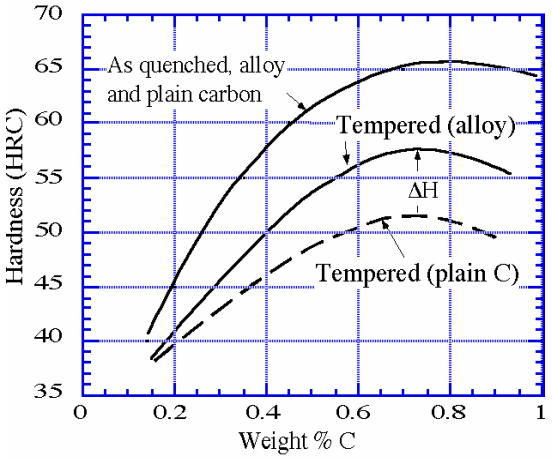

Figure 10.5 As quenched and tempered hardnesses of plain carbon and alloy steel vs. %C.

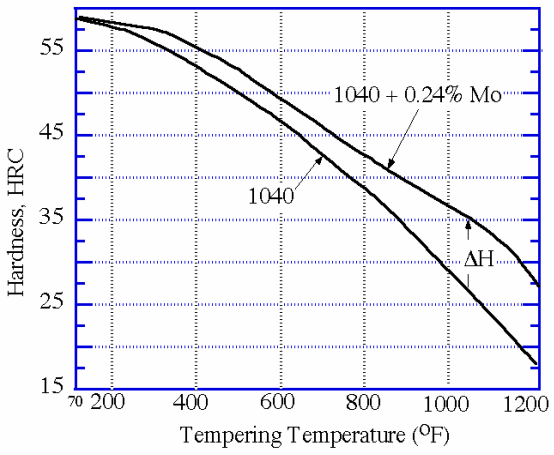

Figure 10.6 Influence of a Mo alloy addition on drop in hardness versus tempering temperature [10.8].

addition of 0.24 %Mo increases the hardness. Again one sees a higher hardness for the alloy steel by an amount indicated as ΔH. The increment in hardness depends on the alloying element added, as well as the tempering temperature utilized. As illustrated in Fig. 10.7, the four main alloying elements in the AISI steels, as well as the small amount of Si present in them, produce a ΔH increment. The magnitude of the ΔH increment for each element varies with the tempering temperature, and Fig. 10.7 illustrates the general trend observed. The main reason for this increment is that very small carbides contribute to hardness, but the contribution drops off as the size of the carbides increases. As explained in Chapter 8, p. 73, the reactive alloying elements segregate into the cementite component of steel. This changes the composition of the carbides from Fe_3C to $(Fe+X)_3C$, (often written as M_3C) where X refers to reactive alloying elements such as Cr and Mo. At higher tempering temperatures the average carbide size increases as larger carbides replace smaller ones. But this **coarsening** process requires diffusion and the alloying element, X, cannot diffuse nearly as fast as C. Therefore, in the alloy carbides formed in low alloy AISI steels, both $M_{2.4}C$ and M_3C, the carbides can maintain smaller sizes to higher tempering temperatures and thereby give increased hardness after tempering.

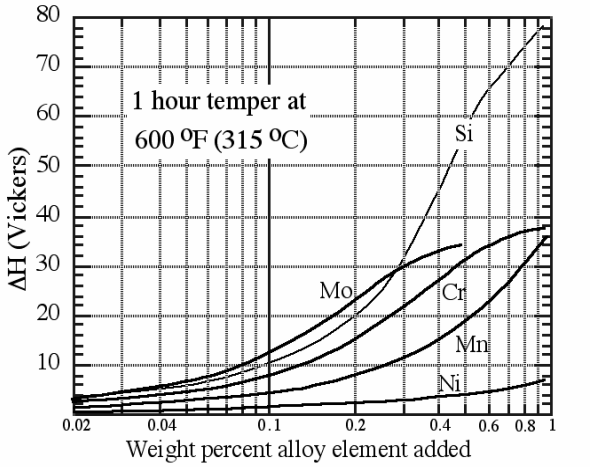

Figure 10.7 Increment in hardness on tempering for Si and the 4 major alloying elements [10.3].

Table 10.2 Two 0.6 % C steels

Steel	%C	%Mn	Alloying Element
1060	0.6	0.75	none
5160	0.6	0.88	0.8 %Cr

To illustrate the beneficial effects produced in tempered alloy steels consider the following comparison of the two steels containing 0.6 % C shown in Table. 10.2. The steels were quenched and tempered for 1 hour at the 4 temperatures shown on Fig. 10.8. At a given level of ductility the low alloy AISI steel is harder (or alternately stronger). At the ductility level of 42 % RA shown by the vertical dashed line, the 5160 is harder by HRC = 43 versus 34 for 1060 (Equivalent tensile strengths of 202 ksi vs. 152 ksi.). Alternately, at a given level of hardness the alloy steel has improved ductility. At HRC = 32 (horizontal dashed line) the %RA of the 5160 is higher by 52% versus 43 % for the 1060 steel.

The point was made in Chap. 8 that the reactive alloying elements tend to form carbides, which leads to two important results. (1) In steels containing cementite carbides the reactive elements will segregate to the cementite, changing its composition from Fe_3C to M_3C, where M =

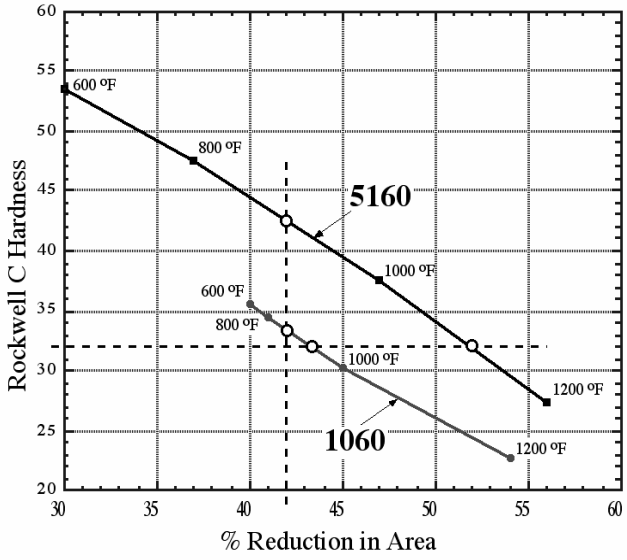

Figure 10.8 Drop in HRC hardness of 1060 versus 5160 steels after tempering for 1 h at temperatues shown (data from [10.5]).

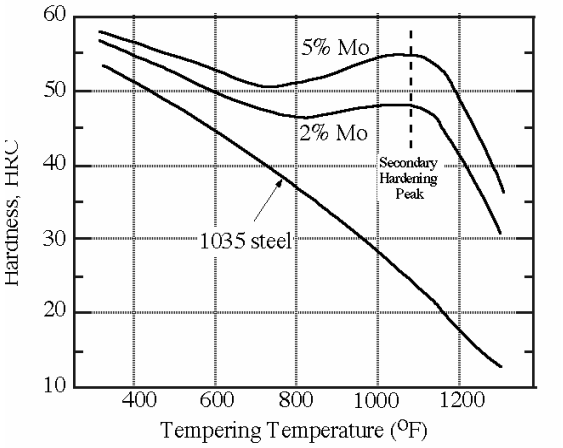

Figure 10.9 Secondary hardening peak formed with large additions of Mo to a 1035 steel [10.8].

Fe + alloying element (2) Cementite is an iron carbide and it will be called a native carbide of iron. Similarly, all of the reactive alloying element form native carbides. These carbides have a different crystal structure, a different melting point and a different hardness than the cementite carbide M_3C. For example, $Cr_{23}C_6$ and Mo_2C are native carbides of Cr and Mo. The hardness and the melting point of the native carbides of the reactive metals are higher than the cementite carbide. The higher melting temperature indicates a reduced mobility of the atoms, which means that if these carbides form on tempering they will **coarsen** less and give improved strength (hardness) at higher tempering temperatures. If adequate amounts of the reactive alloying elements, such as Mo or Cr, are added to a steel their native carbides will form in significant amounts on tempering and give significant increases in tempered strength, as illustrated in Fig. 10.9 for Mo. As shown, the strength on tempering actually increases at higher tempering temperatures when the native Mo carbide forms. This strength increase is sometimes called the 4th stage of tempering, or alternately, the secondary hardening peak. Such high temperature strength is very important in tool steels.

In all of the discussion to this point no mention has been made of the time of the tempering hold at temperature. As one tempers at a given temperature the hardness will fall with increasing time. However, the drop in hardness with time is fairly slow and is often not shown on tempering curves. There have been some extensive studies on the effect of alloying elements, tempering temperature and tempering time on the hardness produced on tempering [10.6, 10.7]. These studies have developed a correlating parameter that allows one to calculate a tempering curve for any AISI steel. Using the method described there, the tempering curves for 1045 steel shown in Fig. 10.10 were determined. The curves show the effect of both time and temperature on hardness. Note, that compared to temperature variations, the time variation from 1 to 4 hours is negligible. Reference [10.2] has several plots of actual data on time and temperature variations which lead to this same conclusion. The curves generally do not mention time of tempering, which is assumed to be 1 hour. However, the time dependence is presented for a few steels. AISI 1045 is one of these steels and the time dependence is similar to that in the calculated curves of Fig. 10.10.

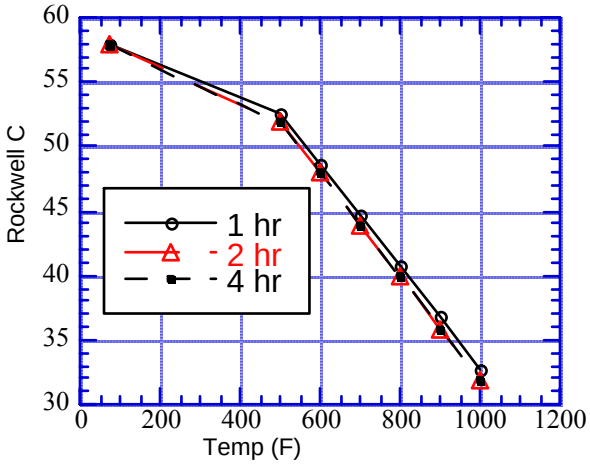

Figure 10.10 Predicted Rc versus tempering temperature for 1045 steel.

References.

10.1 Modern Steels and their Properties, Handbook 2757, Bethlehem Steel Corp. (1972).
10.2 A. Grossmann and E.C. Bain, Principles of Heat Treatment, ASM (1964).
10.3 R.A. Grange et. al., Metallurgical Transactions, vol. 8A, p. 1780 (1977).
10.4 Heat Treater's Guide Practices and Procedures for Irons and Steels, ASM International, 2nd Edition (1995).
10.5 ASM Databook, Metals Progress, vol. 112, June (1977).
10.6 J.H. Hollomon and L.D. Jaffee, Trans. Met. Soc. AIME, vol. 162, 223 (1945).
10.7 R.A. Grange and R.W. Baughman, ASM Trans. vol. 48, 165 (1956).
10.8 E.C. Bain and H.W. Paxton, Alloying Elements in Steel, pp. 198 & 200, ASM (1966).

Summary of Major Ideas of Chapter 10

1 Most all quenched steels are tempered because the toughness of as-quenched steels is generally very poor. Tempering (heating to a low temperature for around 1 hour) significantly increases toughness and ductility, at the sacrifice of both yield strength and tensile strength. Figures 10.2 and 10.3 show the general trend.

2 During tempering the martensite begins to decompose into ferrite and carbides. At the lowest tempering temperatures very fine metastable carbides (usually epsilon carbide, $Fe_{2.4}C$) form (called stage 1 tempering) and at higher temperatures they are replaced by the usual carbide, cementite, Fe_3C, (stage 3). At intermediate temperatures, if retained austenite is present it will decompose (stage 2).

3 Toughness is best measured by notched impact tests such as the Charpy or Izod tests. Such tests, as shown in Fig. 10.4, show that toughness after tempering drops to dangerously low levels as the %C rises above around 0.4%. Because of this fact, combined with the fact that 0.4% C is adequate to produce very strong quenched and tempered steel, the %C level of most all of the various steels used in industrial and commercial machinery, such as trucks and automobiles, is limited to 0.4%.

4 Higher carbon steels find widespread use because of their significant improvement in wear resistance. This wear resistance is due to presence of carbides which have hardnesses superior to martensite. The carbides promote brittleness and this effect is minimized by keeping the carbide size small. Plain carbon steels such as 1080 and 1086 produce improved wear due to the very fine carbides produced in stage 1 of the tempering process. Such steels find wide use in cutting and ploughing applications. Bearing steels such as 52100 as well as tool steels are heat treated to produce arrays of carbide particles of fine sizes. Although fine, around 1 micron, the size range is still much larger than the carbides produced in stage 1 tempering.

5 Two embrittlement mechanisms can occur on tempering steels. The first, tempered martensite embrittlement (TME), occurs for tempering in the range of 500 to 650 ^oF, and this range is to be avoided in tempering. The second, temper embrittlement, TE, occurs for tempering in the range of 1000 to 1200 ^oF. It is easily avoided by quenching from the tempering temperature.

6 The strength of quenched steels drops on tempering. The fine carbide arrays that form in the stage 1 tempering produce a strengthening effect that tends to reduce the inherent rate at which strength drops during tempering. As tempering temperature rises the fine carbides grow in size (**coarsen**) and this reduces their strength contribution. Addition of the reactive alloying elements which prefer to form carbides, such as Cr or Mo, makes the carbides coarsen more slowly and produces higher strengths (hardnesses) after tempering, as is shown in Fig. 10.6. The reduced coarsening rates result because the alloying elements have low diffusion rates in austenite and are therefore difficult to remove from the carbides and hence allow the carbides to remain smaller at higher temperatures.

7 A major advantage of the low alloy AISI steels versus plain carbon steels is this improved tempering response. The improvement shows up as an increase in hardness (or correspondingly strength) at the same level of ductility. Addition of 0.8 %Cr converts a 1060 steel to the low alloy 5160 steel. As shown in Fig. 10.8 after tempering to a ductility of 42% RA (reduction in area), the hardness of 5160 is HRC = 43 compared to 34 for the 1060 steel (equivalent tensile strengths of 202 ksi versus 152 ksi). Alternately, after tempering to an HRC of 32, the ductility of 5160 is superior to 1060 by 52% RA versus 43 % RA. The small Cr addition produces this enhancement by reducing the coarsening rate of the small carbides formed in the stage 1 tempering.

8 The carbides that form in the low alloy AISI steels of Table 6.4 are epsilon and cementite carbides that incorporate the alloying element and change the carbide from $Fe_{2.4}C$ to $M_{2.4}C$ or Fe_3C to M_3C, where M = Fe + X and X = Cr and/or Mo. In high alloy steels, such as tool steels carbide forming elements, like Mo, are added at higher levels and on tempering produce carbides native to that element, and different from $M_{2.4}C$ or M_3C. These native carbides, such as $Cr_{23}C_6$ or Mo_2C, resist coarsening to higher tempering temperatures and often can produce strengths even higher than the as-quenched strengths at tempering temperatures just above a red heat, around 500 ^oC (932 ^oF), see Fig. 10.9.

9 The strength and hardness drop during tempering as one increases either (1) the tempering temperature or (2) the tempering time. For the low alloy AISI steels the reduction is influenced much more strongly by tempering temperature. As shown in Fig. 10.10 increasing the tempering time for a 1045 steel from 1 to 4 hours drops the hardness by only around 1 HRC unit compared to around 5 units for a 100 ^oF increase in tempering temperature. For this reason many of the useful tempering graphs found in ref. [10.4] present tempered hardness versus tempering temperature with no mention of tempering time. In such cases it is safe to assume the tempering time was 1 hour.

11 Austenitization

The first step in the hardening of steel is heating the steel hot enough to form austenite from which martensite can form on quenching. For some steels it is desired or required that carbides be present during this austenitization step and this will be called two-phase austenitization. Because the presence of the carbides produces some significant changes, single phase austenitization and two-phase austenitization will be treated separately in the following discussion.

Single Phase Austenitization Plain carbon and low alloy AISI steels are generally austenitized at temperatures that produce single phase austenite. This means the steel must be heated above the A_3 or the A_{cm} temperature for the steel of interest. The temperature range for the plain carbon steels is shown on Fig. 4.22 and reference [11.1] presents specific recommended temperatures for all the individual steels.

The purpose of the austenitization step is to produce austenite with a homogeneous composition of both carbon and any alloying elements present. The room temperature steel will general consist of ferrite and cementite. In hypoeutectoid steels the cementite will usually be present as pearlite and in hypereutectoid steels it will be present either as pearlite, or a mixture of pearlite and cementite particles. In plain carbon steels ferrite is essentially pure iron (Fe + 0.02 % or less C), and basically all of the C is contained in the pearlite for hypoeutectoid steels. Hence, homogenization of the C requires heating the steel at a hot enough temperature for a long enough time for the carbon to diffuse from the pearlite regions to the center of the largest ferrite regions, see Fig. 11.3. Because the alloying elements are also present at different compositions in the room temperature cementite and ferrite the same rule applies to homogenization of the alloying elements during austenitization. By simply heating hotter one can speed up this homogenization process. However, it is important not to heat so hot that excessive grain growth occurs in the austenite because large grains reduce toughness. Hence the austenitization temperature and time should be selected to control the two factors: (1) homogenization of C and alloying elements, and (2) minimization of austenite grain growth.

Homogenization Homogenization with respect to C and the alloying elements occurs by the process of diffusion discussed in Chapter 7. Consider first, the homogenization of carbon. The homogenization of a ferrite-cementite mixture into austenite occurs by a 2-step process which will first be described for austenitization of pearlite. Figure 11.1(a) shows a ferrite plate (α) in pearlite between two cementite plates. As shown in Fig. 11.1(b), upon heating to A_{c1} austenite will form along the α/Cm boundaries and grow into both the ferrite and cementite plates. Eventually the growing austenite consumes all of the α and Cm, and this is the end of the first step. At this point the C composition is not homogeneous in the austenite, it will be highest at the center of the old Cm plates and lowest at the center

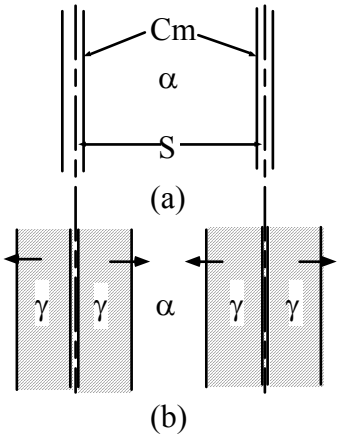

Figure 11.1 (a) Pearlite with spacing = S. (b) Austenite (γ) formation at temperatures of A_{c1} and above.

of the old α plate. In the second step the C composition in the newly formed austenite homogenizes by the process of diffusion. In the first step diffusion also occurs into ferrite, but analysis shows that the first step as well as the second step is controlled by the diffusion of C only in the austenite. To a good approximation then, we can determine how long it will take any ferrite/cementite mixture to homogenize by calculating how long it will take the C atoms to diffuse the required distance in austenite. In Fig. 11.1 the required distance will by the half spacing between plates, S/2, because the C diffuses into the ferrite plate shown from both left and right.

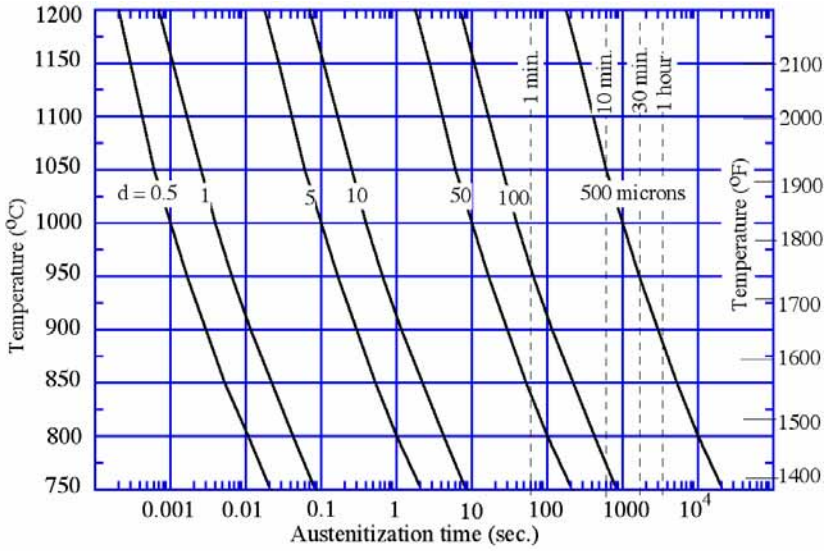

Figure 11.2 Temperature dependence of time required for C atoms to diffuse distances, d, of 0.5, 1, 5, 10 50 100 and 500 microns in austenite.

Equation 7.1 allows us to calculate approximately how long it will take a carbon atom to diffuse some arbitrary distance, d, if we know the diffusion coefficient, D, of carbon in austenite. The values of D for carbon diffusion have been well measured and are given to a good approximation for most steels as $D = 0.12 \times \exp[-16000/(T+273)]$ cm^2/s, where T is temperature in ^oC. Hence, it is possible to construct diagrams like Fig. 11.2 which show the times required to move C atoms distances ranging from d = 0.5 to 500 microns as temperature increases. The line labeled 5 tells us that at 800 ^oC and 1000 ^oC it will take 1 sec. and 0.1 sec., respectively, for a C atom to diffused 5 microns. The pearlite spacing, S, is generally less than 1 micron giving a diffusion distance for homogenization of d = S/2 = less than 0.5 microns. At the recommended temperature range for austenitization of steels of 1500-1550 ^oF in reference [1], Fig. 11.2 shows that the pearlite should form homogeneous austenite in less than 10 milliseconds (0.01 sec.).

Now consider a typical ferrite/pearlite steel as shown in Fig. 11.3 that is to be austenitized. Essentially all the C in this steel is contained in the pearlite regions, marked P. The above discussion shows that these pearlite regions will form homogeneous austenite in a manner of seconds after reaching the A_{c1} temperature. The fresh formed austenite in the old pearlite regions will have the carbon composition of the old pearlite, roughly 0.77 %C. To complete homogenization of the steel this carbon must be redistributed to the center of the surrounding ferrite grains, a maximum distance of z on Fig. 11.3, roughly 1/2 the ferrite grain size. As before, the homogenization occurs in 2 steps. (1) The austenite formed in the old P regions expands into the ferrite grains by migration of the austenite/ferrite boundaries. (2) This newly formed austenite will contain less C at the center of the old ferrite grain and more at the edge and the second step is homogenization of this C variation by

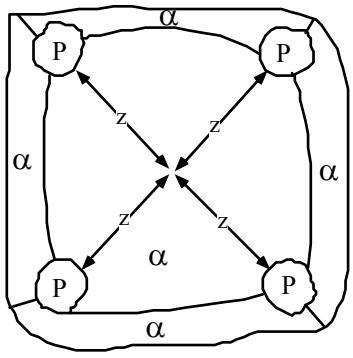

Figure 11.3 A ferrite grain with pearlite at its grain corners.

diffusion. As with the pearlite the total homogenization process is controlled by the diffusion coefficient of C in austenite and the time may be approximated as above with Fig. 11.2. Suppose the ferrite grain size is relatively large, like 100 microns. This gives a diffusion distance d of 50 microns and at typical austenitization temperatures homogenization is predicted to be complete in around a minute. At a more typical ferrite grain size of around 20 microns homogenization is predicted to require less than 10 seconds.

Hypereutectoid steels are supplied from the mill in the spheroidized form with particles of Cm in a ferrite matrix. When these steels are austenitized, homogenization occurs by the formation of spherical regions of austenite which form around the carbides and grow into the surrounding ferrite. Again the process occurs in 2 stages: First the conversion of the surrounding ferrite to austenite as these spherical regions expand and second by the homogenization of the fresh formed austenite with C diffusing to the center of the ferrite regions from the positions of the dissolved Cm particles. Homogenization times can again be approximated with Fig. 11.2. Because the distance between the spheroidized Cm particles in hypereutectoid steels is generally less than around 5 microns, the carbon homogenization times are again predicted to be small, on the order of a matter of seconds after the austenitization temperature is reached.

It is important to bear in mind that these calculations give us the time of homogenization after the steel has achieved the recommended austenitization temperature. After placing a piece of steel in a furnace set at the desired austenitization temperature it will take some time for the center of the steel to reach this temperature. A general rule of thumb is that it will take the steel a time equal to one hour per inch of thickness. When working with propane fired furnaces having considerable gas flow, as is often done by bladesmiths, the times to achieve the austenitization temperature can be considerably reduced. Similarly, austenitizing in salt pots will considerable reduce times to heat to the austenitization temperatures, as the liquid salt transfers heat more rapidly than gases do. Three techniques which produce extremely fast heating rates are flame heating, induction heating and laser heating. As shown with Fig. 11.2, even with these ultrafast heating rates homogenization of austenite with respect to %C is not a big problem as long as the microstructure of the steel is fine. However, such is not the case when considering homogenization of austenite with respect to the alloying elements of a steel.

As pointed out in the diffusion chapter, the alloying elements have diffusion coefficients in austenite that are 1000s of times lower than for carbon. Hence, homogenization of the alloying elements during austenitization is much slower than homogenization of C. As an example alloying element consider Cr whose diffusion distances are given in Fig. 11.4 as calculated from the measured diffusion coefficient of Cr in austenite [7.1]. Diffusion times are now much larger, for example at 850 ^{o}C (1562 ^{o}F) a diffusion distance of 1 micron requires 5 hours for Cr, compared to only 0.02 seconds for C. Air cooled pearlite will generally have a plate spacing, S, of less than 0.2 microns, giving a homogenization diffusion distance of 0.1 microns. Figure 11.4 estimates that at the normal austenitization temperature of 5160 steel (830 ^{o}C

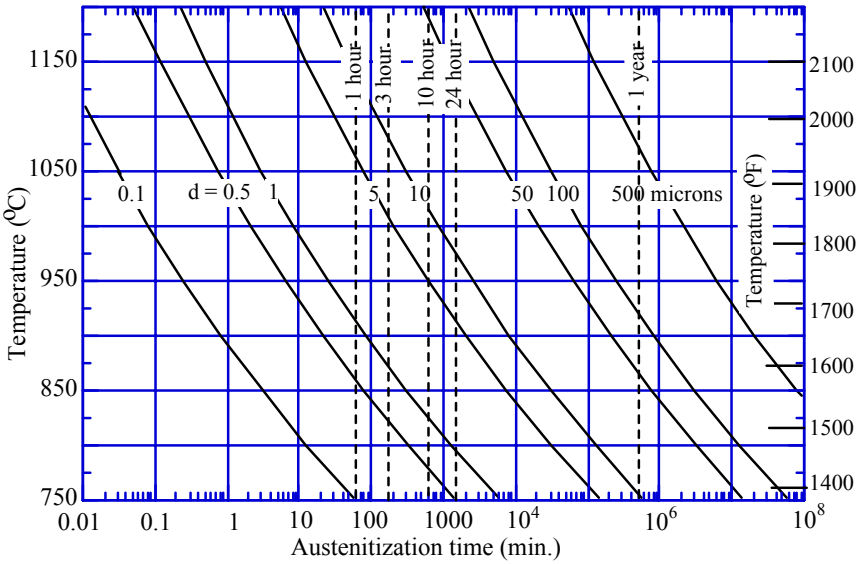

Figure 11.4 Temperature dependence of time required for Cr atoms to diffuse distances, d, of 0.1, 0.5, 1, 5, 10 50 100 and 500 microns in austenite.

recommended in[11.1]), the pearlite should homogenize in around 5 minutes. However, if the Cr containing carbides of a Cr steel are more widely separated than in pearlite, as in a spheroidized steel, homogenization times can be significantly longer. For example, if a spheroidized 5160 or 52100 steel with carbides spaced at 1-2 microns is austenitized at 830 °C, Fig. 11.4 shows that homogenization will take on the order of 100 min. This effect may explain the dramatic improvement of hardenability of a 5160 steel that is achieved by increasing the austenitization temperature from 850 to 950 °C (1562 to 1742 °F), see Fig. 9.15. Another example of slow homogenization of alloying elements was pointed out in the last chapter on tempering. In alloys containing carbides the first step of homogenization is the dissolving of the carbides into the surrounding austenite that forms upon them. The rate of this step is dramatically lowered by the low diffusion coefficient of carbide forming alloying elements. Hence, during tempering the stage one $M_{2.4}C$ epsilon carbides remain smaller than the $Fe_{2.4}C$ epsilon carbides of plain carbon steels resulting in higher tempered strengths at a given tempering temperature as was shown for a Mo alloy in Fig. 10.6 and a Cr alloy in Fig. 10.8.

Austenite Grain Growth The principles of grain growth were discussed in chapter 8. As illustrated in Fig. 8.3 austenite grain size increases rapidly as austenitization temperature is increased. The figure also shows that, in general, the austenite grain size increases more rapidly with increasing temperature than increasing time.

At normal heating rates the new austenite grains will nucleate on the boundaries between cementite and ferrite with their subsequent growth rate controlled by C diffusion in the fresh formed austenite. At very rapid heating rates to temperatures higher than around 910°C (1670 °F), however, new austenite grains can nucleate directly on old ferrite/ferrite boundaries as shown in Fig. 8.4. To understand why rapid heating rates and high temperatures are required remember that the ferrite component of room temperature steel is nearly pure iron. Figure 3.5 shows that the ferrite component will contain around 0.02 %C, and if heated above the A_c temperature of around 910 °C (1670 °F) it can transform directly into austenite with no composition change required. However it must be heated rapidly or it will be transformed into austenite from austenite regions that nucleate first at the cementite/ferrite boundaries and then grow into remaining ferrite. In any case, as discussed on page 69, the first formed austenite grains will have small diameters, which grow rapidly as temperature increases. As shown there the small

grains can effectively be retained by using the trick of rapid cyclic heat treating. It is also shown in Chapter 8 that alloying additions reduce austenite grain growth by two mechanisms, the formation of small particles, Figs. 8.9 and 8.10 and (2) grain boundary segregation, Fig. 8.12.

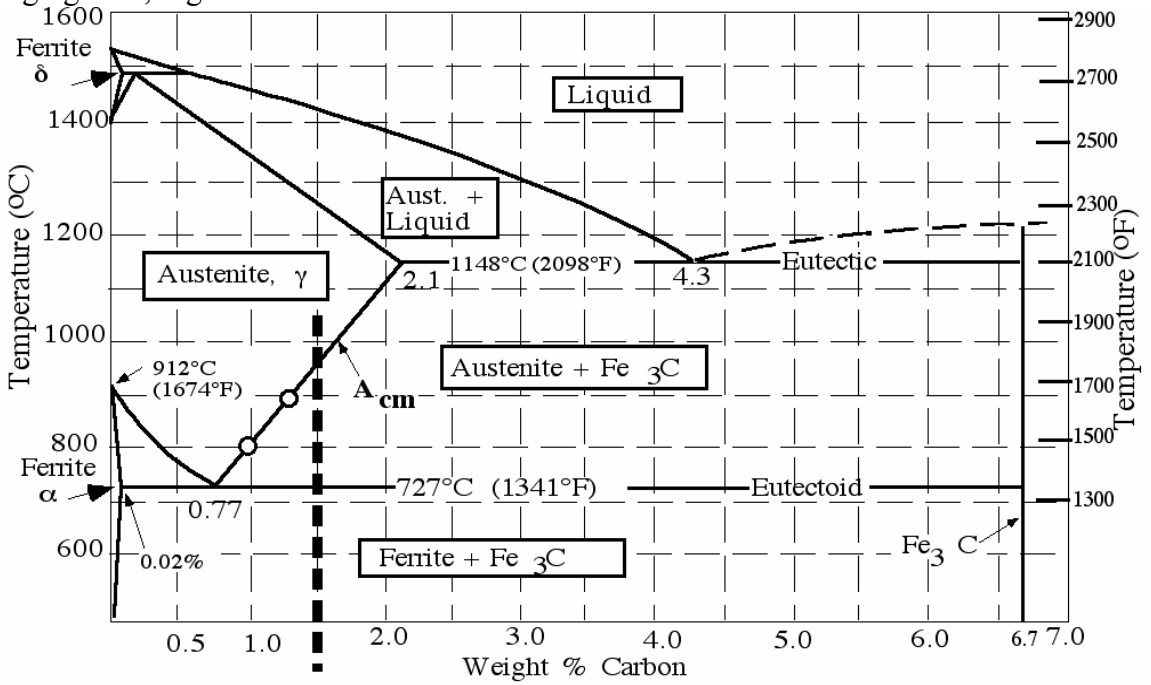

Figure 11.5 The full iron-carbon phase diagram.

Two-Phase Austenitization Steels that are used for superior wear properties generally contain carbides in a tempered martensite matrix. This means that the carbides must be present during the austenitization step in order for them to be present after the austenite transforms to martensite on quenching. Common examples include bearing steels, such as 52100, tool steels and heat treated cast irons such as ductile cast iron. Many tool steels and most all cast irons cannot be heat treated to single phase austenite. To understand why, consider the full Fe-C phase diagram which is shown as Fig. 11.5. (If you compare this to Fig. 3.5 you will see that the diagrams presented in Chapter 3 were all just small portions of the full diagram that did not show any of the liquid region that occurs at very high temperatures.) In our initial discussion of phase diagrams in Chapter 2, the salt-water system was chosen to illustrate the major ideas. Figure 2.2 illustrates that the freezing temperature of water-salt solutions decrease as the % salt in the liquid increases; but it decreases only down to a certain point, called the eutectic point, which occurs at the eutectic temperature of -57.6 ^{o}F and the eutectic composition of 30 % salt content. Figure 11.5 shows that the same thing happens in steel, with the freezing temperature falling to a eutectic temperature of 1148 ^{o}C (2098 ^{o}F) at a composition of 4.3 weight % C in the liquid steel. Most cast irons have carbon compositions above 2.1 % and below 4.3 % C, and can be roughly modeled with the pure Fe-C diagram of Fig. 11.5*. It shows that an Fe-C alloy in the cast iron composition range of 2.1 to 4.3 %C will begin to melt and

* Actual cast irons also contain significant amounts of Si and its effect on their phase diagram is discussed in the chapter on cast irons, Chap. 16.

will become a mixture of liquid steel and cementite at temperatures above 1148 ^{o}C. At temperatures below 1148 these alloys will always contain some cementite (Fe_3C) mixed in with the austenite. Hence, the diagram is showing us that for Fe-C compositions above 2.1 % there is no way that you can form 100 % austenite. Hence, most cast irons cannot be heat treated to form single phase austenite, they will begin to melt before the cementite can be fully dissolved into the austenite. The same is true of many tool steels, their heat treatment always involves two-phase austenitization.

Such is not the case for steels that have carbon compositions under 2.1 %. Consider an alloy of Fe + 1.5 %C shown at the vertical dashed line on Fig. 11.5. If this alloy is austenitized at temperatures above it's A_{cm} value of around 960 ^{o}C it will become single phase austenite. Now consider what must happen if we austenitize this steel at either of the 2 lower temperatures of 800 or 900 ^{o}C. In both cases the steel will contain cementite in the austenite and will be an example of two-phase austenitization. There is a major difference in single-phase and two-phase austenitization which can be illustrated by this example. To understand this difference it might be a good idea to review the discussion of the 1095 alloy whose microstructure is shown at the bottom of Fig. 3.5. After heating to 760 ^{o}C the alloy is located in the 2-phase γ + Cm region of the diagram at a position shown with the circle. The phase diagram tells us that at 760 ^{o}C any alloy having a composition between points O and P will be a 2-phase mixture of austenite and cementite. Furthermore, it tells us the compositions of these two phases. The austenite composition is given by the intersection of the horizontal line at 760^{o}C with the A_{cm} line, point O. This composition is less than the 0.95 %C in the alloy because not all of the C is contained in the austenite, some is lost to the Cm carbides. Now return to consideration of the 1.5 %C alloy shown with the vertical dashed line on Fig. 11.5. The phase diagram tells us that the austenite composition that forms at the two temperatures of 800 and 900 ^{o}C will be given by the open circles located at the A_{cm} line for these temperatures. Hence the %C in the austenite part of the steel will change with temperature, having values of roughly 1% at 800 ^{o}C and 1.3 % at 900 ^{o}C. <u>The result shows that the %C in austenite for two-phase austenitization is controlled by the austenitization temperature.</u> This is a very important result which must be clearly understood when heat treating such alloys as 52100 bearing steel, as will now be discussed.

Figure 4.17 tells us the amount of retained austenite that is obtained in a quenched steel as the %C of the quenched austenite increases. The results show that in hypoeutectoid steels (%C less 0.77) the amount of retained austenite will generally be small enough to be of no consequence. However, in hypereutectoid steels the amount of retained austenite will become large enough to have significant effects on both strength and tempering response. The effect on hardness (strength) is shown by the data of Fig. 4.12, where the drop in hardness at %C values above 0.8 is due to the retained austenite. Because two-phase austenitization can occur in hypereutectoid steels, the austenitization temperature will have an effect on the amount of retained austenite and, hence, the as-quenched hardness of these steels. Such an effect is illustrated nicely by the data for an 8695 steel shown in Figs 11.6. (8620 steel is often used for carburizing, and 8695 would be a typical carburized composition for this steel.) Figure 11.6 (a) shows the seemingly strange result that the as-quenched hardness of the steel drops as the austenitizing temperature increases

from 1400 to 1600 ^{o}F. The A_1 and A_{cm} temperatures are shown on Fig. 11.6(a) and two-phase austenitization must be occurring between these two temperatures. This means that the %C in the austenite will be increasing as the temperature rises from A_1 to A_{cm}. The increase in %C produces an increase in % retained austenite as shown in Fig. 11.6(b) which, in turn, accounts for the drop in as-quenched hardness. Austenitization above the A_{cm} temperature gives a constant %C in the austenite equal to that of the overall alloy (0.95 %C here) and the hardness becomes constant since the amount of retained austenite is no longer changing with austenitization temperature.

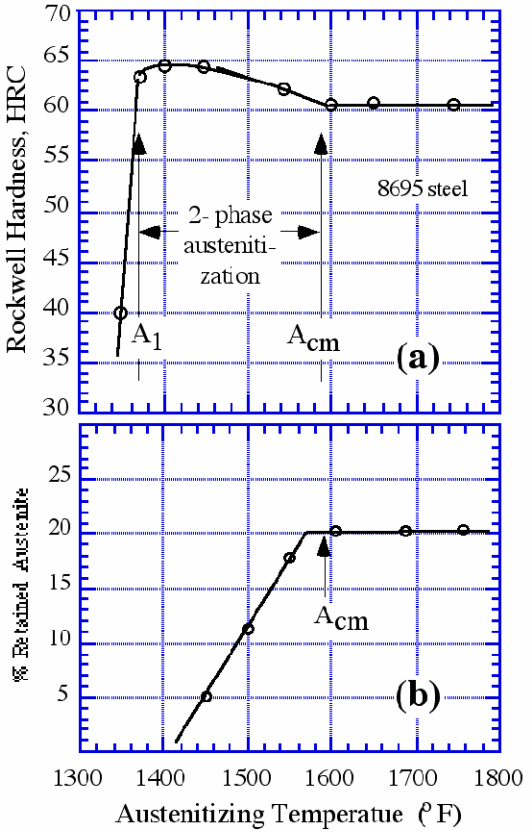

Figure 11.6 Effect of austenitizing temperature on (a) the as-quenched hardness of 8695 steel, and (b) the amount of retained austenite at room temperature [11.2]. (copyright: American Metal Market)

Bearing steels like 52100 are deliberately austenitized below A_{cm} in order to produce arrays of cementite carbides in the final martensite for increased wear resistance. The recommended austenitizing temperature for this steel [11.1] is 845 ^{o}C (1555 ^{o}F) and Fig. 6.3 presents an approximate phase diagram for 52100 showing that at this austenitizing temperature the %C in the austenite will be around 0.78%. Hence, one expects only a modest amount of retained austenite in the quenched product. In addition the martensite should consist of a mixture of lath and plate forms. If however, one were to austenitize this steel at temperatures around 950 ^{o}C, it would become single phase and produce the more brittle plate martensite with more retained austenite. Figure 4.17 predicts that the amount of retained austenite would increase from around 8 to 15 %.

Data is available on 52100 steel [9.3] which nicely illustrate the effect of the Cr alloying element on both the phase diagram and the rate of austenitization. For austenitization at the recommended 845 ^{o}C, Fig. 11.7 presents data showing the measured %C in the austenite as a function of austenitization time for both the 52100 and the corresponding plain carbon steel of the same %C value, 10100. It is seen that the Cr addition in the 52100 steel does 2 things. First, it reduces the rate at which the cementite carbides dissolve. In the plain carbon 10100 steel the carbides are dissolved after around 5 min., while it takes around 100 min. in the 52100 steel for the carbides to dissolve to their final size. Second, the alloy addition has raised the A_{cm} temperature so that austenitization is occurring in the two-phase region for 52100,

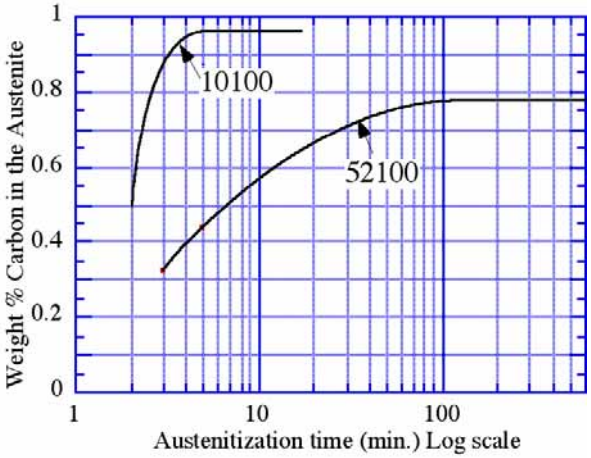

Figure 11.7 Wt. % C increase in austenite at 845 ^{o}C. Adapted from [11.3].

see Fig. 6.3. Hence in the 52100 steel the %C in the austenite has been reduced to the value on the A_{cm} line*, while for the 10100 steel single phase austenitization occurs and the %C is the same as in the starting alloy. (Note: apparently this 10100 steel contained only around 0.95 %C.)

References

11.1 Heat Treater's Guide Practices and Procedures for Iron and Steels, ASM International, 2nd Editions (1995).
11.2 A.R. Troiano and R.F. Hehemann, Effect of Austenitizing Conditions on Medium Alloy Steels, Iron Age, vol. 174, pp. 151-3, No. 21 (1954).
11.3 J.M. Beswick, The Effect of Chromium in High Carbon Bearing Steels, Metallurgical Transactions, vol. 18A, pp. 1897-1906 (1987).

Summary of the Major Ideas of Chapter 11

1 At room temperature most steels consist of a mixture of ferrite and cementite, with the cementite present either as the fine plates in pearlite or as discrete particles. Both C atoms and alloying element atoms have different compositions in ferrite and cementite. For example, cementite contains 6.7 %C compared to only 0.02 %C in ferrite, a huge difference. For carbide forming alloying elements like Cr and Mo, the differences in %Cr and %Mo in cementite versus ferrite are less than for C but can be significant. Hence, when steels are heated to form austenite the fresh austenite inherits a very non-uniform distribution of C and alloying element atoms. It is desirable to make the distribution uniform in the austenite prior to quenching. Therefore an important process that occurs in the austenitization step of heat treating is the homogenization of the fresh formed austenite with respect to %C and % alloying elements.

2 Two important processes occur during austenitization of steels: (1) homogenization of the composition of carbon and alloying elements in the fresh formed austenite, and (2) grain growth of the new austenite grains. Increasing the austenitization temperature will speed up homogenization, but it will also speed up grain growth. Because small grains are required for improved toughness the austenitization temperature is chosen to produce a compromise between these two processes. Reference [11.1] presents recommended austenitization temperatures for the standard hardening of virtually all commercial steels.

3 Homogenization is controlled by the rate of diffusion of carbon and the alloying elements in austenite. These atoms must diffuse from the center of the cementite regions to the center of the ferrite regions during homogenization. The homogenization time is dependent on 2 variables: (1) the diffusion coefficient of the atoms, D, and (2) the distance the atoms must diffuse, d, and both variables have strong effects. Increasing temperature increases D rapidly and drops the homogenization times. Increasing d, the distance from the center of the cementite regions to the center of the largest ferrite regions, increases the homogenization times rapidly. Figure 11.2 shows how the required austenitization time to achieve homogenization of C varies as temperature and diffusion distance are changed.

* Strictly speaking a ternary isothermal diagram is needed to evaluate A_{cm} for steel alloys, but Fig. 6.3 is a reasonable approximation.

4 When austenitizing a steel containing pearlite and ferrite the homogenization occurs in two stages. First the pearlite converts to a homogeneous austenite of the same composition as the pearlite, 0.77 %C. Second, the ferrite around the old pearlite regions converts to austenite and homogenizes on holding. The first stage occurs in seconds after the austenitization temperature is reached because the plate spacing of pearlite is virtually always very small (less than 1 micron) and hence d for diffusion is very small. The second stage is larger because the d value is now set by the ferrite grain size (see Fig. 11.3) which can give d values 10 to 100 times larger than in pearlite. However, even with large ferrite grains size homogenization times for the second stage are still low for carbon, on the order of minutes.

5 Because the D values for the alloying elements are on the order of 1000s of times smaller than for carbon, the homogenization times for alloying elements can be very large at the normal austenitization temperatures. Data are presented for chromium alloys in Fig. 11.4 showing that air cooled pearlite (which has a fine spacing) will homogenize in minutes, but homogenization to the center of the ferrite grains in the second stage can easily take many hours at normal austenitization temperatures. Raising the austenitization temperature can speed up homogenization and produce dramatic increases in hardenability in alloy steels as shown for 5160 steel in Fig. 9.15. One must worry, however, about possible grain growth at the higher temperatures.

6 Grain growth must be minimized during austenitization. Grain growth was discussed in Chapter 8. Grain growth increases with increases of both austenitizing temperature and austenitizing time, and the temperature effect is much stronger, see Fig. 8.3. Grain growth is decreased by the addition of alloying elements, which allows alloy steels to be austenitized hotter than plain carbon steels. Ultrafine austenite grain sizes may be achieved by cyclic heat treatments as demonstrated by the experiment discussed in Chapter 8, see Table 8.2, p 69.

7 For most steels austenitization is carried out at temperatures that produce single phase austenitization, and the general temperature ranges is shown in Fig. 4.22. For high carbon steels used for enhanced wear properties two-phase austenitization is employed. In this case cementite carbides are present in the austenite so that quenching gives arrays of cementite particles in a martensite. The carbides enhance wear resistance as they are harder than the martensite. An important example of two-phase austenitization occurs with the common bearing steel, 52100, and Fig. 6.4 shows the typical carbide arrays that are produced in this steel.

8 Two phase austenitization is tricky because the carbon content of the austenite is controlled by the austenitization temperature. Because austenitization is occurring below the A_{cm} temperature of the steel, the %C in the austenite is given by the location of the A_{cm} line for the temperature of choice, as illustrated for austenitization of a 1.5 %C steel on Fig. 11.5. In this example raising the austenitization temperature from 800 to 900 ^{o}C increases the %C in the austenite from 1.0 to 1.3 %

9 Two phase austenitization occurs for high carbon steels, tool steels and cast irons. As seen in Fig. 4.17, at higher carbon levels significant amounts of retained austenite can occur on quenching which results in reduced hardness and strength. As one raises the two-phase austenitization temperature the %C in the austenite will increase and this can lead to reductions of as-quenched hardness due to increases in % retained austenite, Figure 11.6 illustrates this effect for 8695 steel (a carburized 8620 steel). Austenitizing this steel above it's A_{cm} temperature produces single phase austenitization and as-quenched hardness no longer depends on austenitization temperature because the %C in the austenite is now limited to the overall value of 0.95 %C.

12 Quenching

The quenching process has played an important role in the production of hardened steel implements since ancient blacksmiths first discovered the tricks of hardening carburized iron blades, an event that probably occurred around 1200 BC [12.1]. When reading historical accounts of methods for hardening steel, one cannot help but be impressed by the great emphasis placed on the quenching media as well as the great variety of quenchants that were recommended. Roberts-Austen [12.2] gives a short history of quenchants and states: "The belief in the efficacy of curious nostrums and solutions for hardening steel could hardly have been firmer in the third century BC than in the sixteenth of our era. He quotes a recipe from a 1531 book as: "Take snayles, and first drewn water of a red die, of which water being taken in the two first monthes of harvest when it raynes, boil it with the snails, then heate your iron red hot and quench it thererin, and it shall be hard as steele." C.S. Smith has published several sources on the history of the science of steel which illustrate the importance placed on the quenchant [12.3]. A 1532 pamphlet called, On Steel and Iron, gives several recipes for hardening steel, one of which follows: "Take the stems and leaves of vervain, crush them, and press the juice through a cloth. Pour the juice into a glass vessel and lay it aside. When you wish to harden a piece of iron, add an equal amount of a man's urine and some of the juice obtained from little worms known as cockchafer grubs." A discussion by Wertheim [12.4] shows that there was a widespread belief that special waters were important: "The ever reliable Pliny informs that Roman steelworkers carefully distinguished the waters of various rivers for quenching, a tradition that persisted in western Europe for two millennia and was extant in Asia. In England the waters of the river Derwent, in France of the river Fure were highly regarded." All of these stories reflect the fact that hardening steel was largely an art in early times, plus the fact pointed out by C.S. Smith that the importance of the tempering step was often not understood, so that by slowing the quench rate down some of the exotic recipes probably provided a degree of tempering. Also, recent progress on evaluating the quenching power of water has shown that it is sensitive to various impurity additions, which might well account for some of the early variations that were used.

Special Quenching Techniques By inserting a thermocouple into a piece of steel one may measure the temperature versus time during the quench operation. A plot of this temperature versus time is called a cooling curve. If the cooling curve plot is superimposed on a CT diagram for the steel one may make a reasonable estimate of what austenite transformation products (pearlite, ferrite, bainite or martensite) will form during the quench. Except for thin steel pieces, such as knife blades, the surface of the steel will cool faster than the center region. Figure 12.1 presents a hypothetical cooling curves at the surface and center of a rapidly quenched 5140 steel superimposed on its CT diagram which was previously discussed as Fig. 9.9. Because both the surface and the center have dropped below the M_{90} line without ever crossing the CT lines for ferrite start, F_s, pearlite start, P_s, or bainite start, B_s, we expect the bar to be 100 % martensite to its center. (Note: it is common to use the M_{90} temperature as a reasonable approximation of the martensite finish temperature, M_f.)

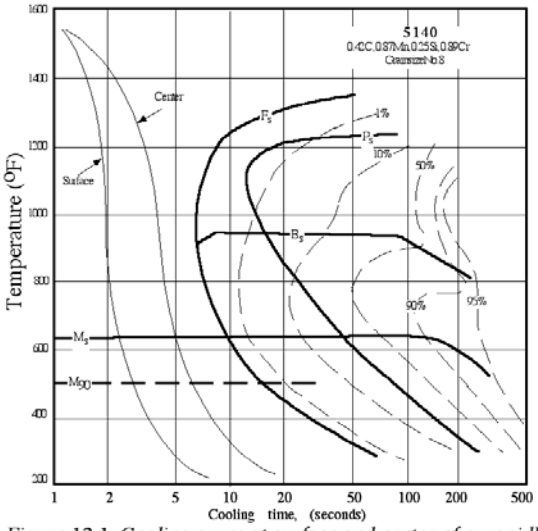

Figure 12.1 Cooling curve at surface and center of a rapidly quenched bar of 5140 steel plotted on top of CT curve.

Martempering A major problem with the rapid quenching of steel is the formation of both distortion and quench cracks in the piece. Experiments have shown that these problems arise from 2 main causes: (1) a non uniform temperature distribution in the piece as its temperature falls through the M_s-M_f range, and (2) too high a cooling rate as the temperature falls through the M_s-M_f temperature range. Quench crack formation leads to embrittlement and sensitivity to this problem depends strongly on the %C in the steel and the cooling rate through the M_s-M_f range. Kern [12.5] claims that water quenching of steels with %C greater than 0.38 % will produce quench cracking unless the piece has a simple shape such as a round with no holes. He recommends use of a slower oil quench for the higher %C steels, which is the usual industrial practice. Distortion on quenching is due mainly to the first cause, large temperature gradients [12.6]. For the example of Fig. 12.1 we would expect extreme temperature gradients, because when the surface reaches M_{90} the center is at around 1350 ^{o}F, which is 850 ^{o}F hotter than M_{90}. Both of these problems can be strongly reduced by employing a special quenching technique first suggested in the 1940's [12.7] which is usually called **martempering**, but also sometimes marquenching.

Martempering is generally done by quenching into a molten salt bath at a temperature just above the M_s temperature. The piece is held in the salt just long enough to equalize the temperature throughout and then it is air cooled. Figure 12.2 shows possible cooling curves plotted on the CT curve for the 5140 steel. The process produces both a uniform temperature in the piece and a reduced cooling rate as it cools through the critical M_s-M_f temperature range where the martensite forms from the austenite. A problem with martempering is that it requires the steel to have a fairly high hardenability, which means that the "nose" of the CT curve must be far enough to the right that the center of the piece cools fast enough to miss it. Hence, except for very thin pieces (such as knife blades) it is difficult to use properly with plain carbon and some low alloy AISI steels. Reference [12.8, p. 104] presents an excellent discussion of martempering giving recommended bath temperatures and compositions as well as maximum section sizes for some plain carbon and several low alloy AISI steels. Martempering can also be

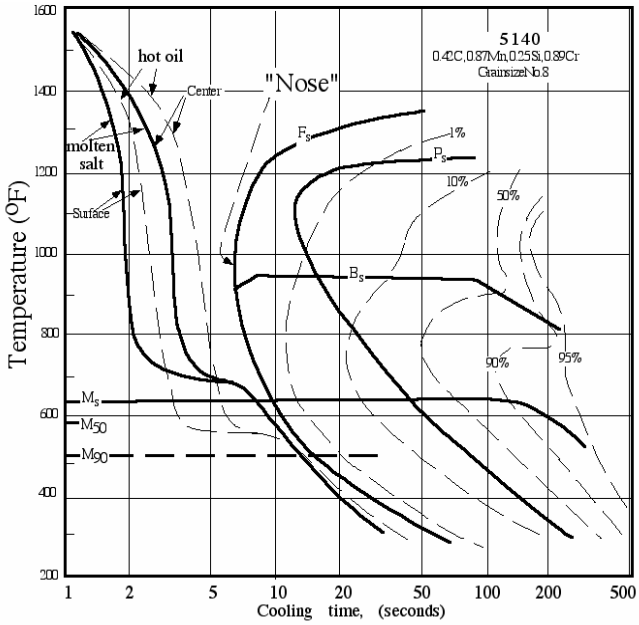

Figure 12.2 Cooling curve at surface and center of a martempered bar of 5140 steel plotted on top of CT curve. Solid curves: molten salt, dashed curves: hot oil.

done using hot oils, so called martempering oils, which can be used at higher temperatures than ordinary quenching oils, and the dashed cooling curves on Fig. 12.2 correspond to such an oil. Experiments [12.6] show that even though the hot oil temperature is below the M_s temperature, significant reduction of distortion is still obtained. Reference [12.8] presents a good discussion of the advantages and disadvantages of salt versus oil for martempering.

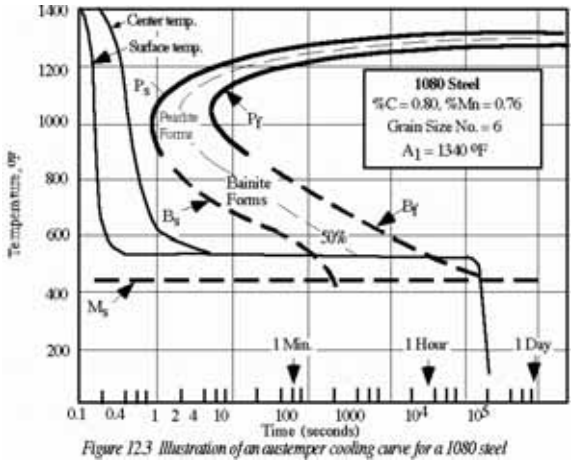

Figure 12.3 Illustration of an austemper cooling curve for a 1080 steel

Austempering The microstructure now called bainite was first discovered with the use of isothermal quenching experiment in the early 1930s by Bain and Davenport at then US Steel. As shown by Fig. 4.22 the bainite has two forms, called upper and lower bainite and on this plot it forms by isothermal holding at temperatures from just above to just below the M_s temperature. To form steels with 100 % bainite it is necessary to quench the steel to temperatures above M_s fast enough to avoid the formation of pearlite or ferrite and hold it until all the austenite transforms to bainite. For plain carbon steels this means that the work piece must be cooled extremely rapidly as is illustrated for a 1080 steel in Fig. 12.3 using the IT diagram of Fig. 9.3. In this example the center of the work piece must cool below roughly 1000 °F in only 1 sec., which illustrates that only quite thin samples of 1080 steel can be successfully austempered. As illustrated in Fig. 9.4, alloy additions shift the pearlite start times to larger values so that the low alloy AISI steels can be austempered in larger section sizes. A problem with austempering the alloys, however, is that the bainite finish curves are shifted to longer times, which, in some cases leads to prohibitively long hold times to complete decomposition of austenite into bainite.

Shortly after the discovery that fully bainitic steels could be produced by isothermal quenching, researchers at US Steel found that such steels had ductilities and toughnesses that were superior to those of quenched and tempered martensites at the same hardness level. Their early work evaluated the hardness of steels transformed completely at isothermal temperatures and Fig. 12.4 presents a graphical summary of the results. The hardness of fresh martensite at room temperature is found at the upper left of the figure and the values are what one expects from the data presented on Fig. 4.12. The curves all show a significant hardness increase as the

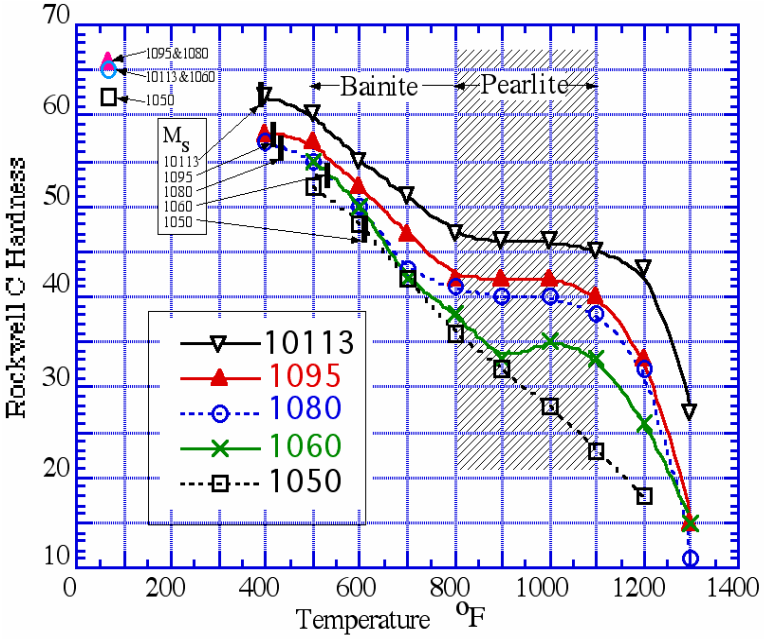

Figure 12.4 Hardness of several plain carbon steels after isothermal quenching. All steels had Mn 0.80-0.90 except 1095 and 10113 which had 0.30%Mn.[12.9]

bainite is formed at decreasing temperatures, which is a reflection of the fact that lower bainite is stronger than upper bainite. The M_s values for the steels are shown by the short vertical line on each curve, and it is seen that the hardest fully bainite structures formed at the M_s temperatures (vertical bars) are not as hard as fresh martensite in each steel. To better illustrate this result Table 12.1 presents a comparison of these hardnesses. The curves of Fig. 12.4 also illustrate that the hardness of fully pearlitic steels depends upon the %C of the steel. At higher % C values the cementite plates of the pearlite increase in relative thickness and make a larger contribution to the total hardness.

Table 12.1 Comparison of fresh mart. hardness to maximum bainite hardness.

Steel	Mart. R_c	Max. Bainite R_c
10113	65	62
1095	66	58
1080	66	57
1060	65	53
1050	62	48

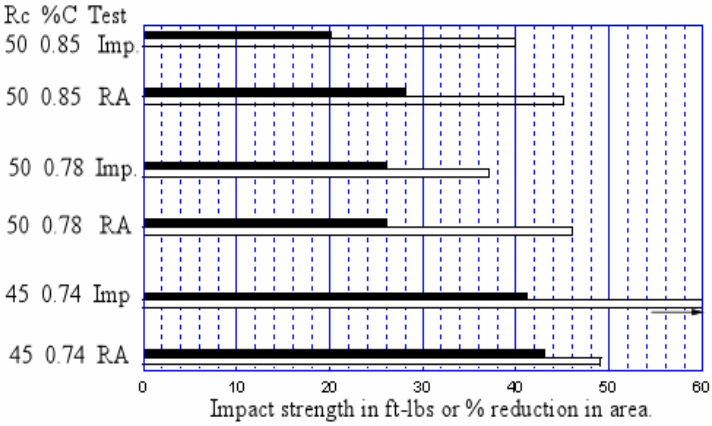

Bar graph 12.1 Comparison of plain carbon Q & T steels (black bars) to austempered steels (open bars). Imp. = impact strength (ft-lbs) and RA =% reduction in area for steels of %C = .74, .78 & .85 with hardness of Rc = 45 & 50. (Imp. test = unnotched Charpy on 0.28 inch rod) [12.10]

To illustrate the advantages of austempered plain carbon steels Bar graph 12.1 presents the early US Steel data comparing the ductility, measured as %RA (percent reduction in area) and the impact strengths on austempered steels versus Q & T (quenched and tempered) steels at the various hardness levels. It is seen that the austempered steels (open bars) produce significantly better ductility and impact strength in the hardness range presented of HRC = 45 to 50. This enhancement in mechanical properties extends to the higher hardness levels possible with austempering as is illustrated dramatically by Fig. 12.5. The austempered rods on the left could be bent to nearly 180 degrees without breaking, while the quenched and tempered rods at the same hardness level of HRC = 58 fractured with little prior bending strain.

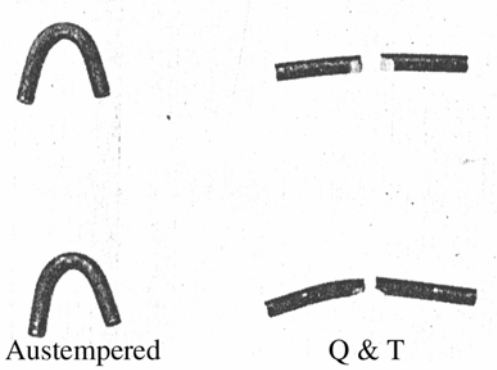

Figure 12.5 Rods of 0.1 inch diameter of 1 %C, 0.4% Mn produced at HRC = 58 and bent under the same conditons.[12.11]

Early industrial work with austempering of plain carbon steels established guidelines for the largest round bar diameters that could be successfully austempered and these data are presented in Table 12.2. Plain carbon steels are available with low and high levels of Mn, and the table illustrates that the hardenability improvement of Mn allows larger section sizes. The final column has been added by utilizing heat transfer calculations to estimate sheet thicknesses that have the same cooling rate at their center for an oil quench that occurs for a round bar. Austempering should be an attractive method of hardening steels for knives as the thin geometry lends itself,

Table 12.2 Maximum secton size for austempering [12.10]

%C	%Mn	Max HRC	Max. Diam. inches	Max. Sheet thickness.
.95-1.05	0.30-0.50	57-60	0.148	0.118
0.95-1.05	0.60-0.90	57-60	0.187	0.150
0.80-0.90	0.30-0.50	55-58	0.156	0.125
0.80-0.90	0.60-0.90	55-58	0.218	0.174
0.60-0.70	0.60-0.90	53-56	0.187	0.150
0.60-0.70	0.0.90-1.20	53-56	0.281	0.225
0.60-0.70	1.60-2.00	53-56	0.625	0.50
1.0 + 0.4-0.6 Cr	0.40-0.60	57-60	0.312	0.250

especially near the cutting edge, to fast cooling rates. And, the final column of Table 12.2 provides a guideline for maximum blade thicknesses of plain carbon steels that should be successfully hardened with austempering. In addition to the improvement in ductility and toughness provided by austempering, it also has the same advantage as martempering for reducing distortion. Also, there is evidence that bainitic structures often show superior wear to that of Q & T steels at the same level of hardness [12.12].

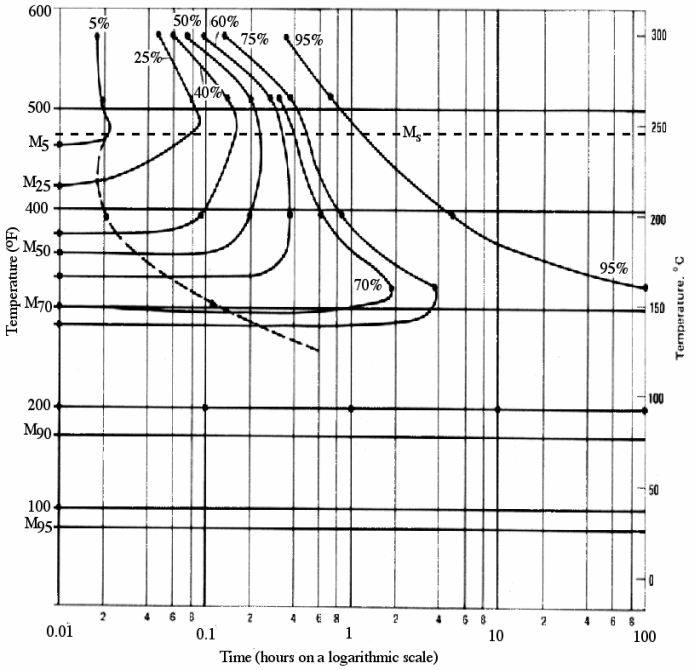

Figure 12.6 IT diagram for a 1075 steel (0.75% C, 0.50% Mn) showing the tranformation times to lower bainite just above M_S and the times for combined transformatin to martensite and bainite just below M_S.[12.16]

Austempering does not always produce an improvement in toughness over the quenched and tempered condition. A review of the data in the literature shows that austempering improves toughness only at the higher hardness levels. The cross-over hardness appears to be around HRC = 40. Below this value the quenched and tempered condition gives as good or better toughness to the austempered condition. [12.13, 12.14].

Variations on Conventional Austempering It is possible to use austempering heat treatments to produce mixtures of bainite and martensite. There is some industrial experience with such mixed structures that indicate they also have excellent ductility and toughness compared to Q & T steels at the same hardness level [12.15]. As an aid to understanding these non conventional austempering treatments the IT diagram at temperatures near the M_s for a 1075 steel is presented in Fig. 12.6, which may also be found in ref. 12.8. The diagram shows the times required to transform the austenite by the percentage values given. Interpretation above the M_s temperature is straight forward. For example, holding at 500 ^oF the austenite transforms to lower bainite going from 5 % transformed at around 0.02 hours to 95 % transformed at around 0.8 hours. Below the M_s the interpretation is a bit more complicated. For example, consider a steel held at the M_{25} temperature, which is about 430 ^oF. After a few milliseconds this steel would contain 25% martensite, that is what the M_{25} temperature designates. The downward curling dashed line tells us when the remaining 75% austenite begins to transform to lower bainite, in this case after about 0.02 hours (72 sec.). Draw a horizontal line across at the M_{25} temperature and you will see that it crosses the 50% line at around 0.25 h (15 min.). At this point the austenite is 50 % transformed so the steel will be 25% martensite (which has been tempered for 15 min.), 25 % lower bainite and 50 % retained austenite. The 95% line is crossed at around 3 h, so here the steel would be 25 % tempered martensite, 70% lower bainite and 5 % retained austenite. Hence, this diagram gives us information on the combined formation of martensite and lower bainite at temperatures below the M_s temperature. The diagram indicates that below around the M_{75} temperature lower bainite will not form in the retained austenite even on extended holding times.

With this information as background, two types of modified austempering heat treatments will be described, both of which produce steels with mixed bainite/martensite structures. Table 12.3 presents the steps in the austempering process following the austenitization step, which is, of course, the beginning step of the process. Conventional austempering (CA) is then a 2 step process as shown in the table and it produces samples that are 100 % bainite. The term ΔT is a conventional scientific nomenclature meaning some specific range of temperature. In our example with Fig. 12.6 austempered at 500°F the value of ΔT would be 27 °F because M_s for this steel is 473 °F (ΔT = 500-473). For CA the final hardness is controlled in one of two ways as shown below the box.

Table 12.3 Three variations on austempering

Conventional Austempering (CA)

step1	step2
Q to (M_s+ΔT) and hold to 100% bainite	Air or oil quench (Piece will be 100 % fresh bainite)

Hardness Control:
(a) Temper to desired HRC.
(b) Adjust hardness with ΔT. Higher values give softer bainite, often upper bainite. Small values give hardest bainite, lower bainite.

Modified Austemper Number 1 (MA1)

step 1	step 2	step3
Q to (M_s-ΔT_1) and hold short time.	Up-quench to (M_s+ small ΔT_2) and hold until all of the retained austenite is transformed to bainite.	Air or oil quench. Piece will contain tempered martensite + fresh lower bainite.

Hardness Control:
(a) Increase ΔT_1 of step 1 to increase %M/%B ratio and increase HRC.
(b) Increase ΔT_2 of step 2 to obtain softer bainite and drop HRC.
(c) Temper the fresh bainite at temperatures above its formation temperature to drop HRC.

Modified Austemper Number 2 (MA2)

step 1	step 2
Q to (M_s±ΔT) and hold time needed to give desired %B. (Note: Is martempering if %B=0 and ΔT small.)	Air or oil quench. Piece will contain mart. + fresh bainite. For positive ΔT values martensite is fresh, for negative values it will be partially tempered. Type bainite (LB vs. UB) and hardness set by ΔT.

Hardness Control:
(a) Temper to desired HRC.
(b) Reduce hold time in step 1 to increase %M/%B ratio and increase HRC prior to tempering.
(c) Change ΔT of step 1 to control hardness of bainite component. Increase ΔT for lower hardness, and decrease ΔT (even to negative values) to increase hardness.

In the first modified austemper process of Table 12.3, MA1, the mix of martensite and bainite is controlled in step 1 by controlling how far the bath temperature is set below M_s. This controls the %martensite which ends up in the sample. Because the sample is held only a short time, little to no bainite will form in this step. The bainite is formed in step 2 after the up-quench. Note that the martensite in the product sample will be in the tempered condition, having been tempered at the temperature of step 2. Three methods of controlling final hardness are listed below the box. Following is an illustration of how one would design an MA1 experiment to produce 50% martensite/50 % lower bainite in a 5140 steel using the CT diagram of Fig. 12.2. After austenitizing the sample would need

to be quenched to a temperature of 580 °F (M_{50} temperature) with the center dropping below the nose temperature in less than around 6 seconds. After the center cools to the 580 °F temperature the sample should be up-quenched to around 650 °C and held for at least 500 sec. before air or oil quenching. The sample should consist of 50% fresh lower bainite and 50% martensite that has been tempered at 650 °C for 500 sec.

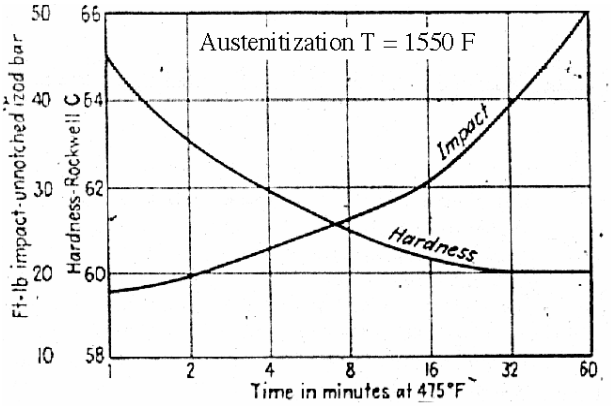

Figure 12.7 Hardness and impact strength of 52100 steel vs hold time at M_S prior to quenching. The %bainite goes from 0 to 100% as time goes from 1 to 60 min. (copyright: American Metal Market)

In the second modified austemper process of Table 12.3, MA2, the mix of martensite and bainite is controlled in step 1 by controlling the %bainite that will end up in the sample. Note that in this case the bath temperature may be set above M_s (positive values of ΔT) or below M_s (negative values of ΔT). For negative values of ΔT the martensite formed in step 1 will end up tempered, but martensite formed in step 2 ends up fresh. Following is an illustration of how one would design an MA2 process to produce 50 % lower bainite in 5140 steel using the CT diagram of Fig. 12.2. After austenitizing the sample would be quenched in salt to 650 °F. Draw a line across Fig. 12.2 at 650 °F and note that the 50% transformation line is crossed at around 60 sec. Therefore, the sample should be held at the 650 °F temperature for 1 minute and then oil quenched to room temperature. It should now consist of 50 % fresh bainite and 50 % fresh martensite.

These variations in austempering techniques offers the bladesmith a rich variety of possibilities for producing knives of varying toughness and hardness. For example as pointed out above, 100% bainite will not be as hard as full martensite. By going to mixed structures one can achieve hardnesses above the limits for 100% bainite given in Table 12.2, and there is industrial evidence that such steels have excellent toughness [12.18].

An interesting possible steel for austempering of knives is 52100 steel. This steel is an excellent candidate for knives as the small carbides in it that produce such good wear properties for its major use as a bearing steel are also attractive for knives. It is sometimes austempered to minimize distortion in bearing races. There is one study in the literature where mixed martensite-bainites were produced in 52100 utilizing process MA2, and here the value of ΔT was set at 0 [12.17]. Figure 12.7 presents the hardness and impact energies of these steels as a function of the time of the hold in step 1. At the shortest times the steel was 100% martensite and at the longest times 100% bainite. It is seen that the bainite improves toughness, but it is not possible to say that the toughness would be higher than the 100% martensite after it was tempered to the same hardness level. However, the known benefits of bainite on toughness would lead one to think the austempered samples would show improve toughness over tempered martensite at the same levels of hardness.

Very little if any systematic studies have been done on the effect of mixed structures on toughness of austempered versus Q & T steels at equal hardnesses. There is

one study showing the effect of %B on the ductility in 3 plain carbon austempered steels [12.18] and the results are summarized in Fig.12.8. This study produced the mixed B/M structures of various hardnesses using method MA1(a&b). At hardnesses of HRC = 50 and 56 it is seen that addition of bainite improves ductility, and more-so as %C increases from 0.65 to 0.95 %C. There are two studies on 4340 alloy steels that show that the mixed austempered structures have superior room temperature toughness for %B levels up to around 30%. [12.19-12.20]. And there is one study on a steel with a composition of 0.9C, 1.6Mn and 0.55Cr, which is not too different than 52100 [12.21]. The comparison of toughness between the austempered versus Q & T condition at specific hardnesses is shown in Fig. 12.9 for this 0.9%C steel. Toughness here was measured with the fracture load in a bend test. The M_s for this steel was 195 ^oC, and the mixed B/M structures were produced by the MA2 method using both positive and negative ΔT values. In the first case the samples were austempered at 300 ^oC ($\Delta T = +105^oC$) to give 10%B, and in the second case the austempering temperature of 180 ^oC ($\Delta T = -15^oC$) was used to produce 13% B. In both methods final hardness was controlled by tempering and the three points of Fig. 12.9 were for tempering at 200, 250 and 300 ^oC. The data of Fig. 12.9 show that the negative ΔT method appears to produce a better toughness at a given hardness level.

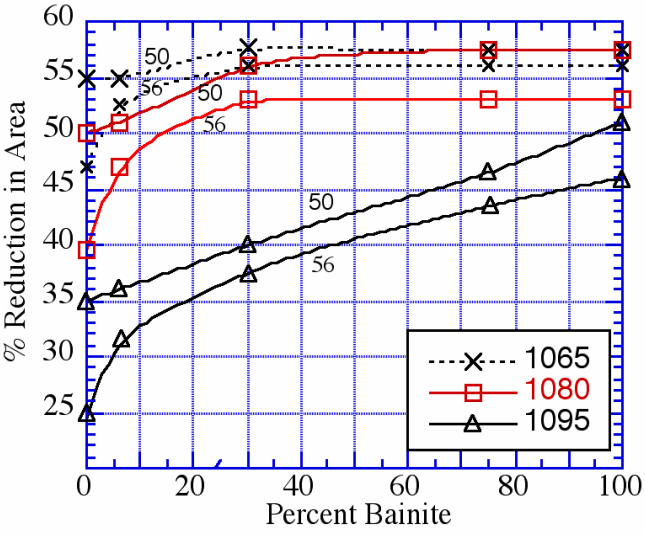

Figure 12.8 Effect of adding bainite to martensite on ductility at a constant hardness levels in plain carbon steels [12.18]

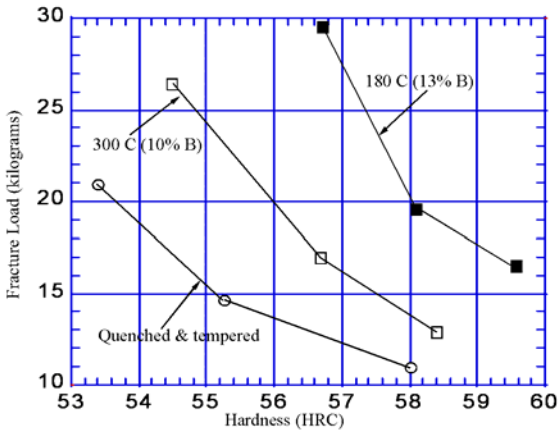

Figure 12.9 Comparison of bend test fracture strengths for quenched & tempered and 2 mixed M/B structures in a 0.9% steel [12.21].

Perhaps the most widespread use of austempering is in the foundry industry where ductile cast iron is so processed to produce what is called ADI, austempered ductile iron. It has been found that the performance of ADI gears rivals that of conventional carburized gears and production is cheaper and more energy efficient. The wear resistance of the bainitic ADI is superior to Q & T steels. This improvement may not carry over to the bainite formed in conventional steels as there is evidence it is related to high degree of retained austenite in the ADI bainites due to the high level of Si in the cast irons. See chapter 16, p 181 for mechanical properties of ADI.

Characterization of Quench Bath Cooling Performance There was a considerable amount of study done on water and oil quenching around the time period when Jominy developed his test in the 1930s and 1940s. The cooling intensity was characterized by a heat transfer parameter called H which has units of 1/inches. Larger values of H gave higher quench intensities and Table 12.4 was established. The table gives one a qualitative idea of the relative increase in quenching speed as (1) the quench

Table 12.4 H values for various quenches.

Movement of piece	H, Severity of Quench			
	Air	Oil	Water	Brine
None	0.02	0.3	1.0	2.2
Moderate	-	0.4-0.6	1.5-3.0	-
Violent	-	0.6-0.8	3.0-6.0	7.5

is changed from air to oil to water and finally to a salt solution and (2) agitation of the quench piece is increased. Heat transfer rates vary enormously during a quenching operation and the use of a single value of H to characterize it is an oversimplification, which is, however, quite useful for some practical purposes.

Quenching a piece of hot steel in water or oil produces copious amounts of vapor around the piece, often called the "vapor blanket". In water the blanket is steam and in oil it is vaporized oil. The presence of this vapor phase around the hot steel leads to the very complex mode of heat transfer that occurs during quenching. There has been considerable research on this problem in the latter decades of the 20th century and a method developed in England has now been adopted as an international standard for characterizing quench fluids, ISO 9950. The test utilizes an Inconel 600 alloy cylinder (basically the same Ni-Cr alloy as used for the heating elements of your electric stove), 12.5 mm in diameter by 60 mm long. A metal clad type K thermocouple (see Appendix A) is fitted into a hole along its center and the output of this thermocouple is monitored during the quench. The output produces a cooling curve such as that shown for an oil bath in Fig. 12.10. The heat transfer during the quench can be partitioned into 3 stages, conventionally called A, B and C. Initially, during the A stage, heat transfer is relatively slow as the heat must pass through the vapor blanket that initially surrounds the immersed sample. Notice that the B stage begins with a rapid increase in the rate at which the temperature drops. When the oil (or water) begins to penetrate through the vapor blanket it contacts the hot steel and immediately boils. The heat required to boil the liquid is removed from the steel and this mode of heat transfer is extremely efficient. It is called "nucleate boiling heat transfer", hence the name of stage B shown on Fig. 12.10. When the boiling stops heat is transferred directly to the liquid touching the steel causing its temperature to increase which, in turn, drops its density. Hence, this liquid rises and is replaced by colder liquid contacting the steel piece. The motion of the liquid is called convection and hence the name of stage C shown on Fig. 12.10.

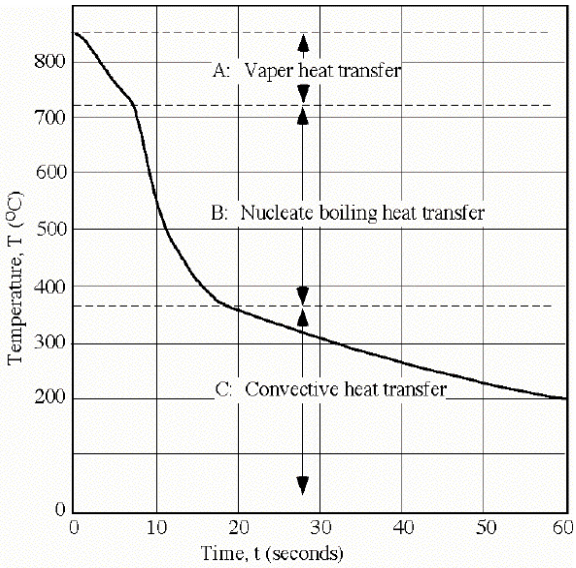

Figure 12.10 Cooling curve measured in the ISO 9950 test on an oil quench bath.

For evaluating quenching intensity we are mainly interested in how fast the temperature is falling and, hence, the most useful parameter is the cooling rate, which will have units of °C/sec. (or °F/sec.). Therefore, it has become common to characterize the quenching

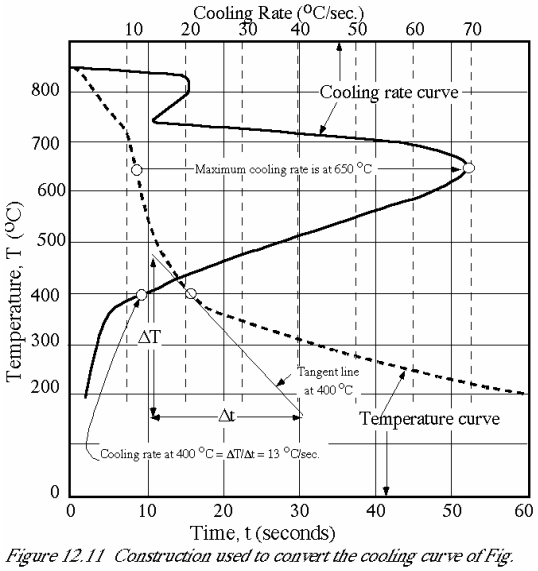

Figure 12.11 Construction used to convert the cooling curve of Fig. 12.5 to a cooling rate curve.

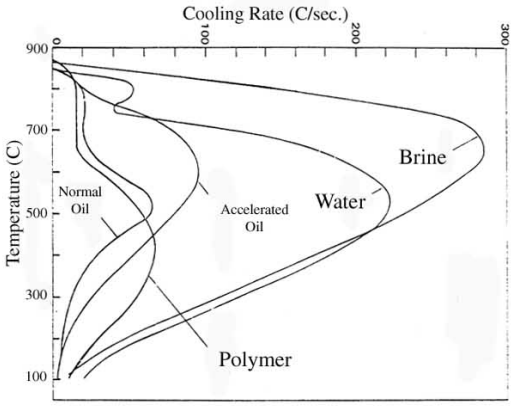

Figure 12.12 Typical cooling rate curves for several types of quenchents at 30 (C) and not agitated [12.22].

power of a quenchant with a plot of cooling rate versus temperature of the Inconel rod, and Fig. 12.11 is presented to show you how such curves are related to the simple cooling curve of Fig. 12.10. In order to obtain the cooling rate at 400 ^{o}C, one constructs a tangent line to the cooling curve at this temperature as shown. Then, moving from the bottom of this line to the top one measures the rise, ΔT, and the run, Δt. The ratio of the rise divided by the run, $\Delta T/\Delta t$ (called the slope in geometry classes) will have units of ^{o}C/sec. and will be the cooling rate when the Inconel center is at 400 ^{o}C. With computer software it is a simple matter to determine the cooling rate at each temperature and the solid line is the corresponding cooling curve with the cooling rates in ^{o}C/sec. given along the top of the diagram. Notice that the maximum cooling rate is 70 ^{o}C/sec. and it occurs at around 650 ^{o}C for this oil. There is an excellent discussion of water, oil and polymer quenchants in reference [12.8], and you will see on pages 78 to 81 that these cooling rate curves are now widely used to characterize the quenching power of the various quenching oils and polymer quenchants that are commercially available. Figure 12.12 presents cooling rate curves for several common quenching fluids. Notice that the maximum cooling rate occurs at different temperatures and varies from a high of 285 ^{o}C/sec. for salt water to a low of 65 ^{o}C/sec. for a normal oil.

For a given quenchant, the speed of the quenching process will depend on the temperature of the bath as well as any agitation used on the work piece during the quenching operation. One can slow down the quench rate of water significantly by heating the water to elevated temperatures. The cooling rate curves given in [12.8] show that the maximum cooling rate for water is decreased from 225 ^{o}C/sec. for a bath at 20 ^{o}C (68 ^{o}F) to only 90 ^{o}C/sec. for a bath at 80 ^{o}C (176 ^{o}F), a decrease of 60 %. The cooling rate data given in [12.8] for hot oils show that the maximum cooling rate is less sensitive to bath temperature and varies in a more complicated manner. As the bath temperature is changed from 200 to 150 to 50 ^{o}C (392, 302, 122 ^{o}F), a maximum cooling rate of 83 ^{o}C/sec. occurs at the intermediate bath temperature of 150 ^{o}C and drops to 80 ^{o}C/sec. at the higher temperature of 200 ^{o}C, and to 75 ^{o}C/sec. at the lowest bath temperature of 50 ^{o}C.

Oil Quenchants One can partition oil quenchants into three categories, normal, accelerated and marquench oils [12.23]. The accelerated oils include additives that produce increased quenching speed as is illustrated by the cooling rate curves in Fig. 12.12, compare the normal oil curve to the accelerated oil curve. The martempering oils are formulated to allow operation at higher temperatures and accelerated and non-accelerated marquench oils are available. Oils can ignite if heated too hot and an oil bath must not be heated too close to its flash point temperature. Reference [12.8, p. 80] presents a table with flash point temperatures for the three types of oils: conventional and accelerated oils have values of around 175 ^{o}C (347 ^{o}F) compared to 300 ^{o}C (572 ^{o}F) for marqenching oils. The table also presents a measure of the quenching speed of these oils labeled GM quenchmeter. This refers to a test developed by General Motors that had been used more in the past to evaluate quenching

speeds. As described in more detail in ref. [12.23], the test measures the time for the quench piece temperature to fall to the magnetic transition temperature (the Curie temperature) of a nickel ball, 354 ^{o}C (669 ^{o}F). So the test number has units of seconds and smaller values mean faster quench speeds.

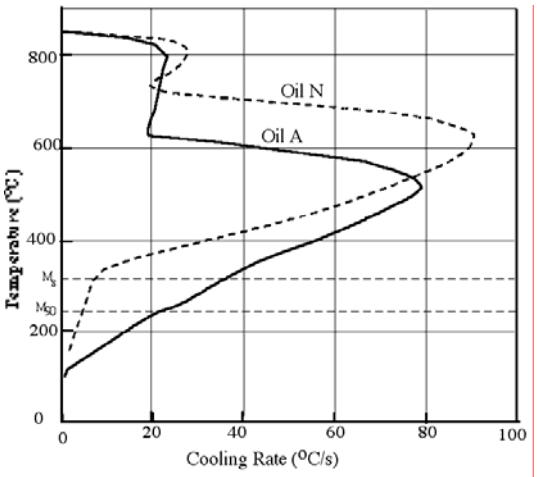

Figure 12.13 Cooling rate data on two different oils [12.24].

Figure 12.13 presents the cooling rate data for two different oils held at 40 ^{o}C, which help to illustrate the usefulness of these cooling rate curves. With the GM quenchmeter test the oils gave essentially the same result, 18.1 s for oil A, and 17.6 s for oil N [12.24]. The cooling rate curves illustrate, however, that there are significant differences in the two oils. Oil N has a faster cooling rate down to temperatures of around 550 ^{o}C (1022 ^{o}F), which means that it would be superior for cooling fast enough to miss the ferrite and pearlite noses of the CT diagrams on low hardenability steels. The temperature axis shows the M_s and M_{90} temperatures for a 1050 steel. Notice that the cooling rates at temperatures between M_s and M_{90} are significantly lower for the N oil. This means that the N oil would be superior for avoiding distortion and quench cracking in parts subject to those problems. Also notice that this occurs even though oil N has a faster maximum cooling rate, which by itself would indicate a higher tendency to cause quench cracking and distortion.

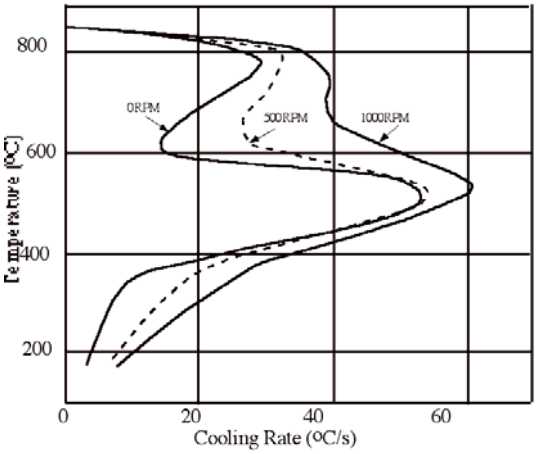

Figure 12.14 Cooling rate curves for conventioal oil at 40 ^{o}C showing effect of agitation [12.22].

The effect of agitation of the quenching oil may be evaluated with these cooling rate curves and Fig. 12.14 presents the results of one study [12.22]. In this case the oil was agitated with a two-blade impeller and the agitation speeds in revolutions per minute are given on the graph. It is seen that the agitation mainly just shifts the curves to higher cooling rates.

Polymer Quenchants These quenchants consist of water with a polymer dissolved in it at some specific concentration level. There are several different types of polymers that have been developed for this purpose and presently the most popular is called PAG, polyalkalene glycol [12.8]. The polymer quenchants produce quenching speeds intermediate to that of water and oils. As illustrated in Fig. 12.15, the quenching speed of a PAG quenchant is progressively reduced as the concentration of the polymer in the water increases from 10 to 20 to 30 %. All quench baths were at 40

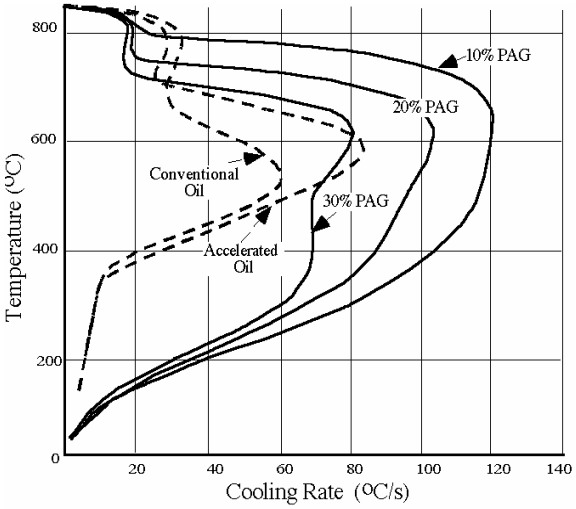

Figure 12.15 Cooling rate curves for a PAG polymer quenchant compared to oil quenchants [12.25].

^{o}C. A problem that sometimes occurs with water quenching is that the cooling can be spotty and produce soft spot regions. The addition of just a small amount of the polymer causes a more uniform contact of the surface during the initial cooling stages and produces a more uniform quench with only a small reduction in quench rate. Also, the polymer quenchants produce much cleaner surfaces than obtained with oil quenchants. Notice that the polymer quench rate in the usual M_s-M_f range would produce more chance of quench cracking than oils.

There are problems with both oil and polymer quenchants related to aging of the bath. Immersion of the very hot steel can lead to oxidation of the liquid components and the continued removal of the steel pieces can produce a selective lose of liquid components. This latter effect is often called "drag out". An excellent discussion of the problems of quench bath maintenance is presented in Chapter 6 of ref. [12.23]. Interestingly, cooling rate curves taken on oil baths used over periods of months show that the cooling rate increases with oxidation effects. Also with oil baths, water buildup in the bath can change the quenching speed significantly. Because the polymer quench speed is strongly dependent on polymer concentration in the water solution, holding constant concentration is a problem. The concentration can be monitored with the refractive index method described in chapter 6 of ref. [12.23].

Salt Bath Quenchants Salt baths can be used for both the quenching and the austenitizing step of heat treating. These baths are composed of mixtures of molten salts. The high temperature salt baths used for austenitizing are usually mixtures of either potassium and sodium nitrates (KNO_3-$NaNO_3$) or potassium-lithium-sodium chlorides (KCL-LiCl-NaCl). The lower temperature salts used for austempering and martempering are mixtures of nitrate and nitrite salts of potassium and sodium. The salts are supplied from the manufacturer with recommended temperature ranges of operation. The advantage of austenitizing in molten salt include very rapid heating, uniform temperature distribution and avoidance of surface oxidation and decarburization. See ref. [12.23, p. 309] for a detailed discussion.

Salt bath quenching is used when one wants to quench very rapidly to elevated temperatures for such processes as austempering and martempering. Tool steels are sometimes quenched in molten salts to the 500-600 ^{o}C (932-1112^{o}F) range prior to additional cooling to reduce scaling, distortion and to minimize cracking. This high temperature quenching is sometimes called interrupted quenching. When hot steel is immersed rapidly in molten salts the vapor blanket does not form as it does with water, polymer and oil quenchants.

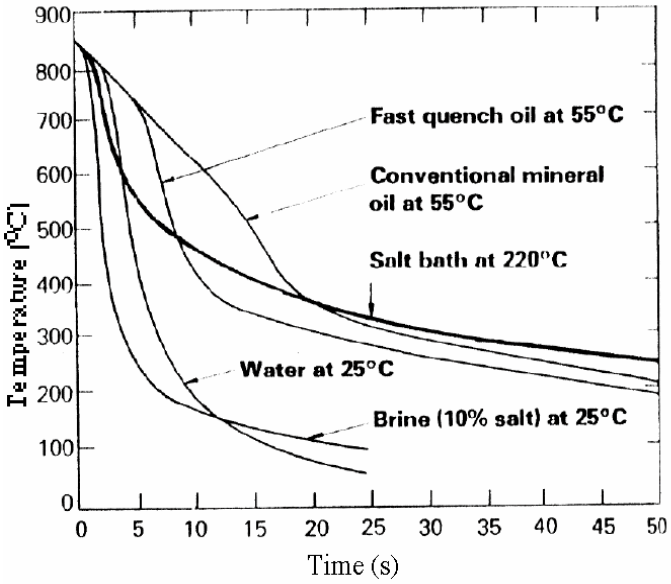

Figure 12.16 Temperature of a stainless steel probe quenched in various quench baths [12.26].

This results in a faster cooling rate initially. However, because the salt is at an elevated temperature the cooling rate at longer times will be slower than the other quenchants that are held at lower temperatures. This is illustrated for a stainless steel probe quenched into 220 ^{o}C (428 ^{o}F) salt in Fig. 12.16. It is seen that the salt cools faster down to temperatures of 600^{o}C (1112 ^{o}F) than does a 25 ^{o}C (77 ^{o}F) water bath and faster down to 490 ^{o}C (914 ^{o}F) than a 55^{o}C (131 ^{o}F) fast quench oil bath. For martempering operations of low hardenability steels it is required that the initial cooling rate by extremely rapid. For such applications it has been shown that the quench rate of salts can be increased by the controlled addition of small amounts of water to the bath [12.23, p 313]. In addition to ref. [12.23] reviews of salt bath quenching are given in [12.26 and 12.27].

Molten metals are an ideal liquid bath for rapid quenching due to the very high thermal conductivity of liquid metals and the lack of vapor blanket formation. Molten lead does not react with steel and it melts at 327 ^{o}C (621 ^{o}F), It can be alloyed with bismuth, which also does not react with steel, giving a eutectic molten bath temperature down to 125 ^{o}C (257 ^{o}F). These baths are normally covered with powdered graphite to avoid surface oxidation, but their use must be done with great caution as the metallic vapors must not be inhaled.

References

12.1 R Maddin, A History of Martensite: Some Thoughts on the Early Hardening of Iron, Chap. 2 in: Martensite, Edited by G.B. Olson and W.S. Owen, ASM International (1992).
12.2 W.C. Roberts-Austen, An Introduction to the Study of Metallurgy, pp 128-9, Charles Griffin and Co., London (1923).
12.3 C.S. Smith, Sources for the History of the Science of Steel 1532-1786, MIT Press (1968).
12.4 T.A. Wertime, The Coming of the Age of Steel, p 193, Univ. Chicago Press (1962).
12.5 R.F. Kern, Steel Selection, p. 132, Wiley-Interscience (1979).
12.6 J.M. Hampshire, User Experience of Hot Oil Quenching, Heat Treatment of Metals, 15-20 (1984.1)
12.7 B.F. Shepherd, Martempering, Iron Age, vol. 151, 50-52 (Jan. 28, 1943).
12.8 Heat Treater's Guide, 2nd Edition, ASM International (1995). [Note: Expanded versions of the treatment on martempering and austempering may be found in: ASM Handbook, Volume 4, Heat Treating, pp 137-163, ASM International (1991).]
12.9 Atlas of Isothermal Transformation and Cooling Transformation Diagrams, ASM (1977).
12.10 EE Legge, The industrial application of austempering, Metals and Alloys, vol. 10, 228-42(Aug. 1939)
12.11 A. Grossman and E.C. Bain, Principles of Heat Treatment, p 178, ASM (1964).
12.12 K.H.Z. Gahr, Microstructure and wear of materials, p. 277, Elsevier (1987).
12.13 P.Payson and W. Hodapp, Metal Progress, vol. 35, 358-62(1939).
12.14 D.L. Turner and F.J. Worzala, Proceedings Int. Sym. for Testing and Failure Analysis, pp 352-56, Long Beach CA (1958).
12.15 Q.D. Mehrkam, Austempering in actual practice, Metal Prog., vol. 86, 134-36 (1964).
12.16 Reference 12.8, p 203.
12.17 H.E. Boyer, Controlling physical properties by the interrupted quench, Iron Age, vol. 160, 49-54 (July 1944).
12.18 H.J. Elmendorf, The effect of varying the amount of martensite upon the isothermal transformation of austenite remaining after controlled quenching, Trans. ASM, vol. 33, 236-60 (1944).
12.19 R.F. Hehemann, V.J. Luhan and A.R. Troiano, The influence of bainite on mechanical properties, Trans. ASM, vol. 49, 409-26 (1957).
12.20 Y. Tomita and K. Okabayashi, Mechanical properties of 0.4%C-Ni-Cr-Mo high strength steel having a mixed structure of martensite and bainite, Metallurgical Transactions, vol. 14A, 485-92 (1983).

12.21 S.M. Sundaram and A.K. Mallik, Effect of lower bainite on mechanical properties after tempering, Jounal Iron Steel Institute London, vol. 205, 876 (1967).
12.22 D. Close, The Wolfson Engineering Group Quench Test-Scope and interpretation of results, Heat Treat. Metals, vol 10, 1-6 (1984.1).
12.23 G.E. Totten, C.E. Bates, and N.A. Clinton, Handbook of Quenchants and Quenching Technology, ASM International, Materials Park, OH (1993).
12.24 D.A. Guisbert and D.L. Moore, Correlating Quenchant Test Data, Adv. Materials and Processes, No. 10, 40Q-40V (1996).
12.25 R.T. von Bergen, Advances in Quenching Technology, Heat Treat. Metals, vol. 10, 7-8 (1984.1).
12.26 C. Skidmore, Salt Bath Quenching-A Review, Heat Treat. Metals, vol 12, 34-38 (1986.2).
12.27 R.W. Foreman, Salt Bath Quenching, pp 87-94 in Conference Proceedings; Quenching and Distortion Control, Edited by G.E. Totten, ASM International (1992).

Summary of the Major Ideas of Chapter 12

1 Heat transfer in the quenching process is complicated by the formation of a vapor blanket around the immersed steel piece as heat transfer through a gas is relatively slow. For a given quenchant 2 main factors can increase cooling rate, (1) increased agitation rate of the liquid, (2) reduction in the temperature of the bath.

2 A relatively new technique has been accepted (ISO 9950) for characterizing the cooling rate of the various liquid quenchants used industrially. Figure 12.12 shows how these cooling rate curves illustrate the relative quenching speed of common liquid quenchants.

3 To through-harden a piece of steel the center must cool fast enough to drop its temperature below the nose of the CT diagram for that steel, as illustrated for a 5140 steel on Fig. 12.1. For low hardenability steels one desires a quench that is very fast. As illustrated on Fig. 12.12, brine and water quenches produce the fastest cooling. However, for steels with %C above around 0.4 %, these quenches will lead to quench cracking and distortion.

4 Quench cracking and distortion are caused primarily by large temperature gradients in the steel piece as martensite is forming in the steel. Hence, a critical factor in avoiding these problems is to have a low cooling rate in the M_s-M_f temperature range. Hence, one desires a quenchant that cools the piece very rapidly from the austenitizing temperature down to just above the M_s temperature, and then slowly down to room temperature. For steels with %C above 0.4 %, oil quenches are often the best compromise.

5. Martempering is a technique that minimizes the problems of quench cracking and distortion. As illustrated in Fig. 12.2, the quench is interrupted at temperatures just above the M_s temperature allowing the temperature gradients in the work piece to flatten out prior to formation of martensite. Martempering is generally done by quenching into hot salt baths.

6. Oil quenchants are available in three ranges, normal oils, accelerated oils and martempering oils. Special additives are used to produce the latter two types. As illustrated in Fig. 12.12 the accelerated oils have a significantly higher maximum cooling rate, but still have a relatively low cooling rate in the M_s-M_f range. The martempering

oils can be used hotter and are effective for martempering some steels, even though the temperature equalization is done just below the M_s temperature, as shown in Fig. 12.2.

7 Polymer quenchants are available which produce cooling rates intermediate to that of oils and water, as illustrated in Fig. 12.15. These baths are solutions of a polymer in water and the higher the concentration of polymer in the water the more the quench rate is reduced. Cleanup following quenching is much easier than for oils, but maintenance of constant polymer concentration over extended use can be a problem.

8 Molten salt bath quenchants are available that are useful over specific temperature ranges, which are controlled by the type of salts. They offer very rapid initial quench rates, but because they are used hot, quench rates at longer times are reduced. In addition to quenching these baths can also be used for austenitizing and annealing and provide protection from oxidation.

9 Austempering is a quenching technique designed to produce bainite in steels. It is usually done by quenching into hot salt baths and holding for times adequate to produce all bainite, and such times may be found on the CT curves for the steels of interest, see Fig. 12.3

10 Bainitic steels display superior toughness to quenched and tempered steels at hardness levels of around HRC = 40 and above, and are therefore an excellent choice for knives, see Bar Graph 12.1 and Figs 12.8 and 12.9. As illustrated in Fig. 12.4, hardness levels in the high 50s range may be obtained in the higher carbon level bainitic steels.

11 Table 12.3 presents two modified forms of austempering which produce a mixture of martensite and bainite. These methods give increased hardness over fully bainitic steels and there is limited experimental evidence (see Fig. 12.9) indicating that toughness can be superior to the quenched and tempered condition (i.e., full martensite) at the same hardness.

13 Stainless Steels

A big problem with steels is that they are easily corroded when exposed to damp conditions, particularly if a salty or acidic atmosphere is around. For example, a piece of steel left in a room in which acids are used will very quickly become highly rusted with the characteristic dirty brown color of steel rust. (Chemically, rust is a hydrated form of iron oxide.) The two major types of stainless steels were both discovered in 1912 by accident because of their unusual resistance to corrosion [13.1]. The austenitic stainless steel type was discovered in Germany by E. Maurer when he noticed that certain Cr-Ni alloys did not rust after being left in a room with acid fumes. The ferritic stainless steel type was discovered in England by H. Brearley when he observed difficulty in trying to etch gun barrels made from a Cr alloy. Brearley first used the name "stainless steel" for the ferritic type of stainless and the name was later also applied to the austenitic stainless.

The good corrosion resistance of stainless steels is the result of a very thin chromium rich oxide film that forms on the surface of the steel. (It is so thin, around 2 nm or 0.002 microns, that it is transparent.) The oxide film protects the underlying steel from further reaction with the environment. When the protective film is present the steel is said to be passivated, or in the passive state. In general, a stainless steel will be passivated when in contact with an oxidizing aqueous solution but not when in contact with a reducing solution. Figure 13.1 presents data on the corrosion rate of Fe-Cr alloys as a function of the % Cr in the alloys when tested in an oxidizing acid, nitric acid, and a reducing acid, sulfuric acid. In nitric acid there is a significant reduction in corrosion rate as the %Cr increases up to values of 11 to 12 %Cr, followed by a plateau out to 15 %Cr and then a second strong reduction as the %Cr increases to just under 20% Cr. At the 11 to 12 %Cr values and above, the steels are generally said to be passivated in this environment. It is therefore commonly stated that **for a steel to be considered stainless it must contain a minimum of just under 12 %Cr.** Figure 1 also illustrates that passivation depends on the type of aqueous liquid contacting the steel. Notice that in the reducing acid, increasing % Cr actually causes loss of the passivated film.

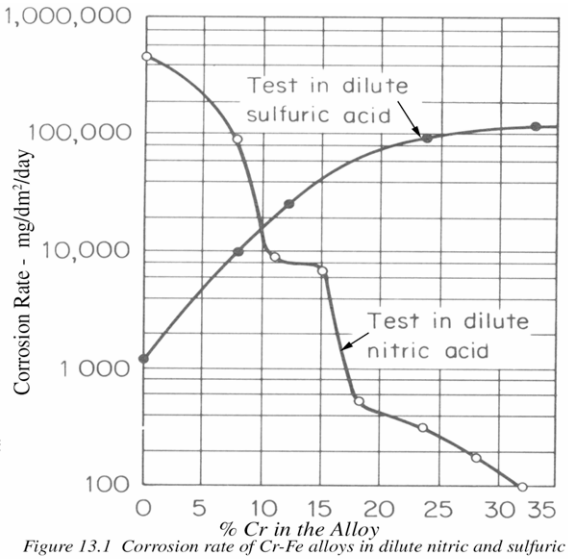

Figure 13.1 Corrosion rate of Cr-Fe alloys in dilute nitric and sulfuric acids [13.2].

Stainless steels also exhibit improved resistance to oxidation at higher temperatures. Figure 13.2 illustrates that oxidation resistance [as measured by loss in weight after 48 h in 1000 °C (1832 °F) air] also improves as % Cr is increased. Again there are two composition ranges where the improvement is dramatic and they are also separated by a plateau

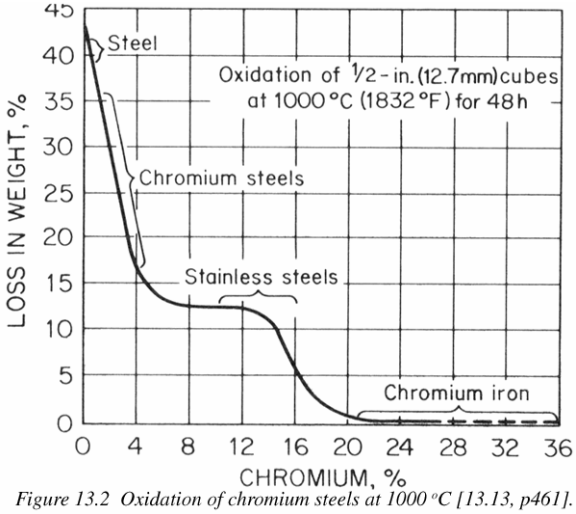

Figure 13.2 Oxidation of chromium steels at 1000 °C [13.13, p461].

region, but the plateau now extends from 15 %Cr down to lower % Cr values, around 6 % Cr.

In general, passivity is promoted by small additions of Mo (molybdenum) or Ni (nickel) to the stainless steel. Loss of passivity is promoted by the presence of chlorine ions such as is present in salt water and, as discussed above, by reducing conditions.

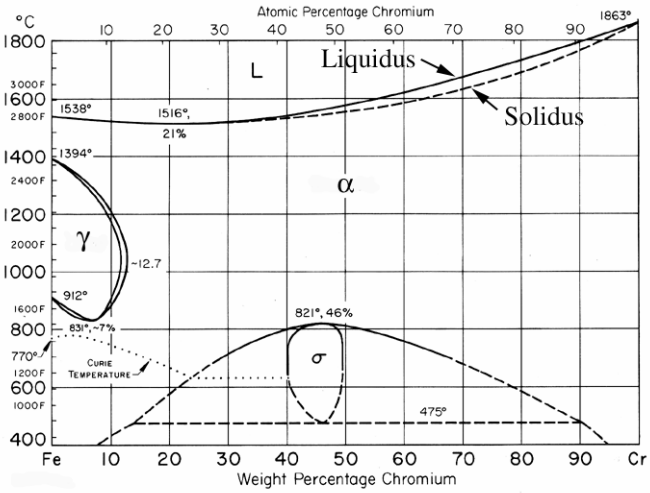

Figure 13.3 The Fe-Cr Phase diagram [13.3].

Ferritic Stainless Steels As a first approximation, ferritic stainless steels can be considered to be alloys of Cr -Fe with Cr compositions exceeding 12 %Cr. As with ordinary steels a good way to understand the structure of these alloys is with a phase diagram, and Fig. 13.3 presents the phase diagram of Fe + Cr alloys with no carbon present. The diagram gives the melting point of pure Cr as 1863 ^{o}C, and pure Fe as 1538 ^{o}C. The solid line extending between these two temperatures is called the "liquidus", and it tells us the freezing temperature of all the alloy compositions. The symbol L above this line tells us the region where alloys are fully liquid. The dashed line between the two pure melting points is called the "solidus" and it tells us the melting point of all alloy compositions. The big open region below the solidus is labeled with the Greek alpha (α) because all alloys in here are ferrite, which is the body centered cubic structure. The looped region at the left center shows us where austenite, γ, can exist on this temperature-composition map. The region labeled sigma, σ, at the bottom center represents a structure that is not body centered cubic ferrite. It has a different crystal structure which turns out to be quite brittle, and consequently this sigma phase is to be avoided. As you might suspect its formation is a problem in the heat treatment of stainless steels that have high Cr compositions. Notice that the lines extending out from the top of the central sigma region become dashed. At the temperature/compositions of these dashed regions the sigma phase will not form without extended holding at temperature. Hence the diagram is telling us that if we forge alloys of Fe-Cr with %Cr in the stainless range of 12 %Cr up to no more than around 26% Cr at high temperatures, upon cooling to room temperature we will have a ferritic (body centered cubic-α) structure.

In the real world it is extremely difficult to make Fe alloys with zero amount of carbon in them. The addition of even a very small amount of C has a large effect on the appearance of the Cr-Fe phase diagram. When carbon is present the appropriate phase diagram becomes a ternary diagram of Cr-Fe-C. Such diagrams were discussed briefly on page 54. By drawing a vertical section through the Cr-Fe-C ternary diagram at a fixed %C one obtains a diagram that will become closer and closer to the pure Cr-Fe phase diagram as the % C approaches zero. Figure 13.4(a) shows a vertical section through the Cr-Fe-C diagram at %C of only 0.05% C. Comparing to Fig. 13.3 one sees that the small addition has had a very pronounced effect on the diagram (note: the sigma phase lines have been removed from Fig. 13.4 to make comparison more simple). Two major changes occur. First, the size of the γ (austenite) region increases significantly. Notice that in the pure alloy at

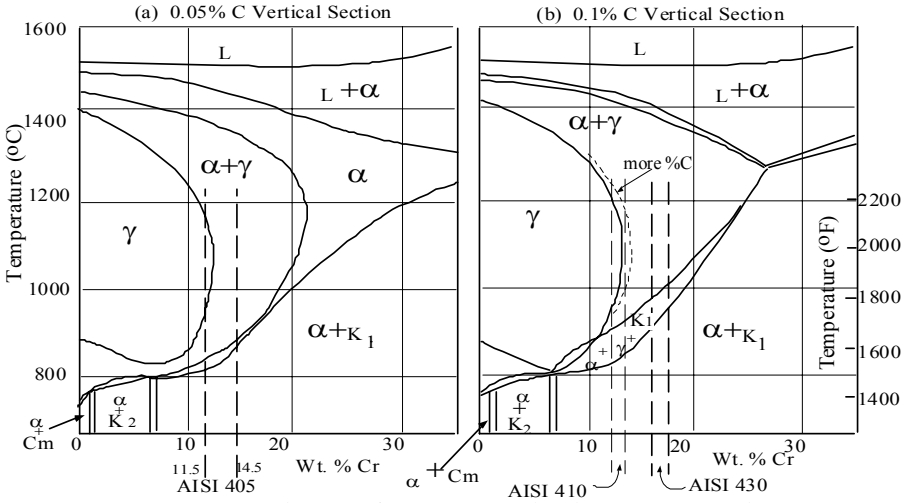

Figure 13.4 Cr-Fe vertical sections of Cr-Fe-C ternary phasediagram at wt. %C values of 0.05% and 0.1% [13.4].(c 1958 Verlag Stahleisen GmbH, Düsseldorf, Germany)

1050 °C one obtains 100% α ferrite down to 12.7%Cr, where now 100% α ferrite only occurs down to around 20 %Cr at 1050 °C. The second effect involves the formation of chromium carbides. The element chromium is a fairly strong carbide forming element and if iron is not around it forms a whole series of different pure chromium carbides with C, all of which have different crystal structures than the iron carbide, cementite (Fe_3C). (As explained on page 99, in alloy steels the cementite carbide is shown as M_3C where M means Fe+X, with X referring to the added alloying element. In an Fe-Cr-C alloy the X would be Cr.) The first two pure chromium carbides have been labeled K_1 and K_2 carbides by German speaking authors. These carbides have the following chemical formulas, $K_1 = M_{23}C_6$ and $K_2 = M_7C_3$, where M means Fe+Cr in Fe-Cr-C alloys like stainless steel. The K_1 carbide is perhaps the most important carbide in stainless steels as its formation often occurs along grain boundaries and promotes localized corrosion along grain boundaries, a type of corrosion called intergranular corrosion (see Table 13.11). There is basically no change in the phase diagrams of Fig. 13.4 down to room temperature, which means that the ferritic stainless steels (12%Cr or more) will consist of α ferrite and K_1 carbides at room temperature, even with %C values as low as 0.05%.

Table 13.1 The AISI ferritic stainless steels.

AISI	%C	%Cr	Other*
405	0.08 max.	11.5-14.5	0.1-0.3 Al
430	0.12 max.	16-18	-
446	0.20 max.	23-27	-

*Both Mn and Si present at around 1%.

There are 3 major AISI grades of ferritic stainless steels which are listed in Table 13.1. Notice that the 3 grades have compositions corresponding to 3 distinct levels of corrosion resistance shown on Fig. 13.1. Notice also that the maximum %C level goes up as the % Cr goes up. The range of Cr compositions for AISI 405 is shown on the lower carbon vertical section of Fig. 13.4(a), and that of the AISI 430 on the higher carbon vertical section of Fig. 13.4(b). AISI 430 is the most popular grade of the ferritic stainless steels. At common forging temperatures (roughly 1900-2100°F) this steel will contain a mixture of ferrite and austenite (α + γ). Upon cooling there is the possibility that the austenite will transform to martensite. In the chapter on hardenability it was shown that high concentrations of Cr promote high hardenability and hence avoiding martensite in 430 might require very slow cooling rates. The required cooling rates to avoid martensite can be estimated from the IT diagram for 430 which is shown as Fig. 13.5. Notice that the steel was austenitized at 2000 °F (1093 °C), and Fig. 13.4(b) would predict the steel should be a mixture of austenite and ferrite (α + γ) at this temperature. Figure 13.5 indicates that the austenitized steel contains 40 % austenite/60 % ferrite. The diagram shows us that

the steel must be cooled below around 1400 °F in less than a second to avoid precipitation of the K_1 carbides. The nose of the transformation curve for the start of ferrite formation occurs at around 1300 with transformation starting at 60 s and not being completed until just under 2 h. If one wants to anneal this stainless steel to the fully ferritic condition it should be held at 1400 °F for at least 2 hours. The diagram shows that the hardnesses of the fully ferritic structures vary from HRB = 78 for a 1500 °F anneal to HRB = 86 for a 1100 °F anneal. Quenching from the austenitizing temperature produced HRB = 101.

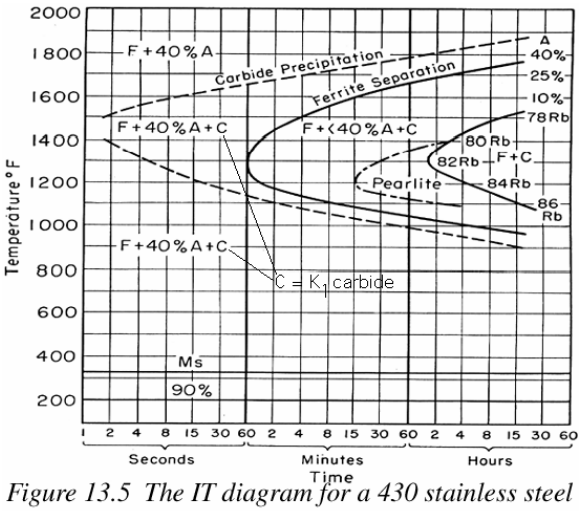

Figure 13.5 The IT diagram for a 430 stainless steel austentized at 2000°C for 15 min. [13.5].

The ferritic stainless steels are subject to embrittlement problems when held at relatively low temperatures. The embrittlement occurs by two different mechanisms. One involves the formation of the sigma phase shown on Fig. 13.2 and the other the formation of ferrite that has a very high percentage of Cr in it. This second mechanism is referred to as 475 °C embrittlement because it occurs for steels held between 400 °C and 540 °C (752-1004 °F). Figure 13.6 presents a schematic IT diagram for the formation of these embrittlement problems. Both problems are more severe as the %Cr in the stainless becomes higher and these curves are representative of alloys containing around 25 % Cr. (Higher %Cr shifts the curves to the left.) Because of these embrittlement problems it is often recommended that ferritic stainless steels be rapidly cooled following an annealing heat treatment. See ref. [13.6, p 759] for good brief discussion of annealing practice for the AISI ferrite stainless steels.

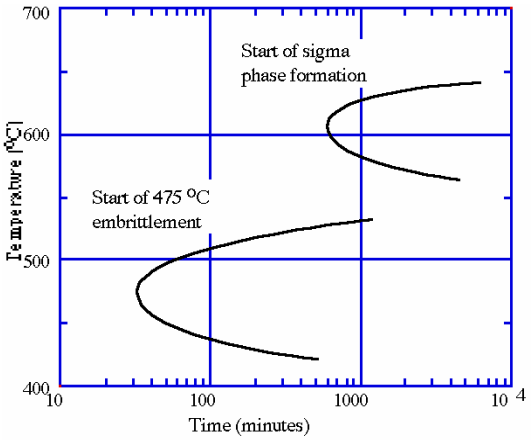

Figure 13.6 An IT diagram of start times for formation of sigma phase and 475° C embrittlement in ferritic SS.

There is a relatively new class of ferritic stainless steels called the superferritics that was developed in the mid 20th century. These steels have improved corrosion resistance and Table 13.2 presents compositions of 3 of them. The improved corrosion resistance is due to the addition of Mo and sometimes Ni and to the very low levels of C and N. The low levels of C and N are produced by special processing techniques and consequently these steels are more costly than the regular AISI ferritic stainless steels. Reference [13.1] presents an excellent review of their corrosion resistance properties in comparison to other stainless steels as well as specialty Ni alloys like Inconel and Hastelloy.

Table 13.2 Examples of superferritic stainless steels.

Name	%Cr	%Mo	%Ni	%C(max)	%N(max)
18-2*	18	2	-	0.025	0.025
26-1*	26	1	0.1	0.005	0.015
29-4-2	29	4	2	0.01	0.02

* Low levels of Ti and/or Cb(Nb) added as scavenger elements.

Martensitic Stainless Steels As the name implies, the martensitic stainless steels can be heat treated to form martensite. All of the martensitic stainless steels classified by the

Table Table 13.3 Some AISI martensitic SSs.

AISI No.	%C	%Cr	Other*
410	0.15	11.5-13	
431	0.20	15-17	1.25-2.5 Ni
440A	0.65-0.75	16-18	0.75 Mo
440B	0.75-0.95	16-18	0.75 Mo
440C	0.95-1.2	16-18	0.75 Mo

* All contain 1% Mn and 1% Si.

AISI have been assigned numbers in the 400 series. Table 13.3 lists the compositions of five of the more popular AISI martensitic stainless steels.

Hardening heat treatments of these steels are basically the same as in plain carbon and low alloy steels in that three steps are involved, austenitization, quenching and tempering. In general, however, things must be done more slowly because of 2 factors: (1) The carbides dissolve much more slowly into the austenite than the cementite carbide because of the presence of Cr in them. (2) The thermal conductivity is much smaller. Factor 1 requires that austenitization times be longer to be sure the carbides have dissolved into the austenite. Factor 2 causes temperature gradients to be much higher which can lead to cracking and warpage even on heating, so that it is often recommended that complex parts be given an intermediate low temperature soak on the austenitization heat-up step to smooth-out temperature variations, and a martempering treatment on cooling.

Table 13.4 Hardness of as-quenched AISI martensitic stainless steels

Carbon Range Wt. %C	As-quenched hardness , Rc
0.06-0.14	38-49
0.2-0.4	44-54
0.65-1.2	56-61

Just as in the plain carbon and alloy steels the hardness of the martensite increases as the %C rises. Table 13.4 presents a rough guideline for the as-quenched hardness dependence on %C in the AISI martensitic stainless steels. Heat treatment of these steels is complicated by a number of factors that will be discussed in the next section, which is devoted to optimizing composition and heat treatment for cutlery applications.

Some guidelines for the heat treatment of the AISI martensitic SSs are presented in ref. [13.6]. As an example we will consider AISI 410. The composition range for this steel has been included on the 0.1 % vertical section of Fig. 13.4(b). The increased %C in 410 up to 0.15% causes the γ region to expand to higher %Cr values as is indicated by the dashed line labeled "more %C". The %C composition range for AISI 410 is shown on the diagram and one sees that the 410 steels are expected to be fully austenite in a narrow temperature range of roughly 1000 to 1200 ^{o}C (1832-2192 ^{o}F). If the steel is austenitized slightly above or below this range it will contain some ferrite that will reduce the hardness of the quenched steel. (Notice on Figure 11.5 that the ferrite formed in Fe-C alloys at around 1450 ^{o}C is designated delta (δ) ferrite and that formed below 912 ^{o}C is called alpha (α) ferrite. The δ ferrite forms from the liquid and the α ferrite forms from austenite. By analogy, if the ferrite of a stainless steel is known to have formed from the liquid it is generally called delta ferrite. However, both ferrites are the same body centered cubic phase and to avoid confusion on ternary diagrams ferrite formed from the liquid is often called α ferrite rather than δ ferrite, as on Fig. 13.4.) As illustrated with micrographs in ref. [13.6], it is common to find stringers of delta ferrite in as-forged samples of this steel.

As with the ferritic stainless steels the high %Cr levels in the martensitic steels produce very high hardenability conditions. Figure 13.7 presents an IT diagram for a 410 steel austenitized at 1800 ^{o}F (982 ^{o}C). Notice that both the position of the transformation curves and the hardness of samples held to full transformation between 1000 to 1400 ^{o}F are similar to the IT diagram for 430 steels shown as Fig. 13.5. A major difference is that

after austenitization, the 410 steel of Fig. 13.7 is 100 % austenite, compared to only 40% for the 430 steel of Fig. 13.5. Even though IT diagrams show that the martensitic stainless steels can be air cooled to form fully martensitic structures, it is generally recommended that samples be oil quenched to optimize corrosion resistance. The quenching minimizes formation of K_1 carbide precipitate formation on cooling, which, as explained in the next paragraph, tends to promote corrosion. (Note: the transformation-start curve for the K_1 carbide precipitation is shown on Fig. 13.5, but not on Fig. 13.7.)

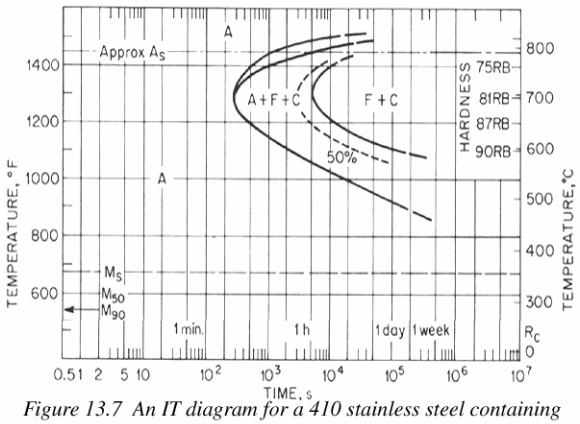

Figure 13.7 An IT diagram for a 410 stainless steel containing 0.11 %C and 12.2 %Cr. Austenitized at 1800 °F (982 °C) [13.4.p6-11].

The corrosion resistance of martensitic stainless steels is generally poorer than the ferritic and austenitic stainless steels. This results from effects of the increased amount of C present in the martensitic stainless steels. As will be explained in the next section, the higher C levels reduce the amount of Cr that will dissolve into austenite. Also, the higher C level increases the possibility of forming the K_1 carbide as small precipitate particles on low temperature heating. As explained above, the K_1 carbide has the chemical formula of $(Cr,Fe)_{23}C_6$ which tells you that it contains significant amounts of Cr. When a small particle of K_1 forms in a matrix of either ferrite or austenite, the Cr atoms in the carbide are subtracted from the matrix iron immediately surrounding the particle. If this causes the %Cr to drop much below 12 %Cr in the surrounding matrix the steels become susceptible to corrosion and are said to be "sensitized". Since the carbides prefer to form along the grain boundaries of the matrix the corrosion occurs along the grain boundaries and this type of corrosion is therefore called intergranular corrosion. Hence, sensitization is said to occur when a low temperature heat treatment, such as tempering, causes K_1 precipitate particle formation to the extent that intergranular corrosion may occur. Figure 13.8 presents corrosion data on a 410 stainless steel showing the loss of corrosion resistance produced by tempering. The steel has become sensitized on tempering in the range of 400 to 700 °C (752-1292 °F).

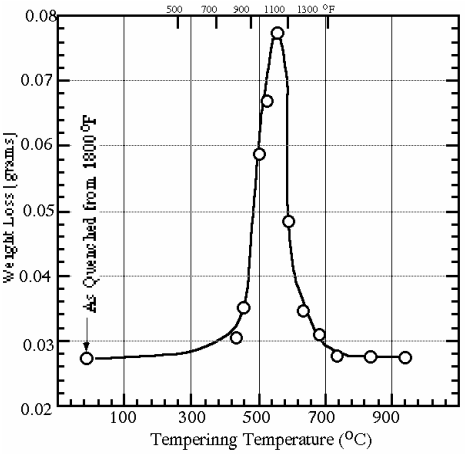

Figure 13.8 Intergranular corrosion produced by sensitizing a 410 steel on tempering. Corrosion test: 14 days in 20% salt fog. [13.7]. (copyright: NACE International YEAR)

The martensitic stainless steels are generally tempered to enhance toughness, just as are plain carbon and alloy steels The variations of hardness on tempering the various AISI martensitic stainless steels are presented in ref. [13.6]. Figure 13.9 presents a summary of data showing the tempered hardnesses of 12 % Cr stainless steels as the %C in the steels varies from 0.055 to 0.14 %. The higher hardnesses in the range shown correspond to the higher %C

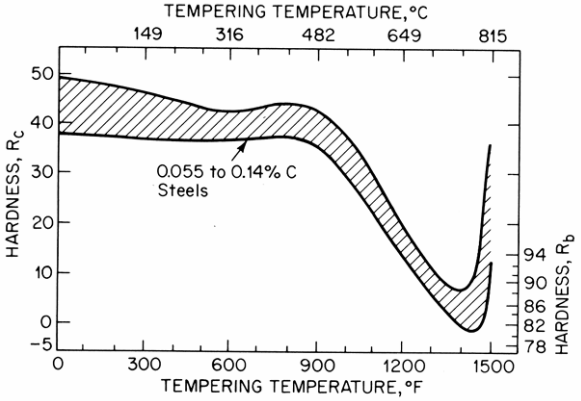

Figure 13.9 Tempering response of 12 % Cr stainless steels, tempered for 2 h [13.4, p20-19].

values. Very little reduction in hardness occurs until the tempering temperature exceeds around 900 ^{o}F (482 ^{o}C). The large reduction of hardness above this temperature has been shown to be due to formation of particles of the K_1 carbide precipitate.

As with the plain carbon and alloy steels it is generally necessary to temper the martensitic stainless steels to improve toughness. Reference [13.4, page 20-21] presents Izod impact data on a 410 stainless steel after tempering to various temperatures. It is found that toughness is improved for tempering to temperatures up to near 500 ^{o}F (260 ^{o}C). Above 500 ^{o}F toughness (impact energy) drops to a minimum at 900 ^{o}F (482 ^{o}C) and then rises strongly at temperatures above around 1000 ^{o}F (538 ^{o}C). The peak loss of toughness at around 900 ^{o}F (482 ^{o}C) is due to the 475 ^{o}C embrittlement discussed above for ferritic steels, see Fig. 13.6. It is due to the formation of carbide precipitates containing Cr and consequently it is more of a problem as the %Cr increases in these stainless steels.

Table 13.4 presents data on Izod impact levels for the 5 AISI martensitic stainless steels in the annealed condition. Figures 13.9 and 13.10 show that tempering of 410 steel at higher temperatures produces hardness and impact strength equivalent to those of annealed samples. The data of Table 13.4 show that even in the annealed condition the 440 martensitic stainless steels suffer from poor toughness. This results in large part from the large carbide particles present at the high levels of C in these steels.

Table 13.4 Izod data for annealed martensitic stainless steels [13.2].

AISI No.	Izod Energy (ft-lbs)
410	90
431	50
440A	15
440B	5
440C	5

Optimizing martensitic stainless steel for cutlery applications To produce a knife with optimum properties one desires high hardness levels and a fine array of carbides to enhance wear resistance and maintain sharpening ability, combined with adequate %Cr to produce corrosion resistance. Hence there are 2 basic requirements:

1- The austenite phase that is quenched requires %C levels of around 0.6 %C or higher to produce Rockwell C hardnesses in the 63 to 64 range.

2- The austenite phase that is quenched requires %Cr levels of 12% or higher to ensure reasonable corrosion resistance.

To understand the various trade-offs involved between composition and austenitization temperature for optimum results, it is helpful to learn how to interpret isothermal sections of the Fe-Cr-C ternary phase diagram. In Chapter 3 it was shown that the Fe-C binary phase diagram is a map with temperature on the vertical axis and composition on the horizontal axis. The various regions on the phase diagram map the temperature-composition values where the various phases of the Fe-C alloys may exist. Ternary phase diagrams are similar to binary diagrams in that the temperature is mapped along a vertical axis. However, composition can no longer be mapped (plotted) along a single line and instead it is mapped along a plane, called the composition plane, with temperature being the height above this plane. The composition plane for an Fe-Cr-C ternary phase diagram is shown on fig. 13.11. The %C is plotted along the horizontal axis and the %Cr along the vertical axis of the composition plane. Consider a 440C

stainless. From Table 13.3 the average composition for this Fe-Cr-C alloy is 17 %Cr and 1.075 %C. A black dot, labeled 440C, has been plotted on the composition plane of Fig. 13.11, and this dot locates the composition of 440C on the ternary diagram.

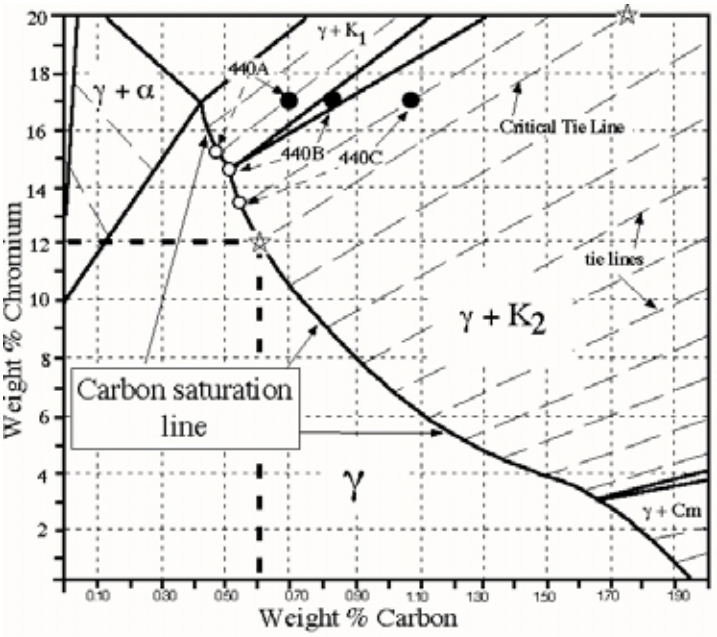

Figure 13.11 Isothermal section of Fe-Cr-C ternary phase diagram at 1100 °C (2012 °F) [13.8].

With composition plotted along a plane, and temperature plotted as distance above the plane, the ternary phase diagram becomes a 3-dimensional plot. We use these complex 3-dimensional diagrams by making sectional cuts through them, either vertical or horizontal sections. The diagrams of Fig. 13.4 are vertical sections through the Fe-Cr-C ternary along a section that holds the %C fixed, at 0.05% in (a) and at 0.1 % in (b). Hence, these vertical sections look similar to binary phase diagrams with temperature plotted vertically and %Cr along the horizontal axis. Figure 13.11 is a horizontal sectional cut through the Fe-Cr-C ternary phase diagram. It is called an isothermal section because the cut is made at one temperature (which is what isothermal means). As indicated by the label, Fig. 13.11 is the 1100 °C (2012 °F) isothermal section and it maps the compositions (%Cr and %C) of the various phases of Fe-Cr-C alloys that can exist at 1100 °C (2012 °F). Figure 13.12 is presented to help explain the interpretation of Fig. 13.11. The large white area is labeled γ, which means austenite. If you plot the composition of an alloy on Fig. 13.12 and it falls in the γ area, this alloy will be 100% austenite when held at 1100 °C. The shaded areas of Fig. 13.12 show the composition regions in which a second phase is present within the austenite at 1100 °C. For example, the composition of 440C is seen to fall inside of the region labeled γ +K_2. This predicts that if 440C is heated to 1100°C (2012 °F) it will consist of austenite with particles of the K_2 carbide in it and upon quenching the martensite formed from the austenite will have the K_2 carbide dispersed within it. (Note: Figure 13.11 should be regarded only as a good approximation for heat treating commercial alloys. For example, experiments on a 14%Cr/7.4%C alloy [13.12] show that the carbides present at 1100 °C are a mixture of K_1 and K_2 with K_1 being predominant.)

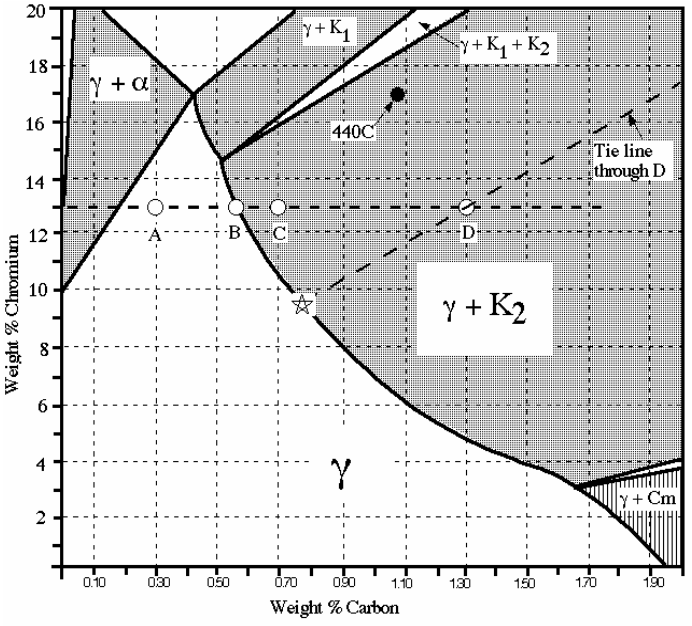

Figure 13.12 The important regions on the 1100 °C isothermal section of Fig. 13.11.

The heat treatment of martensitic stainless steels often involves two-phase austenitization which was previously discussed on page 107. To help understand

Table 13.5 The 4 alloys shown on Fig. 13.12.

Alloy	%Cr	%C
A	13	0.3
B	3	0.58
C	13	0.7
D	13	1.3

the complications that result from this effect for martensitic stainless steels consider the 4 alloys A to D in Table 13.5. All of the alloys have 13 %Cr in them, slightly above the minimum required for stainless passivity. The compositions of the 4 alloys have been plotted on Fig. 13.12. Alloy A lies within the γ region and it will be a 100 % austenite at 1100 ^{o}C with composition 13 %Cr and 0.3 %C. Notice that on Fig. 13.11 the right hand boundary of the austenite region is labeled "carbon saturation line", and alloy B lies directly upon this line with a carbon level of 0.58 %C. The carbon saturation line is very important. It is like the A_{cm} line on the binary Fe-C phase diagram. It tells us the maximum amount of C that austenite can dissolve within itself before addition of more C produces formation of carbide particles. When we go to alloy C, at 0.7 %C, we are in the 2-phase region, $\gamma + K_2$, and the alloy will now consist of austenite with K_2 carbide particles dispersed within the austenite. The diagram provides a measure of how much carbide lies within the austenite. The further the alloy composition lies to the right of the saturation line the larger the volume percent of K_2 carbide it will contain. Hence we expect alloy D to contain a lot more carbides than alloy C because it lies further from the saturation line.

The composition of the austenite formed at 1100 ^{o}C in alloys A and B will be the same as the overall compositions given in Table 13.5. But not so for alloys C and D which contain the K_2 carbides at 1100 ^{o}C. These carbides are rich in both Cr and C and so the austenite is depleted in both elements relative to the overall composition. It is possible to determine the composition of the austenite in alloys C and D from the isothermal phase diagrams. Notice the dashed slanted lines on Fig. 13.11 which are labeled "tie lines". The full isothermal diagram will contain many more such nearly parallel lines, and Fig. 13.12 shows that tie line which passes through alloy D. The austenite composition for alloy D is found at the end of this tie line where it intersects the carbon saturation line, labeled with a star. Hence, even though this alloy contains 1.3%C and 13%Cr overall, the austenite formed in it at 1100 ^{o}C will contain only around 0.78 %C and 9.5 %Cr. Hence the martensite formed on quenching this alloy would have quite poor corrosion resistance with a %Cr level well below the minimum 12% needed for good passivity.

With this background it is possible to demonstrate shortcomings of the 440 stainless steels for knifemaking applications. The 3 alloys 440A, 440B and 440C are shown on Fig. 13.11 with a solid arrow pointing at their average overall compositions and a dashed arrow pointing at the compositions of austenite that forms in them at 1100 ^{o}C (2012 ^{o}F), which are tabulated in Table 13.6. In all 3 alloys the %Cr in the austenite is lowered from the overall 17 %Cr value, but is still above the 12% Cr needed for good passivity. Notice however that the %C in the austenite is lowered a bit below the 0.6% value needed to achieve R_c values in the 63 to 64 range. In addition, the highest %C alloy, 440C, is found to contain large primary carbide particles produced in the solidification process, see p. 162. Reference [13.6, p. 777] presents a series of micrographs of 440C which illustrate these relatively large primary carbide

Table 13.6 Composition overall versus that in 1100 ^{o}C austenite.

Alloy	Overall %C/%Cr	In austenite %C/%Cr
440A	0.70/17	0.48/15.1
440B	0.85/17	0.52/14.6
440C	1.07/17	0.56/13.6

particles present in this stainless steel.

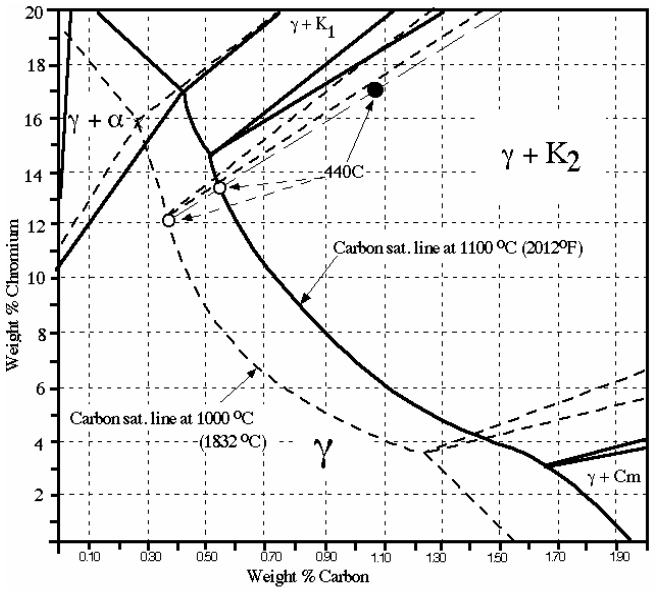

Figure 13.13 Shift in lines of Fe-Cr-C isothermal section for temperature dropping from 1100 to 1000°C[13.8].

To illustrate what effect lowering the austenitizing temperature will have on austenite composition and volume fraction carbides, the change in the position of the carbon saturation line is shown on Fig. 13.13 when the temperature is dropped from 1100 to 1000 °C (2012 to 1832 °F). The overall composition of the 440C on the superimposed diagrams remains fixed. But one sees that the %C/%Cr in the austenite drops from 0.56%C/13.6%Cr to 0.39%C/12.1%Cr. Reference [13.6] recommends that 440 C be austenitized at 1010-1065 °C (1850-1949 °F). Further, they recommend the upper end of the range for maximum corrosion resistance and strength. The reason for this recommendation is understood by the above discussion: the higher austenitization temperatures will increase both %C and %Cr in the austenite.

To produce stainless steel blades that can be heat treated to as-quenched hardnesses in the range of R_c = 63-64 it is necessary to be able to produce austenite with %C values above around 0.6%C and %Cr levels above around 12 %Cr. This composition is shown at the star on Fig. 13.11 and it happens to fall on the carbon saturation line for heat treatment at 1100 °C. As shown for alloy D on Fig. 13.12 if one increases the %C above 0.6 % to 1.3% and holds Cr at 13%, the tie lines through the resulting composition predicts that the resulting austenite will produce a high hardness martensite, as %C is ≈ 0.78%, but its %Cr will fall to around 9.5 %, well below the 12%Cr required for good passivity - see the star composition on Fig. 13.12. If one increases both the %C and the %Cr along the tie line marked with a star at each end on Fig. 13.11, then the austenite composition will match the 0.6%C/12%Cr requirement. This tie line will be called the critical tie line. In alloys with overall compositions along this line, the austenite will contain K_2 carbides with a volume fraction dependent on how far the overall composition lies to the right of the lower star on the carbon saturation line. The composition of the 440 series lies well above the critical tie line. However, there are commercial stainless steels with compositions that lie close to the critical tie line and two of them are shown in Table 13.7. (Note: The position of the compositions of the steels of Table 13.7 lie a bit above the critical tie line. The positions of the carbon saturation line on Figs. 13.11 and 13.13 are, at best, only good approximations for real commercial alloys. In choosing heat treat temperatures for particular alloys it is best to consult the technical data provided by the supplier.)

Table 13.7 Optimum steels for stainless knives.

Steel	%C	%Cr	%Si	%Mn
Sandvik 12C27	0.60	13.5	0.4	0.4
Uddeholm AEB-L	0.65	12.8	0.4	0.65

From the above discussion it should be clear that the austenitization temperature and times are important variables in the heat treat process. In addition, the quench temperature and quench rates are important because these alloys are prone to formation of retained austenite. It was demonstrated on pages 109-110 that in 2-phase austenitization the austenitization temperature controls %C in the austenite, which can

change the amount of retained austenite in the quenched samples. Even though the %C might go up in the austenite, which will give harder martensite, the hardness of the quenched bar can go down because the amount of retained austenite can also go up with increased C in the austenite. In steels prone to retained austenite, such as hypereutectoid alloy steels, tool steels and these stainless steels, there is an important and subtle effect that can occur called, **stabilization**, which will now be briefly discussed.

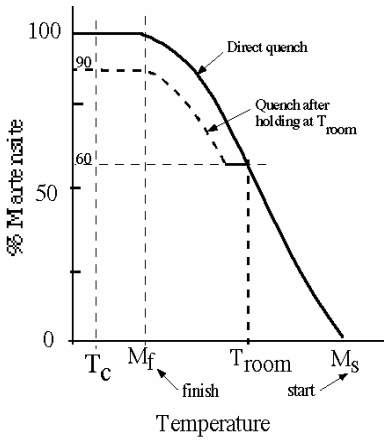

Figure 13.14 Stabilization effect.

The usual way to explain stabilization is with the curves shown in Fig. 13.14. If you refer back to Fig. 4.15 on page 27 you will find the upper curve of Fig. 13.14 explained. The upper solid curve labeled "direct quench" shows the amount of martensite formed in a steel quenched directly to various temperatures between the martensite start temperature, M_s, and the martensite finish temperature, M_f. The curve shows that if this steel is quenched to room temperature, T_{room}, it will contain 40% retained austenite. The dashed curve shows the amount of martensite formed in this steel if it is quenched by a 2-step process, (1) quench to room temperature, (2) hold at room temperature for some time followed by a quench into a cold quenchant. The dashed curve shows that the amount of martensite formed by the cold quench after the room temperature delay is significantly less than would have occurred if the steel had been quenched to the cold temperature with no room temperature delay. A direct quench to the cold temperature, T_c, produces no retained austenite for this steel, but after the room temperature delay one is left with 10 % retained austenite. The room temperature delay is said to have "stabilized" the austenite.

Steels are virtually always quenched to cold temperatures in a 2-step process because a direct quench would promote quench cracking and, other than ice brine, cold quenchants (like liquid nitrogen) have extremely severe problems with vapor blanket formation. In order to minimize retained austenite it is important to minimize the room temperature hold time prior to the cold quench. In addition, if the piece is heated up a bit during the room temperature hold, the stabilization effect is increased. With highly alloyed steels like stainless, there are some subtle effects that result from stabilization that are shown in the study of Sandvik 12C27 in reference [13.9]. A series of heat treatments were carried out in which the amount of retained austenite was measured as a function of the austenitization hold-time with 4 different decreasing quenching rates: (1) water, (2) forced air plus water, (3) forced air plus oil and (4) forced air alone. In all 4 cases the amount of retained austenite increased steadily as the austenitization time increased from 4 to 10 minutes. At longer hold-times more carbides dissolve increasing the %C and %Cr in the austenite and dropping the M_s-M_f range. Perhaps more interestingly, at any given austenitization time the amount of retained austenite increased with decreasing quench rate. For example, with an 8 minute austenitization it increased from 7.5 % to 10% to 14.3% to 15.5% for the 4 quench rates 1 through 4. This increase is due to stabilization as the austenite is cooled more slowly through the temperature range from around 300 ^oC (572 ^oF) to room temperature. In the cooling rates including forced air the steels were cooled with forced air down to 200 ^oC (392 ^oF) and then either water

quenched (rate 2) or oil quenched (rate 3) to room temperature. These results show that the amount of retained austenite formed in this stainless steel is significantly influenced by the cooling rate through the low temperatures. This is a subtle stabilization effect. Hence, there are two reasons to cool these stainless steels by quenching rather than air cooling: (1) to reduce the amount of retained austenite as illustrated here, and (2) to reduce K_1 carbide precipitation on cooling and improve corrosion resistance.

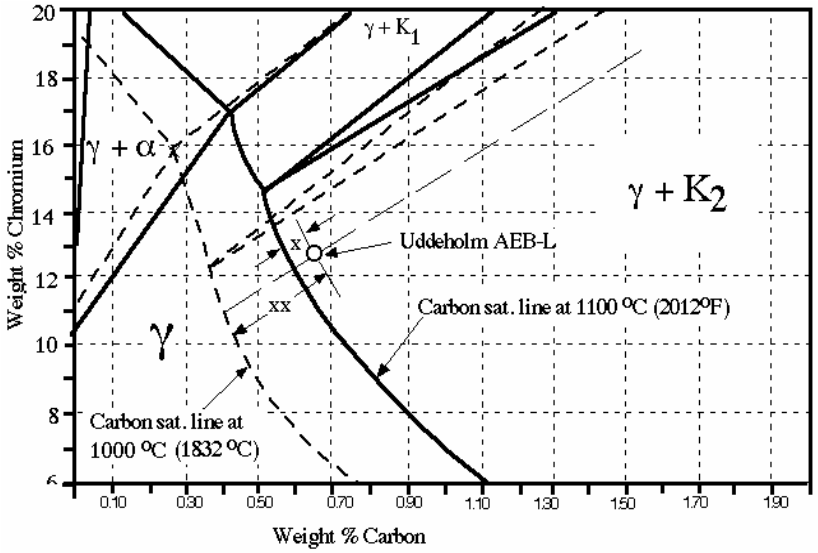

Figure 13.16 Fe-Cr-C isothermal sections at 1000 &1100 °F.

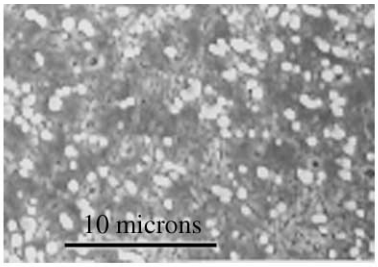

Figure 13.17 SEM micrograph showing K_2 carbides-white particles.

Example Heat Treatment using AEB-L To illustrate some of the important features involved in heat treating these stainless steels, experiments carried out by the author on Uddeholm AEB-L strip of thickness 0.7 mm will be presented. The composition of this alloy is shown on the combined 1000 and 1100 °C isothermal phase diagrams of the Fe-Cr-C ternary alloy in Fig. 13.16. At both temperatures the alloy composition lies in the austenite plus K_2 carbide region and so we expect 2-phase austenitization at both temperatures producing carbides in the austenite which would give martensite + carbides on quenching. Note, however, that the distance from the overall composition to the carbon saturation line is smaller at 1100 °C, distance marked x, than at 1000 °C, distance marked xx. Hence, we expect a higher volume fraction of carbides at the lower austenitization temperature. Strips of the alloy were austenitized for 4 minutes in a resistance heated furnace with an inert atmosphere, helium gas, and they were then forced air cooled to 200 °F in 70 s, followed by water quenching. Metallographic samples were examined in the scanning electron microscope and Fig. 13.17 presents a typical micrograph showing the distribution of carbides in the martensitic matrix. The diameter of the carbides averaged around 0.6 microns, which is somewhat finer than the secondary carbides found in the 440 stainless steels. and no primary carbides were observed The absence of the coarse primary carbides should allow sharpening to a finer radius of curvature at an edge without carbide pullout, which is more likely with the coarse primary carbides of 440C steels. The carbide density was measured as the number of carbides per square inch on micrographs of 2000x magnification, and the results are presented as Fig. 13.18. As expected from the above discussion of Fig. 13.16 it is seen that the carbide density increases as the austenitization temperature decreases.

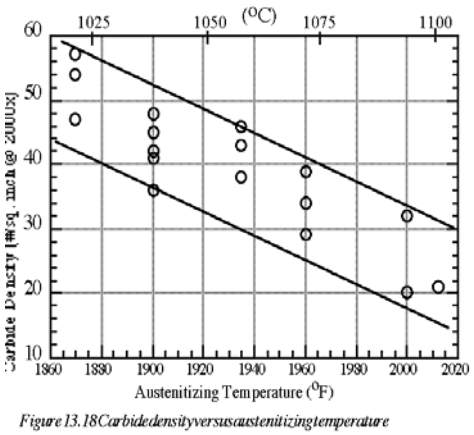

Figure 13.18 Carbide density versus austenitizing temperature

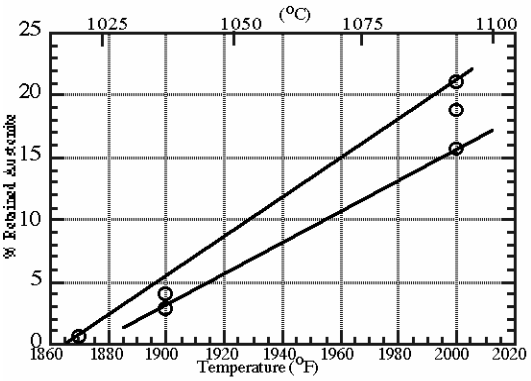

Figure 13.19 % retained austenite versus austentizing temperature for room temperature quench.

The amount of retained austenite in the quenched samples was measured using standard x-ray diffraction techniques and the results are shown in Fig. 13.19. The higher austenitizing temperatures result in a significant amount of retained austenite. As seen on the isotherms of Fig. 13.16, the higher austenitization temperature of 1100 °C (2012 °F) increases both the %C and the %Cr in the austenite (the points where the tie line meets the carbon saturation lines). This, in turn, drops the M_s-M_f range which gives more retained austenite for a room temperature quench.

The effect of cold quenching was evaluated by preparing mixtures of liquid nitrogen and isopentane (also called 2-methyl butane) at temperatures of -75 °F (-59.4 °C) and -140 °F (-95.6 °C). In samples quenched from both 2000 °F and 1900 °F the amount of retained austenite was reduced to zero at the -140 °F temperature and to around 0.4 % at the - 75 °F temperature. The latter temperature is the recommended cold quench temperature [13.10].

Because the steel strip was so thin, it was necessary to measure hardness with a microhardness tester and then convert the DPH values to R_c values. The hardness was found to depend mainly on the amount of retained austenite. Samples quenched to -140 °F from either 1900 or 2000 °F, which had no retained austenite, both gave hardnesses of around R_c = 63.5. Samples quenched to room temperature, which had the amount of retained austenite shown in Fig. 13.19, had hardnesses of R_c = 62 and 60 when quenched from 1900 °F and 2000 °F respectively. Tempering these samples at 380 °F (193 °C), which is near the maximum recommended tempering temperature [13.10], dropped the hardness of both steels by around 1.7 R_c points.

Table 13.8 % Aust. in stabilization experiments.

Aust. Temp.	As Quenched Room Temp.	Quenched -140°C after 3 days
2000 °F	21.1 %	10.2 %
1900 °F	4.3 %	4.3 %
2000 °F	19 %	19%*

* Sample tempered 30 min. at 380 °F

Results of some stabilization experiments are presented in Table 13.8. A sample quenched to room temperature from 2000 °F produced 21.1 % retained austenite (RA). A similar sample quenched immediately to -140 °C produced 0% RA, but the original sample quenched to -140 °F after a 3 day hold at room temperature produced 10.2 % RA. Hence, the 3 day hold had stabilized 10.2 % RA, just under half of the original 21.1 % RA. In the 1900 °F austenitization sample all 4.3 % of the RA was stabilized by the 3 day hold. And in a 2000 °F austenitized sample (bottom row of table) that had been tempered before the 3 day hold, all of the original 19% RA was stabilized, illustrating that heat plus holding increases stabilization of the austenite. These results illustrate the importance of immediate cold quenching prior to tempering to maximize the elimination of retained austenite.

The measurement of retained austenite with x-ray diffraction analysis is a somewhat complicated and non-standard technique. Reference [13.9] presents a simple technique that can be used as a guide to qualitatively evaluate the amount of retained austenite in the steels of Table 13.7 and thereby estimate if the austenitization temperature is near the desired level. Immediately after the room temperature quench and prior to any tempering, blank samples need to be cold quenched to at least -31 ^{o}F (-35 ^{o}C) and their hardness compared to that of the room temperature quenched samples. The cold quench will cause the hardness to rise due to loss of retained austenite. Their guidelines [13.9] are as follows: (1) If hardness rises by more than 1.5 R_c points the austenitization temperature was too high (too much retained austenite). (2) If hardness rises by less than 0.5 R_c points the austenitization temperature was too low.

Table 13.9 Hardness of some carbides [13.11].

Phase	Knoop Hardness	Rc
Martensite	846	65
Cementite(Fe_3C)	1150	70
K_1 carbide ($M_{23}C_6$)		73
K_2 carbide (M_7C_3)	1820	79

The K_1 & K_2 carbides present in the stainless steels of Table 13.7 are significantly harder than the cementite carbide (M_3C) of alloy steels. Table 13.9 presents some measurements of Knoop microhardness values which have been converted to estimated R_c values in the right-hand column. The higher hardness of the K_1 & K_2 carbides has only a small effect on raising the as-measured R_c values of the stainless blades. As seen in Fig. 13.17, the carbides are well isolated from each other and the depth of the diamond indentation of the Rockwell machine therefore measures the resistance to flow of the surrounding martensite matrix with only a small effect from the carbides. However, the presence of the K_1 & K_2 carbides at the surface is effective at increasing the wear resistance over that of a pure martensitic matrix, or of a martensite containing the M_3C carbide of alloy steels such as AISI 52100. Wear tests on both the steels of Table 13.7 [13.9, 13.10] show these steels to have significantly improved wear resistance over conventional steels such as AISI 1095 at the same hardness levels of around $R_c = 60$. The improved wear produced by the fine arrays of the K_1 & K_2 carbides, combined with the lack of coarse primary carbides and the stainless corrosion resistance, make the 2 steels of Table 13.7 among the best choice of steels for most knife applications. See appendix B for a further discussion of the popular stainless steels used to make knives.

Table 13.10 Austenitic stainless steels.*

AISI No.	%Cr	%Ni	Max %C
302	18	9	0.15
304	19	9.3	0.08
304L	19	10	0.03
308	20	11	0.08
309	23	13.5	0.20
310	25	20.5	0.25

*All contain approx. 2%Mn, 1%Si.

Austenitic Stainless Steel As the name implies, the austenitic stainless steels are fully austenite at room temperature. The austenite is stabilized at room temperature by the addition of fairly large amounts of Ni to the steels. The steels may be considered as ternary alloys of Fe-Cr-Ni. Just as with the ferritic stainless steels, carbon is present in these steels at very low levels and the corrosion resistance is enhanced by reducing the %C in them. The average compositions of the common austenitic stainless steels are presented in Table 13.10, and you will notice that as the %Cr is increased so is the %Ni. Both Ni and austenite are face centered cubic structures and, as you might therefore expect, addition of Ni tends to stabilize austenite to lower and lower temperatures. You may understand why the Ni content must be increased as the %Cr goes up by studying the 1100 ^{o}C (2012 ^{o}F)

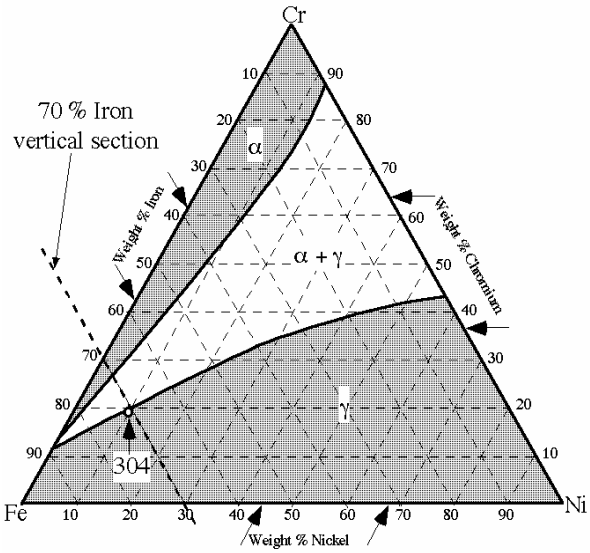

Figure 13.20 Isothermal section of Fe-Cr-Ni phase diagram at 1100 ^{o}C (2012 ^{o}F) [13.3].

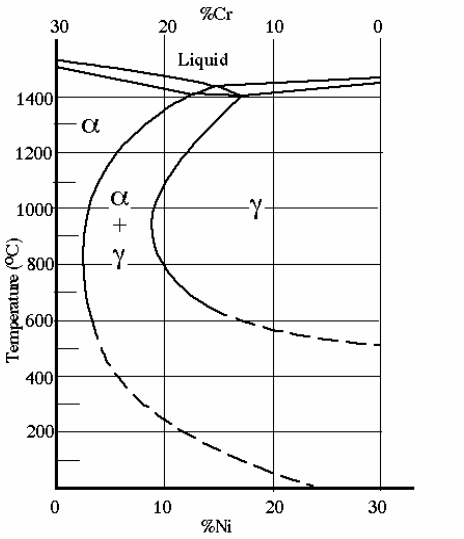

Figure 13.21 Verticle section of Fe-Cr-Ni phase diagram at 70% Fe [13.4, p 4-11].

isothermal section of the Fe-Cr-Ni phase diagram shown in Fig. 13.20. To understand how compositions are plotted on this diagram consider the 304 stainless composition which is shown on the diagram. The %Ni compositions run across the bottom of the diagram and since 304 contains 10% Ni its composition must lie on the line going up from 10%Ni. But 2 lines go up from 10% Ni on the bottom axis. The Ni lines are those going up to your right as shown by the arrows next to Weight % Nickel. (The other lines going up to the left are Fe lines coming in from the left axis as shown by the arrows on Weight % Iron.) Similarly, the Cr lines are the horizontal lines as shown by the arrows on the right axis around Weight % Chromium. Therefore, the composition of the 304 alloy is located at the intersection of the 19%Cr line running in horizontally from the right axis and the 10 %Ni line running up from the bottom axis. Alloy compositions that are 100 % γ at 1100 ^{o}C must lie in the lower shaded region labeled γ on Fig. 13.20. The diagram shows that if you increase %Cr in the 304 alloy it is necessary to also increase %Ni in order to remain in the 100 % austenite region.

In order to understand how the phases might change on cooling it is helpful to be able to look at vertical sections through the ternary phase diagram. Fig. 13.21 presents the vertical section made along the line on Fig. 13.20 labeled 70% Iron vertical section. This vertical section is made through the ternary diagram along alloy compositions that all contain 70 % Fe, which means if you add up the %Cr + %Ni it must come out to 30%. The 70% iron vertical section is shown in Fig. 13.21. The diagram shows that an alloy of 10% Ni+ 20 % Cr (close to 304) will be 100 % austenite at 1100 ^{o}C, but on cooling below around 790 ^{o}C it should become a mixture of γ + α (austenite plus ferrite). Notice that the lines below around 600 ^{o}C are

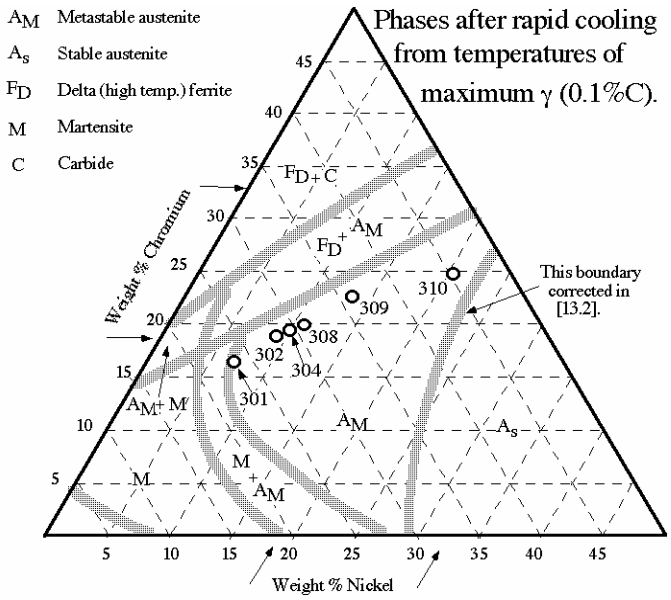

Figure 13.22 Phases present in austenitic stainless steels quenched from temperatures near those of Fig. 13.20 [13.13].

dashed. This is done to show that the austenite will remain stable below these

Table 13.11 The three main types of corrosion in stainless steels

Type of Corrosion	Description	To Avoid [13.4, Ch.15]
Intergranular	As previously discussed this type of corrosion results from the precipitation of the K_1 carbide, usually on grain boundaries, of either ferrite or austenite.	%C less than around 0.02 %
Pitting (Crevice)	Small pits develop holes in the passivating film which set up what is called a galvanic cell producing corrosion.	%Cr greater than 23-24% %Mo greater than 2%
Stress Corrosion Cracking	Localized points of corrosion allow stresses initially unable to crack the steel to concentrate sufficiently to now do so. Details of the mechanism are complex and not well understood. The presence of the chlorine ion (a component of the salt in sea water) makes this type of corrosion a problem in salt waters.	%Cr greater than 20% %Mo greater than 1%

temperature without the formation of ferrite, even though this vertical section predicts that ferrite will form in the austenite. The dashed curves are used because it is found that if you cool down much colder, or if you mechanically deform, particles of martensite will form in the austenite. Hence, the room temperature austenite is said to be "metastable". Phase diagrams do not show us where the metastable phases form. But people have worked out the metastable phase diagram for the austenitic stainless steels and Fig. 13.22 presents the results. The regions on this diagram labeled A_M map the composition of alloys that form metastable austenite on rapid cooling to room temperature from around 1100 ^oC, meaning that particles of martensite might form in this austenite on cold quenching or on severe mechanical deformation at low temperatures. The common austenitic stainless steels of Table 13.10 are plotted on this diagram and you see that all of the austenitic stainless steels lie in the metastable region at room temperature. The fact that the austenitic stainless steels are actually metastable alloys at room temperature is not important from a practical point of view because as long as severe cooling is avoided they remain austenitic at room temperature and elevated temperatures with no problems of ferrite formation.

The austenitic stainless steels are generally considered to have the best corrosion resistance of the 3 types of stainless steels. It is customary to partition corrosion into three types as shown in Table 13.11. As illustrated in the right most column of this table, corrosion resistance is enhanced by three main things: (1) decreasing the %C in the steel, (2) increasing the %Cr in the steel and (3) adding a small amount of Mo to the steel. The Table 13.10 data show that the AISI 308-309-310 series of austenitics employ increased %Cr to achieve improved corrosion resistance. Table 13.12 presents some additional popular austenitic stainless steels with around 18 %Cr that are modified to enhance corrosion resistance. The popular AISI 316 steel has Mo added, and 316L has the Mo addition plus a reduced %C to enhance resistance to intergranular corrosion. The 321 and 347 employ a small addition of a scavenger element to reduce intergranular corrosion. Both Ti and Cb(Nb) are very strong carbide forming elements. Hence when they are present in austenite they will form carbides with C that is dissolved in

Table 13.12 Additional austenitic stainless steels.*

AISI No.	%Cr	%Ni	Max %C	Other
316	17	12	0.08	2.5 Mo
316L	17	12	0.03	2.5 Mo
321	18	10.5	0.08	Ti($5xC_{min}$)
347	18	11	0.08	Cb(Nb)($8xC_{min}$)

*All contain approx. 2%Mn, 1%Si.

the austenite. Essentially, they scavenge the element C from the austenite leaving less of it to form the K_1 carbide. Notice that the amount of the scavenger element added is set to the minimum amount of C in the steel. For example, in 321 the Ti level is set at 5 times the minimum carbon level.

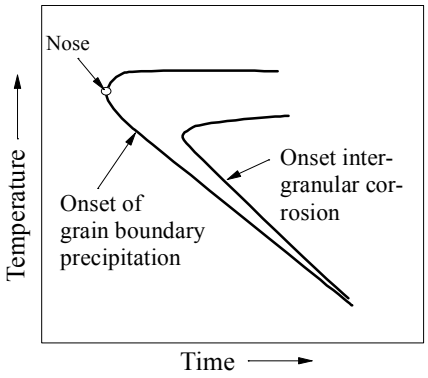

Figure 13.23 Start-times versus temperature for K_1 precipitation and intergranular corrosion.

The resistance to intergranular corrosion can be strongly reduced by heat treatments that cause the K_1 carbide to precipitate. Figure 13.23 is a type of IT diagram that maps the temperature-time conditions needed to cause the K_1 carbide to start to precipitate on the austenite grain boundaries. The diagram also contains the start-curve for the intergranular corrosion that is caused by the carbide precipitation. Reference [13.4] presents data for AISI 304 stainless which gives a temperature-time at the nose of 850°C (1562 °F) & 20 sec. for onset of grain boundary precipitation and 690 °C (1274 °F) & 20 min. for onset of corrosion. They also present recommended annealing temperatures for the austenitic stainless steels and on cooling from these temperatures they advise the use of sufficiently rapid cooling to drop the temperature from 870 to 425°C (1600 to 795°F) in no more than 3 minutes. Figure. 13.23 shows that this recommendation is made to avoid the possibility of promoting intergranular corrosion.

Figure 13.24 is presented to illustrate why it is advisable to hold the carbon level of the austenitic stainless steels as low as possible. Notice how sensitive the minimum start time for K_1 precipitation is to the %C in the steels. Dropping %C from 0.08 to 0.02 % (a factor of 4), increases the minimum start time for K_1 precipitation from 0.1h to around 80 hours (a factor of 800). These data illustrates why Ref. [13.6] recommends care in forging to minimize carburization.

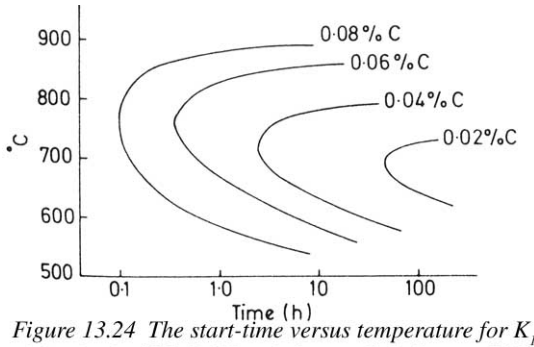

Figure 13.24 The start-time versus temperature for K_1 precipitation in 18Cr/10Ni stainless as %C changes [13.14].

Although the austenitic stainless steels are generally considered to have the best corrosion resistance, the ferritic stainless steels are superior in their resistance to stress corrosion cracking, particularly the superferritics that are low in Ni [13.1].

The austenitic stainless steels cannot be hardened except by cold working. During cold working the strength (and hardness) rises while the ductility falls. Figure 13.22 shows that when the Ni content of 302 is reduced from its value of 9% to a value of 7% in AISI 301, the composition lies in the region where one might expect martensite to form. In 301 martensite does form during the cold working operation and this leads to increased strengths and reduced ductilities. Table 13.13 presents data comparing the tensile strength and ductility of 301 and 302 after a 40 % cold reduction. The tensile strengths have been converted to estimated equivalent hardnesses

Table 13.13 Mechanical properties after 40 % cold reduction [13.2].

Steel	Tensile Strength	Percent Elongation	Equivalent Hardness
301	192 ksi	5 %	42 R_c
302	160 ksi	15 %	36 R_c

(Table 5.3) to provide an idea of expected maximum hardnesses in these cold worked austenitic stainless steels.

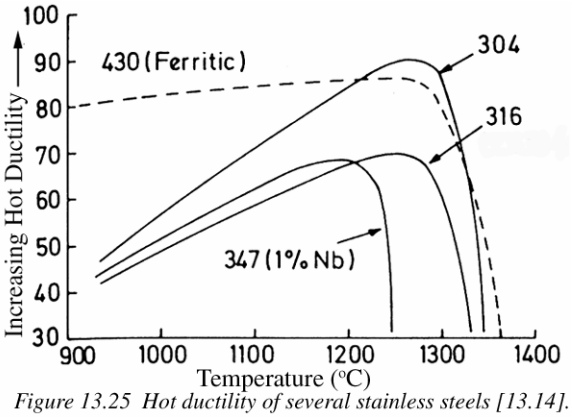

Figure 13.25 Hot ductility of several stainless steels [13.14].

Hot ductility is an important concern in forging knives from stainless steels. Figure 13.25 presents the relative hot ductility of several types of stainless steels. It is seen that the ferritic stainless steels have a nearly constant hot ductility throughout the forging temperature range. The hot ductilities of the austenitic grades are much more sensitive to temperature. The hot ductility of AISI 304 increases strongly with temperature and only becomes equal to the ferritic 430 at around 1250 °C (2282 °F). The falloff in these curves is dramatic and limits the maximum forging temperatures. The falloff is due to either formation of liquid or loss of grain boundary cohesion. The significant reduction of hot ductility in AISI 316 and 347 is thought to be due to inhibition of recrystallization produced by the additions of Mo and Cb(Nb), respectively, in these two steels [13.14].

Precipitation Hardening Stainless Steels (PHSS)

Recall that secondary hardening during the tempering of alloy steels occurs due to the precipitation of small carbide particles, see Fig. 10.9 and discussion. The precipitation hardening stainless steels achieve the same type of hardening increase on heating to modest temperatures, but here it is due to precipitation of compounds that are not carbides. For example, in 17-7 PH stainless steel (see Table 13.14) the Al added to this alloy forms a compound with the Ni atoms of the stainless, such as Ni_3Al or NiAl, on heating to around 1000 °F.

Table 13.14 Composition of 3 precipitation hardening stainless steels.

Type	AISI No.	Trade Name	%Cr	%Ni	%C	Other*
Martensitic	630	17-4 PH Armco	16	4.2	0.04	3.4 Cu, 0.25Cb
Semi-Austenitic	631	17-7 PH Armco	17	7.1	0.07	1.2 Al
Austenitic	600	A-286 Alegheny-Ludlum	14.8	25.3	0.05	Low levels: Mo,Al,Ti,V ,B

*Low levels of Mn and Si are also present, see [13.4].

There are 3 basic types of these steels, called martensitic, semi-austenitic, and austenitic. As an example, one steel of each type is shown in Table 13.14. Some of these steels have been given an AISI number, but they are seldom used as it has become customary to maintain the trade name used by the company that developed the steel. For example, ref. [13.6] describes the recommended heat treat practice for these steels without specifying the AISI numbers. Similar to a quench and temper heat treatment, these steels are also generally heat treated by a 2-step process with the final step being the precipitation anneal. The steel type is related to the matrix that is present when the final precipitation hardening treatment is carried out. For example, in the austenitic A-286 steel the precipitation occurs when the steel is fully austenite. It is helpful to plot the Cr/Ni compositions of the 3 steels of Table 13.14 on Fig. 13. 22, which has been done in

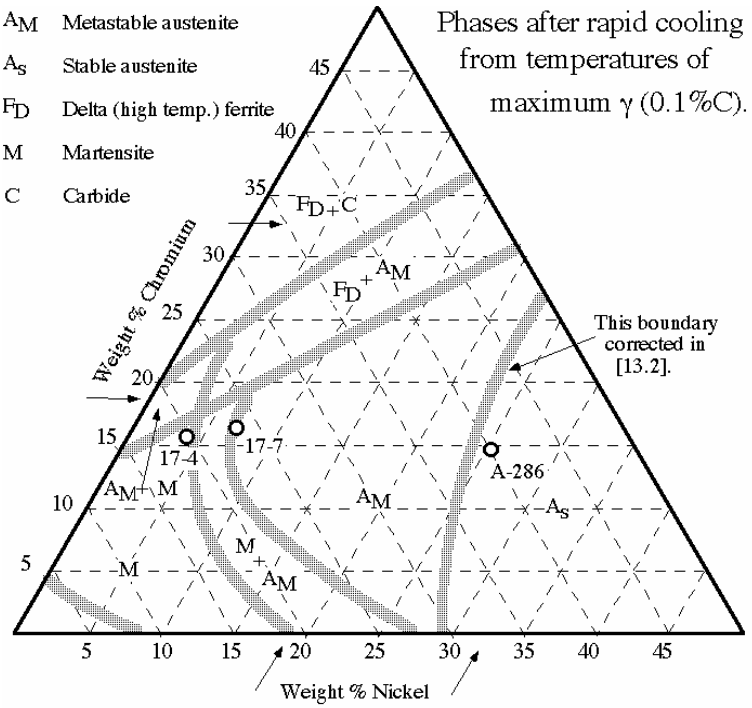

Figure 13.26 Composition of the three PH stainless steels of Table 13.13 plotted on Fig. 13.22.

Fig. 13.26. The austenitic A-286 stainless steel lies in the stable austenite region, and the final step of the heat treatment causes the precipitation to occur in an austenite matrix. The diagram shows that the martensitic 17-4 PH steel lies in the composition region where rapid cooling produces martensite, and in this steel the final precipitation occurs when the steel has a martensite structure.

The semi-austenitic steels are the most complex of the three. It is helpful to realize that 17-7 is essentially the same steel as AISI 301 with a slightly lower carbon composition plus the addition of Al needed to form the precipitate. Figure 13.26 shows that its composition is right on the edge of the metastable austenite region. As described in ref. [13.6], a double heating is employed prior to the final precipitation anneal. The first heat treatment, usually done at the mill, produces an austenite matrix with minor amounts of delta ferrite. The second heating forms chromium carbides along the delta ferrite grain boundaries and changes the composition of the austenite matrix so that on cooling it now becomes a martensite matrix. Hence the final precipitation in the semi-austenitic stainless steels occurs in a predominately martensite matrix.

In the heat treating of these steels it is common to specify the various steps in the process with the term "condition". For example, a second step of heating to 790 °C (1455 °F) for 1.5 h and cooling to room temperature within 1 h and holding for 30 min. is called "condition T". If this is followed by the precipitation anneal of heating to 565 °C (1050 °F) for 1.5 h and air cooling, the final condition is called TH1050, whereas if the precipitation temperature is 510 °C (950 °F) the final condition is called TH950. Reference [13.6] gives information on the hardness achieved for the various conditions of 17-7PH, and condition TH1050 produces a hardness of R_c = 38 to 44 while condition TH 950 produces R_c = 42 to 48.

Table 13.15 [13.6]

Steel	Final Hardness
17-4PH	42-44 R_c
17-7PH	34-49 R_c
A-286	24-45 R_c

It is helpful to realize that the martensite structures of these steels is a low carbon martensite with hardnesses well below that of the martensite of either alloy steels or the martensitic stainless steels. The final hardnesses ranges of the three steels after the heat treatments specified in ref. [13.6] are given in Table 13.15. These alloys provide a stainless steel with improved toughnesses at their level of hardness over the martensitic stainless steels.

A helpful hint in working with stainless steels is to remember that the austenitic form of iron is not magnetic and will not, therefore, be attracted to a magnet. So, fully

austenitic stainless steels will not be attracted to a magnet. Austenitic stainless steels that contain a small amount of ferrite will be weakly attracted to a magnet, with the attraction force dependent on the volume fraction ferrite in the steel. As seen in Fig. 13.21, forging some of the common austenitic stainless steels at higher temperatures will result in formation of the high temperature delta ferrite. Use of a magnet on fully austenitic and ferritic steels as standards might help in gauging levels of residual ferrite. There is a class of stainless steels not discussed here called duplex stainless steels which consist of a mixed ferrite/austenite structure. These steels contain a Cr/Ni composition of 25/5 and you can see on Fig. 13.21 that if such a steel were forged at around 900 ^{o}C it would consist of a mixture of ferrite and austenite. Refer to reference [13.15] for a brief discussion of these stainless steels as well as all the other stainless steels.

References

13.1 M.A. Streicher, Stainless steels: past, present and future, pp 1-34 in Stainless Steel '77, Ed.: R. Q. Barr, Climax Molybdenum Co., (1977).
13.2 Source Book of Stainless Steels, ASM, p 107 (1976).
13.3 Metals Handbook, vol. 8, 8th Edition, American Society for Metals, Metals Park, OH (1973).
13.4 D. Peckner and I.M. Bernstien, Handbook of Stainless Steels, McGraw Hill Book Co, New York (1977).
13.5 A.E. Nehrenberg and P Lillys, High temperature transformations in ferritic stainless steels containing 17 to 25 % Chromium, Transactions American Society for Metals, vol 46, 1177-1213 (1954).
13.6 Heat Treater's Guide, Practice and Procedures for Irons and Steels, ASM International, 2nd Edition (1995).
13.7 F.K. Bloom, Effect of heat treatment on and related factors on straight stainless steels, Corrosion, vol.9, p 61 (1953).
13.8 M. Hillert, Prediction of iron-base phase diagrams, in Hardenability concepts with applications to steel, Ed: D.V. Doane and J.S. Kirkaldy, p 49, Metallurgical Society of AIME, Warrendale, PA (1978).
13.9 P. Ericson, Sandvik 12C27-stainless steel for edge tools, Steel Research Centre, Sandvik, Sweden (1981).
13.10 UHB Stainless AEB-L Technical Data, Uddeholm Strip Steel AB, Munkfors Sweden, Nov. (1990).
13.11 P. Leckie-Ewing, A study of the major carbides in some high speed steels, Trans. ASM, vol. 44, 348 (1952).
13.12 A. Omsen and L.G. Liljestrand, Reactions during heating of a 13.5% Cr Razor Blade Steel, Scandinavian J. Metallurgy, vol. 1, pp 241-246 (1972).
13.13 Metals Handbook, American Society for Metals, p1261, Metals Park, OH (1948).
13.14 F.B. Pickering, Physical metallurgy development of stainless steels, in Stainless Steels '84, pp 1-28, The Institute of Metals, London (1985).
13.15 W.F. Smith, Structure and properties of engineering alloys, McGraw-Hill, New York (1981).

Summary of the Major Ideas of Chapter 13

1 The outstanding feature of stainless steels is their excellent resistance to corrosion. The resistance is due to a thin chrome containing oxide film on the surface of the steel that inhibits reaction with water solutions and moisture. When an effective corrosion inhibiting film is present the steel is said to be "passivated". For a steel to be considered "stainless" it must contain a minimum %Cr level of just under 12% Cr.

2 The corrosion data of Fig. 13.1 illustrates why the 12 % value occurs. It also illustrates that stainless steels are only corrosion resistance in oxidizing water solutions,

like nitric acid. In reducing acid solutions, like sulfuric, the passive film is reduced to the point where it is not effective at inhibiting corrosion.

3 Table 13.11 presents the 3 types of corrosion that occur with stainless steels. It shows the 3 major compositional changes that lead to improved corrosion resistance: (1) Minimizing the %C in the steel, (2) Increasing %Cr up to the 20 to 25% range, and (3) Adding 1 to 2 % Mo to the steels.

4 Stainless steels are generally partitioned into 4 major types: (1) Ferritic, (2) Martensitic, (3) Austenitic and (4) Precipitation Hardened Stainless Steels.

5 The ferritic stainless steels are Fe-Cr-C alloys. At room temperature they have a ferrite (body center cubic) structure, and hence are magnetic. The room temperature ferrite contains a fine dispersion of chrome carbides, called the K_1 carbide which has chemical formula $(Fe+Cr)_{23}C_6$, often abbreviated to $M_{23}C_6$.

As shown by the Fig. 13.4 phase diagrams these steels will contain some austenite at forging temperatures (1900-2100 ^oF). The high Cr level produces excellent hardenability, Fig. 13.5, so that steels air cooled after forging will contain martensite unless annealed adequately at around 1300 ^oF. In addition, 2 forms of embrittlement can occur in these steels for prolonged heating at low temperatures as illustrated in Fig. 13.6.

The ferritic steels have AISI numbers in the 400 range. As shown in Table 13.1 the popular grades are supplied at 3 levels of Cr composition, 12, 17 and 25 %, with increasing corrosion resistance as the %Cr increases. New grades of these steels, not given AISI numbers and called "superferritics" have been developed. As shown in Table 13.2 these steels develop improved corrosion resistance by small additions of Mo and Ni and by reduction of the level of both C and N.

6 Similar to the ferritic stainless steels, the martensitic stainless steels are Fe-Cr-C alloys that have been assigned 400 AISI numbers, Table 13.3. Whereas one usually wants the %C as close to zero as is economically possible in the ferritics, it is necessary to increase %C in the martensitics in order to increase the hardness of the martensite formed in these alloys, Table 13.4. The steels have high hardenability and can be hardened with air cooling, but are generally quenched to avoid problems with embrittlement and reduced corrosion resistance due to K_1 carbide precipitation. They need to be tempered to produce adequate toughness for most uses and their tempering response is similar to alloy steels, see Figs. 13.9 and 13.10.

Similar to plain carbon and alloy steels it is necessary to increase the %C to around 0.6 % to obtain martensite with hardnesses in the low Rockwell 60 range. However, as discussed on pages 135 to 138, one cannot just assume that alloys containing %C at 0.6% or above will produce both adequate hardness and corrosion resistance. The %Cr/%C level in the martensite is controlled by the level in the austenite formed at high temperature before quenching. But the %Cr/%C level in the austenite may not be the same as the overall level in alloys. For example, an overall level of %Cr/%C = 12% Cr/

0.6% C will give a hot austenite of this same composition and lead to as-quenched R_c values in the low 60s while maintaining the minimum 12 %Cr for adequate passivation. If however, one increases %Cr above 12% Cr to improve corrosion resistance, the austenite formed at high temperatures will contain %C below 0.6 % And if one increases the %C above 0.6 % then the austenite formed at high temperature will contain more C, but the %Cr will fall below 12% and reduce corrosion resistance.

The best compositions for knife steels have %Cr/%C values at or just above 12%Cr/0.6% C and Table 13.7 presents two such steels. Optimum heat treatment of these steels is complicated because it involves the 2-phase austenitization discussed on p. 108. Austenitization temperature and time control martensite hardness, volume fraction carbides and amounts of retained austenite. An example illustrating these factors is presented on pp 139-142.

7 The austenitic stainless steels have significant amounts of Ni added to stabilize the austenite phase at room temperature. These alloys may be regarded as Fe-Ni-Cr alloys with impurities of C. They have 300 AISI numbers, Table 13.10. As explained with the help of Figs. 13.20 and 13.22 these alloys have the %Cr/%Ni values balanced to ensure that at room temperature the face centered cubic austenite phase is stable. Since the austenite is non-magnetic these alloys will not be attracted to a magnet unless they contain some residual ferrite. As shown on the Fe-Cr-Ni vertical section, Fig. 13.21, an alloy of 10%Ni/20%Cr (close to AISI 304) will contain ferrite when forged above around 1100^{o}C (2012 ^{o}F), which illustrates that residual ferrite can be present in these steels, depending on prior heat treatment.

The 300 series austenitic stainless steels have the best overall corrosion resistance. Corrosion behavior is generally partitioned into 3 types: Intergranular, Pitting (crevice) and Stress Corrosion. Table 13.11 summarizes the characteristics of each. It also shows how the composition of %C, %Cr and %Mo are varied to optimize corrosion resistance. One can consider AISI 302 as the base steel, %Cr/%Ni = 18/9. Improved corrosion resistance is obtained in 304 and 304L by reducing the %C, in 308-309-310 by increasing %Cr and in 316 by adding Mo. The austenitic stainless steels can be work hardened to reasonably high hardness levels as illustrated in Table 13.12. Their hot ductility is compared to that of a ferritic steels in Fig. 13.25.

8 The precipitation hardening stainless steels (PHSS) are heat treated in a 2 step process similar to the quench and tempering of alloys steels where, instead of tempering, the second heating produces an increased hardness through the precipitation of an alloy compound. Special elements, such as Al and Cu are added to these alloys to produce the precipitate. The alloys can be hardened to maximum values of 44 to 49 HRC and provide a stainless steel in this hardness range with superior corrosion resistance to the martensitic stainless steels.

The %Cr/%Ni balance is altered in these steels to produce 3 types of steels called martensitic, austenitic and semiaustenitic. The names given to these steels are usually the trade names of the producers, even thought some of them have been assigned AISI

numbers. Table 13.14 presents one example steel from each of the 3 types. The final precipitation reaction occurs in a martensitic matrix for the both the martensitic and semi-austenitic types and it occurs in an austenite matrix in the austenitic type. Figure 13.26 shows how the variation of the composition of these steels produces this effect for the 3 steels of Table 13.14.

9 Sensitization A stainless steel is said to be sensitized if it has been held in the low temperature range of roughly 870 to 425 ^{o}C (1600 to 795 ^{o}F). This treatment forms precipitates of the K_1 carbide on grain boundaries that remove Cr from the surrounding matrix and leads to intergranular (grain boundary) corrosion. It occurs in all types of stainless steels, particularly if the %C is high, see Figs. 13.23 and 13.24. Addition of the scavenging elements Ti or Cb(Nb) to the steel is sometimes employed to remove carbon from the austenite or ferrite as a carbide. Examples include the austenitic steels, 321 and 347, see Table 13.12, and the superferritic steels, 18-2 and 26-1, see Table 13.2.

10 Stabilization Retained austenite occurs in steels when the M_s-M_f range extends below room temperature, as is the case for the martensitic stainless steels. The retained austenite can be eliminated by cold quenching. Cold quenching is done in 2 steps, first to room temperature and then to a cold temperature. A time delay before the cold quench often results in an increase in the amount of retained austenite after the cold quench. The time delay has stabilized some of the retained austenite. Stabilization can produce quite subtle problems in martensitic stainless steels, see page 139.

14 Tool Steels

One of the characteristics of our species, Homo sapiens, has been the use of tools. Because our ancient ancestors used rock materials for their tools they have been preserved and archeologists are able to use the "tool kits" of ancient species to characterize differences between our Homo sapiens ancestors and other ancient species, such as Neanderthal man. These tool kits consisted of various shaped rock material, including flints, that were used for such activities as cutting, hammering, punching, etc. Modern day tool steels are essentially the evolved form of these 100,000 year old tool kits because tool steels are the primary die and cutting materials which modern industry uses to shape other materials by such operations as forging, extrusion, shearing, etc. Until the early 1800s the main use of steel was for tools. Nowadays, however, tool steels represent only a small fraction of total steel production, but they continue to play a key role in man's industrial activities, as is evidenced by the fact that many industrial plants have small shops devoted to the tool steels of their machinery.

The first tool steel was developed in England by Mushet around 1868. He accidentally discovered that large additions of tungsten, W, and manganese, Mn, produced air hardening steels. (These additions improved the hardenability of the steels to the point where air cooling rates were adequate to avoid formation of pearlite and bainite, thereby forming martensite directly on air cooling.) He then did systematic research and developed a steel containing 2% C, 2.5% Mn and 7% W that remained the tool steel of choice for around 25 years. It was called Robert Mushet's Specialty steel. Then, in the 1898-1900 time period, two Americans, Taylor and White at Bethlehem steel, discovered what we now call "high speed" tool steels. Their discovery was largely a processing discovery, which showed that by austenitizing high W steels at much higher temperatures than had previously been used it was possible to produce very significant secondary hardening during tempering, similar to that shown on Fig. 10.9. Their steel was demonstrated at the 1900 World Fair in Paris where it was shown that tools could operate for long periods at such high cutting speeds that a red heat (550 ^{o}C (1022 ^{o}F)) was produced in the steels. Their patented steel contained 1.85%C, 3.8% Cr and 8% W. Vigorous research in England and the US quickly established that their %C level was too high and %W too low for optimum performance. By 1910 the optimum composition had been adjusted to 0.68 %C, 4.0% Cr, 18% W, 1.0% V and 0.4% Mn [14.1]. Taylor and White lost their patent claim in a controversial court case in 1908 in a story that is interesting to read about, see ref. [14.2]. It is surprising how close the 1910 composition compares to one of our best modern day high speed tool steels, T1, whose composition is given in Table 14.1.

Tool Steel Classification Tool steels have been classified into several types as illustrated in the left column of Table 14.1. The various types are further subdivided according to a letter code followed by a number, as shown in the second column of this table. Chapter 6 of reference [14.3] presents complete lists of all the tool steels along with an excellent discussion of selection criteria for these steels. There are many different steels for each letter code. For example, the W steels listed in [14.3] include 7 members ranging from W1 to W7. To simplify this presentation Table 14.1 has listed just one of the steels for each letter type. Reference [14.4] presents a listing of the composition of the AISI tool steels which includes most of the steels in the more

*Table 14.1 Classification of AISI Tool Steels showing weight % composition of one alloy for each AISI type[14.3]**

Type	AISI	C	Mn	Si	Cr	V	W	Mo	other	Total Alloy
Carbon(water hardening)	W1	**1.0**	0.25	0.25						0.5
Low Alloy	L6	0.7	0.5	0.25	0.9			0.3	1.6Ni	3.6
Shock resisting	S2	0.47	0.40	**1.05**		0.22		0.45		2.1
Die steels for cold working	O2	0.9	**1.6**	0.25	0.22	**1.8**		0.3		4.2
	A2	1.0	0.62	0.25	**5.1**	0.32		**1.2**		7.5
	D2	**1.5**	0.3	0.25	**12**	0.6		0.95		14.1
Die steels for hot working	H13	**0.39**	0.35	1.0	**5.1**	1.0		**1.4**		8.9
	H21	**0.35**	0.30	0.3	3.5	0.5	**9**			13.6
High speed	M2	0.83	0.27	0.32	4.1	**2**	**6.1**	**5**		17.8
	T1	0.78	0.25	0.30	4.1	1.1	**18.2**	0.7		24.7
	T15	**1.55**	0.27	0.27	4.4	**4.9**	**12.4**	0.5	**5Co**	27.7

* The P steels commonly used for molding plastics have not been included.

complete list of ref. [14.3]. (Note: There are many tool steels in use not having an AISI classification, and ref. [14.3, p. 230] presents a system for classifying all these steels. This system, which assigns a 3 digit number to each steel, is not widely used.)

In the discussion of steel selection in ref [14.3], the major properties of the steels are considered to be (1) wear resistance, (2) toughness and (3) hot hardness. Table 14.2 presents the ratings of these 3 properties for each of the steels of Table 14.1, where a rating of 1 to 10 is used with 10 being the best possible value. In general, one may rationalize the main reason for high values of the 3 properties listed in Table 14.2 as follows:

High wear resistance:	More carbides
High toughness:	Low %C in the steel
High hot hardness:	More alloy carbides

The various types of tool steels will be briefly discussed by reference to the member of the type shown in Tables 14.1 and 14.2.

W Steels The W stands for water hardening. These steels are similar to the plain carbon 1095 steel and have very low hardenability. Therefore, as shown in Table 14.2 the toughness of the steel is improved significantly if the steel is shallow hardened. This means the steel is quenched at a rate that produces martensite only near the surface and allows the core to remain unhardened and therefore tougher. The poor hot hardness of these steels relative to the rest of the steels results because the carbides in the other steels are alloy carbides, i.e. M_3C rather than Fe_3C. The alloy carbides resist coarsening and dissolving at higher temperature and give the improved hot hardness. The final column of Table 14.1 gives the total of the % alloying elements in each steel. Hence, as one moves down in the table the amount of the alloying addition generally increases and therefore the volume fraction of alloy carbides increases.

Table 14.2 Relative values of the three most important properties of tool steels [14.3].

Type	AISI	Wear Resistance	Toughness	Hot Hardness
Carbon(water hardening)	W1 (1095)	4 4	7(shallow hard.) 3(through hard.)	1 1
Low Alloy	L6	3	6	2
Shock resisting	S2	2	8	2
Die steels for cold working	O2	4	3	3
	A2	6	5	5
	D2	8	2	6
Die steels for hot working	H13	3	9	6
	H21	4	6	8
High speed	M2	7	3	8
	T1	7	3	8
	T15	9	1	9

L Steels The L stands for low alloy, and these steels have compositions similar to the AISI alloy steels discussed in Chapter 6. For example, if you compare the composition of the L6 member listed in Table 14.1 to the AISI 4340 steel of Table 6.4 you will find that L6 is essentially a 4340 steel with %C increased from 0.4 to 0.7%.

S Steels The S stands for shock resisting. The high toughness needed for shock load resistance is obtained by reducing the %C in these steel to low levels, which also results in the low wear resistance and hot hardness of the S steels.

O Steels The O stand for oil hardening. The key alloying elements for the various steels is shown in bold print in Table 14.1, and for the O steels Mn and V are mainly responsible for its improved hardenability over the W steels allowing them to generally be oil quenched to through hardness.

A Steels The A stands for air hardening. Hardenability of these steels is improved to the point that they may be air hardened. The key element additions allowing hardenability improvement are Cr and Mo.

D Steels These steels are sometimes called High-Carbon, High Chromium steels and the D symbol has no obvious meaning, although it is usually correlated with the term direct hardening. The steels may be air hardened. As illustrated in Table 14.2, the combination of high carbon and high alloy content results in excellent wear resistance, moderately good hot hardness, but poor toughness.

H Steels The H stands for hot hardness. These are usually the steels of choice for the die steels of extrusion operations that are done hot. Here, the combination of low carbon and moderate to high alloy content gives good toughness and hot hardness but only fair wear resistance.

M and T Steels The M and T stand for the molybdenum and tungsten additions in these high speed tool steels. The carbides of these 2 elements are stable to quite high temperatures. Therefore, the high level of these alloying elements produces large carbide volume fractions which give good wear resistance and hot hardness, but poor toughness. The high carbon T15 steel has been included in Tables 14.1 and 14.2 to provide an example of a tool steel designed to produce a maximum wear resistance and hot hardness at the sacrifice of toughness.

The Carbides in Tool Steels It should be clear from the above discussion that the carbides present in tool steels play a dominant role in the control of the mechanical properties desired in a tool steel. The microstructure of most tool steels following heat treatment is similar to that of 52100 shown in Fig. 6.4. As may be seen from Fig. A2(c) or ref.[14.4, p. 548], the microstructure of A2 contains arrays of carbides that appear similar to Fig. 6.4, but have larger diameters. As with 52100, it is these arrays of carbides that give the tool steels their excellent wear resistance. The type of carbide present in the tool steels varies with the type of alloying elements in the steel. As may be seen from Table 14.1 there are 4 major alloying elements present in varying amounts in

Table 14.3 The carbides in tool steels

Type	HRC	Element distribution in M	
		Most	Least
M_3C	70	Fe, Mn, Cr	W, Mo, V
$M_{23}C_6(K_1)$	73	Cr	Mo, V, W
M_6C	75	Fe, Mo, W	Cr, V, Co
$M_7C_3(K_2)$	79	Cr	?
M_2C	79	W, Mo	Cr
MC	84	V	W, Mo

the tool steels, Cr, V, W, and Mo. As discussed with the aid of Fig. 8.8 on page 72, these elements all form very stable carbides. Table 14.3 lists the 6 major types of carbides found in tool steels. As one goes down in the table it is seen that the hardness of the carbide type increases. (These hardness values, given as Rockwell C, are only estimates based on several sources.) Each of them is characterized by a different crystal structure which corresponds to a different chemical formula. The M_3C carbide may be thought of as having a chemical formula of $(Fe+X)_3C$, where X refers to different combinations of the Mn and the 4 major alloying elements, Cr,V,W,Mo. If X contains only Fe and Mn this is the cementite carbide found in plain carbon steels. Table 14.3 shows that in tool steels the M in M_3C will be mostly Fe, Mn, Cr with minor amounts of W, Mo, and V. The two chromium carbides that are dominant in stainless steels and discussed in Chapter 13, $M_{23}C_6$ (called K_1) and M_7C_3 called K_2), are also present in many tool steels and have M mainly containing Cr. The remaining 3 carbides M_6C, M_2C and MC have M mainly containing Mo, W and V.

On heating a carbide containing steel to high temperature austenite will form and the carbides present in the original steel will begin to get smaller in size as the M atoms in the carbide dissolve into the austenite. The more difficult it is for the M atoms to dissolve, the hotter one can heat the steel and retain small carbides in the matrix. Figure 14.1 presents data showing the fraction of several alloying elements that have dissolved from the carbides into the austenite as the temperature of austenitization rises in an M4 high speed tool steel. This steel contains 3 main carbides in the annealed condition, $M_{23}C_6$, M_6C and MC. The figure shows that the predominantly Cr carbide, $M_{23}C_6$, dissolves at relatively low temperatures while the other two carbides, which contain mainly Mo, W and V, do not dissolve until temperatures are quite high. The secondary hardening, which makes the high speed tool steels have hot hardness, is due to precipitation of fine alloy carbides on tempering. However, this precipitation process requires that the alloying elements have been dissolved into the austenite during the austenitization step. It is apparent from Fig. 14.1, that quite high austenitization temperatures are required to dissolve the Mo-W-V alloy carbides of high speed steels. This relationship between alloy content and recommended austenitization temperature is illustrated in Table 14.4 which has been made up using the recommended heat treat practice for the various steels given in ref. [14.4]. It is seen that the austenitization temperatures increase from values typical of plain carbon and low alloy steels, around 845 ^oC (1553^oF), way up to the extremely high temperatures of around 1230^oC (2246^oF) for the most highly alloyed steels, the high speed tool steels.

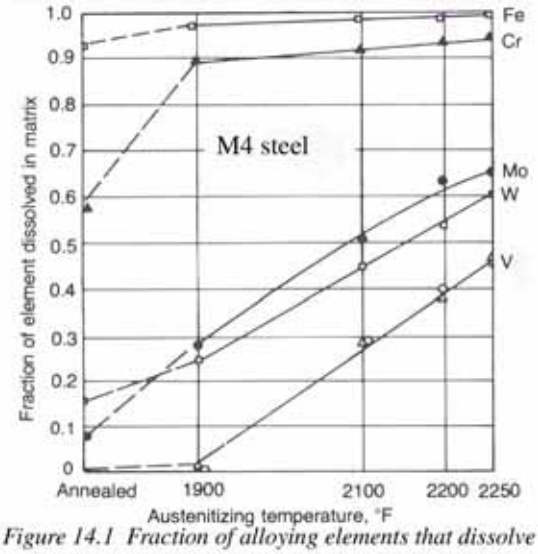

Figure 14.1 Fraction of alloying elements that dissolve as the austenitizing temperature is raised [14.5].

Table 14.4 Recommended heat treat practice for a sampling of tool steels [14.4].

Type	AISI	Austenitization Temp.		Secondary Peak.			Number of. tempers
		°C	°F	Max R_c	Temp. of max R_c °C	Temp. of max R_c °F	
Carbon(W.H.)	W1	760-845	1400-1553	none	none	none	Single
Low Alloy	L6	790-845	1454-1553	none	none	none	Single
Shock resisting	S2	845-900	1553-1652	none	none	none	Single
Die steels for cold working	O2	760-800	1400-1472	57	260	500	Single
	A2	925-980	1697-1796	57	454	850	Double
	D2	980-1025	1796-1877	58-59	482	900	Double
Die steels for hot working	H13	995-1040	1823-1904	52-54	524	975	Triple
	H21	1095-1205	2003-2201	52-56	532	990	Triple
High speed	M2	1190-1230	2174-2246	64-66	543	1010	Double
	T1	1260-1300	2300-2372	65-67	527	980	Double
	T15	1205-1260	2201-2300	67	543	1010	Triple

As shown in ref.[14.3, p. 219], it is possible to characterize the different types of tool steels by the shapes of their hardness versus tempering temperature curves. Figure 14.2 presents the generalized curves. It is seen that as the alloying content of the tool steel increases a well developed secondary hardening peak is formed, which has its maximum hardness for the high speed tool steels. Reference [14.4] presents the hardness versus tempering temperature for most tool steels and Table 14.4 summarizes the temperatures of the secondary hardness peaks and the R_c hardness at the peak for the steels discussed here. You will notice in studying the data of ref. [14.4] that small changes occur in the tempering curves depending on both the quench type (air versus oil versus salt) and on the austenitizing temperature. The higher values of the hardness ranges listed in Table [14.4] correspond to austenitization at the higher temperatures of the austenitizing ranges that are listed. Notice the much lower overall hardness of the H steels shown on Fig. 14.2. This results from the low %C in these steels which is required by the need for high impact strength in their use as hot work die steels for such applications as extrusion.

Special heat treatment effects with tool steels The heat treatment of tool steels involves many subtle effects that are not present in heat treating low alloy and plain carbon steels.

1 Most of these steels are two-phase at their austenitization temperatures and therefore involve the complications previously discussed for this case on pages 107 and 136. The carbon composition and the alloy composition of the austenite is controlled by the austenitization temperature. In general, higher austenitization temperatures will increase both the %C and % alloying elements in the austenite. Increasing %C leads to both higher hardness martensite but also an increase in % retained austenite, unless subzero cooling is employed. Specific 2-phase effects include the following:

(a) The austenitization time and temperature controls the amount of C in the austenite,

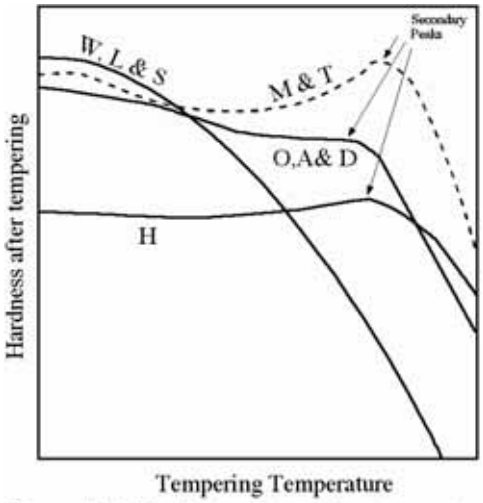

Figure 14.2 Hardness vs. tempering temperature of the various types of tool steels.

which in turn controls the as-quenched hardness, mainly by controlling the amount of retained austenite in these high carbon steels. As and example, see p 623 and 625 of ref. [14.4] for data on T1.

(b) The austenitization temperature affects the secondary hardening peak. Higher temperatures put more alloying elements into the austenite and generally raise the secondary peak hardness. As an example see p. 625 of ref. [14.4] for T1 data.

2 Stabilization of austenite can be a significant factor in tool steels.

(a) Many of the tool steels need to be cold quenched to remove retained austenite. As explained on p. 138 it is important to avoid holding the sample at room temperature between the quench to room temperature and immersion into the cold quench medium. Data on the effect of the room temperature holding time versus % retained austenite may be found for some of the tool steels in ref. [14.4], for example p 625 presents data for T1.

(b) The higher alloyed tool steels are air hardening. However, austenite stabilization effects produce more retained austenite for air quenched steels than oil quenched steels, just as was described for stainless steels on p. 138. Hence, the air hardened steels end up with slightly lower hardness than oil hardened steels, as is illustrated for D2 by the data on p. 562 of ref. [14.4].

3 "Conditioning" of retained austenite As discussed on page 97, during stage 2 of the tempering process the retained austenite decomposes into a mixture of carbides and ferrite (this mixture is often called bainite, although it forms on up-quenching austenite, rather than the usual case of bainite formation on down-quenching austenite). In the highly alloyed tool steels it is found that this stage 2 decomposition of retained austenite into bainite is not complete and some or all of the remaining retained austenite is said to be "conditioned" during the first temper. And, furthermore, during the cooling from the tempering temperature the conditioned retained austenite will transform to fresh martensite, which, not being tempered, is brittle. (For reasons too complex to go into here, the conditioning has raised the M_s of the conditioned austenite which then allows martensite formation on cooling.) Hence, in many tool steels it is often recommended that the steels be given a double or even a triple temper to be sure all fresh martensite has been tempered. The number of temper treatments recommended for various tool steels in ref. [14.4] are given in the right most column of Table 14.4.

4 The high austenitizing temperatures, particularly for the high speed tool steels, requires careful atmosphere control to avoid surface degradation effects. Salt bath heating is an effective method of minimizing scaling and/or surface decarburization. An advantage of the T steels over the M steels is that they are less sensitive to decarburization. In controlled atmosphere furnaces the M steels are found to decarburize even in a reducing CO atmosphere. For example in an 11% CO atmosphere at 2200 ^{o}F (1204 ^{o}C) the M steels decarburize at the surface significantly in just 5 minutes, whereas the T steels actually carburize at short times and then decarburize at longer times [14.3, p 713]. Interestingly, as-quenched surface hardness can be decreased by both surface decarburization and carburization. In the latter case the reduced hardness results from increased amounts of retained austenite, while in the former it results from a reduction of the hardness of the martensite.

5 The recommended heat treatment practice for tool steels is much more complicated than that for the plain carbon and low alloy steels. As evident from the above discussion, one must control austenitization atmospheres, temperature and times carefully to achieve proper amounts of %C and % alloying element in the austenite; and control of retained austenite often requires the use of cold temperature quenching, control of room temperature hold time in this process and the use of double or even triple tempering. In addition, it is often important for tool steel dies that any shape or size changes during the heat treat process be minimized. Also, since these steels are often fairly brittle it is important to avoid any crack formation induced by thermal stresses on heat treating. Therefore it is usually recommended that the steels be given a stress relief anneal after rough machining to shape and also a preheat treatment after finishing machining. In the preheat treatment the tool is held just below the A_1 temperature to minimize temperature gradients and thereby reduce any distortion or possibility of crack formation when the austenite begins to form above the A_1 temperature. Table 14.5 illustrates the complexity of recommended heat treat practice for most of the steels discussed above taken mainly from ref. [14.6]. Reference [14.4] presents similar recommended practice with more details given for each of the various steps.

Table 14 5 Recommended full heat treat practice [14.4 &14.6].

Steel	Stress relief after rough mach.	Preheat after finish mach.	Austenitization. Temp.	Quench* media	Low temp. stabilize	Temper***
W-1	620 °C	565-650 °C	760-840 °C	W or B	not required	To target R_c
S-2	650°C	650 °C	840-900 °C	W or B	-75 to -196 °C	"
O-2	"	650 °C	790-815 °C	O	-75 to -196**	"
A2	675°C	600-700 °C	925-980 °C	A	"	"
D2	"	"	980-1065 °C	"	"	"
H13	650°C	815 °C	995-1040 °C	"	"	D or T (500 °C)
M2	750°C	780-840 °C	1100-1230 °C	A or O	"	D or T (540 °C)
T1	700-750°C	815-870 °C	1260-1300 °C	"	"	D or T (570 °C)

* W = water, B = brine, A = air, O = oil.
** recommend prior 150 °C stress relief treatment.
*** D = double temper, T = triple temper.

References

14.1 O.M. Becker, High Speed Steels, McGraw Hill, N.Y. (1910).
14.2 A.S. Townsend, Alloy tool steels and the development of high speed steels, Trans. Amer. Society Steel Treaters, vol. 21, p769 (1933) [Note: This journal became: Transactions of Amer. Soc. for Metals.]
14.3. G.A. Roberts and R.A. Cary, Tool Steels, Fourth Edition, American Society for Metals (1980).
14.4. Heat Treater's Guide, Practices and Procedures for Irons and Steels, ASM International (1995).
14.5. F. Kayser and M. Cohen, Carbides in high speed steels-their nature and quantity, Metals Progress, vol. 61, p79, [June 1952). See also: ref. 14.3, p. 744.
14.6 R. Wilson, Metallurgy and Heat Treatment of Tool Steels, McGraw-Hill, New York, (1975).

Summary of major ideas of Chapter 14

1 Tool steels are the modern version of the "tool kits" employed by our ancient ancestors to shape the relatively soft materials like wood and animal skins utilized in their daily lives. Modern tool steels are used to shape, cut, punch, deform, etc. the much stronger and varied materials used by modern society. They are specialty steels, produced in relatively low volumes that have various desirable combinations of a triad of desirable properties in tools: wear resistance, toughness and hot hardness. Table 14.1 and 14.2 list a selection of common AISI tool steels along with the relative values of the triad of properties, and the accompanying text presents a brief discussion of the various tool steel types.

2 The wear resistance generally desired in tool steels results from the various alloy carbides formed in these steels. The key alloying elements used in tool steels, Cr, Mo, W and V form the various carbides shown in Table 14.3. This table presents the relative hardness of the carbides. As shown in Fig. 14.2, most of the tool steels produce a strong secondary hardening peak during tempering that plays a key role at enhancing hot hardness. To successfully produce this peak it is necessary to austenitize the tool steels at temperatures high enough to dissolve the carbide present in the steel as supplied from the mill. Figure 14.1 shows that steels high in Mo, W and V must be austenitized hotter than steels high in Cr and Table 14.4 presents recommended austenitizing temperatures which reflect this fact.

3 Heat treatment of tool steels is considerably more complicated than heat treatment of plain carbon and low alloy steels. As illustrated in Table 14.5 possible additional steps involve (1) an initial stress relief after rough machining, (2) a preheat just below the A_1 temperature, (3) cold quenching to avoid retained austenite and (4) double or triple tempering to avoid retained austenite. The reasons for the need of these various additional steps is presented on pages 155-157.

Chapter 15 Solidification

Virtually all steel products have been solidified from the liquid in the first stages of their production. (Even objects made from powders fit this category because most all steel powder is produced from molten metal.) Consequently, the solidification process has an influence on the properties of all steel products. This process exerts a strong influence on three important factors of cast metals:

1) Microsegregation of alloying elements, carbides and inclusions.
2) Microstructure (grain size, grain shape, and phases present)
3) The level of porosity in the cast metal.

It is common for casting processes to produce severe microsegregation, large grains and significant porosity, all of which lead to reduction in mechanical properties. All three of these factors are improved by severe mechanical deformation, such as hot forging or rolling, so that wrought steels generally have improved mechanical properties over cast steels. But even in wrought steel, mechanical properties can be influenced by the original casting operation, so that it is helpful to have an understanding of the solidification process even if you work with wrought steel and not steel castings.

As a material solidifies from the liquid there is a solid front that advances into the liquid. It turns out that the shape of this solid front, sometimes called the solid/liquid interface, plays a strong role in controlling the 3 factors mentioned above. Consider the solidification process occurring on the left of Fig. 15.1, which shows a crucible that has been filled with liquid steel and then allowed to cool until the solid/liquid interface has advanced inward about a third of the way to the center. Because heat is being removed from the bottom as well as the vertical walls, the solid grows upward about an equal distance from the bottom as it solidifies inwards from the mold walls. Because the solid is more dense than the liquid, a volume contraction occurs upon solidification causing the height of the solid to decrease as it freezes toward the crucible center. The inset on the right shows a section from the left side of the crucible where the solid/liquid interface is advancing to your right during solidification. If you have not thought about this process before, when asked what you think the shape of the solid/liquid interface might look like a reasonable guess is that it would be planar, as shown by the inset labeled A. For very pure metals this is generally correct, but not for steels and virtually all metal alloys. The interface actually consists of arrays of small branched structures that look like pine trees all growing into the liquid with branches coming off at right angles as shown in the inset labeled B. Each little tree-like structure is called a dendrite (which is the Greek word for tree). If you could put your eye at the location shown, and if the liquid metal were transparent, you would see all the little trees growing toward you as shown at C. The view would be similar to the view you would see when flying over a pine plantation and looking down on the tree tops. A major difference is that you would need a magnifying glass to see any individual dendrite because they are very small in size.

The spacing of the dendrites depends on how fast the solid liquid interface is moving, which, in turn, depends on how fast heat is being withdrawn from the liquid metal. Figure 15.2 shows the spacing of the main stalks of the dendrites as d. In a large steel casting heat removal is slow and dendrite spacing, d, can approach 1 mm (1000

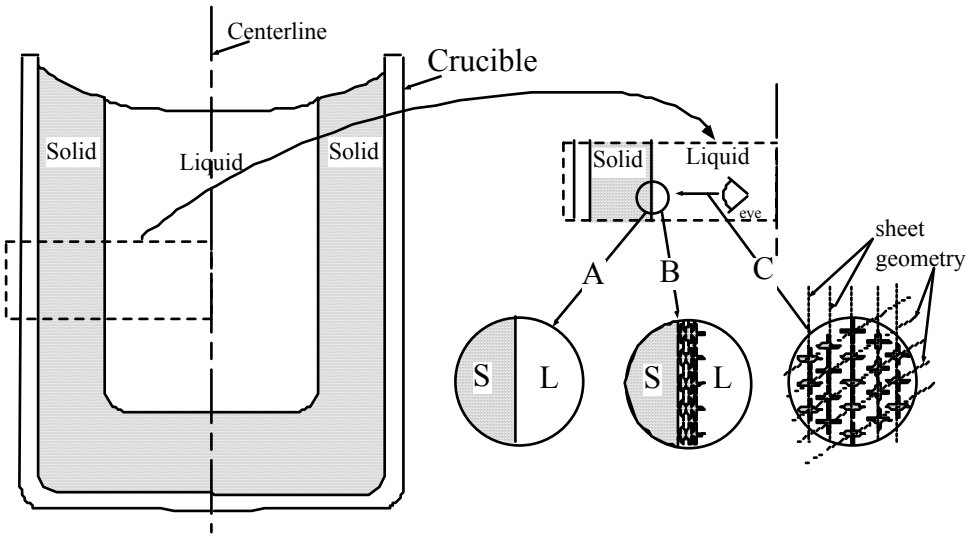

Figure 15.1 Nature of the solid front during solidification of steels.

microns (μm)). For continuous cast steel where heat is removed at high rates the spacing is on the order of 300 μm, and in weld metal where the small liquid pool allows even faster cooling rates the spacings can be as small as 100 μm. The diameters of the dendrite main stalks (called primary dendrite arms) are smaller than their spacing, d, by roughly 10 times. The diameter of a human hair is around 0.002 inches or 50 μm, so you can see that most dendrites have main stalk diameters of sizes comparable or smaller than your hair. These small dendrites play a strong role in controlling factors 1 and 3 listed above, but only a weak role in factor 2, as will now be discussed.

Factor 1 - Microsegregation Liquid iron can dissolve more impurity atoms than solid iron for virtually all types of impurity atoms. Sulfur is an outstanding example. Whereas liquid iron can dissolve 31 weight % S at 1000 ^{o}C, solid iron can dissolve only 0.01% S at this temperature. This means that all of the S impurities in a steel will be dissolved in the liquid prior to solidification, but basically none of the S will be dissolved in the iron after it freezes. The S ends up in the solid in the form of small particles, called inclusions. The sulfide inclusions are a chemical compound of iron sulfide having the formula, (MnFe)S. (The Mn present in all steels is contained in these sulfides in amounts that vary with the overall level of Mn in the steel and in how fast the steel was cooled.) After

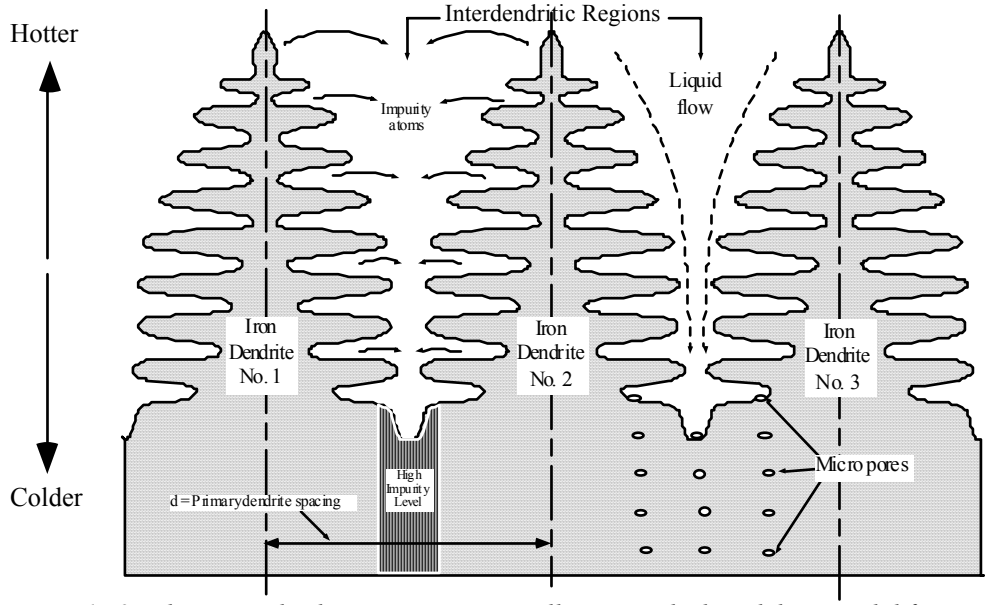

Figure 15.2 Three iron dendrites growing vertically up into the liquid during solidification.

solidification the sulfide particles are distributed non-uniformly throughout the solid in what is called a microsegregated distribution. The dendrites cause the microsegregation as will now be explained by examining dendrites No. 1 and No. 2 in Fig. 15.2. Because the solid dendrites can hold virtually no S atoms, these atoms must be ejected from the growing dendrite arms into the liquid region between the two dendrites as is shown by the arrows on the diagram. The composition of S in the interdendritic liquid will rise as one moves toward the base of the dendrites at the bottom of the picture, and eventually it becomes high enough that particles of the sulfide compound form. Depending on the chemical composition of the steel, the particles form from the liquid as either solid particles or as immiscible liquid droplets which freeze to solid at temperatures lower than that at the base of the dendrite arrays. Hence all of the sulfide particles end up lying in the interdendritic regions, which are shown as the area labeled "high impurity level" on Fig. 15.2. The name microsegregation is used because the segregation spacing is of a microscopic size as dictated by the micron level spacing, d, of the dendrites.

The non-iron atoms deliberately added to the iron of steels, such as Mn, C and alloying elements become microsegregated between the dendrites in the as-solidified steel. This phenomena can lead to formation of particles of compounds in the austenite on cool-down that you would not expect. To understand how this occurs consider the Fe-1.8%C alloy whose composition is shown on the full Fe-C phase diagram in Fig. 15.3. The diagram shows that when this alloy is cooled to 1100 °C it should consist of single phase austenite (no particles present) having the composition of 1.8%C. Consider, however, the effects of the microsegregation of C between the dendrites. The phase diagram of Fig. 15.3 tells us that this alloy will begin to form solid when the liquid temperature falls to 1400 °C. This means that the tips of the primary dendrites on Fig. 15.2, which are the first formed solid, will be positioned in the liquid where the temperature is close to 1400 °C. The phase diagram also tells us that the composition of the first formed solid will only be around 0.7 %C. Hence, as the solid tips form, the %C must drop from the 1.8%C

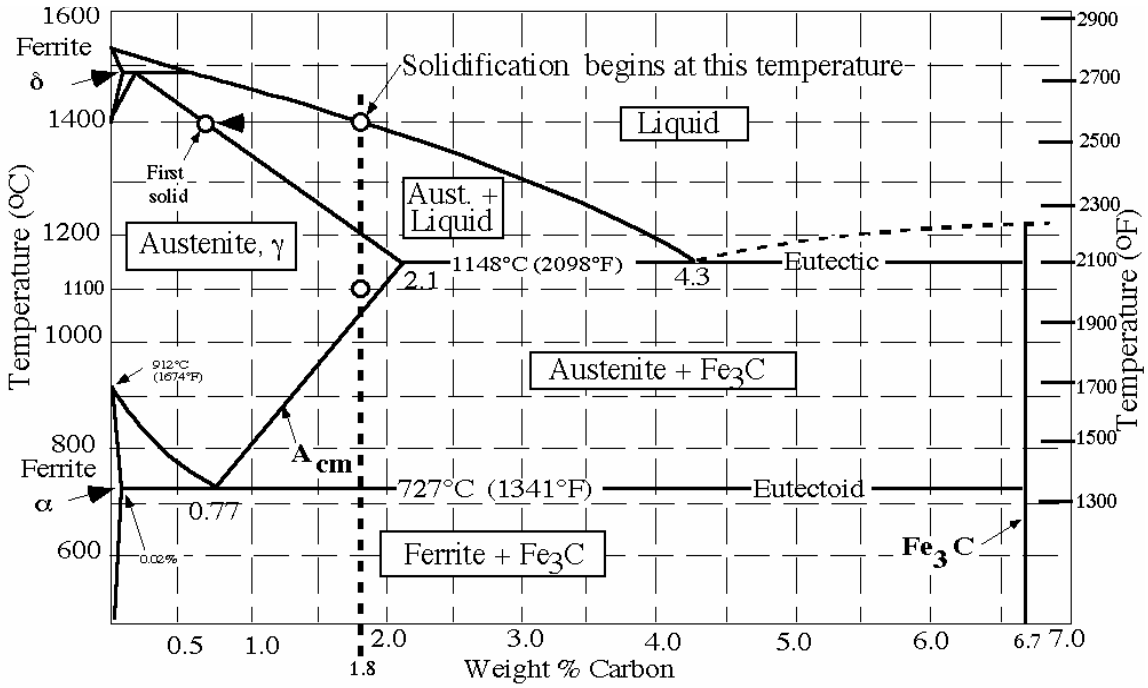

Figure 15.3 Composition of a Fe-1.8%C alloy on the Fe-C phase diagram.

in the liquid down to 0.7%C in the solid and the difference of 1.1%C must be ejected into the liquid in the direction of the arrows shown between the tips of dendrites No. 1 and No. 2 on Fig. 15.2. As you move toward the base of the dendrites on Fig. 15.2 the %C in the interdendritic regions must increase. Also, the temperature must decrease. When the liquid temperature has decreased to 1148 ^{o}C, Fig. 15.3 shows that %C in the interdendritic liquid will reach the eutectic composition of 4.3 % and all of the remaining liquid will solidify at 1148^{o}C as a eutectic mixture of austenite containing cementite particles. Now consider two different cases of what may happen as the temperature drops further from 1148 to the 1100^{o}C temperature discussed above. The core regions of the dendrites initially form with %C values around 0.7%, well below 1.8 %. Hence it is possible that the C in the cementite particles, Fe_3C, will diffuse out into these cores and the cementite particles will dissolve. In this first case you would end up with single phase austenite at 1100 ^{o}C. And if the C diffusion coefficient were high enough and you cooled slow enough, carbon would migrate by diffusion into the core regions of the austenite dendrites sufficiently to produce a homogeneous austenite having %C = 1. 8 throughout at 1100 ^{o}C, as predicted by the equilibrium phase diagram of Fig. 15.3. This case is called **equilibrium freezing**. In the second case, the diffusion rate is not adequate to dissolve all of the cementite particles formed in the solid eutectic at 1148^{o}C as the temperature falls from 1148 to 1100 ^{o}C. So, in case 2 you end up with a mixture of austenite and Fe_3C particles at 1100 ^{o}C. Because the equilibrium phase diagram predicts that a 1.8%C alloy should contain no cementite particles at 1100 ^{o}C, this case is called **non-equilibrium freezing.** Case 2 shows how you can end up with particles between the dendrites after freezing, even though the phase diagram predicts a single phase (particle free) austenite should form. In pure Fe-C alloys the C diffusion coefficient of the tiny C atoms is so large that equilibrium freezing is usually found in cast alloys. Steels, however, contain Mn and alloying elements. The Mn and some of the alloying elements, such as Mo and Cr are carbide formers and hence the cementite carbide particles now become $(FeX)_3C$, where X is a combination of Mn, Mo and Cr. To dissolve these carbide particles you must diffuse the X element atoms as well as the C atoms. As shown in the diffusion chapter (see table on page 64) these elements diffuse thousands of times slower than C and it is found that non-equilibrium freezing generally occurs in low alloy steels as well as in tool and stainless steels.

In working with alloy steels, tool steels and stainless steels you will find that people often talk about **primary carbides** and **secondary carbides**. Consider the non-equilibrium freezing of the 1.8 %C alloy just discussed. The cementite carbides formed out of the liquid between the dendrites are the primary carbides. After the alloy temperature falls below the A_{cm} temperature shown on Fig. 15.3, we expect additional cementite (M_3C in an alloy steel) to form and this carbide is called secondary carbide. There is often a difference in the distribution of these carbides as the primary carbides are distributed along the interdendritic regions and the secondary carbides tend to form along the austenite grain boundaries. Notice that the primary carbides form out of the liquid and the secondary carbides form out of the solid. There is usually a difference in the size of the primary and secondary carbides. In tool steels and stainless steels the primary carbides that form from the liquid are generally much larger than the secondary carbides that form in the solid. The large primary carbides formed in tool steels and stainless

steels can lead to extreme brittleness of as-solidified steels because the carbides are brittle and they form an interconnected network threading through the dendrite arrays in which they formed. For this reason it is often necessary to hot forge many tool and stainless steels to break up the network carbides and achieve adequate toughness for practical uses. By employing rapid solidification one can reduce the size of the primary carbides and refine the networks. This is the reason tool steels are sometimes made from powders. Whereas there is no way to rapidly solidify a big ingot of steel, powders formed from small liquid droplets freeze very rapidly, thus reducing the dendrite spacing. After compaction and high temperature sintering one ends up with much finer primary carbides.

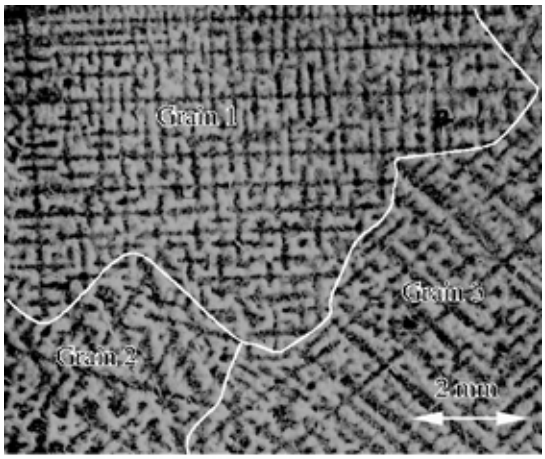

Figure 15.4 Austenite dendrites in a 1.6% C as-cast steel revealed with Stead's etch.

The phenomenon of banding in steels discussed on pages 23 and 40 (Figs 4.9, 5.5 and 5.6) results from microsegregation of the alloying elements in steel. The mechanism that produces this dramatic effect on microstructure is a bit complicated to understand because you first must have a grasp of the concepts of hardenability discussed in Chapter 8. Consider a Mn steel such as AISI 1340 (Table 6.2, page 50) which is often used for train track rails. After solidification, the Mn is microsegregated into the interdendritic regions which, as shown at position C in Fig. 15.1, tends to be aligned into a sheet geometry. The alignment shown at C would occur only within a single grain, with neighboring grains having interdendritic sheets aligned at various angles to that shown in C. Figure 15.4 illustrates the variation of the dendrite orientation between neighboring grains in an as-cast steel. (As explained below, a special etchant causes original austenite regions to appear black.) It is found that forging or rolling causes the sheet geometry of all the various grains to become aligned in the plane of the metal flow produced during the deformation. Hence, after adequate forging or rolling flow to form a plate geometry, you end up with microsegregated sheets of high and low Mn content aligned in the plane of the plate. The high Mn sheets are located at the positions of the prior interdendritic regions and the low Mn sheets at the locations of the austenite dendrite regions. The banded microstructure forms as a result of the effect of Mn on hardenability. In the high Mn bands the ferrite start-curve of the IT diagram is pushed to longer times than in the low Mn band regions. Hence, on adequately slow cooling from the austenite temperature region, the ferrite nucleates first in the low Mn band regions. Remember, ferrite is essentially pure iron. Therefore as the ferrite grows out from the low Mn band regions it ejects carbon into the high Mn band regions. Eventually the %C in those regions becomes high enough that pearlite forms there and you end up with bands of ferrite interspersed with bands of pearlite. This structure is called ferrite/pearlite banding. It is also possible for the microsegregation to form several other types of less common banding such as: ferrite/bainite, ferrite/martensite, pearlite/bainite and bainite/martensite banding.

Figure 15.4 presents an illustration of the microsegregation caused by dendritic solidification. The steel had a phosphorous, P, impurity level of 0.07% P. Similar to the

elements discussed above, the P atoms segregate into the interdendritic liquid between the dendrites during solidification. Early in the 20th century Stead developed a special chemical etch that is sensitive to variation in P levels even though the steels contain only tiny amounts of P [15.1, p. 5]. When a polished steel surface is etched with Stead's etch, regions containing higher concentrations of P are etched white relative to the low P regions. Because most of the P has been microsegregated to the interdendritic regions, Steads etch makes the interdendritic regions white and the dendrite stalks dark as shown in Fig. 15.4.

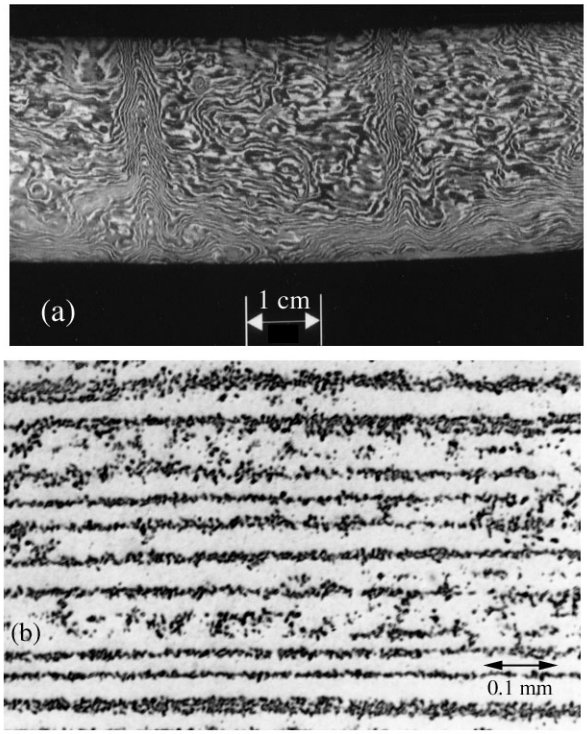

Figure 15.5 (a) Surface pattern of a genuine Damascus blade-17th century blade (Moser blade No. 9). (b) Longitudinal section through blade. Etched to make cementite particles dark and the pearlite matrix white.

The common Damascus steel knives of modern bladesmiths are made using the technique of pattern welding. In this method alternate sheets of 2 different types of steel are forge welded together in bundles which are folded back upon themselves several times to produce blades having around 200 to 400 layers of the alternating sheets. The surface patterns on these blades are the result of the fact that one of the layers will etch darker than the other, thereby revealing the pattern in which the layers intersect the blade surface. Pattern welded steel originated long ago, around 200 AD. The name Damascus steel originates from a type of steel quite different from these pattern welded steels, that was developed around the same time period. These blades will be called genuine Damascus blades simply because the name originated from them. Genuine Damascus blades are named after the city of Damascus in modern day Syria because these Damascus swords were first encountered by Western Europeans in the Crusades and it was thought that they were produced in Damascus.

Most all of the Damascus steel swords found in the arms and armor sections of large modern museums are of the genuine Damascus type. Figure 15.5(a) presents the surface pattern of a museum quality Damascus sword. Genuine Damascus steels are made from small ingots of fairly high purity iron containing around 1.5 to 1.7%C. The original small steel ingots were manufactured on a large scale in India and this steel has come to be called Wootz steel in the English speaking world. The method of making these ingots and the mechanism causing the surface pattern upon forging were not know until recent times [15.2]. The surface pattern on genuine Damascus blades results from a type of carbide banding as is illustrated by the longitudinal section of the sword of Fig. 15.5(a) shown in Fig. 15.5(b). The micrograph is shown at a magnification of 90x and the dark bands consist of arrays of Fe_3C particles that have clustered together into bands during the forging process. Hence, the surface pattern results from a type of carbide banding and recent experiments [15.3] show that the banding is caused by the microsegregation of low levels of carbide forming elements like V and Mn that are present in the original wootz ingots. During the repeated heating and cooling cycles of

the forging process the carbides present in the original casting are continually being partially dissolved and reformed. The microsegregated V and/or Mn atoms cause the reforming carbides to slowly become positioned primarily at their locations on the interdendritic planes. Just as with pearlite/ferrite banding discussed above, the interdendritic planes are rotated into the forging plane during the forging deformation. As seen in Fig. 15.5(b) the alignment of the carbide bands in the final blade is so good that it looks like the carbides might have been aligned by mechanical placement, as is the case for the bands of pattern welded Damascus blades.

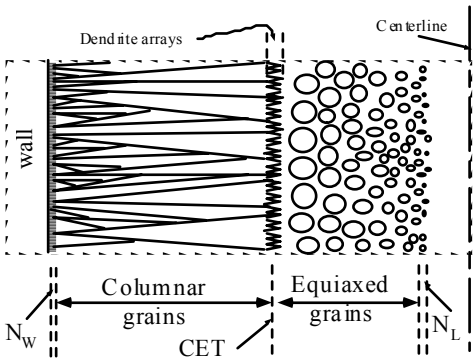

Figure 15.6 Distribution of grains developed in box region shown on Fig. 15.2

Factor 2- Grain Size and Shape Here we are interested mainly in understanding the grain shapes that are produced by the solidification process. After the liquid metal is poured into the crucible shown in Fig. 15.1 it cools most rapidly at the walls of the crucible and it is on the walls that the first solid forms out of the liquid. It is common terminology to say that the solid "nucleates" on the walls. Little particles of solid may nucleate at thousands of sites per square inch of wall and each of these little particles can grow out into the liquid and become individual grains. The growth front of each little particle contains arrays of aligned dendrites, as at the bottom of Fig. 15.2, and those particles that have their dendrite stalks pointed to the right will grow toward the crucible centerline the fastest and crowd out their neighbors. Consequently, right near the wall, in the region labeled N_w on Fig. 15.6, there is a growth competition and the winning grains end up growing into long columnar shapes extending inward from the wall. Meanwhile, the liquid ahead of the advancing columnar grains is cooling and it is possible that small particles of solid can nucleate within this cooling liquid, particularly if small foreign particles are present in this liquid. They can be produced there either by mechanical addition or by precipitation from the liquid of foreign particles, like sulfide, or oxide or carbide or boride compounds. (Also, in some cases, solid particles of the alloy itself are produced there by liquid convection currents that break off side arms of the dendrites on the columnar growth front and carry them out into the liquid. When this occurs the dendrites play an important role in controlling factor 2, grain size and shape, but otherwise they do not.) Figure 15.6 shows small particles of the solid alloy nucleating in the liquid in the region labeled N_L. These particles can grow out in all directions and each particle gives rise to a grain called an "equiaxed grain" because it has roughly equal axial lengths in all directions. When the long columnar grains hit the equiaxed grains formed in the liquid the columnar grains stop growing and the remaining liquid solidifies as equiaxed grains. Hence, it is common to find columnar grains near the crucible wall and equiaxed grains in the center and the transition is often called the CET, columnar to equiaxed transition, as shown on Fig. 15.6.

In metal alloys in which the as-solidified grain structure is directly inherited by the room temperature casting, the presence of the long columnar grains will generally lead to low toughness. As previously discussed, fine grain size is desired to enhance toughness. Depending on the melting point of an alloy, its thermal conductivity and how fast the crucible wall conducts heat, the radial position of the CET in the crucible will change. If the CET does not occur until near the center of the crucible the metal is said to

be a skin forming alloy for the obvious reason that it freezes by forming a solid skin that progressively thickens. If the CET occurs at or very close to the mold wall the metal is said to be a mushy forming alloy because the liquid becomes a mush containing a mixture of small solid particles + liquid which completes solidification by growth of the arrays of small particles. This distinction is important in designing molds in the foundry industry to produce castings with minimized porosity, and the details are too complex to pursue here. In foundry molds steels are skin forming alloys while cast irons, copper alloys and aluminum alloys are mushy forming alloys. But in making the ingots used for production of wrought alloys most all alloys become more skin forming due to higher solidification rates with higher conductivity ingot and continuous casting molds. Because the columnar grains are broken up on hot forging or rolling of these ingots and slabs their inherent brittle nature is not a problem. However, columnar grains are a common feature of weld metal, brazing metal and solder metal joints. So, in many brazing alloys and aluminum alloys, tricks are employed to produce equiaxed grains. These tricks are aimed at avoiding columnar grains by additives that produce nucleating particles in the molten bead to enhance equiaxed grain formation.

For steels the formation of columnar grains is not as much of a problem because the solid phase that forms from the dendrites is not directly inherited in the room temperature product. Such is not the case in most copper and aluminum alloys. Figure 15.3 illustrates that for steels of composition greater than 0.5 %C the dendritic solid will be the face centered cubic austenite, which becomes replaced by a mixture of body centered cubic ferrite and Fe_3C, usually in the form of ferrite + pearlite, on cooling to room temperatures. Hence, the long columnar austenite grains formed from the liquid will be subdivided into finer ferrite + pearlite grains at room temperature. In steels with %C less than 0.5 %C the columnar grains will be the high temperature body centered cubic form of ferrite, called δ (delta) ferrite, which is twice replaced on cooling. As Figure 15.3 shows, on cooling to room temperature δ ferrite will first change to austenite and then to ferrite or a mixture of ferrite + Fe_3C at room temperature. Nevertheless, control of the CET in the continuous casting of steel is an important consideration for plant managers. By preventing the CET from getting too close to the center of the continuous cast billet, both porosity and segregation at the center of the billet are reduced significantly.

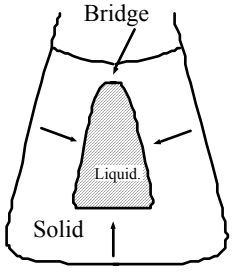

Figure 15.7 Trapped liquid forms cavity porosity.

Factor 3 - Porosity Porosity is produced by the solidification process because when a given volume of liquid metal solidifies, the solid formed from it will occupy a smaller volume. The volume reduction is commonly called the "shrinkage" volume. If this shrinkage volume is filled up by more of the liquid metal there is no porosity. But if it is filled by air or some other gas it often leads to porosity. The reduction of height in the metal shell formed at the crucible wall of Figure 15.1 is due to shrinkage volume. When the final liquid freezes along the centerline of the ingot one would expect to observe a shrinkage pipe going down the centerline, as is familiar to anyone who has cast little lead soldiers. Suppose the walls of the crucible were slanted as shown in Fig. 15.7. Now as the metal advances in from the walls it will form a bridge at the top center before all of the liquid has frozen and trap

a large pocket of metal in the ingot center. After this trapped liquid freezes one ends up with a large internal pore. This type of pore is referred to as "cavity" porosity. It is a problem in the foundry industry where special feeders (or risers) are designed into the molds to ensure that the final liquid to freeze is never inside the surface of the part being cast.

There is a second type of porosity produced by the solidification process that is called "microporosity". This microporosity results because of the dendritic solidification front and its mechanism of formation is a bit complicated. Consider the dendrites, No.2 and No. 3 of Fig. 15.2. As shown by the two downward slanted dashed arrows between these dendrites, there must be a flow of the liquid metal to fill in the shrinkage volume generated as the dendrites solidify. In order to produce this liquid flow the pressure in the liquid at the dendrite tips must be higher than at the dendrite base. Because the pressure at the tips will be close to room pressure, this means that the liquid at the dendrite base must be below room pressure. Therefore, the interdendritic liquid at the base of the dendrites is under a vacuum. To better understand what this implies consider the following experiment. A small glass beaker is filled with a low melting metal like lead or tin and heated to cause the metal to melt. Now the top of the beaker is attached to a vacuum pump which pulls the air out of the beaker. This reduces the pressure above the liquid metal creating a vacuum there. What one observes next is that small gas bubbles begin to form on the walls of the glass container. The gas in these bubbles consists of gaseous atoms, like oxygen, O_2, nitrogen, N_2, or maybe carbon monoxide, CO, that had been dissolved in the liquid metal. Therefore, because the interdendritic liquid at the base of the dendrites is under a vacuum, it is possible that small gas bubble will form there, particularly if the dendrites are long and if the metal contains significant amounts of dissolved gaseous elements. Because the gas bubbles produce quite small pores this form of porosity is called microporosity. It is too small to see with your eye on the polished surface of a metal. Typical diameters are around 5 to 10 microns (μm) in columnar grains and around 25 μm in equiaxed grains and are easily seen in an optical microscope.

The porosity in as-solidified metals can be removed by mechanical deformation as long as the pore walls have not been oxidized. In general micro pores will not be oxidized and cavity pores will only be oxidized if they have an open path to the atmosphere. For example, the cavity formed in Fig. 15.7 will not be exposed to air, unless the ingot cracks, whereas the pipe formed at the center of an unbridged ingot will oxidize. It is found that most porosity formed by the solidification process can be removed by deformation sufficient to cause the pore walls to close on themselves. They simply weld together under the deformation forces.

Steel is a sort of special case when it comes to porosity formation during solidification. Because the molten metal always contains some level of both O and C it is common to form carbon monoxide, CO, gas as the molten metal cools. This is an age old problem that steel producers must deal with. The evolution of CO gas during steel solidification is generally controlled by controlling the level of O dissolved in the liquid steel. Steel producers control the level by adding elements to the liquid steel that selectively form oxides and reduce the dissolved O level of the liquid steel. The resulting

oxide particles end up as small inclusions that are relatively harmless. The common deoxidizers added are aluminum and silicon which produce the alumina (Al_2O_3) and silica (SiO_2) inclusions that collect in the interdendritic liquid of steels. For example, if suppliers refer to a steel as an AK steel they mean that aluminum was added to "kill" the steel. The added Al reduced the O level to the point that no CO bubbling occurred. It is common to have a certain level of microporosity in as-solidified steels which is not a problem as most all steels are used in the wrought form and this porosity has been closed up. One interesting result of the presence of this microporosity is that steel ingots can form with no apparent shrink cavity along their centerline. When the volume of the microporosity equals that of the shrinkage volume the solid solidifies with the same shape as the liquid. This occurs for the small wootz ingots used to make Damascus steel.

References

15.1 G.F. Vandervoort, Metallography, Principles and Practice, McGraw-Hill, New York, N.Y. (1984).
15.2 J.D. Verhoeven, The Mystery of Damascus Blades, Scientific American, vol. 284, 62-67 (2001).
15.3 J. D. Verhoeven, A.H. Pendray, and W.E. Dausch, The Key Role of Impurities in Ancient Damascus Steel Blades, Journal of Metals, vol. 50, 58-64 (Sept. 1998).
http://www.tms.org/pubs/journals/JOM/9809/Verhoeven-9809.html

Summary of major ideas of Chapter 15

1- In general as-cast metals have inferior strength and toughness properties compared to wrought metals, that is metals prepared by forging, rolling or other processes that deforms the as-cast structure.

2 There are 3 primary factors of the solidification process that contribute to this difference in mechanical properties:

1) Microsegregation of alloying elements, carbides and inclusions.
2) Microstructure (grain size, grain shape, and phases present)
3) The level of porosity in the cast metal.

3 As illustrated in Fig. 15.1 when steel solidifies inward from a container wall the advancing solid/liquid interface does not have a planar shape as show at location A, but consists of arrays of dendrites as shown at locations B and C and in blowup in Fig. 15.2. The tree-like dendrite structures have very small main trunk diameters, on the order of the diameter of your hair. These dendrite arrays produce factors 1 and 3 and can influence factor 2 of summary point 2.

4 Microsegregation results because solid steel cannot dissolve nearly as much of the impurity elements or alloying elements as can liquid steel. Hence, these elements tend to segregate into the liquid between the dendrites. Because the dendrites are spaced on the order of microns (fractions of a mm) the segregation is spaced on this small length, which requires a microscope to see, and hence is called microsegregation.

5 The microsegregation can cause several effects in steels, three of which follow.

1. As explained on pages 161-2, one would not expect primary carbides to from in steels with %C less than 2.1 %. Primary carbides are those carbides that form from the liquid, as opposed to carbides that form from austenite on cooling below the A_{cm} or A_1 temperatures. Microsegregation can cause primary carbides to form at compositions well below 2.1% C, particularly in alloy steels.

2. Microsegregation produces the banded structures common in slow cooled steels and illustrated on pages 23 and 40 in Figs. 4.9, 5.5 and 5.6. As explained on page 163, these structures form by a rather complicated mechanism involving the effect of the microsegregated alloy or impurity elements upon hardenability.
3. The attractive structure formed on the surface of genuine Damascus blades, as opposed to pattern welded Damascus blades, also results from a banding due to microsegregation, see page 164.

6 As shown on Fig. 15.6, grains that grow in from the wall have an elongated shape and are called columnar grains. It is also possible for grains of solid to nucleate in the liquid ahead of these columnar grains and these grains grow out with a spherical shape and are called equiaxed grains. Columnar grains are often present in weld and brazing metal and can be a problem there, as columnar grains reduce toughness. They are not as much of a problem in wrought metals because hot mechanical deformation will cause them to be replaced with new sets of smaller recrystallized grains, as explained on p. 70 In as-cast steels the problem is also reduced because on cooling the original austenite or ferrite dendrites are replaced by new ferrite grains due to the A_1 transformation in steels. Such is not the case in many aluminum and copper alloys, where similar type transformations do not occur on cooling.

7 As explained with Fig. 15.6, metal castings often display columnar grains growing in from the mold walls and roughly spherical shaped ("equiaxed") grains in the casting center. The transition point from columnar to equiaxed is called the CET. If this CET occurs near the casting centerline, the casting mode is called "skin forming" and the grains are columnar. If it occurs near the mold wall the casting mode is called "mushy forming" and the grains are equiaxed. For castings that must retain their as-cast grain structure, the mushy mode is preferred if toughness is important.

8 The solidification process gives rise to 2 kinds of porosity that results from the fact that the solid formed from a given volume of liquid will occupy a smaller volume.

1. Cavity porosity This type of porosity results if liquid becomes fully enclosed in a solid shell, often when the top of the liquid is bridged over by solid as shown in Fig. 15.7. Cavity porosity general has sizes of larger than a mm and can be avoided by proper casting design.
2. Microporosity This second type of porosity is characterized by sizes in the very small 10 to 25 μm diameter range. It is produced by problems in feeding the liquid metal into the tiny spaces between freezing dendrites as explained with Fig. 15.2 on page 167. The density of cavity porosity can be reduced by removing dissolved gas from the liquid metal or by casting under pressure. It is most prominent in mushy forming alloys. It can be so severe in some aluminum and bronze alloys that as-cast parts cannot easily be made vacuum tight.

Both types of porosity can be removed by hot deformation adequate to cause the walls of the pores to close in on themselves, provided the walls have not oxidized by exposure to air. The un-oxidized walls simply weld together in the same fashion that hot deformation welds together the alternating sheets in pattern welded Damascus blades.

Chapter 16 Cast Irons

Cast irons differ from high carbon steels in several aspects, two of which are:

1- They cannot be converted to 100% austenite during heat treatment.
2- The other phase present in the austenite is generally graphite as opposed to cementite, Fe_3C, in steels.

To understand point 1, consider again the solidification of a 1.8% Fe-C alloy as discussed with the aid of Fig. 15.3 in the previous chapter. It was explained that the interdendritic liquid will increase its %C all the way up to the eutectic value of 4.3%C at the base of the dendrites where the temperature drops to 1148 ^oC and the cementite carbide, Fe_3C, will form from the liquid as a eutectic mixture of austenite + Fe_3C•. But on cooling to 1100 ^oC this Fe_3C can dissolve into the austenite dendrites so that a single phase austenite may form at 1100 ^oC, as shown at the circle on Fig. 15.3. If, however, the %C in the original alloy is raised to values greater than 2.1% it is no longer possible to produce 100 % austenite on cooling. Notice that an alloy of 2.5% C, for example, upon cooling to 1100 ^oC (open circle on Fig. 16.1) must lie in the 2-phase region and consist of austenite + Fe_3C. As with cast irons, this alloy cannot be converted to 100 % austenite on heating up to its melting point, 1148 ^oC.

The second point says that graphite will form in most cast irons. Graphite is a crystalline form of pure carbon that is quite soft and very easily fractured. Its presence generally leads to a dramatic reduction in toughness in gray cast iron, but not in nodular cast iron as will be discussed below. As pointed out in the footnote on p. 96, the Fe-C phase diagram presented in Chapter 3, and as Fig. 15.3, is not really an equilibrium

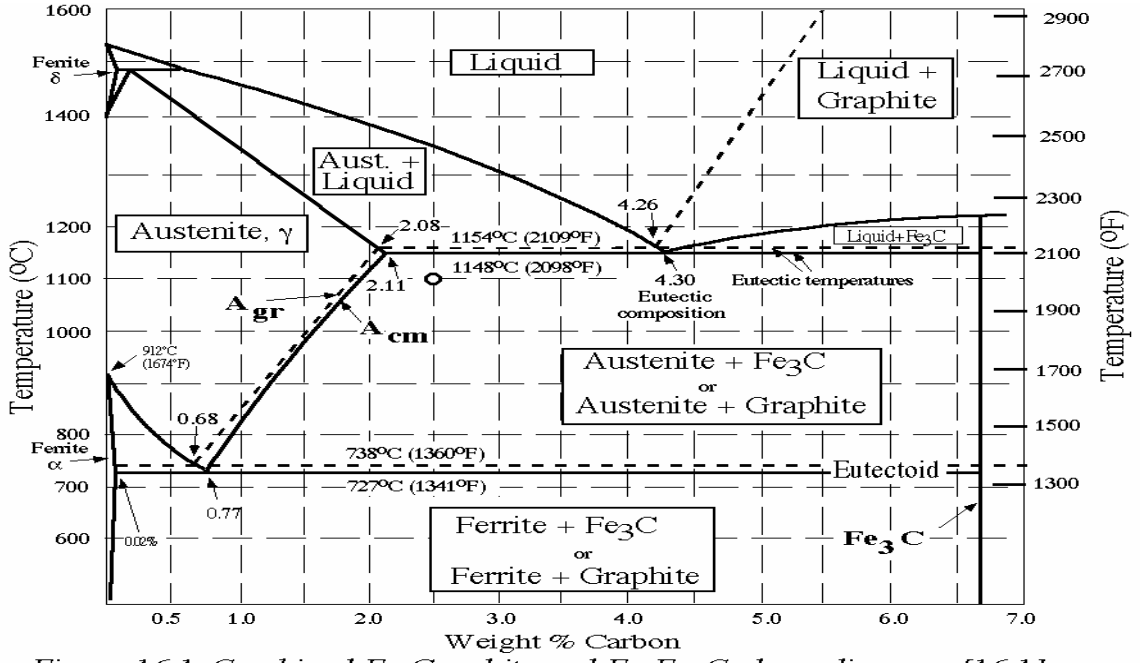

Figure 16.1 Combined Fe-Graphite and Fe-Fe_3C phase diagrams[16.1].

• When liquids of eutectic compositions freeze, the two solids at the ends of the horizontal eutectic line (aust. + Fe_3C here) usually grow side-by-side as a coupled pair from the liquid. If, however, first one solid forms then the other, it is called a "divorced" eutectic.

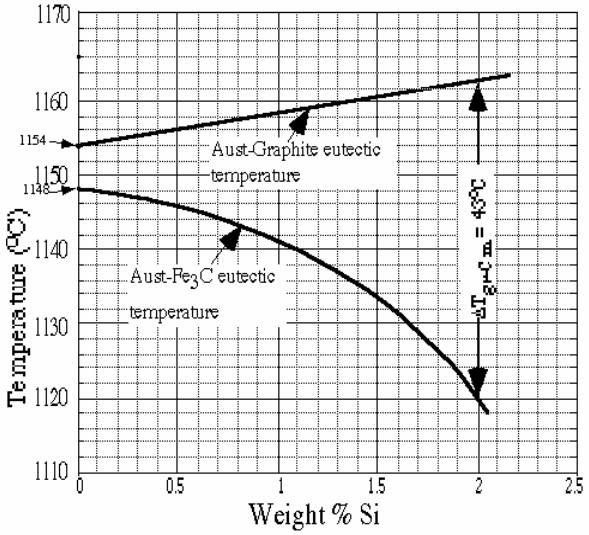

Figure 16.2 Variation of the graphite and Fe_3C eutectic temperatures as %Si increases from 0 to 2% [16.2].

diagram. Strictly speaking, the diagram of Fig. 15.3 should be called the Fe-Fe_3C diagram, because it predicts that at high %C values the Fe_3C compound will form in austenite. There is a second phase diagram called the Fe-Graphite diagram that is in fact the equilibrium phase diagram. Figure 16.1 shows the superposition of both of these diagrams, where the dashed lines give the changes present for the Fe-Graphite diagram. Notice that, whereas the Fe-Fe_3C eutectic occurs at 1148 ^oC, the Fe-Graphite eutectic occurs at 1154 ^oC, 6 degrees higher. This result shows you that it is possible to form graphite from Fe-C liquid at temperatures from 1054 to 1149 ^oC, but not Fe_3C, which means graphite is a more stable phase. Hence, in Fe-C alloys Fe_3C is actually a "metastable" phase. On cooling pure high carbon austenite the graphite phase can form at the higher temperatures (given by the A_{gr} line) than can the Fe_3C cementite phase, (compare to the A_{cm} line). You would therefore expect the more stable graphite to form as you cool a high carbon steel like 1095 or 52100 below the A_{gr} and A_{cm} lines. In steels, however, it is rare to from graphite, the metastable Fe_3C virtually always forms, particularly if carbide forming alloying elements like Cr are present. The motion of atoms at the atomic level to form graphite, either from the liquid or from austenite, is more difficult than that to form Fe_3C and, consequently the metastable Fe_3C forms first and is stable in most all industrial applications. It is possible for graphite to form in steels, in which case we say the steel has graphitized. Graphitization sometimes occurs when steel is held at high temperatures for months or years, as in steam lines. Hence graphite formation in steels is not of general practical importance, but it is in the production and heat treatment of cast irons.

Gray and White Cast Irons Cast irons are ternary alloys of Fe + C + Si. There are 4 main types of cast irons and their composition ranges are specified in Table 16.1 and Fig. 16.4. We will begin our discussion of these irons with gray and white cast iron. In cast irons a eutectic reaction occurs at the base of the austenite dendrites. In gray iron the graphite eutectic occurs and one ends up with the carbon mostly in the graphite form, while in the white irons the Fe_3C eutectic occurs and one ends up with C mostly in the form of Fe_3C, as shown in the final column of Table 16.1.

The addition of silicon is found to allow the formation of graphite more easily, particularly its formation from the liquid. Perhaps it might be more correct to say that the addition of Si makes it more difficult to form Fe_3C. To explain, consider the data of Fig. 16.2 which shows that Si additions lowers the temperature of the austenite-Fe_3C eutectic, while raising that of the austenite-graphite eutectic. To understand how this affects graphite formation in cast irons it is helpful to review the discussion of the meaning of the A_3 and A_{r3} temperatures on

Table 16.1 The 4 main cast iron types

Iron	%C	%Si	%Mn	%S	%P	Carbon form
Gray	2.5-4.0	1-3	0.4-1	0.05-0.25	0.05-1.0	Graphite
White	1.8-3.6	0.5-2	0.2-0.8	0.06-0.2	0.06-0.18	Fe_3C
Malleable	2-2.6	1.1-1.6	Same as white			Graphite
Ductile	3-4	1.8-2.8	0.2-0.9	0.03 max.	0.1 max.	Graphite

page 16. The A_3 line on the phase diagram gives the temperature at which we expect ferrite to precipitate (form) from austenite on cooling. In practice, however, we find that ferrite always forms at a lower temperature, which is termed the A_{r3} temperature. The data in Fig. 3.9 for the 1018 steel show that the ferrite did not form (precipitate) until the austenite had cooled 62 ^{o}C (112 ^{o}F) below the A_3 temperature. This temperature difference of 62 ^{o}C = (A_3 - A_{r3}) is often called the supercooling, because it tells us how far we must cool the austenite below the equilibrium transformation temperature given on the phase diagram by the A_3 line in order to start ferrite formation. If we cool faster the A_{r3} temperature goes down meaning that we need more supercooling to cause ferrite to form, and if we cool slower the opposite occurs.

Now consider the solidification of an Fe-3.5 %C alloy containing 2% Si. Figure 16.2 shows that there are 2 eutectic temperatures for this alloy, 1163 ^{o}C if graphite forms and 1120 ^{o}C if Fe_3C forms. As solidification proceeds the liquid in-between the dendrites continues to become enriched in C as its temperature drops until one of these two eutectics forms. There is a competition between which one will form first. The competition involves 3 important factors.

(1) Both eutectics require some supercooling below their eutectic temperatures shown on Fig. 16.2 before they will form from the interdendritic liquid.

(2) Just as was the case with supercooling required to form ferrite from austenite, the amount of supercooling required increases in both cases as the cooling rate increases.

(3) The amount of supercooling required to form the Fe_3C eutectic is smaller than that required to form the graphite eutectic.

Suppose the interdendritic liquid has cooled to 1130 ^{o}C and neither eutectic has formed (nucleated). Then the liquid will be supercooled by 33^{o}C (1163-1130) for formation of the graphite eutectic, and there will be no supercooling for the Fe_3C eutectic because the liquid temperature has not fallen below 1120^{o}C. Hence the Fe_3C eutectic cannot form. If the 33^{o}C supercooling is adequate to make the graphite eutectic form then one will end up with a gray cast iron.

Now suppose we cool faster, such that the amount of supercooling required to form the graphite eutectic increases to 53 ^{o}C. This means that the graphite eutectic will not form in the interdendritic liquid until it reaches 1110 ^{o}C (1163-53). But at 1110 ^{o}C the liquid is supercooled 10 ^{o}C below the Fe_3C eutectic (1120-1110). Because little supercooling (less than 10^{o}C) is needed to form the Fe_3C eutectic the cast iron will freeze as a white cast iron. This example illustrates why it is found that a given cast iron will form as a white iron on fast cooling and as a gray iron on slow cooling. It also illustrates why the addition of silicon favors formation of gray irons. The value of $\Delta T_{gr\text{-}Cm}$ on Fig. 16.2 drops from 43^{o}C with 2% Si to only 6 ^{o}C (1154-1148) with zero Si. Hence, without Si, it is much more likely that the interdendritic liquid will supercool below the white eutectic temperature before the graphite eutectic has formed. Foundryman do a simple experiment that dramatically demonstrates the effect of cooling rate on white formation. The molten metal is poured into a small sand mold that has a cast iron plate on its bottom. The set-up is called a chill-test casting because the plate on the bottom causes solidification to occur rapidly at the bottom where contact is made with the cast iron. As freezing proceeds upward the solidification rate decreases and one can observe a transition from a white iron to a gray iron by simply fracturing the sample along a vertical

plane. For reasons to be discussed later, the fracture surface of a white iron is white and that of a gray iron is gray. As illustrated in Fig. 16.3, the transition from white to gray is easily seen on the fracture surface and the height above the chill surface is called the chill depth. Note that in the transition zone there is a mixture of white + gray and such regions are called mottled. As the Si content of the cast iron increases the chill depth decreases. By adding certain chemical elements, called inoculants, to the liquid iron ladle just before pouring, the foundryman can also decrease the chill depth. The inoculants form small solid particles in the liquid which make it easier for the graphite eutectic to form, thereby reducing the supercooling needed for its formation and allowing it to form at faster cooling rates. The most effective inoculating element is Ca, and it is likely, but not certain, that its effectiveness results from formation of small sulfide particles by reaction with the S impurities present in the liquid cast iron.

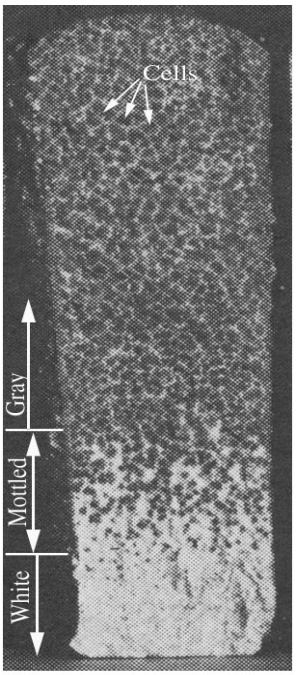

Figure 16.3 Chill casting.

Figure 16.4, presents a graphical plot of the %C + %Si listed in Table 16.1 for the various cast irons. People who make cast irons often refer to the carbon equivalent (the C.E.) of a specific iron. The carbon equivalent is defined as,

$$C.E. = \%C + 1/3\ \%Si.$$

Notice that the dashed line at the top of Fig. 16.4 shows the position of any cast iron whose C.E. = 4.3 %. Suppose such an iron had %Si = 0. It would, hence, consist of only Fe + C and you could plot its location on Fig. 16.1 at %C = 4.3 %. Figure 16.1 shows that this composition lies right at the eutectic composition of Fe-Fe_3C alloys and very close to the eutectic composition of Fe-graphite alloys. The dashed line on Fig. 16.4 gives a good approximation of how these eutectic compositions change as Si is added to Fe-C alloys. Generally, if a cast iron has a composition close to the eutectic the fraction of austenite dendrites will become very small. This means that as the C.E. of a cast iron drops more below the 4.3 value, it will contain a larger volume fraction of solid forming from the liquid as austenite dendrites. Similarly, as the C.E. approaches 4.3 it will contain a larger fraction solid forming from the liquid as the eutectic mixture of either aust. + graphite in gray irons, or aust. + Fe_3C in white irons.

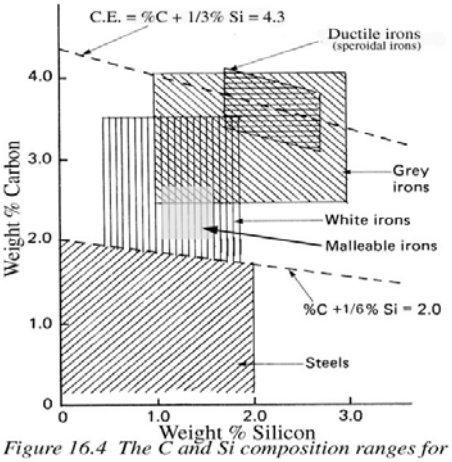

Figure 16.4 The C and Si composition ranges for various cast irons and for Si containing steels.

We will now discuss the geometrical shapes of the eutectic solids which form in gray and white cast irons. The top row of Table 16.2 presents a simple schematic summary in the left 2 columns showing how the microstructure develops during solidification of gray cast irons. The austenite-graphite eutectic solid nucleates (forms) at various locations within the interdendritic liquid. It then grows outward with an overall spherical shape. As shown in the top left column, the spheres grow around and encase the austenite dendrites. They generally grow to sizes larger than the dendrite spacing. Notice that in the mottled region on Fig. 16.3 you can see many of these spherical gray regions, which have became trapped in the white iron that surrounds them. In fully gray

Table 16.2 Summary of some main characteristics of Gray, White and Ductile cast iron.

Gray Cast Iron			
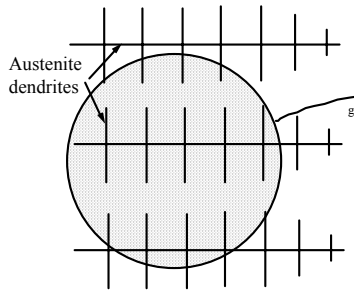	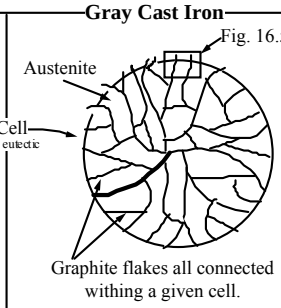	One inoculant used, active elemnt = Ca Hi Ca level → more and smaller cells.	Low strength & toughness High thermal conductivity
White Cast Iron			
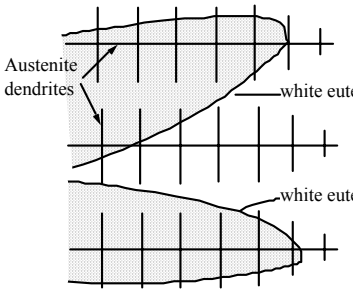	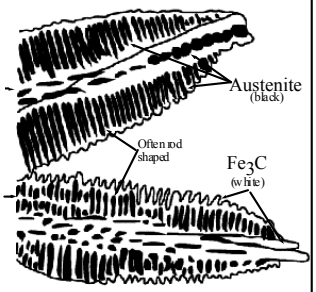	No inoculant used	Very brittle Very hard - good wear resistance
Ductile Cast Iron			
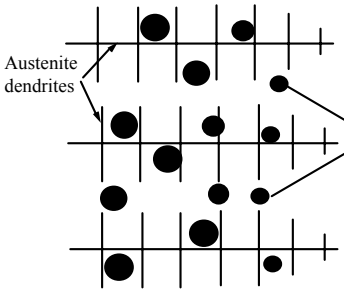	Divorced eutectic (graphite spheres + surrounding aust.) Solid graphite spheroids (Dark lines show orientation of graphites heets)	Two inoculants required Mg- to make graphite form spheroids Ca- to give high density of spheroids Also requires low levels of S impurities.	Heat treatable to moderately high levels of strength and toughness. Spheroids not connected so lower themal conductivity and improved toughness over gray irons.

cast irons, the spherical regions have grow outward until they contact one-another and each of these regions is called a cell. Several cells are located by the arrows at the top of Fig. 16.3. At the growth front between the spherical cells and the liquid, both flake shaped graphite and the austenite grow together into the liquid, as a type of coupled eutectic growth. Figure 16.5 shows an actual growth front preserved by quenching and one sees that the flakes are covered by austenite nearly up to their protruding tips.. Because this sample was made by quenching the liquid surrounding the spherical growing cells solidified rapidly as white iron and preserved the solid austenite/graphite eutectic growth front.

The micrograph of Fig. 16.5 illustrates the typical shape of what is called type A graphite in gray cast irons. This is probably the most common shape of graphite in sand cast gray irons. Gray irons that are solidified more rapidly can have finer distributions of graphite and these have been classified into types B

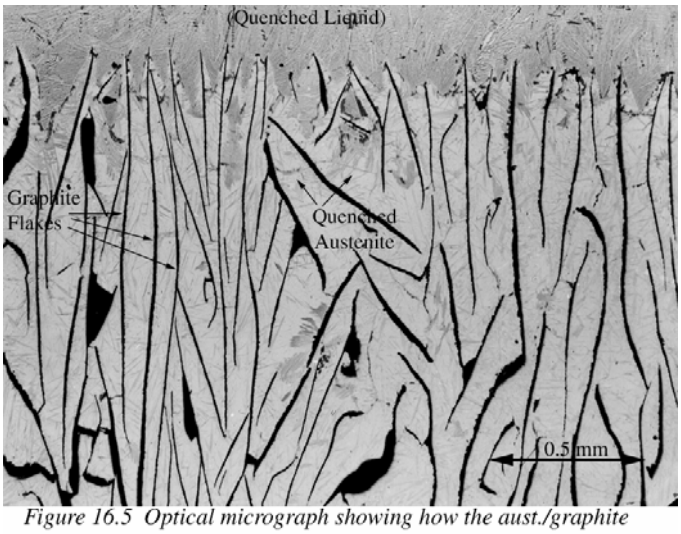

Figure 16.5 Optical micrograph showing how the aust./graphite eutectic grows into the liquid at the cell/liquid interface-40x mag.

through E by the ASTM (American Society for Testing Materials). A comparison of structures of all of the types, A to E, can be found on pages 820 or 874 of ref. [16.3]. Figure 16.6 presents SEM micrographs of a Type A and a Type D gray iron. These are the most common gray irons, with type D forming in thin sections that cool fast and type A forming in fatter sections that cool slower. The samples were first polished to a mirror finish and then immersed in hydrochloric acid, which dissolved away the iron lying between the graphite flakes. So the pictures give you an idea of how the graphite extends down from the original polished surface. Notice that the magnification of the type D graphite in Fig. 16.6(B) is 13 times larger than the type A graphite of Fig. 16.6(A). This illustrates the smaller spacing and the thinner thicknesses of the flakes in the type D graphite.

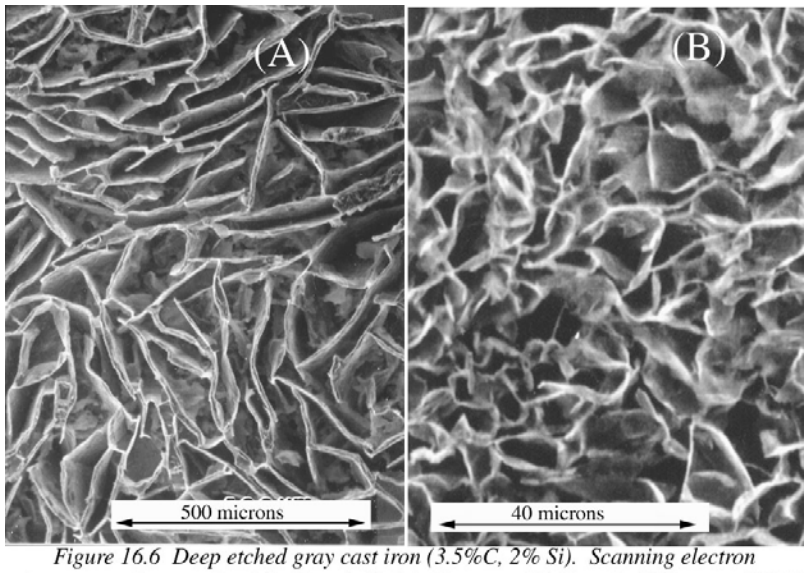

Figure 16.6 Deep etched gray cast iron (3.5%C, 2% Si). Scanning electron microscope micrographs. (A) Type A (flake)-75x mag., (B) Type D-1000x mag.[16.5].

Graphite is a relatively soft material and its presence in gray iron produces some useful properties in these irons. These properties include good resistance to sliding wear, excellent machinability and outstanding damping capacity, from 25 to 100 times better than a 1080 steel [16.4, p 435]. An important characteristic of gray irons is that all of the graphite flakes in a given cell are connected together, like the branches on a tree all interconnect. This feature is illustrated fairly well in the micrographs of deep etched irons shown in Fig. 16.6. Because of the special properties of graphite the interconnectedness of the graphite has a significant effect on the thermal and mechanical properties of gray irons. The thermal conductivity of graphite in the directions along the planes of the flakes is very high, on the order of that in high purity copper. Consequently, the thermal conductivity of gray iron is higher than that of steels. The low mechanical strength of the graphite flakes, particularly in directions at right angles to the plane of the flakes, has a large effect on the mechanical properties of gray cast irons. Gray irons have limited ductility and tend to fracture under impact loading. The fracture surface has a distinctly gray color because it is basically all graphite, except where it penetrates old austenite dendrites. These features are illustrated in the scanning electron microscope pictures of the fracture surfaces of type A graphite shown in Figs 16.7 (A) and (B). In (A) you can see how the relatively large flakes have delaminated into bundles of parallel sheets under the fracture stress. Graphite is similar to mica in that it tends to delaminate into sheets along certain crystal planes called basal planes; and these planes lie along the plane of the flakes in type A irons. In (B) the fractured region is located at a remnant iron dendrite. (Note: the two graphite flakes at the center illustrate nicely how the how these graphite flakes are composed of stacks of sheets, analogous to the structure of mica. It is this sheet structure which causes the strength of the flakes to be so low in directions at right angles to the flakes.) At the dendrite fracture surface in Fig. 16.7(B), you see the white surface characteristic of a microvoid coalescence fracture surface previously discussed in reference to Fig. 5.12 of

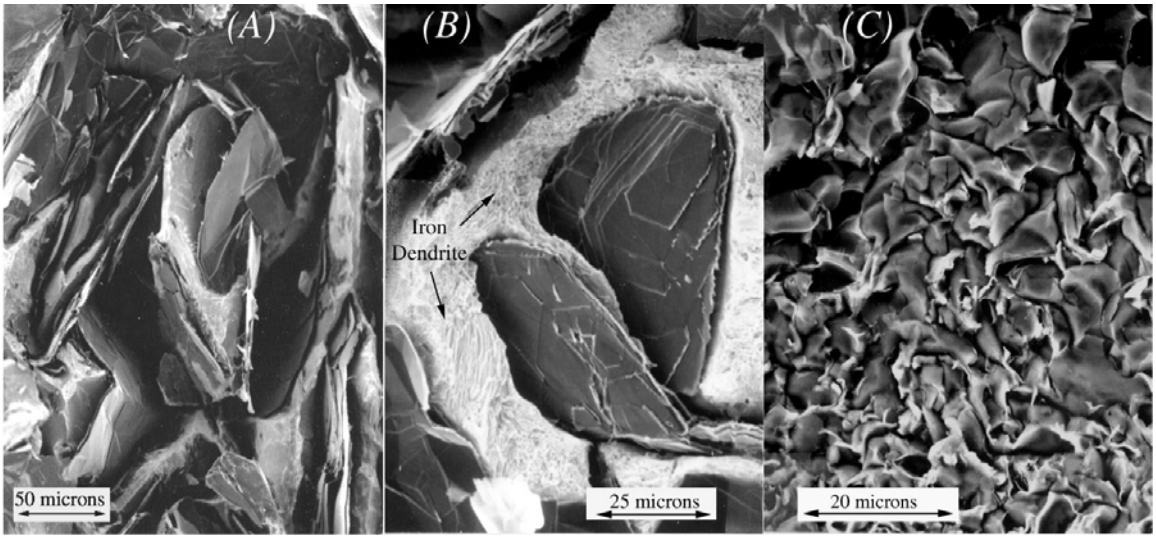

Figure 16.7 Fracture surfaces of gray cast iron (3.5% C, 2 %Si) revealed in scanning electron microscope micrographs. (A) Type A (flake)-220x mag., (B) Type A (flake) at a dendrite-600x mag. , and (C) Type D-1000x mag. [16.5].

Chapter 5. Figure 16.7(B) also illustrates how the flake graphite has managed to grow around the dendrite branches. The overall fracture surface appears gray to your eye because the fractured flakes protrude above the fractured iron dendrite surfaces, and because the dendrites occupy only a minor volume fraction of the gray iron. Figure 16.7(C) illustrates the fracture surface of a Type D iron. It appears essentially similar to the type A fracture surface except that all of the fractured graphite features reflect the finer graphite spacings and flake thicknesses in these irons which result from faster solidification.

Gray cast irons are often classified according to an ASTM code that runs from 20 to 60 as shown in the left column of Table 16.3. The code number approximates the tensile strength. The hardness of gray cast irons is virtually always given with the Brinell scale. The large ball indenter used with the Brinell test provides a much better average hardness over the graphite and iron structure than do the much smaller Rockwell B or C indenters. Using Table 5.3, the measured Brinell hardness numbers have been converted to equivalent R_c values in the final column. This is helpful for people who routinely use the C scale as a measure of hardness and find it difficult to evaluate relative hardness using other scales. The data of Table 16.3 illustrate that gray cast irons are much stronger in compression than in tension, which is a direct result of low strength of the graphite flakes and the interconnectedness of the flakes in gray irons. This is why gray irons find their major use in applications that are subject mainly to compressive stresses and not to tensile stresses, often massive structures such as lath beds, rolling and forging bodies, engine blocks, etc.

Table 16.3 Typical properties of gray cast iron test bars [16.4].

ASTM (A 48 class)	Tensile Strength	Compressive Strength	Hardness Brinell	Hardness (Equivalent R_c)
20	22 ksi*	83 ksi	156	(2)
30	31	109	210	(16)
40	42.5	140	235	22
50	52.5	164	262	27
60	62.5	188	302	30

* The k stands for 1000s, so 22 ksi = 22,000 pounds per square inch.

The strength variation of the irons of Table 16.3 result mainly from variation of the microstructure of the iron phases and the volume fraction of iron dendrites. As the carbon equivalent of an iron falls further

below the 4.3 value of the eutectic, the volume fraction iron dendrites goes up and raises the strength. Iron microstructures that are mainly pearlitic will be stronger than mainly ferrite microstructures. Gray irons are generally not heat treated, and when they are [16.3] the heat treatment usually is an anneal which drops strength. Therefore the variation of iron microstructure in the irons of Table 16.3 arise during the cool-down in the casting process.

To understand how the foundryman controls the microstructure of the iron matrix part of both gray and ductile cast irons it is useful to understand Figure 16.8. This figure shows how the phase diagram of Fig. 16.1 for pure Fe-C alloys is changed when 2% Si is added. It is a vertical section through the ternary Fe-C-Si system at a constant value of 2% Si, and hence is the same type of diagram as those of Fig. 13.4 which were used in discussing Fe-C-Cr stainless steels. As in Fig. 16.1, both the stable graphite lines and the metastable Fe_3C lines are shown, but in this case the stable graphite lines are shown solid and the metastable Fe_3C lines are dashed. Notice that the diagram illustrates the lower temperature of the Fe_3C eutectic relative to the graphite eutectic, previously shown to be $\Delta T_{gr\text{-}Cm} = 43\ ^oC$ on Fig. 16.2.

Consider now an iron of 3.5%C + 2% Si. This iron would have a C.E. of 4.17 and its composition appears on Fig. 16.8 at the vertical 3.5 %C line. The development of the microstructure of this alloy as it forms in a mold after pouring can be divided into 2 stages as cooling occurs along this vertical line. Stage I involves the solidification of the liquid metal as the temperature falls from 1 to 2. During stage I for a gray iron the structure forms as shown in Table 16.2. At completion when the temperature has fallen to point 2, the iron will consist of graphite flakes in an austenite matrix. Stage II involves cooling in the mold from temperature 2 down to temperatures of 3 and below. Consider a gray iron. As the temperature falls to the eutectoid temperatures the austenite must continuously drop its carbon composition as suggested by the A_{gr} line on the diagram. During this time the carbon atoms ejected from the austenite are deposited on the graphite flakes causing them to thicken. When the temperature falls to the eutectoid regions of the diagram, just as with the eutectic reaction in the liquid, there is a competition between the formation of graphite versus Fe_3C. Again, you must supercool more below the graphite eutectoid than below the

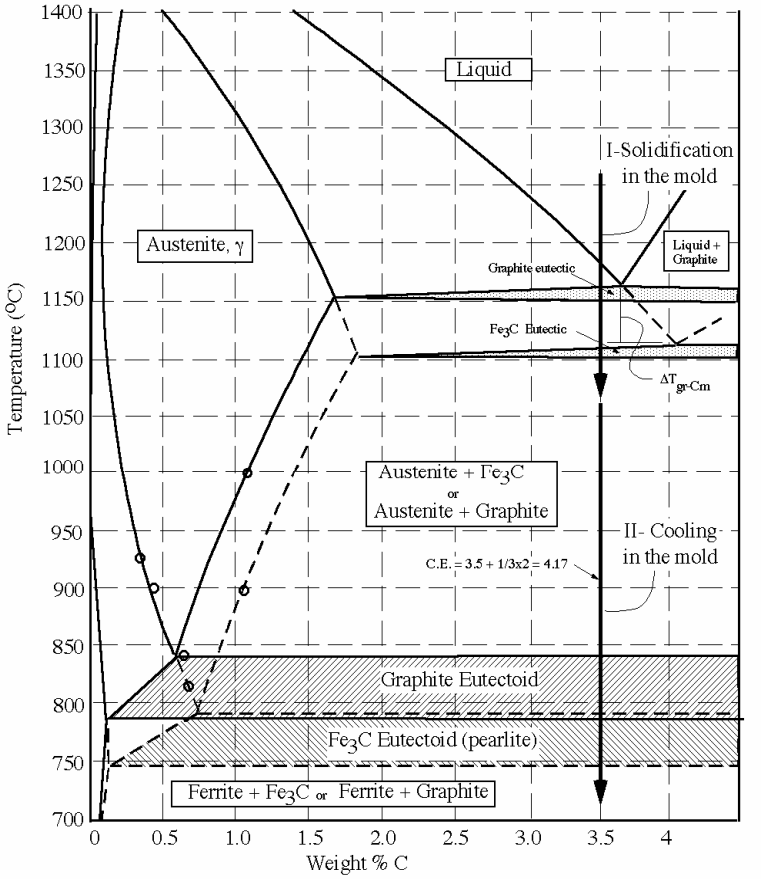

Figure 16.8 Vertical sections of Fe-C-Si phase diagram at %Si = 2. The stable graphite system is solid lines and the metastable Fe_3C system is dashed lines.

Fe_3C eutectoid to cause either to form. If the cooling rate is sufficiently fast in the mold, or if low levels of pearlite stabilizing elements are present, particularly tin or antimony, the graphite eutectoid will not nucleate. In this case all of the austenite surrounding the graphite flakes will transform to pearlite, similar to what happens in steels, as explained on pp. 13-14. One then ends up with what is called a pearlitic gray cast iron, which consists of the flake graphite surrounded by grains that are fully pearlitic.

Figure 16.9 A gray iron with a ferrite-pearlite matrix. Mag. 250x.

If, however, the cooling rate is extremely slow it can happen that no pearlite will form. In this case the graphite eutectoid reaction occurs in preference to the Fe_3C eutectoid, but it occurs in a divorced manner. What happens is that the remaining austenite transforms into rims of ferrite around the flakes. As the ferrite rims grow outward essentially all of the carbon that was in the austenite is deposited on the encased graphite flakes. Hence, one ends up with graphite flakes surrounded by ferrite in what is called a ferritic cast iron. Figure 16.9 shows the intermediate case where some of the graphite flakes are surrounded by rims of ferrite, but the remainder of the iron matrix is pearlite. In this case the divorced eutectoid graphite reaction (called divorced because the graphite & ferrite do not form side-by-side as a coupled pair) occurred first and then as the temperature dropped below the pearlite eutectoid the remaining austenite converted to pearlite (which is the more common coupled eutectoid with Fe_3C & ferrite plates forming side-by-side as a coupled pair). The greater the fraction pearlite in a cast iron the higher its tensile strength. The foundryman controls the fraction pearlite by controlling the cooling rate in the mold and with alloy additions that stabilize the pearlite. The most common heat treatment of gray irons is annealing, which converts some or all of the pearlite to ferrite and reduces tensile strength and improves machinability. See ref. [16.3] for discussion of the heat treatment of gray irons.

As shown in Fig. 16.4, white cast irons have lower C and Si compositions than gray irons. Graphite does not form in these irons so that one ends up with a structure consisting of Fe_3C (cementite) and pearlite. Table 16.2 illustrates that both white cast irons and gray irons begin solidification from the liquid with the formation of austenite dendrites. In white irons the interdendritic liquid solidifies as the eutectic mixture of austenite + Fe_3C, which forms between the dendrites and grows out around them as shown schematically in Table 16.2. The white eutectic has an overall planar shape with a central spine that consists of Fe_3C (white in Table 16.2) with rods of austenite (black) growing out perpendicular to the planes. Figure 16.10 shows an optical micrograph of the eutectic component of a white iron. The Fe_3C also appears white in this micrograph, and the austenite, which has transformed

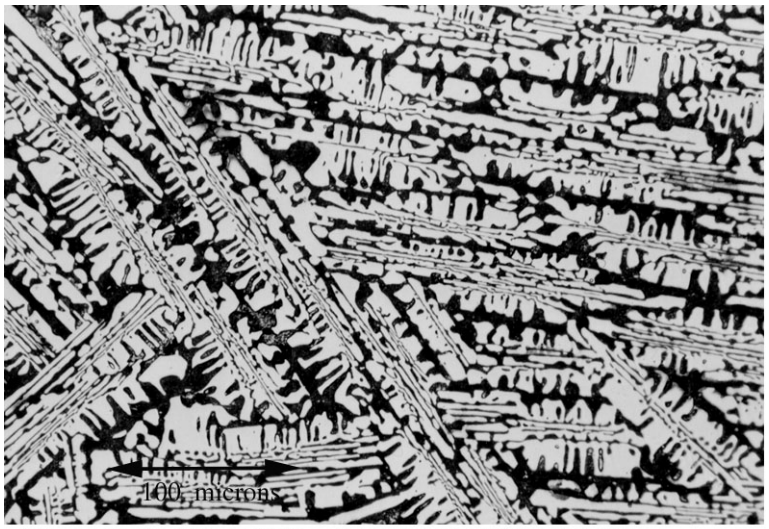

Figure 16.10 The eutectic component of a white cast iron

to pearlite, is black. Because the Fe_3C is very hard and very brittle these irons are also hard but brittle. The high hardness produces very good wear resistance. Because cast irons can be made to freeze with the white structure at fast cooling rates, and gray iron at slower cooling rates, as illustrated in Fig. 16.3, it is possible to make items like large rollers with a very hard white iron surface and a softer gray iron core, with the core having adequate toughness for many industrial applications. Improved toughness may be achieved in white irons by alloying with moderate amounts of Ni and Cr, and a nice discussion of these irons may be found in [16.6]. The fracture surface of a white iron runs along the brittle Fe_3C component of the iron. This component fractures by a cleavage mechanism and produces a bright white surface and hence the name for these irons.

Ductile and Malleable Cast Iron Ductile cast irons represent a triumph of 20th century metallurgical research. These irons were developed independently around 1948 at the International Nickel Company in the U.S. and at the Cast Iron Research Association in England. Both groups discovered that by keeping the S and P levels low and adding very small amounts of a key chemical element, the shape of the graphite could be changed from the interconnected flakes of gray irons into isolated spheres (usually called spheroids) of graphite. (Ductile C.I. is also called nodular C.I. and spheroidal C.I.) The INCO team showed that the effect was produced by the addition of only 0.02 to 0.1 % Mg (magnesium) and the BCIRA team by the addition of only 0.02 to 0.04 % Ce (cerium, the rare earth metal of atomic number 58, see p 57). Current foundry practice in the U.S. uses the Mg addition to produce ductile irons. As illustrated on the bottom row of Table 16.2, the graphite spheroids grow directly out of the interdendritic liquid and are not connected to each other. Their formation is an unusual type of divorced eutectic growth with the other component of the eutectic, the austenite, forming upon the surrounding dendrites of austenite. The spheroids are 100% carbon in the form of graphite, with the characteristic graphite sheets rotated around so as to be nearly parallel to the surface of the spheroids, as shown on Table 16.2. The spheroid diameter of a ductile iron is much smaller than the cell diameter of a gray iron; the typical volume of a single gray iron cell would be occupied by roughly 200 spheroids in a ductile iron. The mechanical properties of a ductile iron are comparable to a high carbon steel filled with very small and isolated spherical voids. The fact that the graphite spheroids are not connected, and that they have smooth surfaces means that they do not act as crack initiation sites. Hence they reduce mechanical properties only in rough proportion to their very small volume fraction. Consequently, as their name implies, ductile cast irons have fairly good toughness and, similar to steels, they are often used in the heat treated condition. See [16.3, p. 824] for a discussion of heat treatment.

Prior to 1948 a type of cast iron similar to ductile cast iron and called malleable cast iron was available. The malleable cast iron produced in the U.S. was an American invention, having its origin in the 1826 work of Seth Boyden, an iron founder from New Jersey. It was called black heart malleable to distinguish it from an inferior European process called white heart malleable. The industry was shrouded in secrecy and the process in mystery until the early 20th century and [16.7] presents an interesting discussion of these times. Malleable irons are produced in a two step process where step

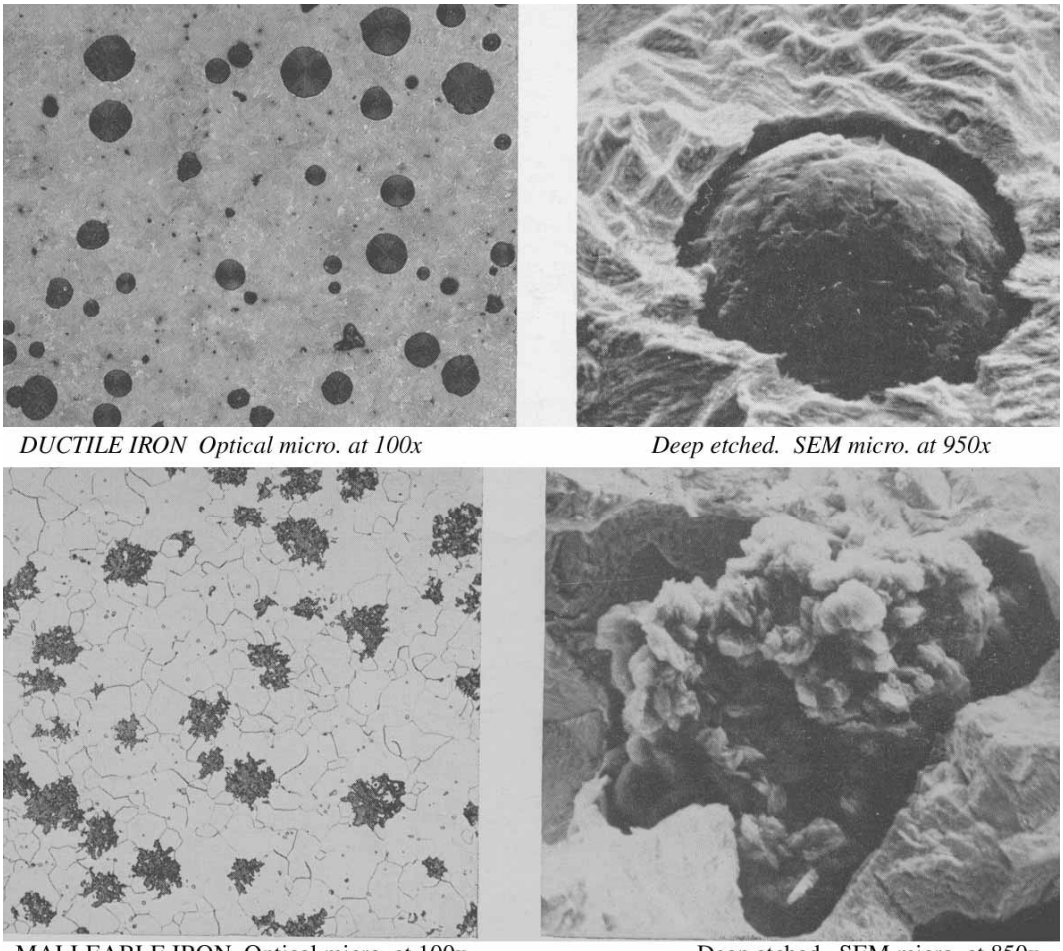
DUCTILE IRON Optical micro. at 100x
Deep etched. SEM micro. at 950x
MALLEABLE IRON Optical micro. at 100x
Deep etched. SEM micro. at 850x

Figure 16.11 Comparison of ductile cast iron (top) to malleable cast iron (bot.) From: Brittish Cast Iron Research Association, Broadsheet number 138 UK (1976).

1 is the production of a white cast iron. In step 2 the white iron is heated to around 950 ^{o}C (1742 ^{o}F) held for a day or two and then slow cooled over around a day or two. As seen on Fig. 16.8, at 950 ^{o}C the prolonged hold is in the temperature range of the austenite + Fe_3C or austenite + graphite region of the phase diagrams. Hence, at this temperature the white structure of austenite + Fe_3C decomposes into the more stable austenite + graphite structure. And, furthermore, if the proper mix of impurity elements, heating rate and holding temperature and times are employed [16.8, p. 656] the graphite forms as discrete isolated clumps, similar to the spheroids of ductile iron. The similarity of the structures of the 2 irons is shown in the micrographs of Fig. 16.11. The right hand micrographs were made in a scanning electron microscope (SEM) after the polished sample surface had been deep etched to allow the graphite to stick up. These micrographs show nicely the difference in the graphite shape in the two irons. As shown, in ductile iron the surface of the graphite is fairly smooth and spherical, while it is more jagged and clumpy in the malleable iron. The malleable cast iron industry has largely been replaced by the ductile industry, although malleable irons continue to be produced and have some limited advantage, especially for thin samples [16.9, p. 57].

Similar to gray irons, the matrix of ductile and malleable cast irons can be controlled by the cooling process, the addition of alloying elements prior to casting and heat treatment subsequent to casting. In the as-cast condition a ductile iron will come out as a ferritic ductile, a pearlitic ductile or more often as some mix of ferritic - pearlitic.

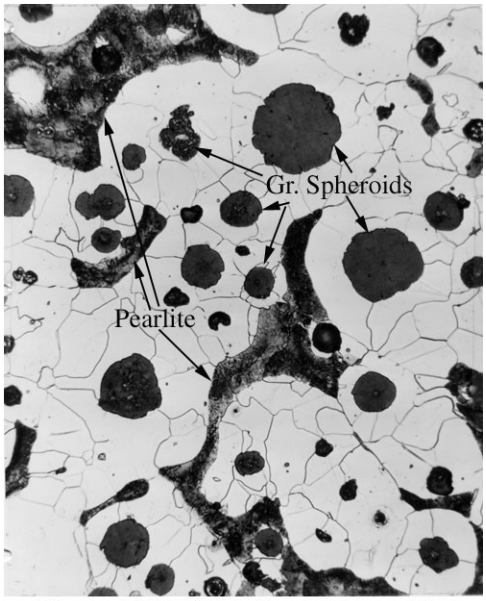

Figure 16.12 A ductile cast iron with a matrix that is dominantly ferrite. (250x)

Figure 16.12 presents a micrograph of a ductile cast iron that has a matrix with a pearlite/ferrite mix that is predominantly the white ferrite. Ductile irons are graded or classified as shown in Table 16.4. The 3 numbers of the specification refer to rough estimates of the 3 mechanical properties: Tensile strength-Yield strength-% Elongation, with strength units of ksi (thousands of pounds per square inch). Hence, the 60-40-18 ferrite ductile will have approximate tensile and yield strengths of 60 and 40 ksi and an approximate elongation at failure of 18%. The fully ferrite structure is produced by an annealing heat treatment. The next two irons down in the table are produced in the as-cast condition by composition control in the casting process, as was described for gray irons on page 178. The fully pearlitic structure is often produced by a normalization heat treatment (normalization means air cooling). The final row of Table 16.4 refers to a special form of ductile iron that has become widely used because of the attractive mechanical properties for the relatively cheap cast iron. It is widely referred to as ADI (austempered ductile iron). As discussed in Chapter 12, the austempering produces a bainite structure which, particularly at the high carbon levels of a cast iron, has excellent toughness compared to quenched and tempered martensite. These irons have found wide use in crankshafts and as a cheaper replacement for carburized gears.

Table 16.4 Types of Ductile Cast Irons

Grade or Class	Matrix Microstructure	Heat Treatment after casting	Structure controlled by:
60-40-18	All ferrite	Anneal	Heat treatment
65-45-12	Ferrite + small % pearl.	None(as-cast)	Composition control
80-55-06	Ferrite + large % pearl.	None(as-cast)	Composition control
100-70-03	All pearlite	Normalized	Heat treatment
120-90-02	Tempered martensite	Quench & temper	Heat treatment
135-100-8*	Bainite	Austempered	Heat treatment

* Austempered Ductile Iron, ADI

Table 16.5 is presented to show the specification of malleable irons. The two most common irons are presented in the table along with their ASTM number. A column is included that gives the tensile strength-yield strength and elongation in units comparable to that of Table 16.4. It is apparent that the mechanical properties of the two irons are comparable with the same type of ferrite/pearlite microstructure.

A relatively new form of cast irons has been developed in the past 20 to 30 years that is called **compact graphite** cast iron. These irons develop their graphite structure in cells, similar to that shown for gray irons in the top row of Table 16.2, only now the graphite has a more cylindrical or "worm-like" shape. They are sometimes called vermicular graphite irons. Research has developed composition controls that allow these irons to be produced reliably [16.6, p. 22]. They have mechanical properties somewhat intermediate between gray and ductile irons, and the interconnectedness of the graphite produces machinabiltiy and thermal conductivity superior to ductile irons.

Table 16.5 Grades of Malleable Cast Iron

Grade	Matrix	TS/YS/El	ASTM No.
Ferritic malleable	Ferrite	53-35-18	35018
Pearlitic malleable	Pearlite + ferrite	65-45-10	45010

References

16.1 Metals Handbook, vol. 8, 8th Edition, ASM, Metals Park, OH (1972).
16.2 I.C.H. Hughes, A Review of Solidification of Cast Irons with Flake Graphite Structures, p 184-192, The Solidification of Metals, ISI London, Publication 110 (1967).
16.3 Heat Treater's Guide, Practices and Procedures for Irons and Steels, ASM International, 2nd Ed. (1995).
16.4. Cast Irons, ASM Specialty Handbook,ASM International, Materials Park, OH (1996).
16.5 J.S. Park, Microstructural Evolution and Control in the Directional Solidification of Fe-C-Si Alloys, PhD Thesis, Parks Library, Iowa State University (1990).
16.6 R. Elliott, Cast Iron technology, p. 33, Butterworth (1988).
16.7 H.A. Schwartz, American Malleable Cast Iron, The Penton Publishing Co. (1922)
16.8 R.W. Heine, C.R. Loper Jr and P.C. Rosenthal, Principles of Metal Casting, McGraw-Hill (1967).
16.9 Metals Handbook, Ninth Edition, Vol. 1, Properties and Selection: Iron and Steels, ASM Metals Park OH (1978).

Summary of the major ideas of Chapter 16

1. There are 4 main types of cast irons. As shown in Table 16.1 carbon is present mainly as graphite in gray, malleable and ductile cast iron, while it is present as Fe_3C in white cast iron. The 3 irons, gray, ductile and white form directly in the mold, while malleable iron is produced by a special heat treatment of a white iron.

2. Cast irons are ternary alloys of Fe-C-Si. The addition of Si makes it more difficult for Fe_3C to form in these alloys and instead graphite forms in the 3 irons, gray, ductile and malleable.

3. There are dramatic differences in the properties of the cast irons. The white irons are hard but brittle due to the relatively large volume fraction Fe_3C in them. The graphite in gray iron is largely interconnected which produces excellent machinability, damping capacity and thermal conductivity, but low strength and toughness. As shown in Table 16.3, strength in tension is much less than in compression. The graphite in ductile and malleable cast iron is present as isolated spheres, or clumps, respectively. These irons can have mechanical properties approaching steels and are often heat treated as shown in Table 16.4 for ductile iron.

4. The top two rows of Table 16.2 show that both gray and white irons begin solidification by formation of austenite dendrites. In gray irons the interdendritic liquid then solidifies as the gray eutectic in the form of large spherical "cells" with graphite flakes and austenite growing outward at the spherical growth front as shown in Fig. 16.5. In white irons the interdendritic liquid solidifies as the white eutectic in the form of plate shaped structures composed of Fe_3C + austenite having the shapes shown in Fig. 16.10. As explained with the aid of Figs. 16.1 and 16.2 on pp 171-2, a competition occurs between the formation of the gray eutectic and the white eutectic during solidification after the dendrites have formed. As illustrated by Fig. 16.3 fast cooling allows the white eutectic to win the competition. The bottom of this casting froze fast in contact with a metal chill plate, and the top froze slowly in contact with a sand mold.

5 The composition ranges of the 4 cast irons are shown on Fig. 16.4. Foundryman talk of the carbon equivalent (the C.E.) of cast irons which equals %C +1/3%Si. This number may be calculated for any iron. The farther below a value of 4.3 the larger the volume fraction austenite dendrites in the iron.

6. The fracture surface of a gray iron appears gray because it is covered with graphite. Figure 16.7 shows how the graphite flakes pull up and cover the fracture surface nearly completely in these irons. The fracture surface of a white iron appears white because the brittle Fe_3C fractures by cleavage giving a smooth surface that reflects light well. Notice that in Fig. 16.3 one can actually see the spherical gray "cells" of the gray iron encased within the white iron in the mottled region where both forms have solidified.

7. Like gray and white irons, ductile iron begins solidification by formation of austenite dendrites (bottom row of Table 16.2). Only now a special addition of a minute amount of Mg (magnesium) to an iron low in S and P impurities changes the form of the graphite formation in the interdendritic liquid to the production of small discrete spheroids of 100% graphite. The isolated spheroids detract little from the mechanical properties and hence these irons are called ductile cast iron. They are often heat treated as shown in Table 16.4. Austempering to lower bainite produces excellent mechanical properties and these irons, called ADI (austempered ductile iron) have wide industrial use.

8 In both gray and ductile irons the matrix between the graphite that is present after solidification can be ferrite, pearlite or a mixture of the two. As explained with Fig. 16.8, a competition occurs between the formation of the pearlite eutectoid and the graphite eutectoid on cooling. And, high cooling rates and/or the addition of special alloying elements will enhance the formation of the pearlite eutectoid. Such an iron is called a pearlitic gray or pearlitic ductile iron, as opposed to a ferritic gray or a ferritic ductile iron.

9. Malleable cast iron is produced by a prolonged heat treatment of white cast iron as discussed on p. 180. The graphite distribution is similar to that of ductile irons except that, as shown in Fig. 16.11, the isolated clumps of graphite (often called temper carbon) are more irregular. Malleable irons, developed around 1830, have now been largely replaced by ductile irons, developed in the late 1940's and cheaper to manufacture.

Index

AISI	8,50
410	133,134
430	130,131
440	132,135
1035	100
1060	78,84,89
1075	118
1080	85,120
1086	83,98
4340	97
5140	114
5150	83, 97, 99
5160	78,84,89,97
8695	109
9260	31,97
52100	55,109,119
154-CM	A8
17-4, 17-7	145,146
301, 302, 304, 308, 309, 310, 316, 321, 347	141-145
475 C embrittlement	131
A steels	152-3
A-286	145145
Ac and Ar lines	15,54
ADI austempered cast iron	181
AK steels	74, 168
alpha iron	2
ASTM	50
austempered cast iron	181
austempering	115
austenite	2,9,103
austenitic stainless steel	141
austenitization	103
austenitization- 2 phase	107, 136, 156
bainite	29
banded, banding	23, 40, 161
black body	A5
body centered cubic	2
Brinell hardness	39
brittle fracture	43
C.E. (carbon equivalent)	173
carbides in tool steels	154
carburization	58,61
carbon equivalent	173
cast iron	170
cementite	12-Nov
CET	165
chill-test casting	172
Charpy impact test	42
Chromel-Alumel	A1
coarsening	99
cold junction	A2
cold junction compensation	A2
color band wave lengths	A4
columnar grains	165
columnar-to-equiaxed transition	165
compact graphite cast iron	181
compressive stress	45
conditioning of retained austenite	156
continuous cooling transformation	79,86
controlled rolling	75
convective heat transfer	121
corrosion of stainless steels	143
crevice corrosion	143
crystal	2
CT diagram	79,86
cutlery	134
CVN energy	43
D steels	152-3
Damascus steels	60,164
DBTT	42,97
decarburization	59,61
dendrites	160
DET- divorced eutectoid transformation	33
diamond pyramid hardness, DPH	40
diffusion	58
dislocations	70
divorced eutectic	179
divorced eutectoid	33, 178
double & triple tempering	156
ductile brittle transition temperature	42, 97
ductile cast iron	179
ductile fracture	43
ductility	37
duplex stainless steels	146
elastic deformation	36
electromagnetic	A4
emissivity	A6
endothermic gas	63

epsilon carbide	96
equiaxed grains	165
equilibrium freezing	162
eta carbide	96
eutectic	6
eutectoid	10,13
face centered cubic	2,9
fatigue failure	44
ferrite	2
ferritic stainless steels	129
fresh martensite	25
gamma iron	2
GM quench meter	122
grain boundaries	2
grain boundary segregation	75
grain growth	67,107
grain size	66
grain size number	67
graphite	170
graphitization	171
gray cast iron	171
H steels	91, 152-3
H, severity of quench	120
Hagg carbide	96
Hardenability	78
Hardenability bands	91
hardness test	38
HASLA steels	74
Hastelloy	132, A3
heat flux	A5
homogenization of austenite	103
hot shortness	53
hypereutectoid	11
hypoeutectoid	10,80
impact test	42
impurity elements in steel	51
inclusions in steel	54,72
Inconel 600	121, 132, A3
infrared	A4
infrared pyrometer	A4
interdendritic regions	160
intergranular corrosion	133, 143
iron-carbon phase diagram	10,12,14,107,161
ISO 9950	121
isothermal transformation	30,79
IT diagram	79
Izod impact test	42, 96, 134
Jominy end quench	88
K1 and K2 carbides	130,131,141,154
killed ingot	73, 167
Knoop hardness	40
L steels	152-3
lath martensite	25
lattice	1
Low alloy steels	50-51
lower bainite	30
M steels	152-3
M4	154
malleable cast iron	179
manganese sulfide	53
martempering	114
martensite	24
Martensitic stainless steel	132
microalloyed steels	74
microsegregation	160
microstructures	20-26
microvoid coalescence	44
Ms and Mf temperatures	26
neutral gas	63
nital	1
nodular cast iron	179
non-equilibrium freezing	162
normalizing	32
nucleate boiling heat transfer	121
O steels	152-3
oil quenchants	122
optical pyrometer	A4
particle dray	73
passivation, passivated	128
pearlite	13,20
percent elongation	37
periodic table	57
phase	6,9
phase diagram	6
phase transformation	4
PHSS	145
primary carbides	162
Pitting corrosion	143
plastic deformation	36
plate martensite	25
polymer quenchants	123
porosity	166
precipitation hardening stainless steels	145
proeutectoid	21-23
quench cracks	98
Quenching	113

radiancy	A5
Rc hardness versus tensile strength	41
recrystallization	70
reduction in area	37
residual stress	44
retained austenite	27
rimming ingot	73
Robert Mushet Specialty steel	151
Rockwell hardness	39
S steels	152-3
salt bath quenchants	124
Samuri swords	46
Sandvik 12C27	137
secondary carbides	162
SEM scanning electron microscope	30
sensitized, sensitization	133
severity of quench, H	120
shot peening	47
sigma phase	129
single phase austenitization	103
solidification	159
solute	75
solute drag	74
solutions	5
spectral emissivity	A6
spectral radiancy	A5
spheroidal cast iron	179
spheroidized steels	32
stabilization	138, 156
stainless steels	128
Stainless steels for knifemakers	A8
strain	36
stress	36
stress corrosion cracking	143
superferritic stainless steel	131
T steels	152-3
TE	97
temper carbon	183
Temper colors	95
Temper embrittlement	97
temperature colors	A3
Tempered martensite embrittlement	96
Tempering	95
tensile strength	37
tensile test	36
thermocouples	A1
thermoelectric effect	A1
through hardened	79
TME	96
tool steel classification	151-2
tool steels	151
toughness	43,98
two phase austenitization	107, 136, 156
Uddeholm AEB-L	137,139,140
ultimate tensile strength	37
ultraviolet	A4
upper bainite	30
vermicular graphite	181
Vickers hardness	40
W steels	152-3
white cast iron	171
yield strength	36

A Appendix A - Temperature measurement

One of the most important measurements that needs to be made in the heat treatment and forging of steel is the measurement of the temperature of the steel. These measurements are most often made utilizing either thermocouples or infrared pyrometers. A very useful resource for both temperature measuring equipment and information about temperature measurements is the Omega Company (www.omega.com). They will supply free copies of their Temperature book that contains information on temperature measurement along with both thermocouple and infrared pyrometer products.

Thermocouples

Perhaps the most common thermocouple used to measure temperature during the heat treatment of steel is the Chromel-Alumel thermocouple. The device is very simple and the general principles of its operation will be discussed using this material as an example. A Chromel wire is welded to an Alumel wire and the weld bead is placed at the location in a furnace where temperature is to be measured. Chromel is the trade name for an alloy made up of nickel plus chromium and Alumel for an alloy that is mostly nickel. Leads, often made from copper (Cu) wire, are attached to the ends of the thermocouple wires protruding out of the furnace and these leads connect to a digital voltmeter as shown in Fig. A1. Alumel is attracted to a magnet and Chromel is not so that when hooking up to the voltmeter one can determine the negative lead (Alumel) using a magnet.

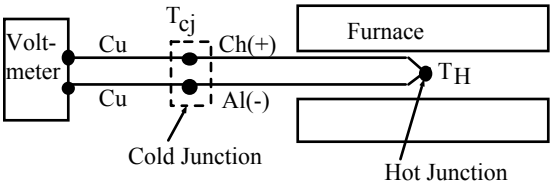

Figure A1 Common set-up for measuring furnace temperatures with a Chromel/Alumel thermocouple.

Thermocouples utilize a physical phenomena that occurs in nature called the thermoelectric effect. It requires that when wires of any two dissimilar metals are welded together and connected to a high impedance voltmeter (like a digital voltmeter) a small d.c. (direct current) voltage will be detected. For the configuration of Fig. A1, a voltage will be registered on the voltmeter if the temperature of the weld bead (called T_H and hot junction in Fig. A1) is higher or lower than the temperature of the Cu junctions (called T_{cj} and cold junction in Fig. A1).

Figure A2 presents the thermoelectric output voltage for Chromel-Alumel. An equation for this curve can be found in the Omega Temperature book. The book also contains long tables listing the voltages at given temperatures in both ^oC and ^oF. Figure A2 shows that as the temperature rises the output voltage increases in almost a straight line. If the hot temperature, T_H, is at 750 ^oC the figure indicates that a voltage of V_H equal to around 32 millivolts will be produced. However the hookup of Fig. A1 will not measure this voltage because of a complication that is important to understand. The

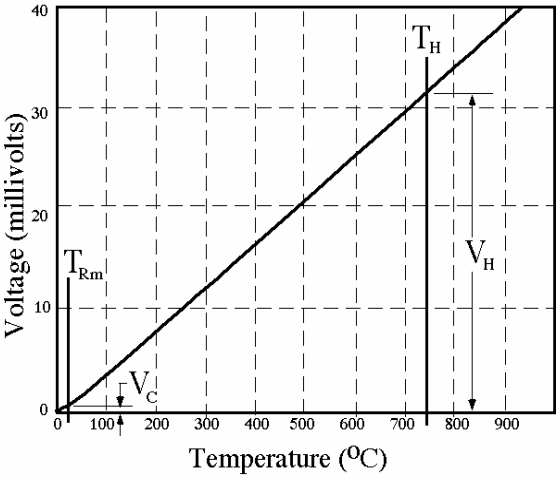

Figure A2 Voltage output of Chromel-Alumel thermocouples.

voltage measured by the voltmeter in the circuit of Fig. 1 is reduced by the voltage called V_C on Fig. A2. Hence the measure voltage is given as,

$$V = \text{measured voltage} = V_H - V_C \qquad \text{Equation A1}$$

The voltage V_C is often called the cold-junction voltage. It is the voltage given by the line on Fig. A1 at the temperature of the junction of the copper lead wires and the Chromel-Alumel wires, T_{cj}. If the cold junction is held at 0 ^oC (by immersion in an ice bath) then $V_C = 0$, and the measured voltage = V_H, the value given in the tables. However, the cold junction temperatures is usually room temperature, T_{Rm}. But this temperature, T_{Rm}, will not be constant because room temperature can vary and, if the junction gets close to the furnace it can rise significantly. Consequently, to produce reliable temperature measurements with a thermocouple one needs to apply what is called, cold junction compensation. Figure A3 presents a thermocouple hookup that uses an electronic cold junction compensator. The electronic compensator contains a battery and circuit components that can measure the local temperature. The unit becomes the cold junction and it automatically generates the required voltage V_C depending on the temperature and adds it to the voltage given in Equation A1 so that now the measured voltage at the voltmeter is equal to V_H no matter how the cold junction temperature might change.

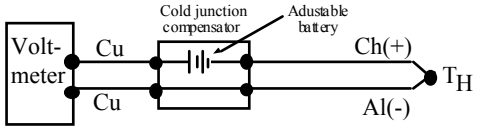

Figure A3 Cold junction compensator automatically adds the required V_C voltage into the thermocouple circuit.

Several commercial devices are available from places like Omega that read out the temperature from a thermocouple directly on a digital display. Some of these devices require that you use a cold junction compensator in the circuit as shown in Fig. A3, while others incorporate the compensator within themselves, so that the thermocouple wires can be hooked up directly to the device. If the device (or the cold junction compensator) is located far from the thermocouple one must use some type of hook-up wire to connect the two. If standard copper hook-up wire is used small errors will be generated if the temperature at the thermocouple connection is not the same as at the device connection. This problem can be overcome by using the thermocouple wire as the hook-up wire. Alternately, one may purchase special so called "compensation wire", and such wire is generally cheaper than the thermocouple wire and is compensated in composition to avoid problems produced by temperature variations between the hook-up connections.

There are various types of thermocouples that are commercially available and Table A1 presents a list of several of these. In recent years it has become common to refer to the various thermocouples with the Type letter code shown in Table A1. For example, the Chromel-Alumel thermocouple is now a type K thermocouple. One of the problems with the use of

Table A1 Some common thermocouple materials

Type	Elements	Comments	Max. Temp.
K	Chromel/Alumel	Most popular type	1800 ^oF (982 ^oC)
J	Iron/Constantine	High output	900 ^oF (482 ^oC)
E	Chromel/Constantin	High output	1100 ^oF (593 ^oC)
T	Copper/Constantin	High output, but low temperature limit	260 ^oF (260^oC)
R	Pt/Pt-13% Rh	High temperature, no oxidation	2642 ^oF (1450 ^oC)
B	Pt-6%Rh/Pt-30%Rh	Similar, but less grain growth	3092 ^oF (1700 ^oC)

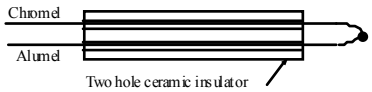

Figure A4 A basic thermocouple

thermocouples in hot furnaces is that the metal thermocouple wires will oxidize. If the oxide films extend too far below the surface the thermocouple will no longer operate correctly. Oxidation rates increase rapidly with rising temperature and Table A1 lists the maximum recommended temperatures for use of the various thermocouple types in air. The temperature limits shown in Table A1 are for a normal lifetime. The lifetime may be extended by using very large diameter thermocouple wire. Another problem with the use of thermocouples at high temperatures is that grain growth will occur and make the wires brittle. For very high temperatures such as those used for forging and for melting steel, the best choice thermocouple is one of the platinum varieties, which do not oxidize. The type B thermocouple has the advantage of reduced grain growth and will, therefore, resist breakage in use better than the other platinum thermocouples.

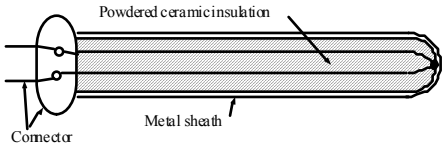

Figure A5 Metal sheathed thermocouple.

Thermocouples come in a variety of forms. They can be made up to suit ones needs from spools of wire. For high temperature applications it is necessary to thread the wires through some type of ceramic insulator so that the wires do not make electrical contact anywhere except at the weld bead. Fig. A4 shows a homemade thermocouple where the wires are threaded through a 2-hole ceramic insulator. At lower temperatures one may get by using fiberglass insulated thermocouple wires. Rolls of such wire are available commercially. Metal sheathed thermocouples are now widely available commercially. As shown in Fig. A5, these thermocouples have an external metal sheath and the wires are insulated from the sheath and each other by a finely powdered ceramic material that gives adequate electrical insulation up to the recommended maximum temperature of the thermocouple, often close to the melting temperature of the sheath metal. Various sheath metals are available having excellent oxidation resistances at high temperatures, such as the nickel based alloys, Inconel and Hastelloy. These metal sheathed thermocouples can be used to higher temperatures than unclad thermocouples. Omega sells a type K metal sheathed thermocouple rated for a maximum temperature of 2201 ^{o}F (1205 ^{o}C). These thermocouples are supplied with an electrical connector on the end as shown in Fig. A5, and various connector sizes and types are available. When using these thermocouples the cold junction will occur at the connector. If the connector might get warm it is important that either it be connected directly to a cold junction compensator or a meter containing such a compensator. If it is necessary to use lead wire to connect to the compensated measuring device, one may simply use lengths of the thermocouple wire. Alternately, spools of compensating wire mentioned above are commercially available for the various thermocouple types at cheaper prices.

Radiation Pyrometers

Blacksmiths have been heating and quenching steels for many centuries and they have been able to control the temperature of the hot steel by observing the color of the light (radiation) coming from it. Table A2 presents a typical approximation of the color of a hot body and its temperature. The color transitions on heating, from red to orange to yellow to white are

Table A2 Approximate temperature colors [A1].

Color	^{o}C	^{o}F
Faint red	500	932
Blood or dark red	550-625	1022-1157
Dark cherry	635	1175
Full cherry red	700	1292
Bright cherry	800	1472
Dark orange	900	1652
Orange	950	1742
Full yellow or lemon	950-1000	1742-1832
Light yellow	1100	2012
White	1150 and up	2012 and up

easily seen by observing the heat-up of a furnace. It is necessary to keep the room dark to observe the first red color listed in the table. Dramatic advances in our understanding of the nature of the light emitted from hot surfaces were made by physicists at the beginning of the 20th century, which led to devices called pyrometers that now allow us to measure the temperature of a hot body more accurately than can be done by a well trained blacksmith. My experience while using infrared pyrometers in working with bladesmiths has found that they can estimate temperatures fairly consistently within about 20 °C or so.

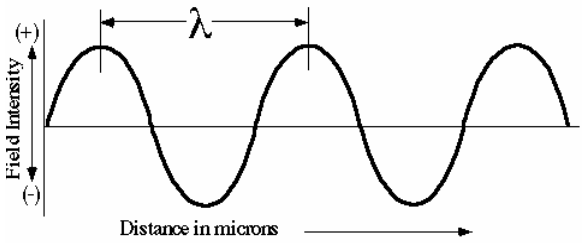

Figure A6 Variation of field intensity of a light wave of wavelength λ.

Figure A8 The cavity radiator

The light that we see coming from a white hot piece of steel is the same kind of light we see coming from the stars and the sun. It is a form of radiating energy that physics books call electromagnetic radiation. It consists of combined alternating electric and magnetic fields that give rise to the name electromagnetic. Light rays are thought of as waves propagating in some direction (at the "speed of light", 186,000 mile/sec.) and having field intensities that vary as shown in Fig. A6 for the electrical field component. It is customary to call the wave length, the distance between peaks or valleys, by the Greek letter lambda, λ. The energy of the light wave becomes higher as λ becomes smaller. If the wave length of the light is restricted to a narrow band of wave lengths in a range that is visible to our eyes our brains see specific colors.* Table A3 lists the bands of wave lengths of the common colors. However, as illustrated in Fig. A7, if the light contains wave lengths of several color bands it appears white to us. Also, our eyes can only see light having wave lengths over a relatively narrow range, generally referred to as the optical range. Light with wave lengths slightly larger than this range is called infrared light, while light with wave lengths shorter is call ultraviolet light.

Table A3 Wave lengths of color bands

Color	Wave Length band
Red	0.65-0.77 microns*
Orange	0.59-0.65 microns
Yellow	0.55-0.59 microns
Green	0.48-0.55 microns
Blue	0.43-0.48 microns
Violet	0.36-0.43 microns

* 25 microns = 1 mil = 0.001 inches

Heated bodies radiate energy and it is possible to measure the temperature of a body by measuring an intensity of the radiation being emitted from it. If the device that measures the temperature examines radiation in the optical range it is called an optical pyrometer. With the development of solid state detectors in the 1960-1970s that efficiently measure radiation in the infrared range shown to the right in Fig. A7, infrared pyrometers became available. These devices are very effective in measuring the temperature of hot metals and furnaces and they have now largely replaced the optical pyrometers, as they are much more convenient to use.

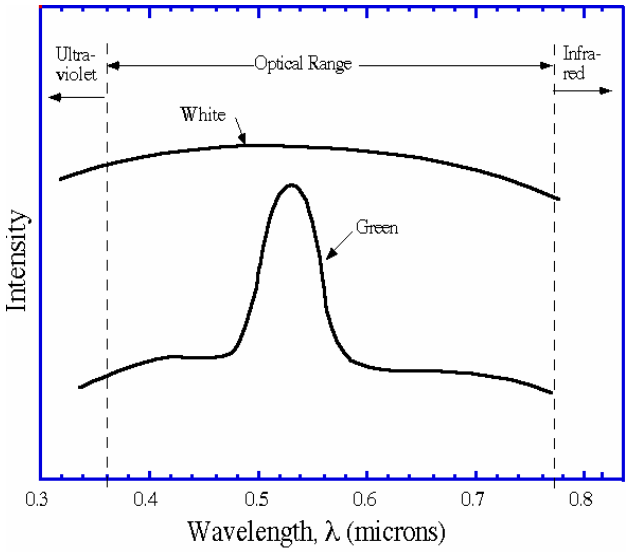

Figure A7 Intesity versus wave length of a white light and of a green light.

* For a clear description of how our brains assign the colors see Chapter 23 of A Vision of the Brain by S. Zeki, (1993).

To understand how radiation pyrometers work, one may start with the definition of a cavity radiator which is shown in Fig. A8. The opening in the ideal cavity radiator is so small that all light coming into it is absorbed in its walls, and it is customary to call it a perfect "black body". The light emerging from the cavity radiator is called black body radiation and its intensity can be measured experimentally and one obtains a value of power per area of the opening, or watts/m^2 or (joules/s)/m^2, where /m^2 means per square meter. Physics books call this quantity the radiancy, R, while engineering heat transfer books call it the heat flux, Q. The wave lengths, λ, of the emerging radiation varies over a wide range. It is possible to spread the light into its wave length components using spectroscopy techniques and hence it is possible to measure R versus λ. In a first approach one would normally just plot R versus λ to observe the dependence. However, if one plots the ratio of R/λ vs λ, a fascinating result is observed: the resulting curve is found to fit data from all cavity radiators, independent of the material from which they are made. The ratio is called the spectral radiancy, R_λ, and the universal plots have the form shown in Fig. A9. The units of spectral radiancy are sometimes given as (watts/m^2)/micron, where the micron refers to the wave length of the radiation and the m^2 to the area of the radiator in square meters. On Fig. A9, however, the units have been changed to watts/in^2-micron, so that if one multiplies this spectral radiancy times the wave length of interest one obtains the watts per square inch (power per area) emitted at that wave length. Figure A9 shows you why the color of hot steel changes in the sequence red-orange-yellow-white as the temperature rises. The intensity of the emitted light shifts to lower wave lengths (higher energies) as the temperature rises. The highest intensity in the optical range always occurs (at least up to 3000 ^oC) at the red end of the range. Hence, as the metal heats the first light intense enough for your eye to see is in the red band. Further heating increases the intensity of the smaller wavelengths visible to the eye so that the colors change progressively through the color bands of Table A3 until there is enough of the shorter wavelengths visible to mix the wavelengths to the degree that your brain sees white light. So, you never see colors beyond the yellow band of Table A3 because when objects become hot enough for green wave lengths to be sufficiently intense for detection by your eye, the mix of red-orange-yellow wave lengths also present causes your brain to see the light as white.

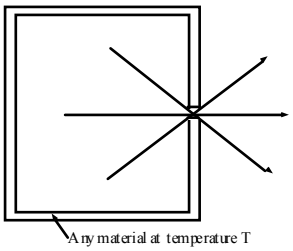

Figure A8 The cavity radiator

The radiation being emitted from the surface of metals and alloys is not blackbody radiation. The spectral radiancy versus wave length for the light emitted from hot steel surfaces will have a functional shape similar to that for black body radiation, but it will be depressed as shown for unoxidized steel at 2000 ^oC in Fig. A10. It is common to characterize the reduced radiation intensity simply as a fraction of the blackbody radiation utilizing a ratio called the **emissivity**. If the fractional drop in spectral radiancy is measured

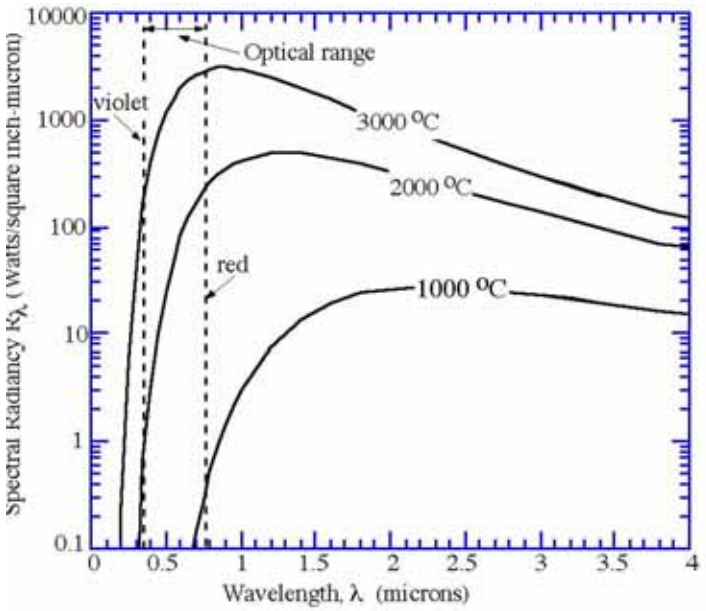

Figure A9 Spectral radiancy versus wavelength for cavity radiator, black body radiation, at 3 temperatures.

at a specific wave length, then the emissivity is called the "spectral emissivity".

$$\text{Spectral emissivity} = e_\lambda = \frac{(R_\lambda)_{surface}}{(R_\lambda)_{cavity}}$$

where the wave length λ must be specified. For example, the spectral emissivity at a wave length of 0.65 microns for the steel of Fig. A10 is found to be, e_λ = 43/122 = 0.35. At λ = 2.0 microns e_λ falls to 66/331 = 0.20. This result shows a general trend for the spectral emissivity of metals, it falls progressively further below 1.0 as λ increases.

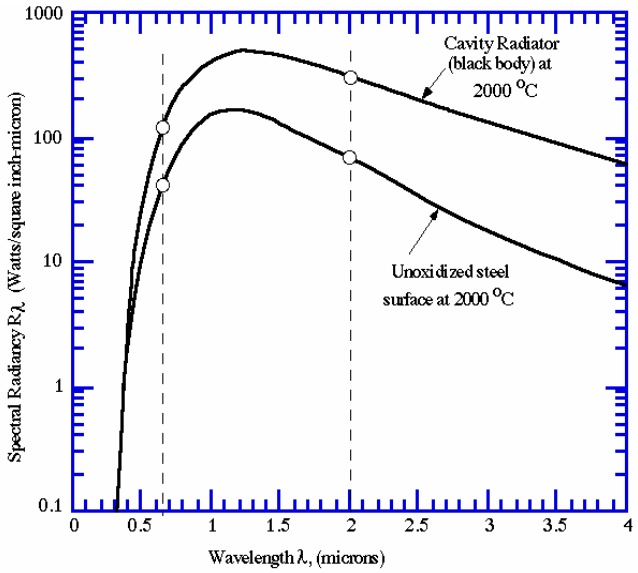

Figure A10 Spectral radiancy from a black body (cavity radiator) versus that from the surface of steel at 2000 °C.

For metals the values of the emissivities are very sensitive to the presence of surface films, such as oxides, on the metal. Table 4.1 presents values of the spectral emissivities for steel and copper in both the oxidized and unoxidized conditions and it is seen that oxidation has a large effect on emissivity. Heat treated and forged steels almost always are oxidized to some extent unless special laboratory conditions are used. These data clearly illustrate the importance of making reliable emissivity corrections when using pyrometers to measure steel temperatures during heat treating and forging operations. The temperature indicated by the infrared pyrometer is an apparent temperature which will be lower than the true value depending on how far the emissivity falls below 1.0.

Table A4 Emissivity Values [A1, p 490]

Material	e_λ *(λ = 0.65 microns)*
Steel (unoxidized)	*0.35*
Steel (oxidized)	*≈0.7*
Copper (unoxidized)	*0.10*
Copper (oxidized)	*≈0.7*

There are several approaches to making emissivity corrections, three of which will be discussed here. In the first method a hole is drilled into the surface of the sample with an aspect ratio, length/diameter ratio, greater than around 5. The hole diameter must be large enough that the pyrometer optics allow it to be focused inside the hole. Radiation coming from such a hole gives a good approximation of black body radiation and it may be assumed that the emissivity is one. A second method is to simply attach a thermocouple to the sample under study and experimentally measure a correction factor for the pyrometer under the conditions of the measurement. This is the most accurate method assuming that the thermocouple bead is securely enough attached to the steel that it is at the same temperature as the steel surface being imaged in the pyrometer. A third method is to use a two-color pyrometer. The two color pyrometer measures the spectral radiancy at two specific wave lengths, λ_1 and λ_2 and then determines the ratio, $R_{\lambda_1}/R_{\lambda_2}$. It turns out that this ratio is less dependent on changes in emissivity than are the values of R_λ themselves. Therefore two-color pyrometers require a much smaller emissivity correction than single color pyrometers. However, they are more expensive.

Infrared pyrometers are easy to use and are becoming available in great variety with many useful features, such as laser beam pointers that locate the position where the unit is focused. Both the variety of instruments available and technical information on the use of these

Table A5 Typical Infrared Pyrometer Ranges Available

Spectral Range *(Range in microns where works)*	*Temperature Range of Operation*	
	minimum	*maximum*
0.76 - 1.06 microns	*600°C*	3000 °C
1.0 - 1.6	250	2000
8 - 14	-50	1000

instruments are available from the commercial company, Omega. Table 4.2 presents information on infrared pyrometers for typical temperature ranges that were available in the late 1990's. A general rule of thumb is to use units with the lowest λ range available for metal samples. As shown above, this reduces the emissivity correction which leads to improved accuracy. Both the single and two color pyrometers have a dial-in knob which allows one to increase the apparent temperature to the corrected temperature corresponding to the emissivity set on the dial. So, if the emissivity is constant and the required correction has been measured, the apparent temperature on the digital read out can be automatically adjusted to give the correct values for emissivities less than one.

References

A1 G.L. Kehl, Metallographic Laboratory Practice, McGraw-Hill, New York, NY (1949).

B Appendix B - Stainless Steels for Knife-makers

Chapter 13 discussed two specific steels that are used for making knives of stainless steel, Sandvik 12C27 and Uddeholm AEB-L. There are several other stainless steels often used by knife-makers and Table B-1 presents most of the popular types. These steels often contain the addition of Mo. In addition to enhancing passivity, as mentioned in Chap. 13, Mo also improves toughness in the tempered condition.

Table B-1 Stainless steels often used for knives

Steel	Mft	%C	%Cr	%Si	%Mn	%Mo	Other
440A	AISI Steel	0.7	17	1	1	0.75	-
440B	AISI Steel	0.85	17	1	1	0.75	-
440C	AISI Steel	1.1	17	1	1	0.75	-
12C27	Sandvik	0.6	13.5	0.4	0.4	-	-
AEB-L	Uddeholm	0.65	12.8	0.4	0.65	-	-
DD400	Minebea	0.61	12.9	0.32	0.67	-	-
425 M	Crucible	0.54	14.2	0.8	0.5	0.8	-
154-CM	Crucible	1.05`	14	0.3	0.5	4	-
ATS-55	Hitachi	1	14	0.4	0.5	0.6	0.4Co,0.2Cu
ATS-34	Hitachi	1.05	14	0.35	0.4	4	-
AUS-6		0.6	13.8	1	1	-	0.13V,0.49Ni
AUS-8		0.73	13.81	0.5	0.5	0.2	0.13V,0.49Ni
AUS-10		1.03	13.8	1	0.5	0.2	0.13V,0.49Ni

In the discussion of AISI 440C in Chapter 13 the 1100 Fe-Cr-C ternary phase diagram was used to illustrate the expected composition of the austenite prior to quenching. To simplify the presentation the addition of the 0.75% Mo in this steel was ignored by plotting the composition on the 1100 ^{o}C Fe-Cr-C ternary phase diagram, Fig. 13.11. Because Mo is a strong carbide forming element one would expect that the 0.75% Mo addition would make small changes to the pure Fe-Cr-C phase diagram. The diagram of Fig. 13.11 was produced by combining experimental measurements with theoretical thermodynamic calculations by a group of Swedish researchers headed by M. Hillert [13.8]. This work led to the development of a sophisticated computer software program called ThermoCalc. At the request of the author, Dr. A. Kajinic at Crucible Research in Pittsburgh PA, has used this program to calculate several Fe-Cr-C isothermal diagrams with a constant amount of Mo added. Figure B1 presents the isothermal Fe-0.8Mo-Cr-C diagram. This diagram matches the Mo level in 425M and provides a good approximation to the 0.75% Mo of the AISI 440 series of stainless steels.

Figure B1 presents the isothermal sections at both 1100 ^{o}C (the solid lines) and at 1000 ^{o}C (the dashed lines). Comparing this diagram to that of the non Mo diagrams of Fig. 13.13, one sees that the carbon saturation line at 1000 ^{o}C is shifted just slightly to lower %C values. Notice that a larger change has occurred in the position of the $\gamma + K_1 + K_2$ region (shaded regions) that lies between the $\gamma + K_1$ and $\gamma + K_2$ regions. This is illustrated well by looking at the position of the overall composition of 440C alloy located at the solid dots on the two diagrams, Figs. 13.13 versus Fig. B1. (The open circle labeled 440C gives the austenite composition at 1100 C.) The Mo addition shifts the $\gamma + K_1 + K_2$ region down and to the right on these diagrams, which favors formation of

the K_1 carbide over the K_2 carbide for a given alloy composition. This result might be expected to reduce wear resistance (as K_2 is the harder carbide, see Table 13.9) if the non-Mo steels did contain mostly K_2 carbides as predicted by Fig. 13.11. However, experiments [13.12] indicate non-Mo steels have mainly K_1 carbides, so this effect is unlikely. But the Mo addition should produce some improvement in the corrosion resistance at the same level of %Cr. Calculations [B1] predict that the austenite formed at 1100 ^{o}C in 440C should contain around 0.73%Mo in addition to 12.2 %Cr.

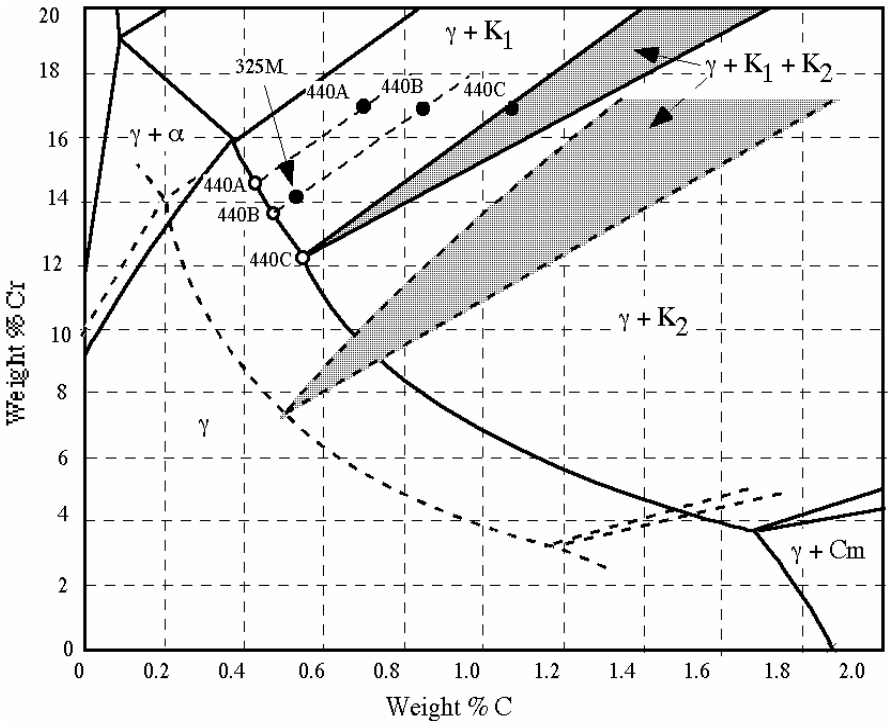

Figure B1 Isothermal sections of the Fe-C-Cr-0.8%Mo alloy system. Solide lines, 1100 ^{o}C and dashed lines at 1000 ^{o}C. ThermoCalc diagram provided by A. Kajinic [B1].

The alloy 325M is shown on Fig. B1 and it is seen to fall essentially on the tie line for AISI 440B (dashed line connecting closed and open circles labeled 440B). However its overall composition lies much closer to the carbon saturation line so that one would expect this alloy to be similar to 440B except the carbides should be present in a smaller volume fraction and the fraction of primary carbides should be negligible. The ThermoCalc predictions for the 1100 ^{o}C austenite of 325M are 13.5%Cr, 0.475%C and 0.77%Mo [B1]. Hence, one would expect this alloy to be not quite as hard as the AEB-L alloy discussed at length in Chapter 13 because of the slightly lower %C, but a bit better in corrosion resistance due to the Mo in the austenite.

The alloys ATS 34 from Hitachi and 154CM from Crucible are essentially the same alloy with the relatively high Mo addition of 4 %. The ThermoCalc prediction of the 1100 ^{o}C isotherm of the Fe-C-Cr-4 Mo system [B1] is presented in Fig. B2. At 1100 ^{o}C the isothermal section of Fig. B2 predicts that the alloy will consist of austenite plus the K_1 carbide. Additional calculations find that the composition of the austenite will be 10.6% Cr, 3.4% Mo, 0.58%C. Because the overall composition of 154CM lies off of the carbon saturation line about the same amount as 440C it is expected that the volume fraction carbides will be similar. The similar overall %C and total %Cr + %Mo in these two steels will probably result in the same problem of formation of

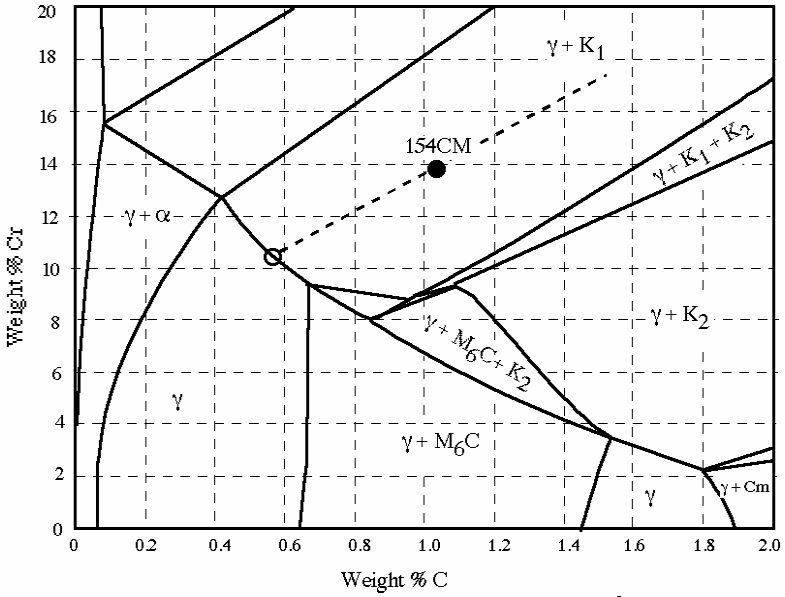

Figure B2 Isothermal section of the Fe-C-Cr-4.0%Mo alloy system at1100 ^{o}C [B1].

large primary carbides in the solidification process.

Research on 154CM at Crucible [B1] has found that the %Cr in the austenite produced at 1065 ^{o}C (1949 ^{o}F) is approximately 10%. This result agrees well with the predicted ThermoCalc value of 10.6% at 1100 ^{o}C, because one would expect a value slightly less than 10.6 at the lower austenitizing temperature of 1065 ^{o}C. The fact that the Cr level lies below the 12% Cr value generally desired for good passivity might indicate that this steel would have poor corrosion resistance. However, the 3.4 % Mo present in the austenite should compensate for this reduction. Experiments at Crucible [B1] have confirmed this to be pretty much the case.

From this discussion it appears that the two steels discussed in Chapter 13, Uddeholm AEB-L and Sandvik 12C27, along with the similar steels of Table B1, (DD400 and AUS6) provide the best combination of properties desired in a knife blade:

(1) An as-quenched hardness in the 63 to 64 R_c range which should provide high wear resistance.
(2) An adequate level of Cr in the austenite formed prior to quenching to provide good corrosion resistance, a bit above the minimum 12 %Cr.
(3) The presence of fine arrays of the $K_1 + K_2$ chromium carbides to enhance wear resistance plus the absence of the larger primary chrome carbides that promote pull-out at sharpened edges.

Sandvik produces a series of stainless steels having compositions close to the value of the 12C27 that was considered in Chapter 13. Table B-2 presents a comparison of these steels to that of the Uddeholm AEB-L that was studied in Chapter 13. The overall compositions shown in the table were plotted on Fig. 13.11 and the predicted values of %C and %Cr in austenite at 1100 ^{o}C are shown in the 4th and 5th columns of the table. The volume fraction carbide in the 1000 ^{o}C austenite can be determined by measurement of the distance of the overall composition from the carbon saturation line. The fraction carbide in the Uddeholm AEB-L, which may be estimated from Fig. 13.17, was taken as a standard and the final column of the table presents the factor telling you fraction carbide relative to this standard. For example, the high carbon in Sandvik 19C27 produces 5.6 times more carbides at 1000^{o}C than found in AEB-L. This steel will produce the highest hardness in the Sandvik series, but the carbides might be larger than desired on the cutting edge due to formation of primary carbides resulting from the increased C level. And the corrosion resistance will be the poorest due to a %Cr of only 11.3%. As shown in Chapter 13 the as-quenched hardness, % retained austenite and volume fraction carbides in AEB-L is very sensitive to heat treat temperature, time and quench rate. Because the compositions of the Sandvik 12C27 and 13C26 are so similar to AEB-L it seems likely that the properties of these three steels may be more sensitive to the austenitization heat treatment than to choice of composition, unless precise heat treat conditions are utilized. The 12C27M of the Sandvik series should have the best corrosion resistance due to the highest %Cr in the austenite, but the lowered %C will produce the lowest as-quenched hardness.

Table B-2 Additional stainless steels available from Sandvik

Steel	Overall		In Austenite at 1000 ^{o}C		Relative volume fraction carbides (Is multiple of amount in AEB-L)
	%C	%Cr	%C	%Cr	
Ud. AEB-L	0.65	12.8	0.59	12.3	1.0 (Standard value)
Sand. 12C27M	0.52	14.5	0.52	14.5	no carbides at 1000 ^{o}C
Sand. 12C27	0.60	13.5	0.56	13.2	0.7
Sand. 13C26	0.65	13	0.58	12.5	1.1
Sand. 19C27	0.95	13.5	0.60	11.3	5.6

As seen in Table B-1, the Minebea steel, DD400 has a very similar composition to the Uddeholm and Sandvik steels of Table 13.7. A fairly recent paper [B.2] has compared this steel to 440C for use in bearings hardened to the HRC = 61 to 64 range. The DD400 bearings are reported to have longer bearing life, reduced noise and vibration levels. Micrographs are presented to show large primary carbides present in 440C and their absence in DD400. The improved bearing properties are attributed to the absence of the primary carbides. As explained on p 162, primary carbides are produced by formation from the interdendritic liquid during solidification. Increased levels of %C will lead to primary carbide formation due to the combination of high Cr content and non-equilibrium freezing in these stainless steels. The absence of primary carbides in the DD400 steel and the AEB-L experiments of page 139 indicate that dropping the %C level from around 1% in 440C to around 0.6% in steels containing around 13 %Cr is sufficient to reduce primary carbide formation to negligible levels during solidification.

References

B1 A. Kajinic, personal communication, Crucible Research, Pittsburgh, PA (2002).

B2 J. Rideout, Bearing steel bests type 440C, Advanced Mat. and Proc. p39, Dec. (1992).